**Universidade de Aveiro** Departamento de Biologia
**2017**

**MÓNICA ALEXANDRA DOS SANTOS FERREIRA**

# CONTROLO EPIGENÉTICO DAS CÉLULAS PRIMORDIAIS DA LINHA GERMINATIVA MASCULINA PELA PROTEÍNA FOSFATASE PP1-NIPP1

# EPIGENETIC CONTROL OF THE MALE PROGENITOR GERMLINE BY THE PROTEIN PHOSPHATASE PP1-NIPP1

**Universidade de Aveiro** Departamento de Biologia
**2017**

**MÓNICA ALEXANDRA DOS SANTOS FERREIRA**

# CONTROLO EPIGENÉTICO DAS CÉLULAS PRIMORDIAIS DA LINHA GERMINATIVA MASCULINA PELA PROTEÍNA FOSFATASE PP1-NIPP1

# EPIGENETIC CONTROL OF THE MALE PROGENITOR GERMLINE BY THE PROTEIN PHOSPHATASE PP1-NIPP1

Tese apresentada à Universidade de Aveiro para cumprimento dos requisitos necessários à obtenção do grau de Doutor em Biologia realizada em cotutela com a Universidade de Leuven para a obtenção do grau de Doutor em Ciências Biomédicas, sob a orientação científica da Professora Doutora Margarida Sâncio da Cruz Fardilha, Professora Auxiliar do Departamento de Ciências Médicas da Universidade de Aveiro e do Professor Doutor Mathieu Bollen, Professor Catedrático e Diretor do Departamento de Medicina Celular e Molecular da Universidade de Leuven, e sob co-orientação científica da Professora Aleyde Van Eynde, Professora Associada do Departamento de Medicina Celular e Molecular da Universidade de Leuven.

**Bolsa de Doutoramento concedida pela Fundação para a Ciência e Tecnologia (FCT) com referência SFRH/BD/73000/2010.**

**PhD Scholarship granted by Fundação para a Ciência e Tecnologia (FCT) under SFRH/BD/73000/2010.**

**Apoio Financeiro da FCT e do programa POPH/FSE no âmbito bolsa individual.**

*We are always slow in admitting any great change of which we do not see the intermediate steps*

The Origin of Species, Charles Darwin (1809-1882)

**o júri**

presidente

Doutor Luís António Ferreira Martins Dias Carlos
professor catedrático do Departamento de Física da Universidade de Aveiro

Doutor Mathieu Bollen
professor catedrático do Departamento de Medicina Celular e Molecular da Universidade de Leuven

Doutora Margarida Sâncio da Cruz Fardilha
professora auxiliar do Departamento de Ciências Médicas da Universidade de Aveiro

Doutor Carlos Pedro Fontes de Oliveira
professor afiliado do Departamento de Microscopia do Instituto de Ciências Biomédicas Abel Salazar da Universidade do Porto

Doutora Maria de Lourdes Gomes Pereira
professora associada com agregação do Departamento de Biologia da Universidade de Aveiro

Doutor Antonius Roebroek
professor do Departamento de Genética Humana da Universidade de Leuven

Agradecimentos/
Acknowledgments

I would like to express my deepest gratitude to my promoters, Prof. Mathieu Bollen and Prof. Margarida Fardilha, for giving me the opportunity to enroll for this PhD, and for their endless support, advice and trust. Over the years, I have been deeply inspired by Prof. Mathieu Bollen's scientific excellence and enthusiasm, and I am grateful to Prof. Margarida Fardilha for introducing me to the fascinating world of phosphatases during my Master's course, and for leading me to take my first steps in science. I feel extremely fortunate to have been mentored by them both, from the beginning to the end of this journey. I also would like to thank my co-promotor Prof. Aleyde Van Eynde for her kind support, guidance and advice regarding the execution of experiments, and Prof. Monique Beullens for her suggestions during our 'round table' meetings.

I wish to express my gratitude to the invited Jury members for their willingness to review my PhD thesis.

I also want to thank my current and former colleagues from the Institute for Biomedicine (University of Aveiro) in Portugal and the Laboratory of Biosignaling and Therapeutics (University of Leuven) in Belgium. A special thank you to my colleagues from the 'South Park Lab' with whom I have had countless enjoyable and friendly moments, inside and outside work.

À Fundação para a Ciência e Tecnologia (FCT), pelo apoio financeiro concebido através da bolsa de doutoramento SFRH/BD/73000/2010.

I acknowledge the Laboratory of Biosignaling and Therapeutics, University of Leuven, for the PhD fellowship provided during the last two years of my doctoral studies.

Agradeço profundamente à minha familia, em especial os meus pais, irmã, cunhado e sobrinhos, o apoiado incondicional e afecto partilhado ao longo desta longa jornada.

Non potevo non ringraziare Franco per l'instancabile supporto e la dedizione dimostratomi nel corso degli anni.

Ik wil iedereen bedanken die mij heeft bijgestaan in het uitvoeren van mijn passie voor de wetenschap. Dankzij jullie steun waren de opofferingen die ik maakte het allemaal waard.

**Palavras-chave**

Epigenética, células germinativas, fosforilação de proteinas, proliferação, spermatogónia, testículo.

**Resumo**

NIPP1, inhibidor nuclear da protein phosphatase 1 (PP1), é uma proteina multifuncional que regula a sinalização celular, splicing do pre-mRNA e transcrição mediante o direcionamento da PP1 para substratos nucleares específicos. A deleção global da NIPP1 é letal durante o desenvolvimento embrionário no início da gastrulação, impedindo assim a sua análise funcional em tecidos de adultos. Este facto incitou-nos a gerar um modelo de ratinho *knockout* induzível (iKO) para a NIPP1. Inesperadamente, a remoção da NIPP1 não foi eficiente na maioria dos órgãos analisados, com exceção do testículo. A deleção da NIPP1 causou uma perda progressiva de células germinativas do testículo dependente da idade, culminando num fenótipo denominado *Sertoli cells-only phenotype*. O testículo adulto nos ratinhos iKO apresentaram uma diminuição na proliferação das espermatogónias (in)diferenciadas e aumento dos níveis de apoptose. De modo análogo, o testículo dos neonatos exibiu uma perda quase completa das espermatogónias (in)diferenciadas derivadas de gonócitos, durante o primeiro ciclo de espermatogénese. Adicionalmente, culturas celulares enriquecidas em células progenitoras $GFRA1^{+}$ isoladas do testículo dos ratinhos iKO apresentaram uma diminuição do seu potencial proliferativo. Estes resultados sugerem que a NIPP1 é necessária para a manutenção das espermatogónias indiferenciadas. Demonstrámos também que fenótipo observado está associado à desregulação de genes implicados no controlo da proliferação e viabilidade celular. No que concerne o mecanismo molecular, a deleção da NIPP1 resultou na perda dos componentes centrais do complexo PRC2 (*Polycomb Repressive Complex 2*), o que afetou a expressão genética através da trimetilação da histone H3 no resíduo Lys27 (H3K27me3). A perda dos componentes integrantes do complexo PRC2 foi explanada pela hiperfosforilação e degradação da proteína EZH2, o componente catalítico central do complexo PRC2, resultando na subsequente destabilização de outros componentes deste complexo. Em conformidade, o fenótipo foi reproduzido através da inibição química da proteína EZH1/2 em culturas organotípicas de testículos. De modo geral, este estudo revela a importância da fosfatase PP1-NIPP1 para a regulação da fosforilação e estabilização da proteína EZH2, essencial para a manutenção das células germinativas.

**Keywords** Epigenetics, germ cells, proliferation, protein phosphorylation, spermatogonia, testis.

**Abstract**

NIPP1, for nuclear inhibitor of protein phosphatase 1 (PP1), is a multifunctional scaffold protein that regulates cell signaling, pre-mRNA splicing and transcription by targeting PP1 to specific nuclear substrates. The global deletion of NIPP1 in mice is embryonic lethal at the onset of gastrulation, precluding its functional analysis in adult tissues. This prompted us to generate a tamoxifen-inducible NIPP1 knockout (iKO) mouse model. Unexpectedly, the deletion of NIPP1 was not efficient in the examined organs except for testis. The loss of NIPP1 caused an age-dependent progressive loss of testicular germ cells, culminating in a Sertoli cells-only phenotype. iKO testis showed a decreased proliferation of (un)differentiated spermatogonia and an increased level of apoptosis. Likewise, neonatal iKO testis exhibited an almost complete loss of gonocyte-derived (un)differentiated spermatogonia during the first wave of spermatogenesis. In addition, $GFRA1^+$ progenitor cells isolated from induced iKO testis displayed a reduced proliferation potential. These data suggest that NIPP1 is required for the maintenance of undifferentiated spermatogonia. We also found that the observed phenotype was associated with the deregulation of genes that are implicated in the control of cell proliferation and survival. At the molecular level, the deletion of NIPP1 was associated with the loss of core components of the Polycomb Repressive Complex 2 (PRC2), which affects gene expression through trimethylation of histone H3 at Lys 27. The loss of PRC2 components could be explained by the hyperphosphorylation and degradation of EZH2, the catalytic subunit of the PRC2 complex, resulting in the destabilization of other PRC2 core components. The testis phenotype of the iKOs could be phenocopied by the chemical inhibition of EZH1/2 in organotypic testis cultures. Overall, our study uncovers a key function for PP1-NIPP1 in the regulation of EZH2 phosphorylation and stability, which is essential for the maintenance of germ cells.

# Table of contents

## List of Figures (Chapter 1 and 5)



## List of Figures (Chapter 2)



## List of Figures (Chapter 4)

## List of Tables (Chapter 1)

## List of Supplemental Tables (Chapter 4)

## Abbreviations

| | |
|---|---|
| As | A single |
| Ap | A paired |
| Aal | A aligned |
| ATP | Adenosine triphosphate |
| BTB | Blood-testis barrier |
| BrdU | 5'-bromo-2'deoxyuridine |
| ChIP | Chromatin immunoprecipitation |
| DAPI | 4',6-diamidino-2-phenylindole |
| DNA | Deoxyribonucleic acid |
| Dpc | Days post-coitum |
| Dpp | Days post-partum |
| ESC | Embryonic stem cells |
| FHA | Forkhead associated domain |
| H2A | Histone 2A |
| H2Aul19 | Monoubiquitination of H2A at lysine 119 |
| H3 | Histone 3 |
| H3K27me2/3 | Di-/tri-methylation of lysine 27 on histone 3 |
| H3K9me3 | Tri-methylation of lysine 9 on histone 3 |
| H3K4me3 | Tri-methylation of lysine 4 on histone 3 |
| LC | Leydig cells |
| MEF | Mouse embryonic fibroblast |
| PcG | Polycomb group proteins |
| PCR | Polymerase chain reaction |
| PGC | Primordial germ cells |
| PI | Propidium iodide |
| PIP | Protein phosphatase 1- interacting protein |
| PPP | Phosphoprotein phosphatase |
| PRC | Polycomb repressive complex |
| PRC1 | Polycomb repressive complex 1 |
| PRC2 | Polycomb repressive complex 2 |
| Pro | Proline |

| | |
|---|---|
| PTM | Post-translational modification |
| pTP | Thr-Pro-dipeptide motifs |
| RA | Retinoic acid |
| RNA | Ribonucleic acid |
| SC | Sertoli cells |
| SLiM | Short linear motif |
| Ser | Serine |
| Spc | Spermatocytes |
| Spg | Spermatogonia |
| Spt | Spermatids |
| SSC | Spermatogonial stem cells |
| Thr | Threonine |
| TM | Tamoxifen |
| TP | Proline-Threonine |
| Tyr | Tyrosine |

## Gene acronyms

| | |
|---|---|
| *Ar* | Androgen receptor |
| *Ddx4 (aka Vasa)* | DEAD (Asp-Glu-Ala-Asp) box polypeptide 4 |
| *Dmrt1* | Doublesex and mab-3 related transcription factor 1 |
| *Eed* | Embryonic ectoderm development |
| *Ezh1* | Enhancer of zeste 1 polycomb repressive complex 2 subunit |
| *Ezh2* | Enhancer of zeste 2 polycomb repressive complex 2 subunit |
| *Gfra1* | GDNF family receptor alpha-1 |
| *Hox* | Homeobox |
| *Hprt* | Hypoxanthine phosphoribosyltransferase |
| *Kit (aka c-Kit)* | KIT proto-oncogene receptor tyrosine kinase |
| *Lhx9* | LIM homeobox 9 |
| *Nanos2* | Nanos homolog 2 |
| *Ngn3* | Neurogenin 3 |
| *Plzf (aka Zbtb16)* | Zinc finger and BTB domain containing 16 |
| *Pou5f1 (aka Oct3/4)* | POU domain, class 5, transcription factor 1 |
| *Ppp1* | Protein phosphatase 1 |
| *Ppp1c* | Protein phosphatase 1 catalytic subunit |
| *Ppp1r8* | Protein phosphatase 1 regulatory subunit 8 |
| *Rbbp4* | RB binding protein 4 |
| *Ret* | c-Ret proto-oncogene |
| *Sf3b1* | Splicing factor 3B subunit 1 |
| *Sohlh2* | Spermatogenesis and oogenesis specific basic helix-loop-helix 2 |
| *Sox2* | Sry-box 2 |
| *Sox9* | Sry-box 9 |
| *Stra8* | Stimulated by retinoic acid 8 |
| *Sry* | Sex-determining region Y |
| *Suz12* | SUZ12 polycomb repressive complex 2 subunit |
| *Wt1* | Wilms tumor 1 |

## Protein acronyms

| | |
|---|---|
| AR | Androgen receptor |
| ATM | Ataxia telangiectasia mutated |
| BMP | Bone morphogenic protein |
| BMP4 | Bone morphogenic protein 4 |
| CDC5L | Cell division cycle 5-like protein |
| CDK | Cyclin dependent kinase |
| DMRT | Doublesex and mab-3-related transcription factor |
| DNMT3A | DNA (cytosine-5)-methyltransferase 3A |
| DNMT3B | DNA (cytosine-5)-methyltransferase 3B |
| DNMT3L | DNA (cytosine-5)-methyltransferase 3-like |
| EED | Embryonic ectoderm development |
| EZH1 | Enhancer of zeste homolog 1 |
| EZH2 | Enhancer of zeste homolog 2 |
| FSH | Follicle-stimulating hormone |
| GAPDH | Glyceraldehyde-3-phosphate dehydrogenase |
| GDNF | Glial cell-line derived neurotrophic factor |
| GFRA1 | GDNF family receptor alpha 1 |
| GnRH | Gonadotropin-releasing hormone |
| I2 | Inhibitor 2 |
| I3 | Inhibitor 3 |
| KIT (aka: SCFR or c-KIT) | Mast/stem cell growth factor receptor |
| LH | Luteinizing hormone |
| MAPK | Mitogen-activated protein kinase |
| MELK | Maternal embryonic leucine zipper kinase |
| NIPP1 | Nuclear inhibitor of protein phosphatase 1 |
| PCNA | Proliferating cell nuclear antigen |
| PLZF | Promyelocytic leukemia zinc finger protein |
| PP1 | Protein phosphatase 1 |
| PP2A | Protein phosphatase 2A |
| PRM1 | Protamine 1 |
| PRM2 | Protamine 2 |

| | |
|---|---|
| Rb | Retinoblastoma |
| RbAp48 | Retinoblastoma-associated protein 48 |
| RET (aka: c-RET) | Proto-oncogene tyrosine kinase receptor Ret |
| SAP155 (aka: SF3b155) | Spliceosome-associated protein 155 |
| SCF | Stem cell factor |
| SDS22 | Protein phosphatase 1 regulatory subunit 22 |
| SOHLH1 | Spermatogenesis- and oogenesis-specific basic helix-loop-helix-containing protein 1 |
| SOHLH2 | Spermatogenesis- and oogenesis-specific basic helix-loop-helix-containing protein 2 |
| SOX9 | Transcription factor SOX9 |
| STRA8 | Stimulated by retinoic acid 8 |
| SUZ12 | Suppressor of zeste 12 protein homolog |
| TBP | TATA-box-binding protein |
| TNP1 | Spermatid nuclear transition protein 1 |
| TNP2 | Spermatid nuclear transition protein 2 |
| UBC | Ubiquitin C |

# CHAPTER 1

# General Introduction

# 1.1 Testis structure and function

The testicles are paired organs that perform two essential functions: sex steroid hormone secretion and production of spermatozoa. A testis consists of seminiferous tubules surrounded by a specialized interstitial space containing steroidogenic Leydig cells (LC), the vasculature, immune cells (macrophages and lymphoid cells) and rare fibroblast-like cells. Within the tubules the highly organized seminiferous epithelium consists of a layer of polarized Sertoli cells (SC) that sustain germ cells at all stages of maturation (Figure 1A) [1–3]. Sertoli cells cease to divide by birth in humans and their numbers remain relatively constant through adulthood at about 130 million per testis [4]. Each SC supports approximately 30-50 germ cells [5,6]. The seminiferous epithelium is compartmentalized by tight junctions between Sertoli cells that create the blood-testis barrier (BTB). The BTB segregates the events of meiotic and post-meiotic germ cell development from the systematic circulation, conferring immune privilege to the testis by avoiding immune responses against gametogenic antigens [7].

## 1.1.1 Spermatogenesis: the male gametogenic process

The development of haploid mature spermatozoa from diploid spermatogonial cells after puberty is known as spermatogenesis. This process is one of the most productive cell-proliferating systems in adult mammalian, generating about 100 million spermatozoa each day in man [8]. It takes approximately 75 days in man and 35 days in mice to complete one spermatogenic cycle [9] (Figure 1B). During spermatogenesis, maturation of germ cells is subdivided in three-phases: (1) a replicative/mitotic phase where spermatogonia (see section 1.2.4) undergo a series of mitotic divisions [10], (2) a meiotic phase in which meiosis and genetic recombination occurs resulting in the formation of haploid spermatids from spermatocytes [11] and (3) spermiogenesis, involving the transformation of round germ cells into specialized spermatozoa [9]. Finally, spermatozoa are released into the lumen of the seminiferous tubules, a process called spermiation [8], and ejaculated via the epididymis and vas deferens.

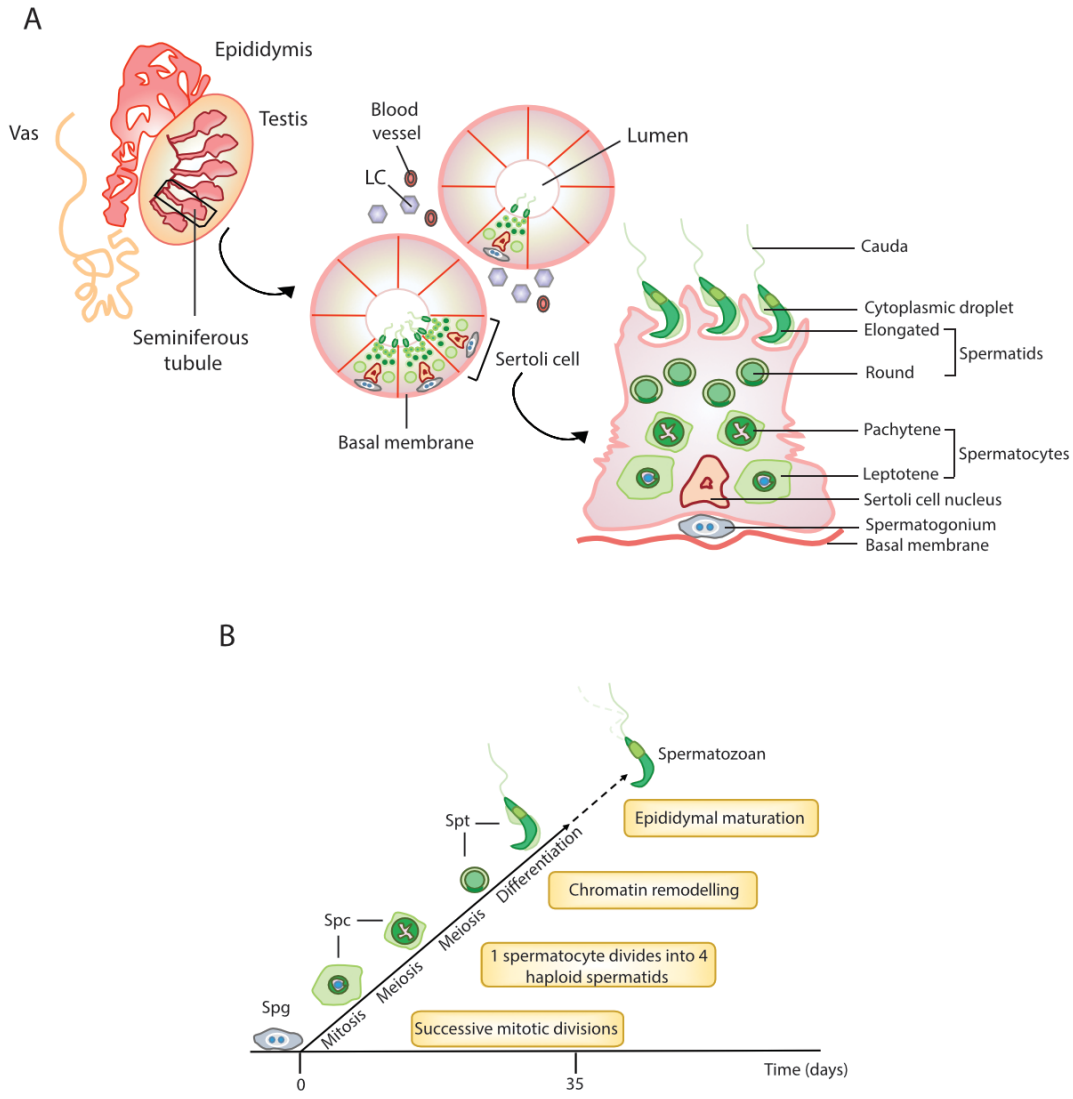


**Figure 1: Organization and regulation of germ cell development in the testis.** (A) Cross-section of the testis showing the localization of the vas deferens, epididymis and the seminiferous tubules. Enlarged representation of the seminiferous tubules surrounded by interstitial cells and magnification of a single Sertoli cell with associated germ cells at different stages of development. (B) Representation of the proliferation, differentiation and maturation of germ cells during one murine spermatogenic cycle. Spg, spermatogonia; Spc, spermatocytes; Spt, spermatids; SC, Sertoli cells; LC, Leydig cells. Adapted from [12]

## 1.2 Regulators of germ-cell fate decision

Primordial germ cells (PGCs) are derived from the epiblast and are maintained throughout life [13,14]. This formation of PGCs requires both cell intrinsic and extrinsic factors, as summarized below.

### 1.2.1 Initiation of fetal germ-cell development

PGCs are formed through the specification of embryonic cells, which is induced by signals from the extraembryonic ectoderm and the visceral endoderm. In mice, this process involves bone morphogenic proteins (BMPs), such as BMP4 and BMP8B, which initiate the formation of PGC precursors at embryonic day 6.25 (E6.25) [15,16] (Figure 2A). Subsequently, these sexually undifferentiated PGCs start migrating towards the genital ridge at embryonic day 10.5 (E10.5), a process that involves the interaction of the receptor KIT (mast/stem cell growth factor receptor) and the CXCR4 (C-X-C chemokine receptor type 4)/G-protein ligand complex, associated with their corresponding ligands, SCF (stem cell factor) and SDF1 (stromal cell-derived factor 1), respectively [17]. PGC migration also requires the pluripotency-associated genes *Pou5f1* (aka: *Oct3/4*; POU domain class 5 transcription factor 1) and *Nanog 3* (nanog homeobox 3) [18,19]. Once PGCs have reached the genital ridge they become surrounded by differentiating SC, forming the testicular cords at E12.5. As soon as testicular cords have been formed, PGCs are called gonocytes [20–22] (Figure 2B). Thereafter, masculinization signals from somatic cells in the gonad direct gonocytes towards a path of male development [23–25].

### 1.2.2 Gonadal sex determination

The gonad is an organ primordia with bipotential capacity: a testis or ovary can develop from a single primordium. The expression of several genes is required between 10.5 dpc and 11.5 dpc for the outgrowth of the early bipotential gonad, including *Nr5a1* (aka *Sf1*, steroidogenic factor 1) [26], *Wt1* (Wilms tumor 1) [27], *Lhx9* (Lim homeobox 9) [28], *Emx2* (empty spiracles homeobox 2) [29] and *Igfr1* (insulin-like growth factor 1 receptor)/*Ir* (insulin receptor)/*Irr* (insulin receptor-related receptor) receptor family [30] (Figure 2B).

In mammals, sex determination is genetically controlled by the presence or absence of the Y chromosome. The initiation of the male pathway at E10.5 depends on gonadal expression of *Sry* (sex-determining region Y), a gene located in the male specific region of the Y chromosome [31–38]. The expression of *Sry* in the genital ridges is regulated by transcription (co)factors (WT1, GATA4 and FOG2) and typically results in their development into testis, whereas absence or dysfunction of *Sry* leads to development of ovaries [39,40]. Accordingly, XY mice with no functional *Sry* develop ovaries and the addition of *Sry* to XX mice triggers the testis pathway [32,34,38]. In humans, patients who show partial to complete sex reversal carry mutations in *SRY* gene [41].

*Sry* encodes a transcriptional factor that binds to and activates the testis-specific gene *Sox9* (*Sry*-box 9) [42–44], *Fgf9* (fibroblast growth factor 9) [45], *Dax1* (nuclear receptor subfamily 0 group B member 1) [46] and *Nr5a1* [43], thereby directing the supporting cells of the genital ridges towards the fate of SC. These cells start to differentiate at E12.0-E12.5 [36] and aggregate around germ cells that separate the gonads into two compartments: the tubular testis cord composed of SC and germ cells, and the interstitial space between the cords which include LC and fibroblasts [47]. The maintenance of the SC phenotype is driven by *Dmrt1* (double sex and mab-3 related transcription factor 1), a transcription factor that is responsible for sex determination in metazoa. Strikingly, the expression of *Dmrt1* in a XX mouse fetal gonad is sufficient to drive testicular differentiation and male secondary sex development [48–50].

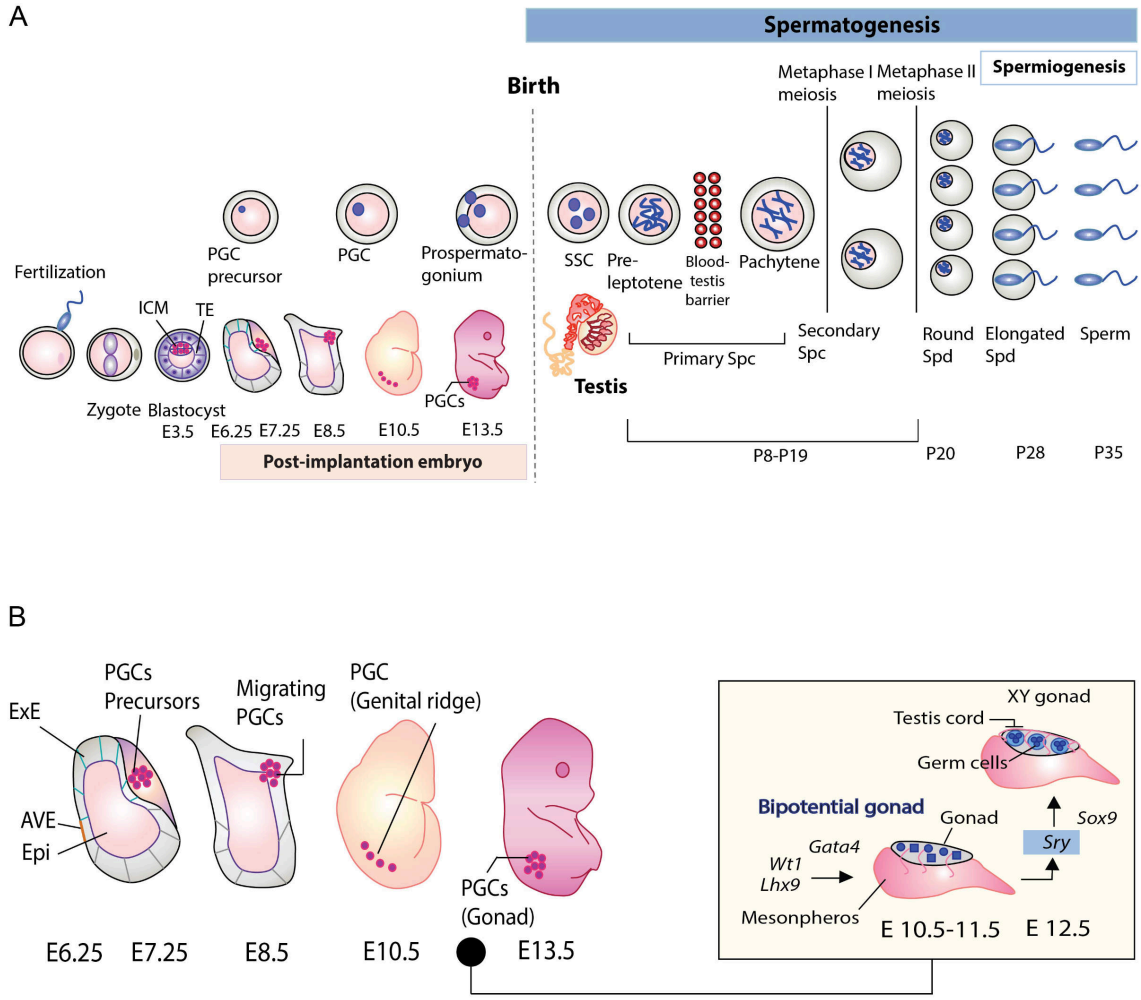


**Figure 2: Schematic representation of germ-cell development during murine embryogenesis and early post-natal life.** (A) Male germ cells start developing shortly after fertilization, when a

population of pluripotent cells form precursors of primordial germ cells (PGCs) in the epiblast at embryonic day E3.5-6.25. Mature PGCs are formed by embryonic day E7.5. They form a cluster of cells in the fetal gonads that proliferate rapidly and migrate to the genital ridge, where sex determination takes place at E12.5. At embryonic day 13.5, PGCs are called gonocytes and are mitotically arrested. Shortly after birth, the first wave of spermatogenesis starts in the neonatal testis and lasts 35 days in mice. Pro-spermatogonia develop into spermatogonial stem cells (SSCs), which proliferate by consecutive mitotic divisions to maintain the SSC population (self-renewal) or differentiate into spermatocytes during the first postnatal week. Spermatocytes enter meiosis and cross the blood barrier established by Sertoli cells to form post-meiotic cells (round spermatids) around day P20-P22. These cells differentiate into elongating spermatids and finally mature into functionally inactive sperm cells. Male mice become fertile five to six weeks after birth. In rodents, the first wave of spermatogenesis is synchronous, but in adulthood, the germ cells of the seminiferous epithelium exist at defined cellular stages. (B) Formation of the XY gonad and gonocytes at E6.25-E13.5. P, postnatal; E, embryonic day; PGCs, primordial germ cells; SSC, spermatogonia stem cell; ICM, inner cell mass; TE, trophectoderm; ExE, extra embryonic ectoderm; AVE, anterior visceral endoderm; Epi, epiblast. Adapted from [2,51–53].

### 1.2.3 Signals regulating the switch from gonad to spermatogonia

Shortly after reaching the genital ridges and their maturation into male germ cells, the PGCs (gonocytes) in mice continue to proliferate until they enter quiescence at E15-16 [21,54–56] (Figure 2). Some authors propose that gonocytes give rise to a special type of stem cells, termed pro-spermatogonia, that subsequently generate the adult-type spermatogonia stem cells (SSC) [57–59]. In any case, this period is marked by changes in expression of cell-cycle proteins and numerous signaling pathways are involved in the inhibition of gonocyte proliferation, including the transforming growth factor beta (TGFb) pathway [56,60,61].

After birth, gonocytes start moving from the center of the seminiferous tubules towards the basement membrane, a process that involves the KIT/SCF signaling pathway [62]. Concomitantly, proliferation resumes and male SSC are formed [54,57,63] (Figure 2). In male mice, transformation of gonocytes into SSCs occurs between 0 and 6 days post-partum (dpp) and the first appearance of active SSC occurs between 3-4 dpp [21,57,58,64]. Signaling from somatic cells markedly influences the molecular mechanism governing the transition from gonocytes to SSC. SIN3A (swi-independent 3a), a component of a large transcriptional remodeling complex in SCs, is specifically required to retain SSC pluripotency, since its deletion from perinatal male gonocytes results in the downregulation

of the SSC genes *Oct3/4*, *Gfra1* (GDNF family receptor alpha-1), *c-Ret* (proto-oncogene tyrosine kinase receptor RET) and *Plzf* (zinc finger and BTB domain containing 16) [65–67] (see section 1.2.4).

### 1.2.4 Postnatal germ-cell development

The early postnatal gonad contains a heterogeneous group of germ cells with respect to morphology, gene-expression pattern and function. As described above, SSCs are derived from a population of perinatal germ cells that migrate during prepubertal development from their perinatal luminal position in the seminiferous tubule to the basal lamina. Here, they remain in a functional niche that is established to maintain self-renewal of SSCs during spermatogenesis. I will elaborate here on the hormonal control of spermatogenesis (1.2.4.1) and the regulation of spermatogonial-cells identity (1.2.4.2), including extrinsic and intrinsic factors that influence self-renewal and differentiation of spermatogonia in mice. Epigenetic regulation and the importance of reversible protein phosphorylation in germ-cells development will be discussed in sections 1.2.5 and 1.2.6, respectively.

#### 1.2.4.1 Hormonal and germ-cell-soma regulation

Testicular function is influenced by endocrine (extra-testicular) and paracrine (intra-testicular) factors. The endocrine pathway involves a hypothalamic-pituitary-testicular axis that functionally interconnects the brain and testis [12,68–70] (Figure 3), while the paracrine pathway comprises interactions between germ cells and somatic testis cells that are essential for normal spermatogenesis.

The endocrine pathway is tightly regulated by a complex network of hormones, involving the gonadotropin-releasing hormone (GnRH) produced by the hypothalamus, which stimulates the production of the follicle-stimulating hormone (FSH) and luteinizing hormone (LH) by the pituitary gland. FSH regulates SC replication before puberty and functions in the seminiferous epithelium throughout adulthood. LH regulates the steroidogenic activity of LCs, leading to the secretion of testosterone and estradiol-17β in the interstitial space [71–74]. FSH and LH signal through specific receptors (FSHR and LHR) that are expressed by SCs and LCs, respectively. LHR knockout mice are phenotypically characterized by spermatogenic arrest [75], while the deletion of FSHR results in a reduced testis size and lower testosterone levels [76]. The production of testosterone and estradiol-17β by LCs, and the secretion of inhibin by SCs [69,70] provide a negative feedback loop that reduces the secretion of LH and FSH. This maintains a fine

hormonal homeostasis within the hypothalamic-pituitary-testicular axis [69,70,74,77]. In addition, the inhibin-antagonist activin hormone, produced by a wide variety of tissues besides gonads, has a positive endocrine effect on FSH stimulation and a paracrine effect on germ-cell maturation [78].

The paracrine regulation is provided by steroids (e.g. testosterone) and growth factors (see next section) produced by testicular somatic cells. The function of testosterone in the maintenance of spermatogenesis, development of reproductive organs and secondary sex characteristics is well understood [79]. LC-secreted testosterone binds to androgen receptors (AR) expressed by SCs, LCs and peritubular myoid cells, to regulate androgen responsive genes [69]. Genetic ablation of AR in mice results in infertility due to loss of spermatids [80]. In human males, hypogonadism is a clinical syndrome that results from the failure to produce normal levels of testosterone (primary hypogonadism) or dysfunction of the hypothalamic-pituitary-testicular axis (secondary hypogonadism) [81].

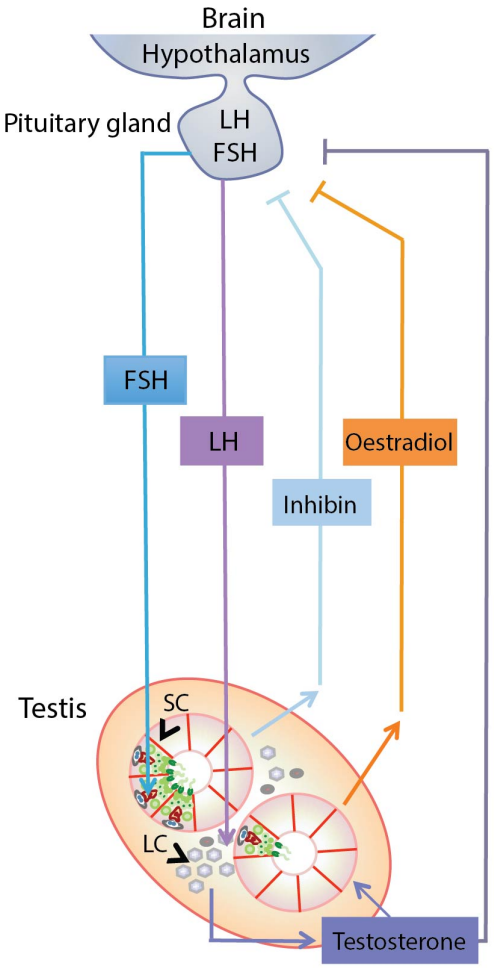


**Figure 3: Hormonal control of spermatogenesis.** The figure shows the main endocrine factors secreted by the pituitary gland (LH, luteinizing hormone; FSH, follicle-stimulating hormone) and

local regulators of testis function (androgens and estrogens). SC, Sertoli cell; LC, Leydig cell. Adapted from [12].

### 1.2.4.2 Regulation of spermatogonial-cell identity and fate

Spermatogenesis in mammals is a continuous process throughout adulthood that depends on a lasting supply of self-dividing and differentiating SSCs. The latter cells are rare, representing only 0.03% of the total testicular germ cells [82]. In adult male mice, SSCs represent a small set of spermatogonia that are referred to as undifferentiated spermatogonia. They divide with incomplete cytokinesis to form clusters of interconnected spermatogonia. The most primitive SSC type, spermatogonia A single (As), divides to form two new As cells, or divides to form paired spermatogonia (Apr) cells connected by an intercellular bridge. Apr spermatogonia further divide to form a chain of aligned cells (Aal 1-4), which can divide to form large syncytial chains of 8 (Al-8), 16 (al-16) and even 32 (Al 32) cells [64,83,84] (Figure 4A-C). All these cell types have been shown to have stem cell potential, since they can form colonies that repopulate a recipient testis after transplantation [85–88]. In primates, there are three morphologically distinct spermatogonia: dark type A (Ad), pale type A (Apr) and type B [89].

In addition to self-renewing, mouse undifferentiated spermatogonia generate differentiated spermatogonia (A1-A4), intermediate (In) and spermatogonia B, which then differentiate into meiotic spermatocytes. SSCs are therefore capable of undergoing self-renewal and differentiation, but whether their division is symmetric or asymmetric in mammals is still a topic of debate. As most stem cells, SSCs can presumably divide by either asymmetric or symmetric modes of division and the balance between those modes is controlled by developmental and environmental signals [90]. When dividing symmetrically, each stem cell generates either self-renewing or differentiating daughter cells [90,91] (Figure 4A). During asymmetric division, each stem cell divides to generate one daughter cell with a stem cell fate (self-renewal) and one daughter cell committed to differentiate (Figure 4B). The balance between self-renewal and differentiating SSC is regulated by both micro-environmental stimuli (niche) and gene expression (see next sections).

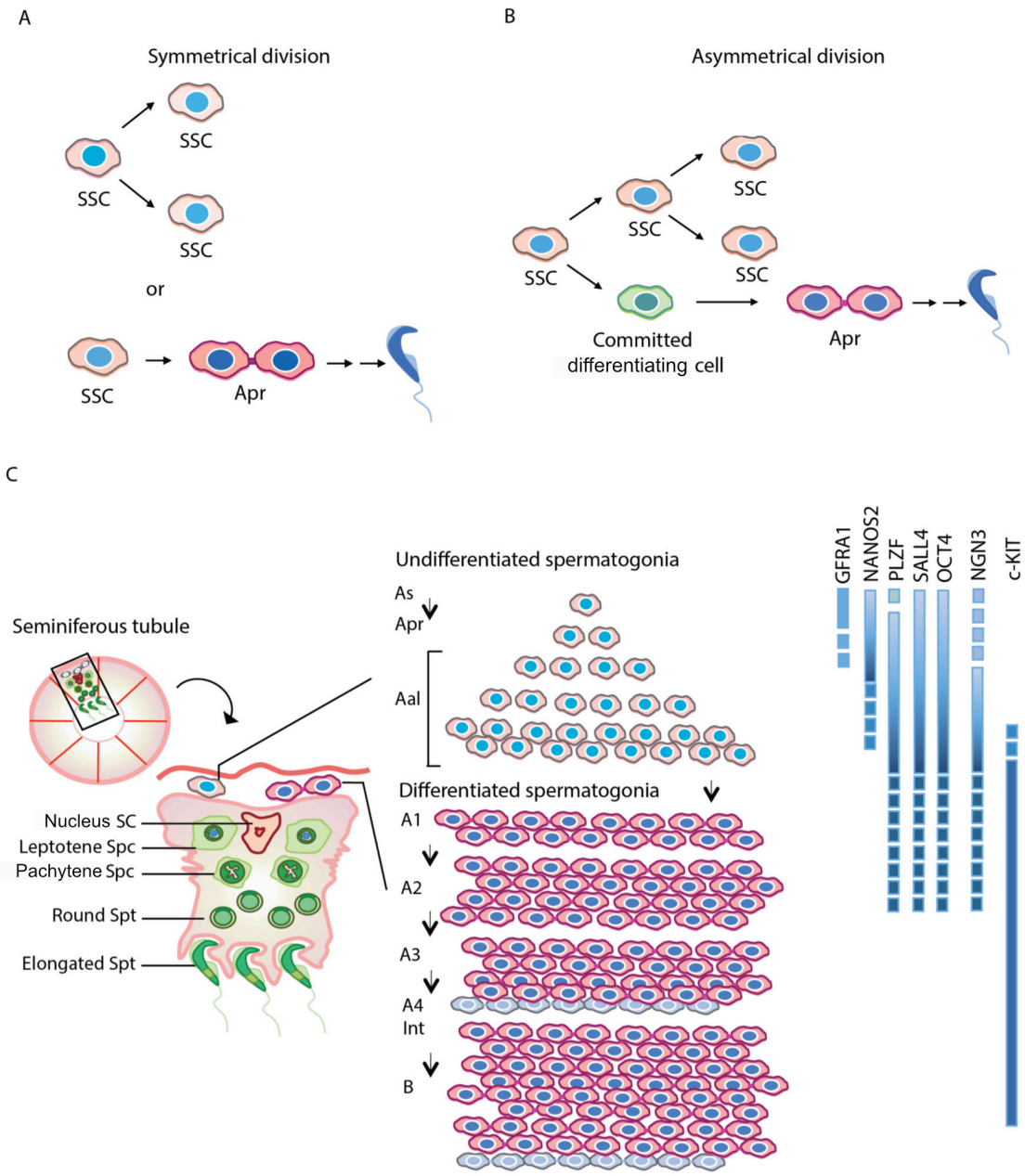


**Figure 4: Germline stem-cell lineage**. (A-B) Possible cell division modes that maintain the balance between stem cells and differentiating progeny of spermatogonial stem cells (SSCs). (A) Symmetrical division: each SSC generates either two SSC daughter cells or two differentiating cells (Apr spermatogonia). (B) Asymmetrical division: each SSC can divide to generate one daughter stem cell and one daughter cell destined to differentiate (Apr spermatogonia). (C) Schematic representation of the spermatogonial development. (Left) Cross-section of a mouse seminiferous tubule and associated Sertoli cells showing the localization of SSCs and differentiated spermatogonia near the basal membrane. (Middle) Self-renewal and differentiation of different spermatogonia pools. (Right) Main genes expressed by undifferentiated and differentiated

spermatogonia. As, A single; Aal, A aligned; Apr, A paired; SC, Sertoli cell; Spc, spermatocyte; Spt, spermatid; I, intermediate [91–93].

#### 1.2.4.2.1 Extrinsic regulation of spermatogonia proliferation

Factors within specialized microenvironments, referred to as niches, provide support to SSCs through architectural support and growth-factor stimulation [94,95]. In mammalian testis, SCs are the major contributor to the SSCs niche, but contributions from other testicular somatic cells are likely to occur, as LCs and myoid cells produce the cytokine colony-stimulating factor 1 (CSF-1), which influences SSC self-renewal [96].

Sertoli cells express GDNF (glial cell-line derived neurotrophic factor), a supporting factor of SSC self-renewal [1,97–102]. The GDNF receptor in SSCs consists of RET and GFRA1 (encoded by the *Gfra1* gene) [103], and target disruption of this receptor impairs spermatogenesis [104]. GDNF activation upregulates expression of the transcriptional factors *Bcl6* (B-cell leukemia/lymphoma 6*)* and *Lhx1* (LIM homeobox 1), which influence SSC self-renewal [97,105]. Other growth factors, including IGF-1 (insulin-like growth factor 1 precursor) and FGF2 (fibroblast growth factor 2) have been implicated in the survival or expansion of SSCs in culture [100,101].

#### 1.2.4.2.2 Intrinsic regulation of spermatogonia proliferation

SSCs are unipotent stem cells that, similarly to embryonic stem cells (ESCs), grow on feeder cells in islands or clumps, and express the *Oct3/4* gene. However, unlike ESCs, transplanted SSCs do not rapidly generate teratocarcinomas [1,85,101]. In fact, pluripotency was for many years believed to be limited to the embryogenic stage [106–108]. In addition, *Nanog* regulation by *Oct3/4* and *Sry*-box containing gene 2 (*Sox2*), a key determinant of ESC self-renewal and pluripotency [109], is not explicitly required for SSC maintenance [1,110,111], indicating that SSCs and ESCs have distinct signaling mechanisms of self-renewal [1].

Several SSC-expressed genes are essential for the autonomous maintenance of stem-cell identity (Table 1). Most of the genes expressed in undifferentiated spermatogonia are also expressed in gonocytes [91,94], with exception of the transcription factor *Ngn3* (neurogenin 3) [112]. A small subset of $Ngn3^{-}$ gonocytes can bypass the SSC phase to directly differentiate into $Ngn3^{-}$ spermatogonia during the first wave of spermatogenesis. This contrasts with the pool of $Ngn3^{+}$ spermatogonia that originate from SSCs during

subsequent waves of spermatogenesis [112,113]. As a result, a heterogeneous pool of gonocyte-derived spermatogonia can be found in the neonatal testis.

**Table 1: Genes involved in spermatogonial stem-cell maintenance**

| Gene | Knockout phenotype | Proposed function in germ cells |
|---|---|---|
| *Dazl* | Failure of spermatogonia Aal-A1 transition [114] | Encodes a RNA binding protein essential for differentiation of spermatogonia Aal [114] |
| *Gfra1* | SSC depletion [104] | Component of GDNF receptor required for spermatogonial self-renewal [104] |
| *Nanos2* | Gradual loss of spermatogonia by apoptosis [110] | Maintenance of stem-cell population and germ-cell differentiation [110,115] |
| *Ngn3* | Failure of embryonic-cell specification and differentiation [112] | SSC fate specification during early stages of spermatogenesis [112] |
| *Oct3/4* | Loss of pluripotency in embryonic stem cells [116] | Regulation of spermatogonia pluripotency [117], fate commitment [118] and germ-line development [119,120] |
| *Plzf (aka Zbtb16)* | SSC depletion and increased apoptosis [121] | Transcription factor required for spermatogonia self-renewal [121,122] |
| *Ret* | SSC depletion [104] | Component of GDNF receptor required for spermatogonial self-renewal [104] |
| *Sall4* | Embryonic germ cells loss. Postnatal deletion causes tubular degeneration in adulthood [123]. | Maintenance of SSC pool homeostasis [123] |
| *Taf4b* | Spermatogonia depletion in adulthood [124] | SSC specification and proliferation [124] |

*Dazl,* deleted in azoospermia like*;* GDNF*,* glial cell-derived neurotrophic factor; *Gfra1,* GDNF family receptor alpha 1*;* *Nanos2*, nanos homolog 2; *Ngn3*, neurogenin 3; *Oct3/4*, POU class 5 homeobox 1; *Plzf*, zinc finger and BTB domain containing 16*;* *Ret, c*-Ret proto-oncogene*;* *Sall4,* spalt-like transcription factor 4*;* *Taf4b,* transcription initiation factor TFIID subunit 4B. SSC, spermatogonial stem cells; al, A aligned.

### 1.2.4.2.3 Differentiation of spermatogonia

Compared to the regulation of SSC maintenance, the transition from undifferentiated to differentiated spermatogonia is regulated by fewer genes [125]. Retinoic acid (RA), the active metabolite of vitamin A, is required for the differentiation of spermatogonia and the onset of meiosis. Whereas the expression of RA during male fetal development is prevented by the expression of the RA-degrading enzyme CYP26B1 (cytochrome P450 family 26 subfamily B member 1) by SCs (Figure 5), RA-stimulated retinoic acid 8 (*Stra8*) expression induces spermatogonia differentiation and meiotic entry during puberty [126–128]. Other RA-induced genes are regulated during spermatogonia differentiation, such as *Kit* and the spermatogenesis- and oogenesis-specific basic helix-loop-helix genes 1 and 2 (*Sohlh1 and Sohlh2).* Additionally, RA downregulates *Plzf* during SSCs differentiation [129]. *Plzf* acts as a transcriptional repressor of *Kit*, a key regulator of spermatogonial

differentiation [130]. Likewise, reduction of *Nanos2* expression by RA is concomitant with induced *Kit* and *Stra8* expression [131]. RA also regulates the expression of BMP4 in mouse testis [132], which decreases the maintenance of adult SSCs. RA-regulated BMP4 induces differentiation by promoting *Sohlh2* and *Kit* expression [129,133,134]. *Ngn3* was also proposed to drive differentiation of mouse SSCs as a downstream effector of the signal transducer and activator of transcription 3 (STAT3)-regulated differentiation [135,136]. Additional genes, including the spermatogonial doublesex-related transcription factors (DMRTs), regulate the transition between mitotic and meiotic developmental programs during spermatogenesis (Figure 5) [49,129,137–139]. In conclusion, multiple signaling pathways modulate SSC self-renewal and commitment to differentiate.

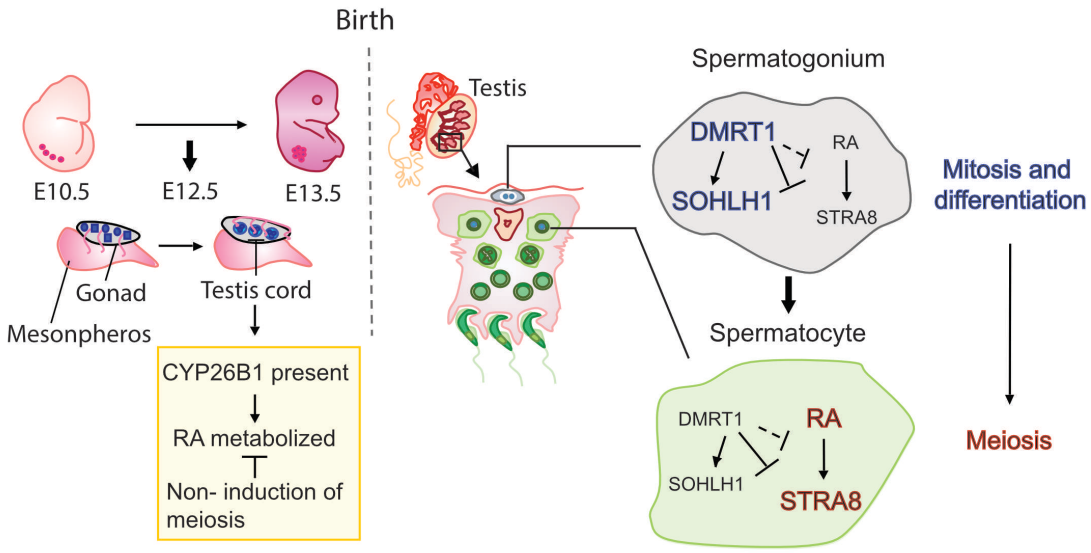


**Figure 5: Schematic representation of the spermatogonial differentiation program.** Retinoic acid (RA) in mice is required for the postnatal differentiation of spermatogonia, which is kept inactive due to the catabolic effect of CYP26B1 during testis embryonic development. CYP26B1 is a cytochrome P450 enzyme that oxidizes RA to its hydroxylated forms [140]. RA responsive genes (e.g. *Stra8)* and other genes *(*e.g. *Dmrt1)* dictate the spermatogonial differentiation fate and regulate the switch from mitosis (spermatogonia) to meiosis (spermatocytes) programs. DMRT1 acts in spermatogonia to restrict RA responsiveness, directly repress *Stra8* transcription, and activate transcription of the spermatogonial differentiation factor *Sohlh1*, thereby preventing meiosis and promoting spermatogonial development. RA, retinoic acid; E, embryonic day. Adapted from [49,128,141,142].

#### 1.2.4.2.4 Potential pluripotency of germ stem cells

Embryonic germ cells and SSCs from neonatal mouse testis have a similar pluripotency and differentiation potential [106,143,144]. Indeed, embryonic-like stem cells (ES-like cells) have been derived from mouse SSCs [100,145–148] that can differentiate into cells of three embryonic germ layers [147]. However, these ES-like multipotent cells can not contribute to spermatogenesis in the seminiferous tubules after transplantation, hinting at a loss of their SSC potential [143], possibly caused by an altered DNA methylation pattern. Remarkably, the plasticity of these SSC unipotent cells is not limited to pluripotency reversal. In fact, direct conversion of SSC cells into somatic cells has been reported [149–151]. SSC-derived ES-like cells can potentially be used for purposes of regenerative medicine [143,144,152,153]. However, a key question is whether results obtained in mice also apply to humans, in particular since spermatogonial self-renewal in primates is still poorly understood [64,154].

### 1.2.5 Epigenetic control of germ-cell development

The process of germ-cell development is regulated by both genetic and epigenetic mechanisms. Epigenetics is defined by chromatin modifications, including DNA methylation, histone modifications (Figure 6), remodeling of the nucleosomes and chromatin reorganization, thereby regulating gene expression without changes in DNA sequence. In germ cells, the epigenetic program contributes to the gene-expression program required for germ-cell development and genomic integrity.

Polycomb group (PcG) proteins are a family of epigenetic regulators of transcription that have roles in stem-cell identity, differentiation and disease. PcG proteins were first described in *Drosophila melanogaster* as silencers of homeobox (*Hox*) genes expression [155–157]. PcG proteins can alter the chromatin environment by their catalytic activity, imposing post-translational modifications (PTMs) such as phosphorylation, ubiquitination, acetylation and methylation. In addition, PcG proteins can also induce chromatin condensation by mechanisms that do not require catalytic activity [158–160], thereby restricting the action of the ATP-dependent chromatin remodeling complexes [158,159].

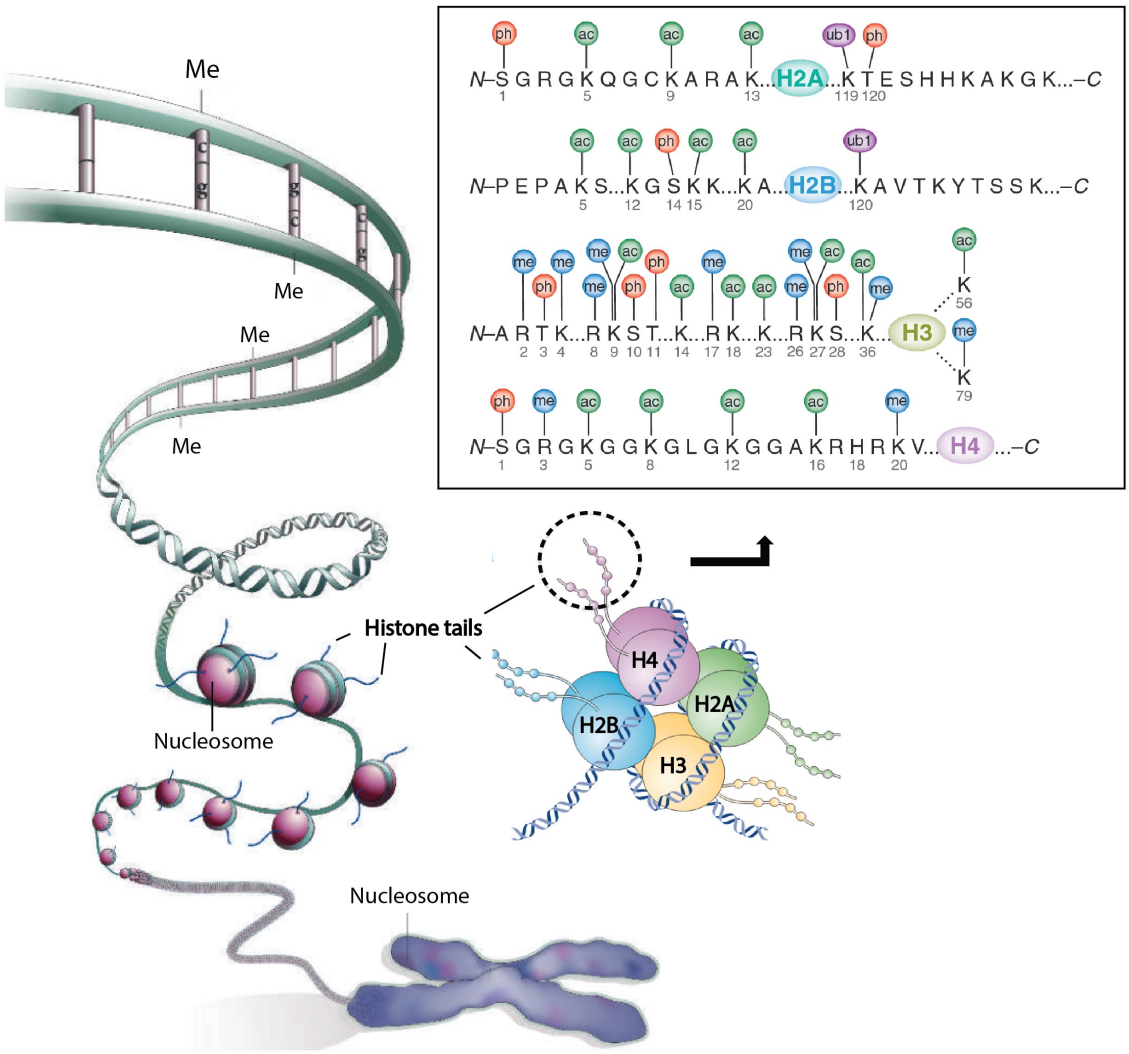


**Figure 6: DNA methylation and the histone code.** DNA is epigenetically modified by methylation on CpG (cytosine-phosphate-guanine) dinucleotides, promoting epigenetic silencing. Moreover, the N-terminus of histone tails protrude from the nucleosome and can be post-translationally modified, determining the chromatin structure. The histone modifications thus act in a combinatorial manner, referred as the histone code. H, histone; Me, methylation; ph, phosphorylation; ac, acetylation; ub: ubiquitination. Adapted from [161–163].

Distinct subsets of PcG proteins associate to form multiprotein complexes called Polycomb repressive complexes (PRCs), which modify histones and mainly silence target genes. PRCs belong to two major families: the polycomb repressive complexes 1 and 2 (PRC1 and PRC2) (Figure 7). PRC1 complexes have E3 ligase activity and their main substrate is histone H2A that is mono-ubiquitinated at lysine 119 (H2Au119) [164–167]. PRC2 complexes contain methyltransferase activity and are mainly involved in the di-trimethylation of histone H3 at lysine 27 (H3K27me2/3) [168]. PRC1 core components

include the E3 ubiquitin protein ligase RING1, BMI1 (aka PCGF4, polycomb group of RING finger 4) and the chromodomain-containing protein Pc (CBX homologue, *Homo sapiens*). The core components of the PRC2 complex are SUZ12 (suppressor of zeste 12 protein homolog), EED (embryonic ectoderm development), RbAp48 (retinoblastoma-associated protein 48) and EZH1/2 (enhancer of zeste homolog 1/2), which contains a SET domain that is responsible for the methyltransferase activity of the complex [156,164,169–176]. EZH1 and EZH2 proteins are mutually exclusive in the complex, but their expression is complementary: EZH2 is highly expressed in embryonic tissues and proliferating cells, whereas EZH1 is mostly present in adult tissues and differentiating cells [174,177–179]. Also, EZH1 has only a minor methyltransferase activity as compared to that of PRC2 [173,177]. PRC2 is important both for the maintenance of embryonic stem (ES) cell pluripotency [180,181] and as a regulator of cell differentiation [182–184] .

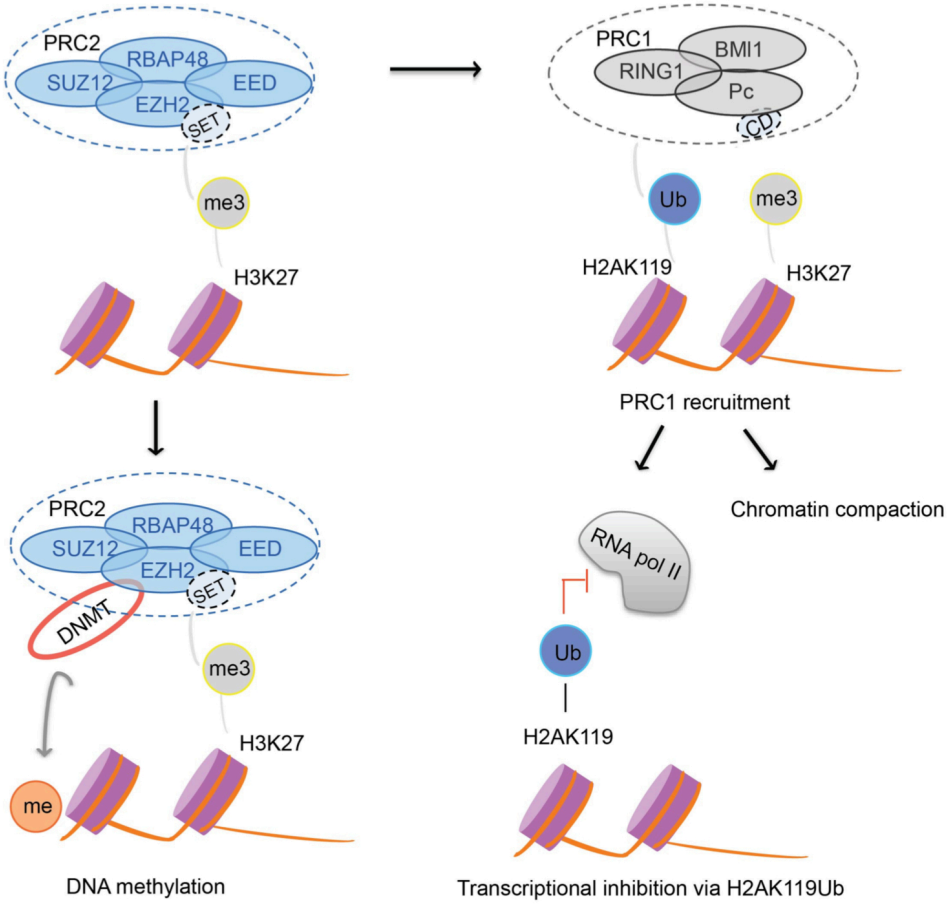


**Figure 7: Epigenetic gene silencing by PcG proteins.** Gene silencing is mediated by tri-methylation of H3 (H3K27me3) by the SET domain of the methyltransferase EZH2, one of the core components of the polycomb repressive complex 2 (PRC2). DNMTs can be recruited to PRC2

target genes via direct interaction with EZH2 to promote DNA methylation. Trimethylated H3K27 (H3K27me3) is recognized by the polycomb repressive complex 1 (PRC1). RING1, a component of the PRC1 complex, catalyzes the monoubiquitination of H2AK119, a histone mark associated with the inhibition of RNA polymerase II binding and progression. In addition, the PRC1 complex induces chromatin compaction independent of RING1. SET, (Su-[var]3-9; E(z); Thrithorax) domain family of proteins; CD, Chromodomain; me, methylation; Ub, ubiquitination. Adapted from [185,186].

Germ cells have specific fates and go through a series of epigenetic events that are unique to this cell type [187]. DNA methylation is particularly important for early testis development due to its role in germline programming, which involves erasure and re-establishment of DNA methylation patterns in germ cells [187,188]. There are two critical stages that require extensive epigenetic regulation during germ-cell development: the genome-wide epigenome reprograming event during PGCs development before birth and the epigenomic fine-tuning that occurs in SSCs postnatally [187,189] (Figure 8).

When germ cell-fate is established at E7.25, the level of DNA methylation is similar to those in the surrounding somatic cells, but decreases as PGCs proliferate and migrate by undergoing a genome-wide DNA demethylation (Figure 8). Methylation in PGCs decreases from ≈70% at E6.5 to ≈30% at E9.5, and is further reduced to ≈10% in male PGCs after gonad formation at E13.5 [190–193]. Subsequently, global DNA methylation by the DNMT3 methyltransferases (DNA (cytosine-5)-methyltransferases 3A/3B/3L) [194,195] rises by some 40% from PGCs at E13.5 to gonocytes at E16.5 to re-establish the epigenome at perinatal germ cells [172,191,196]. Additional histone modifications occur during prenatal development, including repressive H3K27me3, H3K9me3 and H2AK119 monoubiquitination marks, and activating H3K4me3 marks [197–199]. The erasure and establishment of parental imprints[1] occur in PGCs when they arrive in the genital ridges at E11.5 [187], as reflected by demethylation of the imprinted loci [200]. New imprints involving DNMT3 [196,201–204] are established after sex determination has been initiated in G1-arrested gonocytes between E14.5 and birth [192,196,201,205], and are maintained throughout male germ-cell development [206].

[1]Genomic imprinting refers to the selective inactivation of paternal or maternal genes/chromosomes by epigenetic modifications.

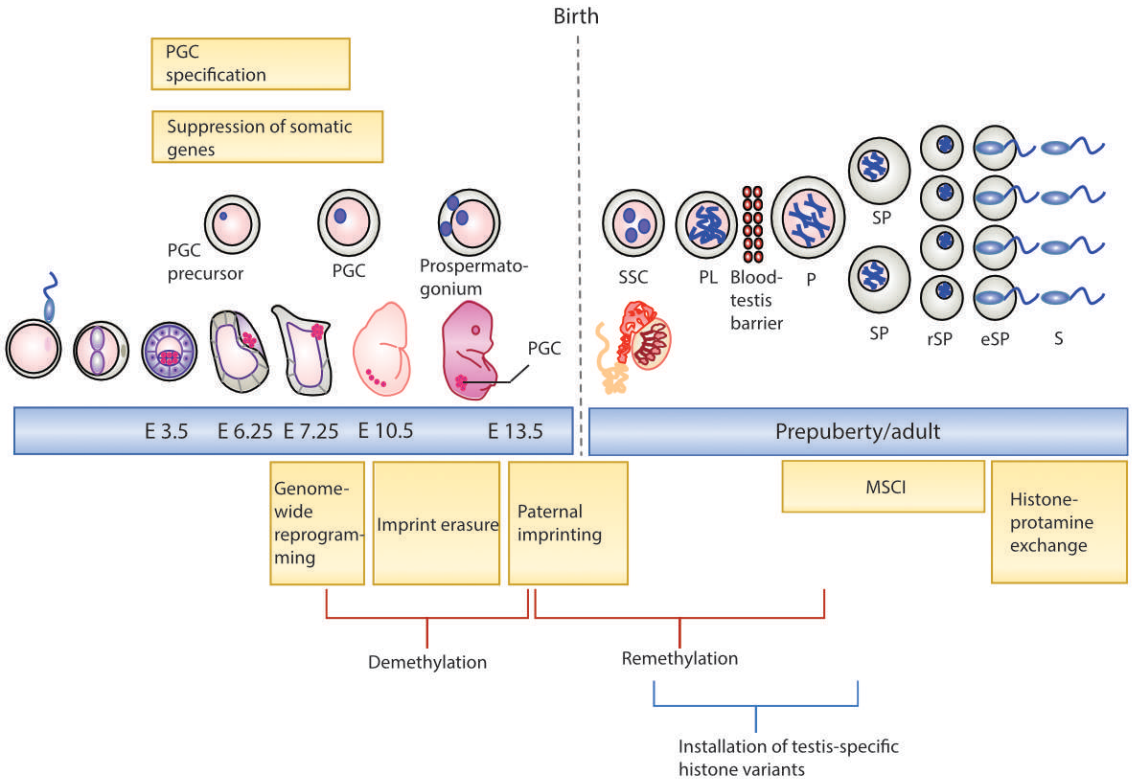


**Figure 8: Chronology of mouse epigenetic regulation of germ-cell development.** After fertilization, the imprinting marks are erased by the epigenetic machinery of the zygote and new paternal imprints are established in a unique pattern dependent on the sexual fate. During neonatal and postnatal testis development, dynamic epigenetic events involve erasure and re-establishment of DNA methylation patterns to guarantee the correct germ-line programming. Adapted from [51,206]. MSCI, meiotic sex-chromosome inactivation.

Postnatally, differential gene expression patterns among undifferentiated spermatogonia subpopulations suggest a modification in the epigenetic programming related to cell-fate determination [207–209] (Figure 8). This is also suggested by differences in DNA methylation [210,211] between self-renewing spermatogonia and those committed to differentiate. In addition, the latter cells exhibit chromatin bivalency (the co-occurrence of H3K4me3 and H3K27me3) at promoters of developmental genes [210–212]. Indeed, conditional mutagenesis of the PRC2 subunits EED and SUZ12 during perinatal germ cell development results in a paucity of mutant SSCs in testis, suggesting a role for PRC2 in the maintenance of these cells [213].

Male germ cells also express a high number of testis-variant histones (e.g. TH2B, TH3, H3.3 and HT1), which are incorporated in the nucleosomes of spermatogonia and spermatocytes [214–217] and probably contribute to meiosis and the subsequent

maturation of gametes [214]. There also exists a mechanism of meiotic sex-chromosome inactivation (MSCI) involving a H2A variant (H2Ax), which includes the condensation of chromatin in a macrochromatin body (XY body) to form transcriptionally silenced chromosomes [218,219] (Figure 8). After meiosis, haploid round spermatids undergo morphological and epigenomic changes to allow fertilization [220,221], where the testis-specific histone variant H1T2 has a function in chromatin condensation [222]. A later process involves the histone-protamine exchange to facilitate DNA compaction, where histones are first almost completely replaced by spermatid nuclear transition proteins 1 and 2 (TPN1 and TPN2), and are subsequently replaced by highly basic protamines 1 and 2 (PRM1 and PRM2) [214,223–227] (Figure 2 and 8). The retained spermatid histones represent a mechanism to transfer epigenetic information to the offspring [206].

### 1.2.6 Regulation of germ-cell function by protein phosphorylation

Reversible protein phosphorylation is an important process for the control of virtually all biological processes, including spermatogenesis (Figure 9). Although in the last decades a series of protein kinases and phosphatases have been shown to be crucial during spermatogenesis, only a few of these enzymes have been functionally characterized in spermatogonia (Table 2). Most phosphorylations occur on serine or threonine residues and, to a lesser extent, on tyrosine residues [228].

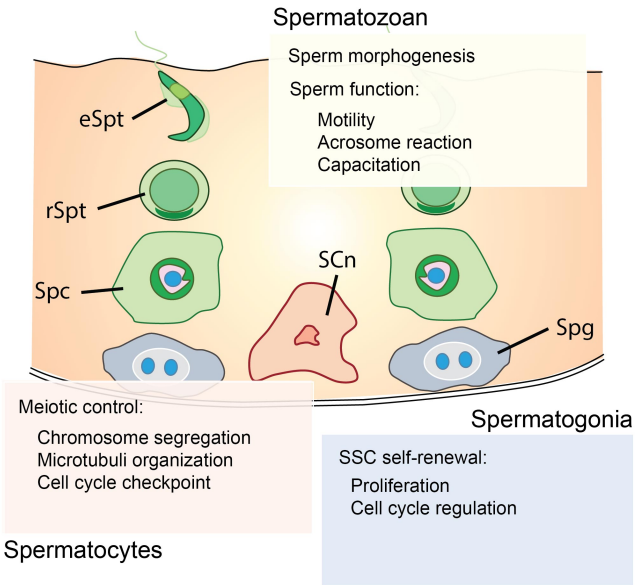

**Figure 9: Schematic representation of the cellular processes controlled by reversible protein phosphorylation during spermatogenesis.** SCn, Sertoli cell nucleus; Spg, spermatogonia; Spc, spermatocytes; rSpt, round spermatids; eSpt, elongated spermatids.

Many serine/threonine protein kinases play pivotal roles in mitosis, meiosis and the post-meiotic differentiation of germ cells. For instance, Aurora like kinase 3 (ALK3) is involved in chromosome segregation, the microtubule associated polo-like kinases (Plks) are required for the organization of the meiotic apparatus [229], and the cAMP dependent protein kinase A (PKA) functions in sperm motility, capacitation and acrosome reaction [230–232]. Other kinases, such as the cell-cycle checkpoint protein kinases (Chk1 and Chk2), prevent cell cycle progressing of germ cells as a result of extrinsic or intrinsic (meiotic recombination) DNA damage events. This process also involves the upstream DNA sensing kinases ATM/ATR, that operate in the recognition and initiation of the DNA damage-repair pathway in testicular cells [233–235], including undifferentiated spermatogonia [236]. Another group of serine/threonine protein kinases, including mitogen activated protein-kinases (MAPKs) such as ERK1/2, are essential for the growth, division and differentiation of both somatic and germ cells. MAPKs also play a role in the capacitation [237] and acrosome reaction of spermatozoa [238,239]. An important spermatogonia signaling pathway involves the growth factor GDNF, as shown by studies on cultured SSCs. Downstream GDNF effectors include members of the Src family of tyrosine protein kinases and the Ras/ERK1/2 signaling pathway. In addition, phosphoinositide 3-kinase and AKT are components of the pathway that is activated by GDNF [101,105,240–242]. Several other tyrosine kinases have been implicated in sperm motility, capacitation and acrosome reaction [243,244].

Compared to protein kinases, little is known about the counteracting protein phosphatases (PPs) in spermatogenesis, particularly in spermatogonia (Table 2). Nevertheless, tyrosine protein phosphatases and serine/threonine protein phosphatases, including the protein phosphatase PP1, have established functions in meiosis, spermatid elongation and sperm acquisition of motility during epididymis maturation [245–248]. (Figure 9).

**Table 2: Kinases and phosphatases involved in spermatogonial development**

| Sub-family/Name | | Proposed function |
|---|---|---|
| **Kinases** | | |
| Serine/threonine protein kinases | | |
| | MAPK (ERK1/2) | SSC proliferation and self-renewal [98,101,242] |
| | Akt | SSC proliferation and self-renewal [241] |
| | Cyclin A1, 2/ CDK 1, 2 | Cell cycle regulation [229] |
| | Cyclin D 1, 2, 3/ CDK 4, 6 | Cell cycle regulation [249] |
| | ATM | Maintenance of SSC [236] |
| Tyrosine protein kinases | | |
| | Src | SSC proliferation and self-renewal [105,240] |
| **Phosphatases** | | |
| Tyrosine protein phosphatases | | |
| | PTPRE | ND [250] |
| | SHP2 | SSC maintenance [251] |
| Serine/threonine protein phosphatases | | |
| | PP1α, β and γ1 | ND [252,253] |
| | PP2A | Present but no spermatogonial phenotype was observed after *Ppp2ca* CKO in mice [61,254] |
| Threonine/tyrosine protein phosphatases | | |
| | DUSP1 | ND [250] |
| | CDC25A | Mitotic regulation [255] |
| | PTEN | ND [256] |

SSC, spermatogonial stem cells; MAPK, mitogen-activated protein kinase; ERK, extracellular signal regulated kinase; Akt (aka PKB), protein kinase B; CDK, cyclin dependent kinase; ATM, ataxia-telangiectasia mutated; Src, proto-oncogene tyrosine-protein kinase*;* PTPRE, Receptor-type tyrosine-protein phosphatase epsilon; SHP2 (Aka PTP-1D), protein-tyrosine phosphatase 1D; PP1C*,* protein phosphatase 1 catalytic subunit; PP2CA, protein phosphatase 2 catalytic subunit; DUSP1, dual specificity protein phosphatase 1 (aka: MKP1, MAP kinase protein phosphatase); CDC25A, cell division cycle 25A phosphatase; PTEN**,** phosphatidylinositol 3,4,5-trisphosphate 3-phosphatase and dual-specificity protein phosphatase; ND, not determined; CKO, conditional knockout.

The catalytic-subunit of PP1 is encoded by three different genes; *Ppp1ca*, *Ppp1cb* and *Ppp1cc* encoding the PP1α, PP1β and PP1γ isoforms, respectively. PP1γ undergoes tissue specific splicing, giving rise to a ubiquitously expressed isoform, PP1γ1, and the testis-enriched isoform PP1γ2. These two splice variants differ in the amino-acid sequence of the C-terminus. The localization of each PP1 isoform in testis has been determined in detail [247,252]. PP1α, PP1β and PP1γ1 are expressed in both somatic cells and germ cells

(spermatogonia and pre-meiotic cells), while PP1γ2 is only present in post-meiotic cells (secondary spermatocytes, round spermatids and elongated spermatids). The redundancy of PP1 isoforms in all testicular cells, except for PP1γ2, explains why the only phenotype associated with the deletion of *Ppp1cc* in mouse males is infertility, mostly due to impaired sperm morphogenesis and motility [247,252,253,257–259]. This observation prompted the identification of several PP1γ-interacting proteins (PIPs) that modulate sperm motility. A large number of testis/sperm-specific PIPs have been identified [260–262], including the spermatogenic zip protein 1 (Szp1), which binds specifically to the PP1γ2 isoform [263]. Conversely, the function of the other PP1 isoforms and isoform-specific PP1-PIP complexes in testis have not been explored yet [252,253].

In Chapter 2, the activity regulation of PP1 by associated proteins is described in the review manuscript entitled 'Biogenesis and activity regulation of protein phosphatase 1'.

## 1.3 NIPP1, a nuclear targeting subunit of Protein Phosphatase 1

NIPP1 is a regulatory subunit of PP1, initially identified in bovine thymus nuclear extracts [264]. Further studies demonstrated that NIPP1 is ubiquitously expressed in multicellular eukaryotes (see section 1.3.1) and recruits a subset of substrates for regulated dephosphorylation by associated PP1 (see section 1.3.3). In this final introductory section, I will elaborate on the structure, interactome and functions of NIPP1.

### 1.3.1 NIPP1 is a nuclear PIP

NIPP1 is one of the most ancient regulators of PP1 (Figure 10). It is expressed in both animals and plants, but not in fungi [265]. The most conserved domain of NIPP1 is the N-terminal ForkHead-associated (FHA) domain, which serves as a platform for the phosphorylation-dependent recruitment of PP1 substrates (see below).

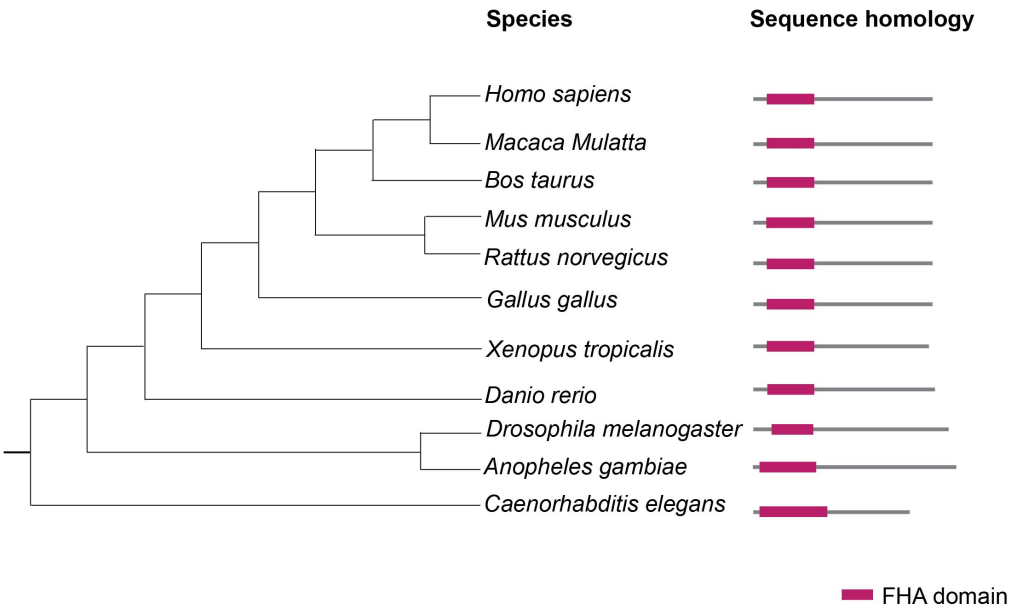


**Figure 10: The phylogenetic tree of NIPP1.** Shown are NIPP1 orthologues in various metazoa. The phylogenetic tree was built by multiple protein sequence alignments and pairwise similarity analyses using the software version MEGA 7.0.21 (www.megasoftware.net). The latter software is based on the CLUSTEL OMEGA multiple sequence alignment. Sequences were retrieved from the database https://www.ncbi.nlm.nhi.gov.

NIPP1 is encoded by *PPP1R8*, localized to chromosome 1p35 and composed of 7 exons in human (*Homo sapiens*). One processed pseudogene (*PPP1R8P*) was mapped to chromosome 1p33. *PPP1R8* encodes 5 distinct transcripts generated by alternative

splicing: NIPP1α, β, γ, δ, and the testis-specific variant NIPP1T/ε [266,267]. By far the most abundant transcript encodes NIPP1α, further referred to as NIPP1. It encodes a polypeptide of 351 residues (38.5 kDa). The other transcripts, termed NIPP1 β, γ and δ are generated by alternative 5' splice site usage, exon skipping and/or alternative polyadenylation [266]. The testis-specific NIPP1 isoform, NIPP1T/ε, is generated by intron retention and has a different C-terminus.

NIPP1 is enriched in the nucleus. Its nuclear targeting is mediated by two independent polybasic nuclear localization signals (NLS) in the central domain of NIPP1, comprising residues 185-209 and 210-240. These NLSs overlap with a PP1-binding domain (see below), but the nuclear targeting of NIPP1 does not depend on its interaction with PP1 [268]. In the nucleus, NIPP1 is excluded from the nucleoli and is enriched in the nuclear 'speckles', which represent storage sites for pre-mRNA splicing factors. The enrichment in the nuclear speckles is mediated by the FHA domain [268]. NIPP1 contains three functional domains: an N-terminal domain (residues 17-126) largely consisting of a substrate recruiting FHA domain, a central PP1-regulatory domain (residues 134-225), and a C-terminal PP1-inhibitory and RNA-binding domain (residues 226-351) [269–271] (Figure 11). A number of substrates have been identified for the PP1-NIPP1 holoenzyme, which determine PP1-dependent functions of NIPP1 in transcription, pre-mRNA splicing, cell cycle progression and chromatin remodeling [272–274]. The diversity of cellular functions via interaction with many functionally distinct interactors suggests that NIPP1 functions as a scaffold protein. Among its established interaction partners are PP1 (see section 1.3.3), the Polycomb proteins EZH2 [275] and EED [276], the protein kinase MELK (maternal embryonic leucine zipper kinase) [277], and the splicing factors CDC5L (cell division cycle 5-like) [278] and SAP155 (spliceosome-associated protein of 155 kDa) [278]. Besides its interaction with proteins, NIPP1 can also bind to RNA, preferentially A/U reach sequences, via a lysine-rich motif in its C-terminal domain [269,271,279] (Figure 11A). The C-terminal two-thirds of NIPP1 is intrinsically disordered but partially folds into a defined secondary structure upon binding to PP1 [280] (Figure 11B).

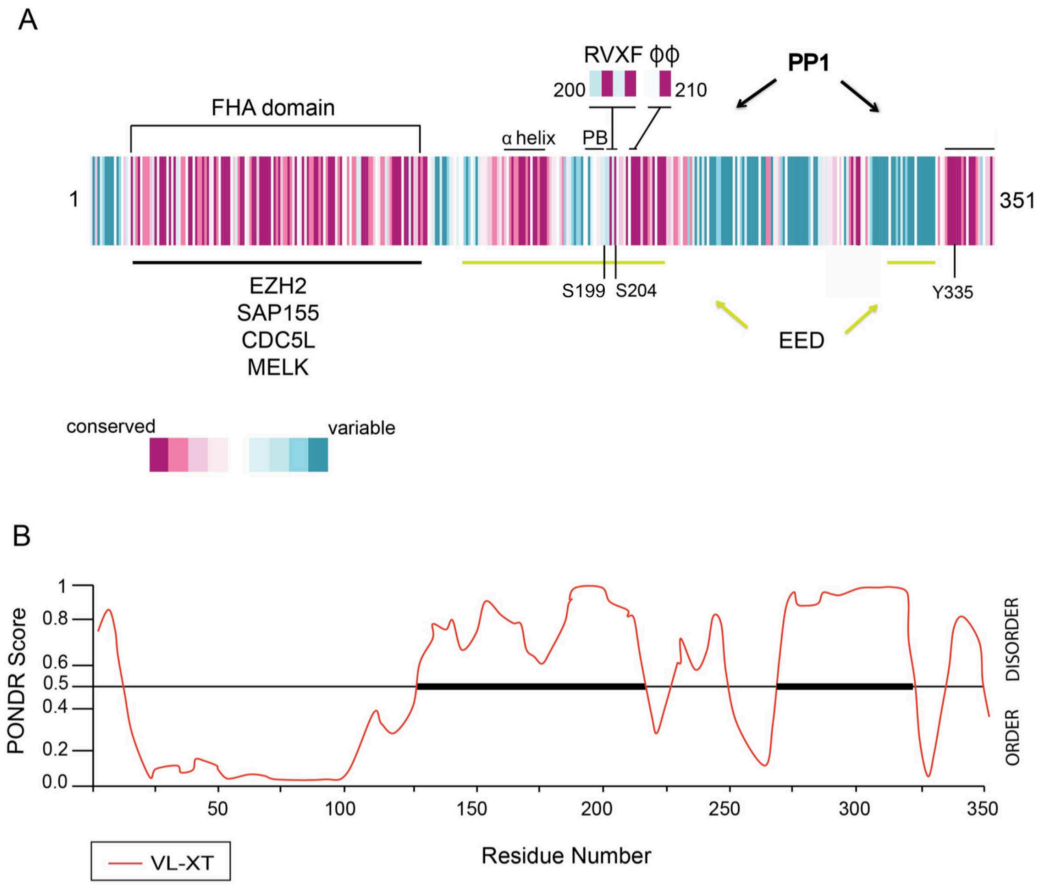


**Figure 11: Domain structure, conservation and interaction partners of NIPP1.** (A) The N-terminal domain of NIPP1 (residues 17-126) largely consists of a highly conserved and well folded ForkHead-associated domain (FHA domain) that binds to pThr-Pro dipeptide motifs (pTP) of the indicated proteins. The intrinsically disordered central and C-terminal domains contain binding sites for PP1 (α- helix, polybasic stretch, RVTF motif, φφ and C-terminus) and EED (residues 143-224 and 310-329). The C-terminus (residues 330-351) is also known to bind nucleic acids. Phosphorylation of NIPP1 at Ser199, S204 and Y335 decreases its interaction with PP1. Colored bars represent aminoacid sequences and conservation based on multiple sequences alignment of metazoa species using ConSurf (www.consurf.tau.ac.il/2016). (B) PONDR score indicating that the N-terminal third of NIPP1 is well folded and the C-terminal two thirds are disordered. (www.pondr.com).

## 1.3.2 Structure and function of the FHA domain

FHA domains are present in hundreds of different proteins and have a binding loop for phosphorylated Thr residues in a specific sequence context [281–284]. For example, RAD53 contains two FHA domains, FHA1 and FHA2, that bind a pThr followed at position +3 by an Asp or Ile/Leu/Val, respectively [285]. Other FHA domains make

additional contacts with residues that are both N- and C-terminal to pThr (e.g. the FHA domain of PNK) or with residues that are remote from pThr (e.g. the FHA domain of Ki67) [282,286,287].

Despite their different binding specificity FHA domains adopt a similar fold: eleven β-strands (β1-β11) form two β-sheets, one containing six antiparallel strands (β1-2, β7-8 and β10-11) and the other containing five mixed β strands (β3-6, β9) [282,288] (Figure 12).

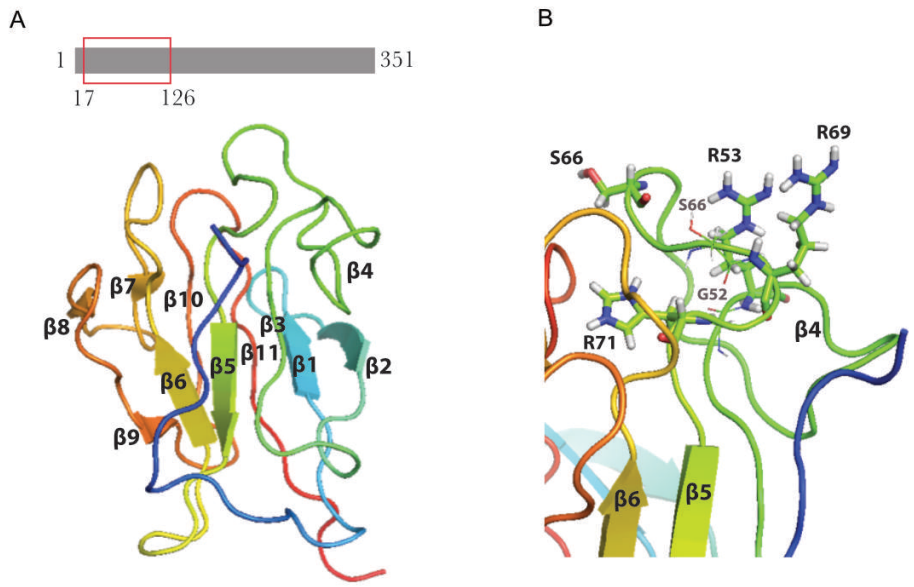


**Figure 12: The FHA domain of NIPP1.** (A) The core structure of the FHA domain of NIPP1 (residues 17-126) comprises 11 β-strands linked by several loops to form two antiparallel β-sheets. (B) Structure showing the binding of residues 470-487 of MELK to the FHA domain of NIPP1. The pThr binding loop resides between β-strands 4 and 5. The residues of this loop that are involved in the binding of pThr are indicated [288]. The structure was drawn using PyMOL (*www.pymol.com*; PDB ID:2JPE).

The FHA domain of NIPP1 binds ligands with a pThr that is followed by a Pro [277,278,289,290]. In this sense, the FHA domains of NIPP1 and Ki67 have a similar specificity. Interestingly, the FHA domain of Ki67 not only binds to a pTP but also interacts with an extended binding surface of 44 residues of NIFK, one of its ligands [291]. Together these two binding sites account for the high-affinity interaction between Ki67 and NIFK. The FHA domain of NIPP1 also interacts rather poorly ($K_d \approx$ 1mM) with pThr416 of EZH2, one of its established ligands [290]. Yet, mutation of Thr416 completely abolishes the interaction with NIPP1. This suggests that Thr416 is essential but not sufficient to account for the high-affinity binding of EZH2 to NIPP1. The same reasoning

applies to Thr478 of MELK, which also binds to the phosphate binding loop of the NIPP1 FHA domain [288]. The available data suggest that secondary interactions are important to account for the stable interactions between NIPP1 and its FHA ligands. However, sequence alignments of established FHA ligands of NIPP1 (Figure 13A) or a comparison with other pTP containing FHA ligands (Figure 13B) did not reveal additional conserved features close to the FHA binding pThr-Pro that could mediate additional interactions.

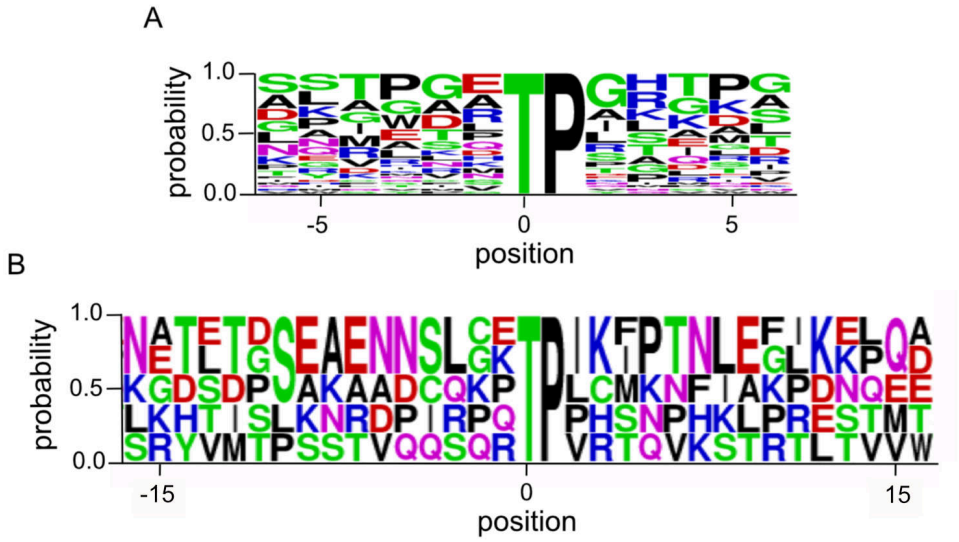


**Figure 13: Binding preference for the NIPP1 FHA domain.** (A) Alignment of established NIPP1 FHA ligands (EZH2, MELK, CDC5L and SAP155) shows that the FHA domain of NIPP1 binds to pThr-Pro dipeptide motifs. (B) Alignment of NIPP1 FHA ligands EZH2 and MELK with other pTP-containing FHA ligands (NIFK, Hklp2 and NDD1) indicates that close to the pTP-dipeptide motif there are no other predicted common motifs. Weblogo (http://weblogo.berkeley.edu/logo.cgi) was used to predict the conservation motifs.

### 1.3.3 NIPP1 modulates the activity of associated PP1

NIPP1 was originally identified as a potent inhibitor of PP1 [292]. However, the central domain of NIPP1 only inhibits the dephosphorylation of a subset of substrates by a non-competitive mechanism [269,280]. The PP1-binding module in the central domain of NIPP1 (residues 159-214) (Figure 14) is intrinsically disordered but becomes partially structured when bound to PP1 [280]. The central domain of NIPP1 has three binding sites for PP1: (1) residues $^{199}$SRVTFS$^{204}$ dock to the hydrophobic RVxF-binding groove on PP1, (2) residues Ile209 and Ile210 bind to another hydrophobic pocket, known as the φφ-binding pocket, and (3) residues 160-175 fold into a four turn α-helix that docks onto the bottom surface of PP1, mainly via electrostatic interactions (Figure 14). Strikingly, a

polybasic stretch (residues 185-198) that is important for the non-competitive inhibition of associated PP1 [269] is not visible in the crystal structure, indicating that it remains unstructured (Figure 14). The binding of the central domain of NIPP1 to PP1 has a significant impact on its overall surface charge, which may contribute to substrate selection by the PP1-NIPP1 holoenzyme.

The C-terminal segment of NIPP1 contains a PP1-binding site that causes the inhibition of PP1 towards all substrates. It acts as a competitive inhibitor, indicating that it binds at or close to the active site [269].

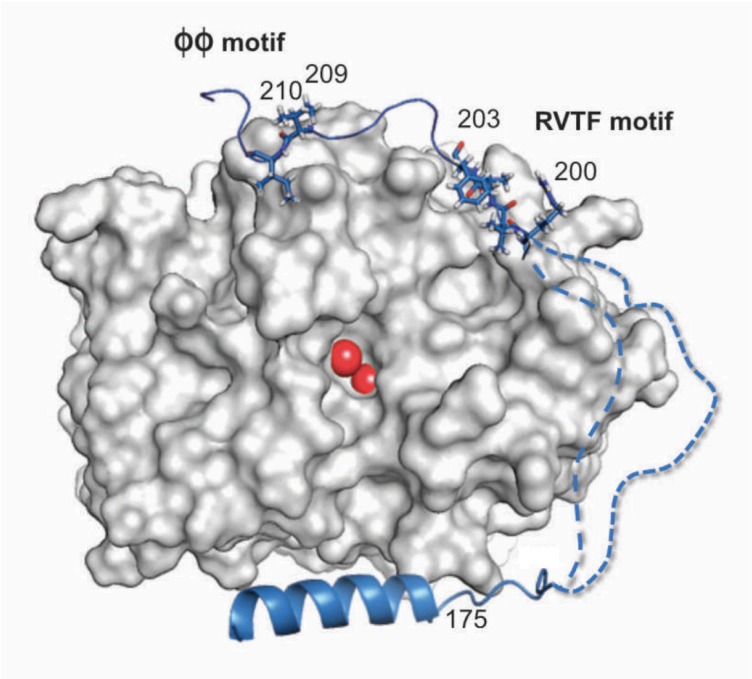


**Figure 14: The crystal structure of PP1 complexed to the central domain of NIPP1.** Cartoon representation of the three primary PP1-binding regions of NIPP1 (blue) and PP1 (gray surface) complex. The $Mn^{2+}$ ions located at the active site of PP1 are represented as red spheres. The residues V201 and F203 of the NIPP1 RVxF (RVTF) motif and residues 209-210 of the φφ motif is shown as sticks. The blue dotted lines represent NIPP1 residues 185-198 that were not visible. Cartoon representation was drawn using *PyMOL* (*www.pymol.com*; PDB ID:3v4y).

### 1.3.4 NIPP1 regulates Polycomb-mediated gene silencing

NIPP1 functions as a PRC2-dependent transcriptional repressor by forming a complex with PP1 and the PRC2 components EZH2 and EED [274–276] (see Introduction). Previous studies indicated that NIPP1 is required for the global trimethylation of H3K27 and is implicated in gene silencing [293]. This transcriptional repression was alleviated by the RNAi-mediated knockdown of EED and EZH2, or by overexpression of a catalytically

dead mutant of EZH2 [275]. Moreover, EZH2 and NIPP1 silence a common set of genes, as revealed by gene-expression profiling in human cells [293]. Accordingly, NIPP1$^{-/-}$ embryos exhibited a reduced global trimethylation of histone H3 at Lys27 [294]. More recent studies have shown that pThr416 of EZH2 binds to the phosphate-binding loop of the FHA domain of NIPP1 (Figure 11A, 12 and 13). In HeLa cells, the recruitment of NIPP1 was found to be essential to maintain the CDK-mediated phosphorylation of EZH2 at this site by opposing dephosphorylation by PP1 [290]. Accordingly, a NIPP1-binding mutant of EZH2 was hypophosphorylated and the knockdown of NIPP1 resulted in a reduced phosphorylation of endogenous EZH2. Conversely, a loss of PP1 was associated with a hyperphosphorylation of EZH2 [290]. NIPP1 has also been implicated in the targeting of EZH2 to specific PcG target genes [274,290,293]. Indeed, a genome-wide promotor profiling in HeLa cells revealed that NIPP1-binding mutants of EZH2 show a deficient association with proliferation-enriched Polycomb target genes [290]. The binding of EED to NIPP1 occurs via two regions in the central and C-terminal thirds of NIPP1 **(Figure 11A)**, but it is not known yet how this contributes to PRC2 signaling.

### 1.3.5 NIPP1 regulates (pre)mRNA splicing

The enrichment of NIPP1 in the nuclear speckles is mediated by its FHA domain, possibly because it binds to phosphorylated forms of the splicing factors SAP155 and CDC5L (Figure 11A) [268,289]. The FHA domain of NIPP1 is essential for the recruitment of phosphorylated forms of SAP155 and CDC5L. Accordingly, mutation of the pThr-binding loop of the FHA domain (Figure 11B, 12 and 13) abrogates their binding to NIPP1 and the targeting of NIPP1 to the nuclear speckles and spliceosomes [268,295]. Mechanistically, NIPP1 recruits PP1 to SAP155, an essential component of the U2 small ribonucleoprotein particle [289,296,297], and promotes subsequent SAP155 dephosphorylation [273]. The expression of a C-terminally truncated NIPP1 (NIPP1-ΔC) that forms a hyperactive PP1-NIPP1 holoenzyme (see previous sections), results in SAP155 hypophosphorylation and splicing inhibition [273]. Similarly, NIPP1 stimulates SAP155 dephosphorylation by PP1 *in vitro*. The dephosphorylation of SAP155 by PP1 further stimulates dissociation from NIPP1 FHA domain [273]. The stimulating effect of NIPP1 on SAP155 dephosphorylation by PP1 suggests that the inhibitory activity of NIPP1 is substrate-dependent and is subject to regulation. This resembles the PP1-regulatory protein MYPT1, which inhibits PP1 activity against non-physiological substrates (e.g. phosphorylase *a*), but stimulates PP1 activity towards myosin light chain [298].

Protein kinase MELK has also been implicated in the early spliceosome assembly (inhibitory activity) independently of its kinase activity [277]. MELK binds to the FHA domain of NIPP1 via pThr478 residue (Figure 11A, 12 and 13) [277,288]. The inhibition of spliceosome assembly by MELK depends on this binding, indicating that MELK probably competes with other splicing factors (SAP155 and CDC5L) for binding to the FHA domain of NIPP1 thereby preventing the recruitment of NIPP1 to the spliceosomes [277].

### 1.3.6 NIPP1 is required for early embryonic development

As described above, NIPP1 emerges as an integrator of transcription, RNA processing and cell signaling. To study the *in vivo* function of NIPP1 in mammals, a global mouse knockout for the NIPP1 encoding gene (*Ppp1r8*) was generated by homologous recombination [294]. NIPP1 knockout (*Ppp1r8*$^{-/-}$) embryos showed growth retardation and died at around embryonic day 6.5 (E6.5), coinciding with the onset of gastrulation. A decreased proliferation was also noted in NIPP1 deficient blastocyst outgrowths for both cells from the inner cell mass and trophoblast giant cells. Since the latter cells grow by repeated replication without an intervenient mitosis, this hints at a role for NIPP1 in the G1/S transition or DNA replication.

### 1.3.7 The C-terminus of NIPP1 displays RNA-binding and endoribonuclease activities

The C-terminal third of NIPP1α corresponds to the NIPP1γ/ARD-1 isoform, which displays an endoribonuclease activity with a specificity that is similar to that of bacterial RNAse E [266,299,300]. Strikingly, ARD-1 was originally identified as a human protein that can rescue lethal mutations in the *Escherichia. coli* (*E. coli*) RNase E encoding gene *rne* [299,301]. Additional studies revealed that ARD-1 displays RNA-binding and endoribonuclease activities [271,279]. However, NIPP1α does not display an endoribonuclease activity, indicating that this activity is either not biologically relevant or subject to inhibitory regulation by the N-terminal two thirds of the protein. ARD-1 and RNase E both bind preferentially to U-rich sequences. In bacteria RNAse E cleaves short oligonucleotides and complex RNAse E substrates in A/U-rich regions and generates 5'-phosphate termini [299]. RNAse E is an essential part of the RNA degradosome which is involved in the turnover of mRNAs [302–304]. In addition, RNAse E has been implicated in the processing of precursor RNAs [305–308]. Orthologues of RNAse E are expressed in

the chloroplasts of higher plants where they participate in endonucleolytic cleavage of the polyadenylation stimulated RNA-degradation process [309].

PP1-binding to the C-terminal segment of NIPP1 is controlled by both phosphorylation and electrostatic interaction between nucleic acids and basic residues. Phosphorylation of NIPP1 at Tyr-335 by protein kinase LYN only occurs in the presence of RNA, and reduces the affinity of the C-terminal domain of NIPP1 for PP1, resulting in a 'de-inhibition' of the PP1-NIPP1 holoenzyme [269].

# CHAPTER 2

# Review

# Biogenesis and activity regulation of protein phosphatase 1

Derived from:

Iris Verbinnen, **Monica Ferreira** and Mathieu Bollen

Laboratory of Biosignaling & Therapeutics, KU Leuven Department of Cellular and Molecular Medicine, University of Leuven, B-3000 Leuven, Belgium

Review article published in *Biochemical Society Transactions* Journal
*(Biochem Soc Trans. 2017; 45 (1):89-99)*

*Journal cover*

## 2.1 Abstract

Protein phosphatase-1 (PP1) is expressed in all eukaryotic cells and catalyzes a substantial fraction of phospho-serine/threonine dephosphorylation reactions. It forms stable complexes with PP1-interacting proteins (PIPs) that guide the phosphatase throughout its life cycle and control its fate and function. The diversity of PIPs is huge (≈200 in vertebrates) and most of them combine short linear motifs to form large and unique interaction interfaces with PP1. Many PIPs have separate domains for PP1 anchoring, PP1 regulation, substrate recruitment and subcellular targeting, which enable them to direct associated PP1 to a specific subset of substrates and mediate acute activity control. Hence, PP1 functions as the catalytic subunit of a large number of multimeric holoenzymes, each with its own subset of substrates and mechanism(s) of regulation.

## 2.2 Introduction

PP1 belongs to the phosphoprotein phosphatase (PPP) superfamily of hydrolases [1–3]. It catalyzes the hydrolysis of serine/threonine-linked phosphate monoesters by a nucleophilic attack of the incoming phosphorus atom with a metal-activated water molecule. PP1 increases the reaction rate by a staggering $10^{21}$ fold, making it one of the most proficient of all known enzymes [4]. It also ranks among the structurally and functionally most conserved proteins: PP1 from yeast and man show >80 % sequence identity and human PP1 can rescue the lethal phenotype associated with the deletion of PP1 in yeast [5]. PP1 is expressed in all eukaryotic cells at moderately high levels. Human U2OS and HeLa cancer cells, for example, contain about 250,000 copies of PP1 isoforms α, β and γ, corresponding to a calculated concentration of ≈ 0,2 μM [6,7]. Biochemical data indicate that PP1 catalyzes a major fraction of all protein dephosphorylation events in eukaryotic cells and regulates a wide array of processes [8]. Consistent with its pleiotropic action PP1 displays a broad substrate specificity. However, PP1 is not completely aspecific and shows a substrate preference that is different from that of the other PPP-type phosphatases, namely PP2A, PP2B and PP4-7 [8]. The recently published structure of a PP5-substrate complex sheds some light on the molecular basis of substrate recognition by PPP phosphatases [9]. The side chains of the peptide substrate engage in water-mediated hydrogen bonds with residues in pockets that radiate from the catalytic site and are known as the hydrophobic and C-terminal grooves (Figure 1). These pockets are spacious and can accommodate highly divergent sequences, accounting for the sequence plasticity of PPP substrates. Most

phosphatase residues that mediate substrate binding are highly conserved among PPP phosphatases. However, a residue that interacts with the substrate -2 position differs between PPP members and therefore probably functions as a substrate-specifying element.

There is no evidence for the existence of cellular pools of unbound PP1. In fact, artificially generated free PP1 causes uncontrolled protein dephosphorylation and results in cell death [10]. Cells prevent the accumulation of unleashed PP1 by expressing PP1 interacting proteins (PIPs) in a large molar excess [3,6,7]. From a biological perspective it is therefore only meaningful to discuss the properties and regulation of PP1 as the catalytic subunit of a large array of multi-subunit complexes or holoenzymes. In general, PIPs guide PP1 throughout its life cycle and determine when and where the phosphatase acts. In the following sections we will consecutively describe PP1-PIP interaction modes, the involvement of PIPs in the biogenesis and turnover of PP1, their role in substrate selection, and their contribution to holoenzyme abundance and activity regulation. The available data suggest that most PIPs serve a dual function: they restrain PP1 and enable the controlled dephosphorylation of a small subset of PP1 substrates.

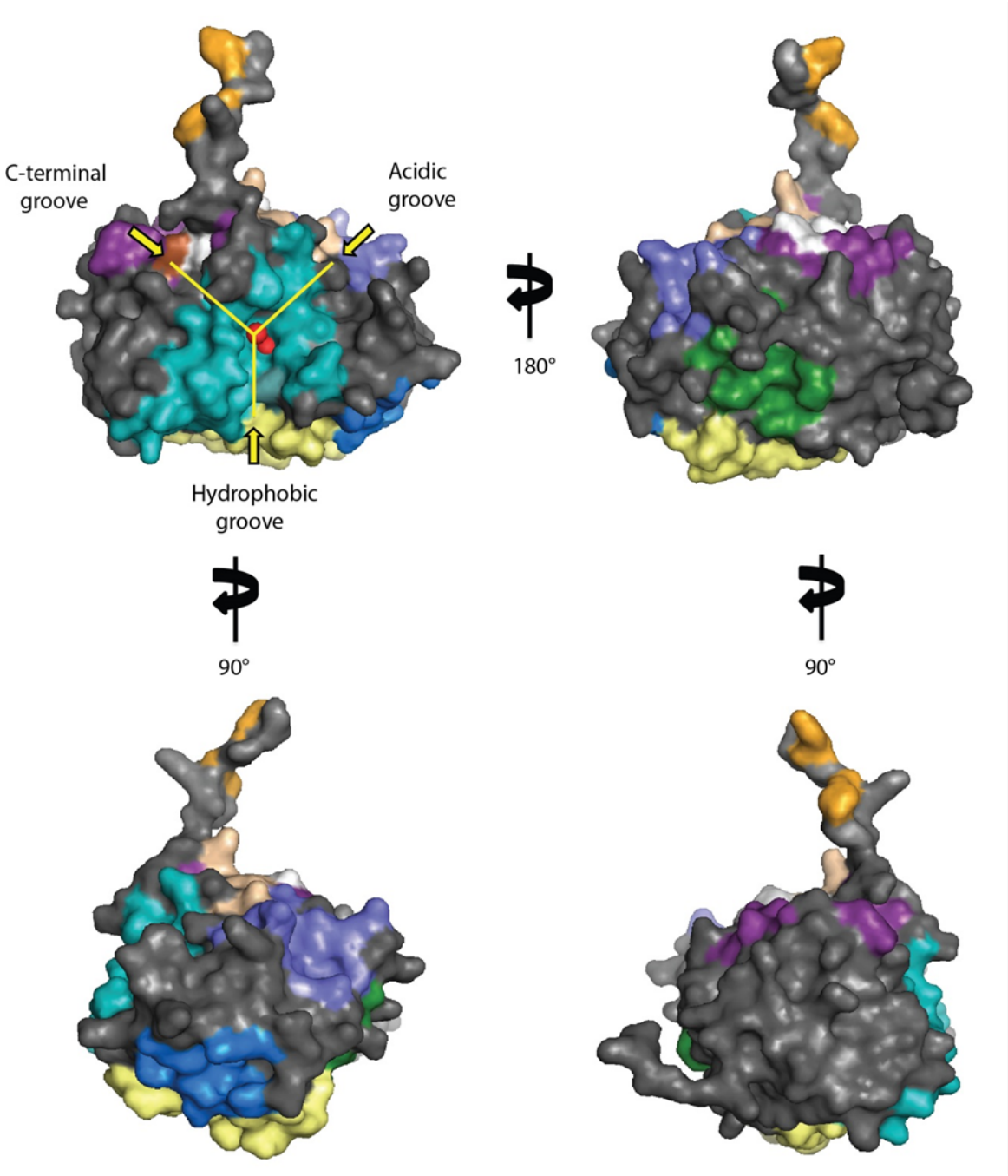


**Figure 1: PIP docking sites on PP1.** The figure shows a surface model of four different orientations of mammalian PP1β (PDB 1S70). Indicated are the two metals in the active site (red circles) and the substrate-binding channels that emanate from the active site. The residues of PP1 that mediate binding to SLiMs are colored: violet, RVxF motif; magenta, Ki67-RepoMan SLIM (KIR-SLiM) motif; green, SILK motif; dark blue, Myosin phosphatase N-terminal element (MyPHONE) motif; yellow, NIPP1 α-helix motif; wheat, φφ motif; cyan, Inhibitor-2 SLiM for docking at the hydrophobic and acidic grooves (IDoHA); Brown, Spinophilin SLiM for docking at the C-terminal groove (SpiDoC). Also shown are the residues in the C-terminus of PP1β that interact with the ankyrin-repeat domain (AnkCap) of MYPT1 (orange). Overlapping binding

residues for the SpiDoC, KIR-SLIM and φφ motifs are depicted in white. Figures were made using *PyMOL* (www.pymol.com).

## 2.3 PP1-PIP interaction modes

More than 200 mammalian genes encode validated PIPs [1,3]. Some are ubiquitously expressed (e.g. Inhibitor-2), others show a more restricted expression (e.g. Spinophilin in neurons) or are expressed conditionally (e.g. Ki-67 in proliferating cells). Most PIPs have an intrinsically disordered domain of 40-60 residues that mediates binding to PP1 with high affinity, as reflected by $K_d$ values of 5-200 nM [11–16]. These PP1-anchoring domains contain short linear motifs (SLiMs) that dock to surface grooves of PP1 (Figure 1). PIPs typically combine several SLiMs to create an interaction area of 1,500-5,000 $Å^2$, thereby covering 5-20% of the surface of PP1. Nearly a dozen PP1-binding SLiMs have already been identified but it seems likely that additional SLiMs remain to be discovered that bind to surface areas of PP1 that have no known interaction partner (Figure 1). Some of the well-characterized SLiMs are present in many PIPs but others are less widespread. For example, the RVxF-type PP1-binding motif is shared by 70% of all known PIPs, while the recently discovered KiR-SLiM motif is only found in the nuclear proteins RepoMan and Ki-67 [3,14,16].

The diversity and concomitance of PP1-binding SLiMs creates a huge combinatorial potential that has been referred to as the 'PP1-binding code' [1,3,17]. This code enables PIPs to create unique interaction interfaces with PP1 and has particular properties (for references and more details see [3]). First, the code is *specific* in that PP1-binding SLiMs do not interact with other phosphatases. Second, it is *universal* and applies to all eukaryotes. Third, the code is partially *overlapping* as it excludes combinations of SLiMs that bind to the same PP1 surface residues. Fourth, it is *degenerate*, implying that SLiMs come in sequence variants that differ in their affinity for PP1. Fifth, the code is *non-exclusive*, allowing two PIPs to bind simultaneously to the same molecule of PP1 as long as they have at least one non-shared SLiM. Sixth, it is *dynamic* and tolerates competition between PIPs within and between PP1 holoenzymes for the same binding sites. The elucidation of the SLiM-based PP1-binding code is yielding structural insights that gradually make it feasible to predict the PP1-interaction mode of poorly characterized PIPs. It can also be expected that the obtained insights will inspire investigators to design artificial PIPs that can be used as tools to explore PP1 signaling and its therapeutic potential.

In addition to the SLiMs in PP1-anchoring domains some PIPs also have PP1-binding SLiMs in regulatory domains. Biochemically well-defined examples are the phosphorylation-regulated PP1-inhibitory SLiMs of Inhibitor-1 and NIPP1 [18,19]. The prevalence and importance of PP1-binding SLiMs in regulatory PIP domains has probably been grossly underestimated because they contribute little to the overall binding affinity for PP1 and are therefore easily overlooked using classical mapping strategies for PP1-binding domains. SLiMs in PP1-regulatory domains add to the flexibility of the PP1-binding code and are important mediators of acute activity regulation (see below). Further diversification of PP1-PIP interaction modes comes from the existence of highly structured PP1-binding domains. For example, Sds22 has a PP1-binding domain that consists of an array of well-folded leucine-rich repeats [20]. Another example is the ankyrin-repeat domain of MYPT1, which specifically binds to the intrinsically disordered C-terminus of PP1β (Figure 1), accounting for the PP1-isoform binding specificity of this myosin-targeting PIP [11]. Interestingly, recent data show that the PP1 isoform selectivity of some PIPs is not only achieved through interactions with the C-terminus but also through interactions with the structured catalytic domain [16]. Thus, the L1 loop of PP1β/γ is ordered by an arginine-mediated salt bridge (Arg19 for PP1β and Arg20 for PP1γ), making it more available for binding of Ki67 and RepoMan. The corresponding residue of PP1α (Gln20) does not order this pocket, explaining why Ki67 and RepoMan preferentially bind to the β/γ isoforms.

## 2.4 PIPs in the biogenesis and turnover of PP1

At an early point in the PP1 biogenesis process, during or shortly after translation, the metal ions $Fe^{2+}$ and $Zn^{2+}$ are incorporated into the active site to generate a catalytically competent enzyme [21]. Eukaryotes probably have dedicated chaperones for $Fe^{2+}$ and $Zn^{2+}$ loading of PP1 that are absent in bacteria because the latter can express eukaryotic PP1 but erroneously incorporate two $Mn^{2+}$ ions in the active site, even when $Fe^{2+}$ and $Zn^{2+}$ are abundant. The nature of the incorporated metals is important because PP1 with $Mn^{2+}$ in its active site has a manifold lower specific activity than native PP1 and is less specific, as it also dephosphorylates tyrosine residues and even non-protein substrates [21]. The identity of the putative PP1 metal-loading chaperones is still unknown but Inhibitor-2 is an excellent candidate (Figure 2). Actually, an *in vitro* reconstituted inactive complex of PP1 and Inhibitor-2, known as the MgATP-dependent phosphatase, can be reactivated by the transient phosphorylation of Inhibitor-2 and considerable biochemical evidence suggests

that this activation process involves the incorporation of metal(s) in the active site (reviewed in [22]).

In yeast, also Sds22 and Ypi1 have been identified as PIPs that are required for an early step in the biogenesis of PP1 [23]. In the absence of functional Sds22 or Ypi1 newly translated PP1 forms aggregates that require the proteasome for clearance. Sds22 and Ypi1 (or its orthologue Inhibitor-3 in vertebrates) form a heterotrimeric complex with PP1, both *in vitro* and *in vivo* ([24,25], Figure 2). Sds22 and Ypi1 also interact with each other. Intriguingly, the assembly of the Sds22-PP1-Ypi3 complex requires a chaperone complex consisting of the AAA-ATPase Cdc48 and its adaptor Shp1, which transiently binds to Sds22 [23]. Sds22 has a structured PP1-binding domain but the binding of Ypi1/Inhibitor-3 to PP1 is SLiM-based [3,20]. The combined binding of Sds22 and Ypi1/Inhibitor-3 is expected to cover a large part of the surface of PP1. Ypi1/Inhibitor-3 inhibits PP1 [24,25], while Sds22 stabilizes a partially unfolded form of PP1 [24], hinting at its preferential binding to newly translated, incompletely folded PP1. Hence, Sds22 and Ypi1/Inhibitor-3 probably serve to keep newly synthesized PP1 soluble and inhibited. We speculate that the resulting heterotrimeric complex is used as a source of PP1 for the assembly of functional holoenzymes.

Virtually nothing is known about the mechanisms underlying the formation and turnover of PP1 holoenzymes. Possibly, the biogenesis factors Sds22, Ypi1/Inhibitor-3 and Inhibitor-2 are also implicated in these processes. It is indeed striking that Sds22 can be present as a 'third' subunit in at least some PP1 holoenzymes and that Inhibitor-3 competes with other PIPs for binding to PP1-Sds22 [26]. Does Sds22 in these complexes serve to recruit an AAA-ATPase complex that extracts PP1 for recycling or degradation (Figure 2)? *In vitro*, Inhibitor-2 removes $Fe^{2+}$ from the active site of PP1 [21] and the bacterially expressed PP1/Inhibitor-2 complex lacks one or both metals [27]. Does Inhibitor-2 remove metals from PP1 once the catalytic subunit is extracted from a holoenzyme and does this represent a key step in its degradation process (Figure 2)?

Sds22, Inhibitor-2 and Ypi1/Inhibitor-3 are the most ancient PIPs [28], suggesting that their functions in the biogenesis and turnover of PP1 are possibly also phylogenetically conserved. Strikingly, the much better studied biogenesis factors of the PPP-type PP2A phosphatase are structurally unrelated to those of PP1 but nevertheless appear to fulfill similar functions. During or shortly after its translation the catalytic subunit of PP2A also forms a heterotrimeric complex with polypeptides that stabilize its inactive conformation (the α4 protein, similar to Sds22 for PP1) and inhibit is activity (the TIPRL protein, similar

to Inhibitor-3 for PP1) [29–32]. Moreover, a chaperone complex (TriC/CCT, similar to AAA-ATPases for PP1) may be involved in the assembly of this complex [30]. In addition, the PP2A interactor PTPA appears to be functionally equivalent to Inhibitor-2 as it has been demonstrated to play a role in the metal-loading of PP2A [33].

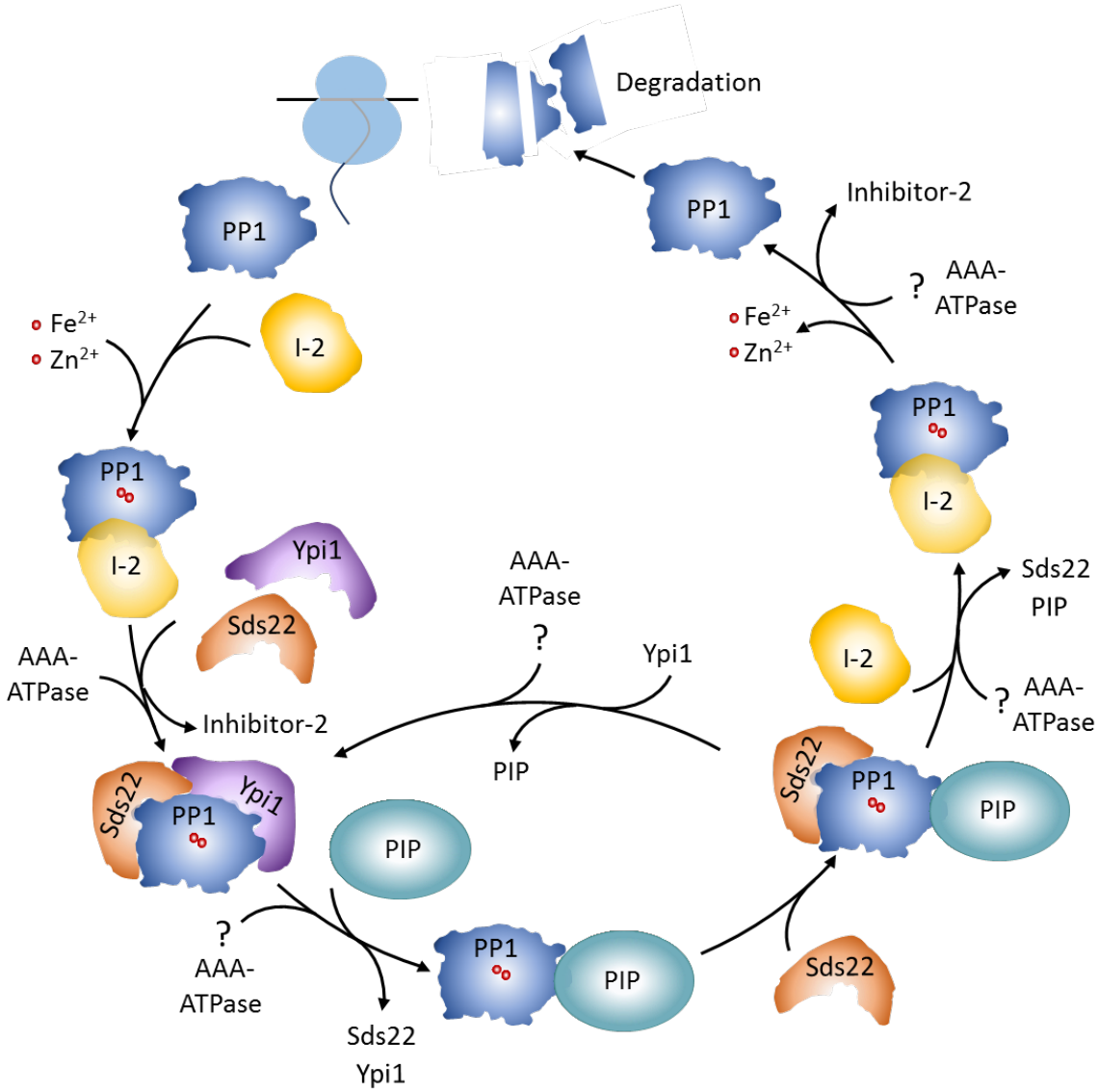


**Figure 2: The hypothetical life cycle of PP1.** During or shortly after the translation of PP1 the metals $Fe^{2+}$ and $Zn^{2+}$ are incorporated into the active site by a mechanism that probably involves the transient phosphorylation of Inhibitor-2 by protein kinase GSK-3. Subsequently, PP1 is extracted by an AAA-type ATPase (Cdc48 and the cofactor Shp1 in yeast) to form a soluble, inhibited trimeric complex with Sds22 and Ypi1 (Inhibitor-3 in vertebrates). This complex serves as the source of PP1 for the assembly of PP1 holoenzymes. At least some PP1 holoenzymes can recruit Sds22 as a third subunit. It is suggested that Sds22 mediates the recruitment of an AAA-

ATPase to extract PP1 from these holoenzymes, either for (phosphorylation-independent) metal unloading by Inhibitor-2 and its subsequent proteolytic degradation or for recycling to form a trimeric complex with Sds22 and Ypi1/Inhibitor-3.

## 2.5 PIPs as substrate-specifiers

Eukaryotic cells contain hundreds if not thousands of distinct PP1 substrates, in various amounts. A key function of PIPs is to limit the action of associated PP1 to a subset of substrates or (transiently) inhibit PP1 altogether. PIPs have evolved multiple strategies to restrain PP1 (Figure 3A). The SpiDoC SLiM of Spinophilin docks to the C-terminal groove of PP1 (Figures 1 and 3A) and sterically hinders the dephosphorylation of substrates that are recruited via this groove [12]. PNUTS occludes the same groove using a different SLiM that has, however, an Arg in common with the SpiDoC motif and was therefore termed the Arg motif [14]. The PP1-anchoring central domain of NIPP1 inhibits the dephosphorylation of many but not all PP1 substrates [19]. A key inhibitory element in this domain was mapped to a polybasic region close to the PP1-binding RVxF-type SLiM. Interestingly, this polybasic stretch of residues was not visible in the electron density map of the PP1-NIPP1 heterodimer, suggesting that it remains flexible in the complex and prevents the dephosphorylation of a subset of substrates through dynamic electrostatic interactions with PP1 (Figure 3A). NIPP1 also has a PP1-regulatory C-terminal domain that prevents the dephosphorylation of all substrates, possibly because it binds at or near the catalytic site [19]. The IDoHA motif of Inhibitor-2 adopts a largely α-helical structure that occupies the acidic and hydrophobic grooves of PP1 but also occludes the active site (Figures 1 and 3A, [27]). In addition, local interactions at the active site cause the displacement of one or both metals. Other PIPs (e.g. Inhibitor-1, CPI-17, MYPT1) have a PP1-regulatory domain that inhibits PP1 but only when it is phosphorylated [1,18,34,35]. Probably these PIPs inhibit PP1 by binding as pseudosubstrates.

Many PIPs have also acquired structural features for positive substrate selection (Figure 3B). They often contain a domain that mediates binding to a specific subcellular compartment. This enhances the local concentration of PP1 and thereby promotes the dephosphorylation of resident substrates. PIPs target PP1 to a wide range of subcellular structures [3], including centrosomes (e.g. Cep192), chromosomes (e.g. RepoMan), endoplasmic reticulum (e.g. GADD34), glycogen particles (e.g. PTG), microtubules (e.g. Kif18A), actin (e.g. Spinophilin), myofibrils (e.g. MYPT1), nuclear speckles (e.g. NIPP1), nucleoli (e.g. NOM1) and the plasma membrane (e.g. TIMAP). Some PIPs have multiple

subcellular targeting domains (e.g. a few glycogen-targeting subunits also have a membrane-targeting domain), which enables them to function as signal integrators [1].

Substrate-recruitment domains of PIPs also contribute to substrate selection and dephosphorylation (Figure 3B). This is because substrates bind relatively poorly to PP1 itself ($K_m$ in the micromolar range, often far above the cellular concentration of the substrate), but their binding affinity and dephosphorylation rate is massively increased if the associated PIP contains an additional substrate-binding site. Examples of substrate-recruitment domains are the ForkHead-associated domain (FHA) of NIPP1 and two eIF2α-binding elements of GADD34 [13,15,36]. Subcellular-targeting and substrate-recruitment domains may be different or the same. Thus, the targeting of NIPP1 to the nuclear speckles is mediated by its substrate-binding FHA domain [37], but GADD34 has distinct binding domains for the endoplasmic reticulum and eIF2α (Figure 3B, [15,36,38]). Some PIPs may simply enhance the affinity for a subset of substrates by extending a substrate-binding groove of PP1. For example, some ankyrin-repeats of MYPT1 lengthen the acidic groove of PP1, which has been suggested to promote the recruitment of a subset of substrates (Figure 3B, [11]).

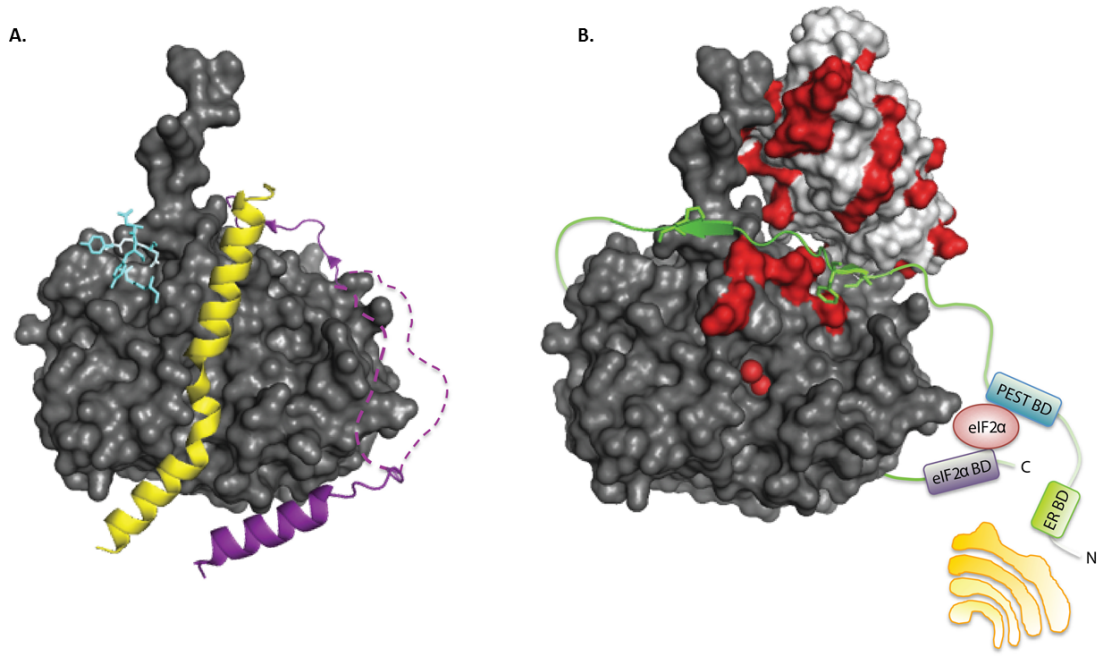


**Figure 3: Mechanisms of substrate selection by PP1.** The figure shows strategies for restricted (A) and facilitated (B) substrate recruitment by PIPs. (A). The SpiDoC motif (cyan) sterically hinders the recruitment of PP1 substrates via the C-terminal groove. The IDoHA motif of Inhibitor-2 (yellow) prevents the dephosphorylation of all substrates by occluding the hydrophobic and acidic grooves as well as the active site. A polybasic stretch in the PP1-anchoring domain of NIPP1

(purple) hampers the dephosphorylation of a large subset of substrates through dynamic electrostatic interactions, as suggested by the dotted lines. (B) Some ankyrin-repeats of MYPT1 (light grey) may promote the binding of a subset of PP1 substrates through extension of the acidic groove (acidic residues highlighted in red). GADD34 (green) promotes the dephosphorylation of eIF2α by providing binding domains (BD) for the endoplasmic reticulum (ER- BD) and eIF2α itself (PEST-BD + eIF2α BD).

## 2.6 Determinants of PP1-holoenzyme abundance

PIPs compete with each other for binding to the limited cellular pool of PP1 (Figure 4). This is nicely illustrated by repeated observations that the overexpression of a single PIP results in a reduced association of PP1 with endogenous PIPs [39–41] (Figure 4A). The measles virus escapes sensing by the host cell using a similar competition strategy. Indeed, the viral V protein titrates PP1 away from the sensor protein MDA5, thereby preventing its PP1-mediated activation [42]. Similarly, a prolonged unfolded-protein-response triggers the assembly of the PP1-GADD34 complex at the endoplasmic reticulum [43]. This reduces the nuclear accumulation of PP1, resulting in the hyperphosphorylation of the Hippo signaling effector Yap and apoptosis. There are also examples of competition between PP1 and other signaling molecules for binding to overlapping PIP binding sites (Figure 4B). Thus, PP1 and cyclin-dependent kinases compete for an overlapping binding motif on the Retinoblastoma protein [44]. Likewise, PP1 and protein tyrosine phosphatase Shp1 compete for binding to Spinophilin [45].

Since the global cellular level of PP1 is kept more or less constant during the cell cycle [46,47], its distribution between PIPs is determined in the first place by the relative abundance of PIPs. Numerous data show that the concentration of PIPs is tightly regulated at multiple levels. Their expression is regulated in a cell-type (e.g. glycogen targeting G-subunits [48]) or cell-cycle (e.g. PNUTS [49]) dependent manner, but can also be induced by specific stimuli (e.g. GADD34 by stress signals [15]). In addition, the level of PIPs can be adjusted post-translationally through regulated proteolysis by caspases (e.g. Inhibitor-3, [50]), the proteasome (e.g. MYPT1 [51]) or lysosomes (e.g. glycogen-targeting R6 [52]) (Figure 4C). The abundance of specific PP1-PIP complexes is also affected by the binding affinity of the components, which is subject to regulation (Figure 4D). Many PIPs show a reduced affinity for PP1 after phosphorylation of residues in or near PP1-binding SLiMs in PP1-anchoring domains (e.g. RepoMan, CENP-E and KNL1 in the first half of mitosis

[16,53–55]). Conversely, microtubule binding by the spindle- and kinetochore-associated (SKA) complex possibly serves to promote the recruitment of PP1 by SKA [56].

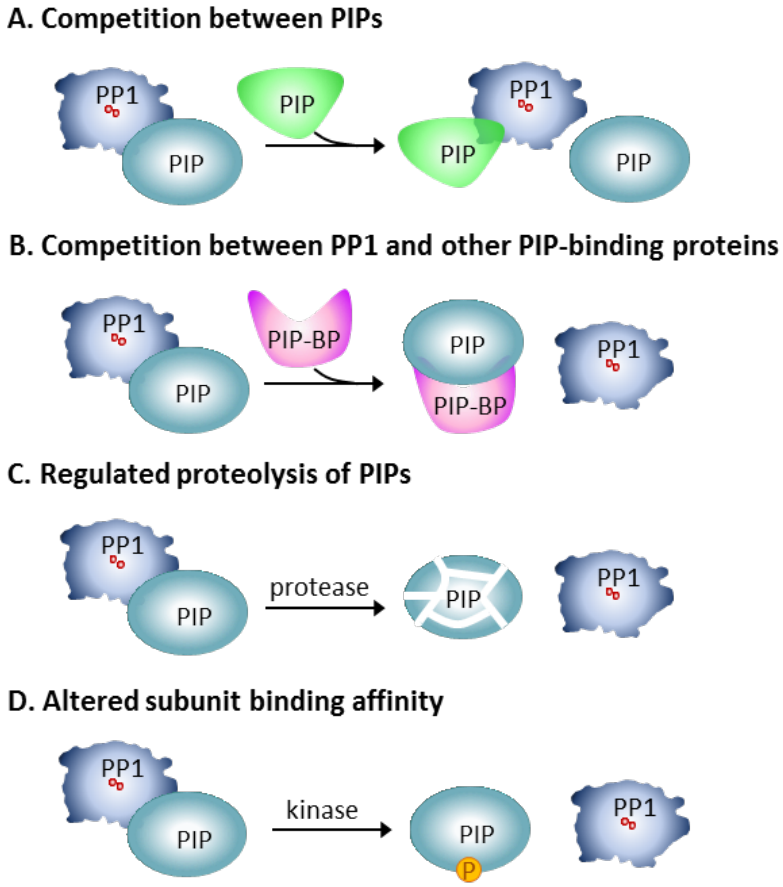


**Figure 4: Regulation of PP1 holoenzyme abundance.** The concentration of PP1 holoenzymes is regulated by different mechanisms. (A) PIPs compete with each other for binding to PP1. (B) PP1 can compete with other PIP-binding proteins (PIP-BPs) for binding to PIPs. (C) The cellular abundance of PIPs can be modulated post-translationally by proteolysis. (D) The binding affinity of PIPs for PP1 is regulated by phosphorylation (P).

## 2.7 Acute activity regulation of PP1 holoenzymes

Most if not all PP1-PIP complexes, similar to the PPP-phosphatases PP2B and PP5 [9,57], are (largely) inactive under basal circumstances. Phosphatase assays have indeed revealed that a majority of bacterially expressed PP1-anchoring domains are inhibitory [40]. In addition, many PIPs also have a PP1-regulatory domain that is inhibitory under basal conditions [18,19]. Furthermore, at least some PP1-holoenzymes can recruit inhibitory proteins (e.g. Inhibitor-1, CPI-17) as a second regulatory subunit [58–60]. If PP1-PIP

complexes are mostly kept inactive in the cell, specific signaling mechanisms must exist for their transient and controlled (in)activation. It indeed appears that multiple, holoenzyme-specific strategies have evolved for acute phosphatase activity regulation (Figure 5), although the underlying molecular mechanisms are often still poorly understood.

Some PP1 holoenzymes are activated by the (de)phosphorylation-regulated release of an inhibitory subunit (e.g. CPI-17 [35]) or dissociation of an inhibitory SLiM (e.g. NIPP1 [19]) (Figures 5A and 5B). Other holoenzymes are activated by the transfer of PP1 from an inhibitory to an activatory PIP within the same complex. For example, the dephosphorylation of protein kinase Raf by the SHOC2-PP1-SCRIB complex is regulated by internal competition between the inhibitory SCRIB and activatory SHOC2 for binding to PP1 [61] (Figure 5C). Activation of PP1-PNUTS requires both its recruitment to target genes via non coding RNAs and the reversal of PP1 inhibition through binding of PNUTS to acetylated histones [62]. Other (in)activation mechanisms target the catalytic subunit itself. GADD34 can recruit the NADPH oxidase 4, which inhibits GADD34-associated PP1 via oxidation of active site metal(s) [63]. It is not clear whether such oxidation is reversible but if it is, this would be an elegant mechanism for acute activity regulation. In addition to metal oxidation, metal (un)loading by Inhibitor-2 may also represent an efficient mechanism for the transient (in)activation of PP1 holoenzymes [22], (Figure 5D). Finally, the inhibitory phosphorylation of the C-terminus of PP1 by cyclin-dependent kinases can be reversed by autodephosphorylation, which appears to be modulated by Inhibitor-2 [64] (Figure 5E).

Another type of PP1 holoenzyme regulation concerns substrate recruitment. Phosphorylation of PIPs has been associated with an altered substrate binding affinity (e.g. binding of phospholamban to glycogen-targeting $G_M$ in heart [65]) (Figure 5F). Sometimes substrate recruitment depends on covalent modifications or allosteric regulation of the substrates themselves. For example, the FHA domain of NIPP1 only binds substrates for dephosphorylation by associated PP1 when they are phosphorylated on a threonine that is followed by a proline ([66], Figure 5G). The recruitment of the glycogen-degrading enzyme phosphorylase *a* by the liver-specific PP1-$G_L$ phosphatase is enhanced by the glucose-induced acetylation of phosphorylase *a*, which increases its affinity for the substrate-binding site of $G_L$ [67]. Interestingly, the $G_L$ subunit also has a second, higher-affinity binding site for phosphorylase *a* and the occupation of this site allosterically prevents the dephosphorylation (and activation) of glycogen synthase by PP1-$G_L$ [68]. This

substrate-level control mechanism serves to prevent glycogen synthesis as long as the glycogenolytic phosphorylase *a* is present. Yet another mechanism of substrate-recruitment regulation relates to conformational changes within a pre-existing complex. For example, ligand binding to the NMDA-receptor complex induces conformational changes that bring PP1 within reach of its substrate protein kinase CaMKII ([69], Figure 5H).

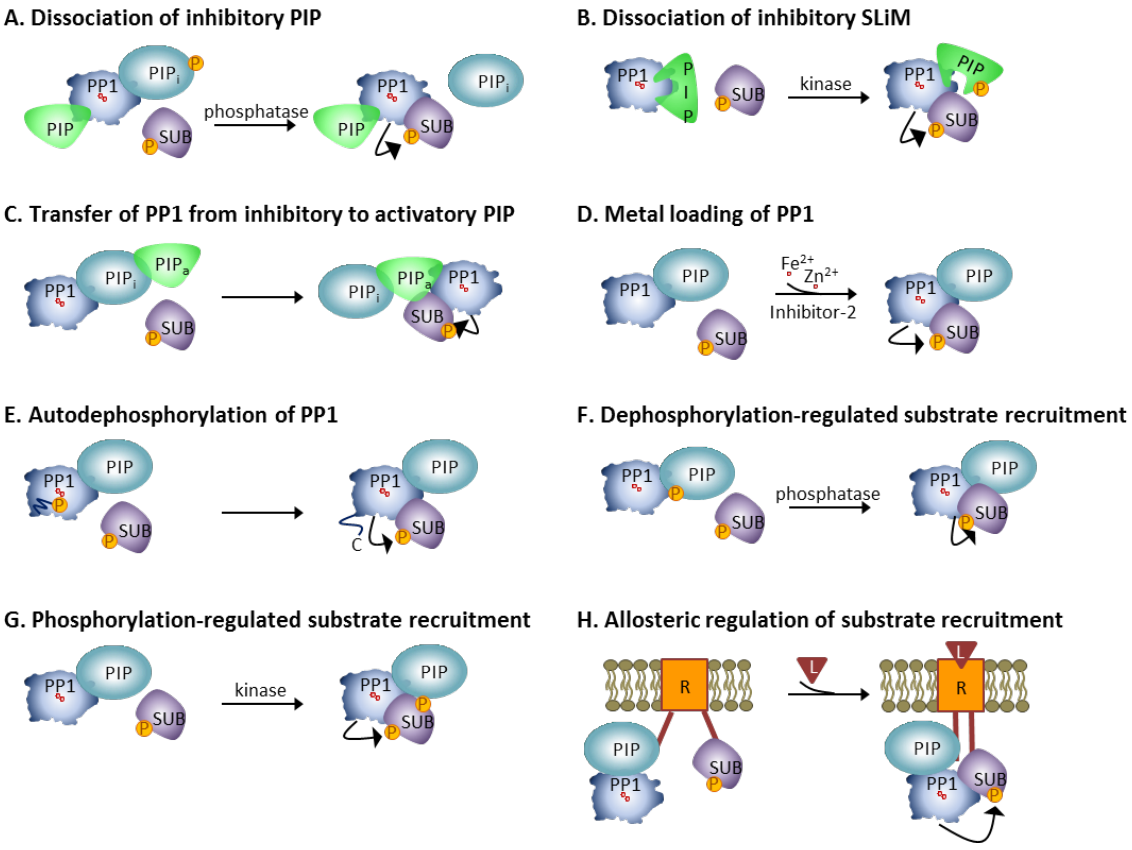


**Figure 5: Activation mechanisms of PP1 holoenzymes.** Different modes of PP1 holoenzyme activation are depicted. (A) Dephosphorylation of an inhibitory PIP causes its dissociation and activation of a PP1 holoenzyme. (B) Phosphorylation-dependent dissociation of an inhibitory SLiM activates a PP1-complex. (C) A PP1 holoenzyme can be activated by transfer of PP1 from an inhibitory to an activatory PIP. (D, E) Targeting of the catalytic subunit of PP1 itself can modulate activation, e.g. by metal loading of PP1 (D) or by autodephosphorylation of an inhibitory site in the C-terminus of PP1 (E). (F) The phosphorylation state of PIPs determines their binding affinity for substrates. (G) Substrate recruitment can depend on its prior phosphorylation state. (H) Ligand binding to a receptor complex can induce conformational changes that brings PP1 within reach of its substrate. P, phosphorylation; SUB, substrate; i, inhibitory; a, activatory; R, receptor; L, ligand.

## 2.8 Conclusions

The ubiquitous expression and low *in vitro* substrate specificity of PP1 originally led to the widespread belief that it is a constitutively active phosphatase that only serves to end kinase signaling. This is clearly a misconception as it is now firmly established that PP1 forms stable complexes with a large variety of PIPs that direct the phosphatase to a small subset of substrates and tightly regulate its activity. PP1 holoenzymes have turned out to be as specific and tightly regulated as any protein kinase. Recently acquired insights in PP1-PIP interaction modes and mechanisms of activity regulation and substrate recruitment offer exciting perspectives for the development of PP1-holoenzyme specific small-molecule inhibitors or activators that can be used therapeutically. Once named an ugly duckling [70], PP1 has truly become a beautiful swan.

## 2.9 References


1. Bollen M, Peti W, Ragusa MJ, Beullens M. (2010) The extended PP1 toolkit: Designed to create specificity. Trends Biochem. Sci. 35, 450–458.
2. Choy MS, Page R, Peti W. (2012) Regulation of protein phosphatase 1 by intrinsically disordered proteins. Biochem. Soc. Trans. 40, 969–74.
3. Heroes E, Lesage B, Görnemann J, Beullens M, Van Meervelt L, Bollen M. (2013) The PP1 binding code: A molecular-lego strategy that governs specificity. FEBS J. 280, 584–595.
4. Lad C, Williams NH, Wolfenden R. (2003) The rate of hydrolysis of phosphomonoester dianions and the exceptional catalytic proficiencies of protein and inositol phosphatases. Proc. Natl. Acad. Sci. U. S. A. 100, 5607–5610.
5. Gibbons JA, Kozubowski L, Tatchell K, Shenolikar S. (2007) Expression of human protein phosphatase-1 in Saccharomyces cerevisiae highlights the role of phosphatase isoforms in regulating eukaryotic functions. J. Biol. Chem. 282, 21838–21847.
6. Lundberg E, Fagerberg L, Klevebring D, Matic I, Geiger T, Cox J, et al. (2010) Defining the transcriptome and proteome in three functionally different human cell lines. Mol. Syst. Biol. 6, 450.
7. Nagaraj N, Wisniewski JR, Geiger T, Cox J, Kircher M, Kelso J, et al. (2011) Deep proteome and transcriptome mapping of a human cancer cell line. Mol. Syst. Biol. 7, 548.
8. Ceulemans H, Bollen M. (2004) Functional diversity of protein phosphatase-1, a cellular economizer and reset button. Physiol. Rev. 84, 1–39.
9. Oberoi J, Dunn DM, Woodford MR, Mariotti L, Schulman J, Bourboulia D, et al. (2016) Structural and functional basis of protein phosphatase 5 substrate specificity. Proc. Natl. Acad. Sci. U. S. A. 113, 9009–14.
10. Chatterjee J, Beullens M, Sukackaite R, Qian J, Lesage B, Hart DJ, et al. (2012) Development of a peptide that selectively activates protein phosphatase-1 in living cells. Angew. Chemie - Int. Ed. 51, 10054–10059.
11. Terrak M, Kerff F, Langsetmo K, Tao T, Dominguez R. (2004) Structural basis of protein phosphatase 1 regulation. Nature 429, 780–4.
12. Ragusa MJ, Dancheck B, Critton DA, Nairn AC, Page R, Peti W. (2010) Spinophilin directs protein phosphatase 1 specificity by blocking substrate binding sites. Nat. Struct. 38; Mol. Biol. 17, 459–464.
13. O'Connell N, Nichols SR, Heroes E, Beullens M, Bollen M, Peti W, et al. (2012) The molecular basis for substrate specificity of the nuclear NIPP1:PP1 holoenzyme. Structure. 20, 1746–1756.

14. Choy MS, Hieke M, Kumar GS, Lewis GR, Gonzalez-Dewhitt KR, Kessler RP, et al. (2014) Understanding the antagonism of retinoblastoma protein dephosphorylation by PNUTS provides insights into the PP1 regulatory code. Proc. Natl. Acad. Sci. U. S. A. 1–6.
15. Choy MS, Yusoff P, Lee IC, Newton JC, Goh CW, Page R, et al. (2015) Structural and Functional Analysis of the GADD34:PP1 eIF2α Phosphatase. 2015.
16. Kumar GS, Gokhan E, De Munter S, Bollen M, Vagnarelli P, Peti W, et al. (2016) The Ki-67 and RepoMan mitotic phosphatases assemble via an identical, yet novel mechanism. Elife 5, 450–458.
17. Bollen M. (2001) Combinatorial control of protein phosphatase-1. Trends Biochem. Sci. 26, 426–431.
18. Endo S, Zhou X, Connor J, Wang B, Shenolikar S. (1996) Multiple structural elements define the specificity of recombinant human inhibitor-1 as a protein phosphatase-1 inhibitor. Biochemistry. 35, 5220–5228.
19. Beullens M, Vulsteke V, Van Eynde A, Jagiello I, Stalmans W, Bollen M. (2000) The C-terminus of NIPP1 (nuclear inhibitor of protein phosphatase-1) contains a novel binding site for protein phosphatase-1 that is controlled by tyrosine phosphorylation and RNA binding. Biochem. J. 352 Pt 3, 651–8.
20. Ceulemans H, Vulsteke V, De Maeyer M, Tatchell K, Stalmans W, Bollen M. (2002) Binding of the concave surface of the Sds22 superhelix to the α4/α5/α6-triangle of protein phosphatase-1. J. Biol. Chem. 277, 47331–47337.
21. Heroes E, Rip J, Beullens M, Van Meervelt L, De Gendt S, Bollen M. (2015) Metals in the active site of native protein phosphatase-1. J. Inorg. Biochem. 149, 1–5.
22. Bollen M, Stalmans W. (1992) The structure, role, and regulation of type 1 protein phosphatases. Crit. Rev. Biochem. Mol. Biol. 27, 227–281.
23. Cheng Y-L, Chen R-H. (2015) Assembly and quality control of the protein phosphatase 1 holoenzyme involves the Cdc48-Shp1 chaperone. J. Cell Sci. 128, 1180–92.
24. Lesage B, Beullens M, Pedelini L, Garcia-Gimeno MA, Waelkens E, Sanz P, et al. (2007) A complex of catalytically inactive protein phosphatase-1 sandwiched between Sds22 and inhibitor-3. Biochemistry. 46, 8909–8919.
25. Pedelini L, Marquina M, Ariño J, Casamayor A, Sanz L, Bollen M, et al. (2007) YPI1 and SDS22 proteins regulate the nuclear localization and function of yeast type 1 phosphatase Glc7. J. Biol. Chem. 282, 3282–3292.
26. Eiteneuer A, Seiler J, Weith M, Beullens M, Lesage B, Krenn V, et al. (2014) Inhibitor-3 ensures bipolar mitotic spindle attachment by limiting association of SDS22 with kinetochore-bound protein phosphatase-1. EMBO J. 33, 2704–2720.
27. Hurley TD, Yang J, Zhang L, Goodwin KD, Zou Q, Cortese M, et al. (2007) Structural basis for regulation of protein phosphatase 1 by inhibitor-2. J. Biol. Chem. 282, 28874–83.
28. Ceulemans H, Stalmans W, Bollen M. (2002) Regulator-driven functional diversification of protein phosphatase-1 in eukaryotic evolution. BioEssays. 24, 371–381.
29. Smetana JHC, Zanchin NIT. (2007) Interaction analysis of the heterotrimer formed by the phosphatase 2A catalytic subunit, α4 and the mammalian ortholog of yeast Tip41 (TIPRL). FEBS J. 274, 5891–5904.
30. Sents W, Ivanova E, Lambrecht C, Haesen D, Janssens V. (2013) The biogenesis of active protein phosphatase 2A holoenzymes: A tightly regulated process creating phosphatase specificity. FEBS J. 280, 644–661.
31. Jiang L, Stanevich V, Satyshur K a, Kong M, Watkins GR, Wadzinski BE, et al. (2013) Structural basis of protein phosphatase 2A stable latency. Nat. Commun. 4, 1699.
32. Scorsato V, Lima TB, Righetto GL, Zanchin NIT, Brandão-Neto J, Sandy J, et al. (2016) Crystal structure of the human Tip41 orthologue, TIPRL, reveals a novel fold and a binding site for the PP2Ac C-terminus. Sci. Rep. 6, 30813.
33. Guo F, Stanevich V, Wlodarchak N, Sengupta R, Jiang L, Satyshur K a, et al. (2014) Structural basis of PP2A activation by PTPA, an ATP-dependent activation chaperone. Cell Res. 24, 190–203.
34. Khromov A, Choudhury N, Stevenson AS, Somiyo A V., Eto M. (2009) Phosphorylation-dependent autoinhibition of myosin light chain phosphatase accounts for Ca2+ sensitization

force of smooth muscle contraction. J. Biol. Chem. 284, 21569–21579.
35. Matsuzawa F, Aikawa SI, Ohki SY, Eto M. (2005) Phospho-pivot modeling predicts specific interactions of protein phosphatase-1 with a phospho-inhibitor protein CPI-17. J. Biochem. 137, 633–641.
36. Rojas M, Vasconcelos G, Dever TE. (2015) An eIF2α-binding motif in protein phosphatase 1 subunit GADD34 and its viral orthologs is required to promote dephosphorylation of eIF2α. Proc. Natl. Acad. Sci. U. S. A. 112, E3466-75.
37. Jagiello I, Van Eynde a, Vulsteke V, Beullens M, Boudrez a, Keppens S, et al. (2000) Nuclear and subnuclear targeting sequences of the protein phosphatase-1 regulator NIPP1. J. Cell Sci. 113 Pt 21, 3761–3768.
38. Zhou W, Brush MH, Choy MS, Shenolikar S. (2011) Association with endoplasmic reticulum promotes proteasomal degradation of GADD34 protein. J. Biol. Chem. 286, 21687–21696.
39. Trinkle-Mulcahy L, Sleeman JE, Lamond a I. (2001) Dynamic targeting of protein phosphatase 1 within the nuclei of living mammalian cells. J. Cell Sci. 114, 4219–4228.
40. Hendrickx A, Beullens M, Ceulemans H, Den Abt T, Van Eynde A, Nicolaescu E, et al. (2009) Docking Motif-Guided Mapping of the Interactome of Protein Phosphatase-1. Chem. Biol. 16, 365–371.
41. Winkler C, Munter S De, Dessel N Van, Lesage B, Heroes E. (2015) The selective inhibition of protein phosphatase-1 results in mitotic catastrophe and impaired tumor growth. J. Cell Sci. 128, 4526–4537.
42. Davis ME, Wang MK, Rennick LJ, Full F, Gableske S, Mesman AW, et al. (2014) Antagonism of the phosphatase PP1 by the measles virus v protein is required for innate immune escape of MDA5. Cell Host Microbe. 16, 19–30.
43. Wu H, Wei L, Fan F, Ji S, Zhang S, Geng J, et al. (2015) Integration of Hippo signalling and the unfolded protein response to restrain liver overgrowth and tumorigenesis. Nat. Commun. 6, 6239.
44. Hirschi A, Cecchini M, Steinhardt RC, Schamber MR, Dick F a, Rubin SM. (2010) An overlapping kinase and phosphatase docking site regulates activity of the retinoblastoma protein. Nat. Struct. Mol. Biol. 17, 1051–7.
45. Ma P, Foote DC, Sinnamon AJ, Brass LF. (2015) Dissociation of SHP-1 from spinophilin during platelet activation exposes an inhibitory binding site for Protein Phosphatase-1 (PP1). PLoS One. 10.
46. Dohadwala M, da Cruz e Silva EF, Hall FL, Williams RT, Carbonaro-Hall DA, Nairn AC, et al. (1994) Phosphorylation and inactivation of protein phosphatase 1 by cyclin-dependent kinases. Proc Natl Acad Sci U S A. 91, 6408–6412.
47. Nigavekar SS, Tan YSH, Cannon JF. (2002) Glc8 is a glucose-repressible activator of Glc7 protein phosphatase-1. Arch. Biochem. Biophys. 404, 71–79.
48. Kelsall IR, Voss M, Munro S, Cuthbertson DJR, Cohen PTW. (2011) R3F, a novel membrane-associated glycogen targeting subunit of protein phosphatase 1 regulates glycogen synthase in astrocytoma cells in response to glucose and extracellular signals. J. Neurochem. 118, 596–610.
49. Fisher LA, Wang L, Wu L, Peng A. (2014) Phosphatase 1 nuclear targeting subunit is an essential regulator of M-phase entry, maintenance, and exit. J. Biol. Chem. 289, 23745–23752.
50. Huang HS, Lee EYC. (2008) Protein phosphatase-1 inhibitor-3 is an in vivo target of caspase-3 and participates in the apoptotic response. J. Biol. Chem. 283, 18135–18146.
51. Twomey E, Li Y, Lei J, Sodja C, Ribecco-Lutkiewicz M, Smith B, et al. (2010) Regulation of MYPT1 stability by the E3 ubiquitin ligase SIAH2. Exp. Cell Res. 316, 68–77.
52. Rubio-Villena C, Sanz P, Garcia-Gimeno MA. (2015) Structure-Function Analysis of PPP1R3D, a Protein Phosphatase 1 Targeting Subunit, Reveals a Binding Motif for 14-3-3 Proteins which Regulates its Glycogenic Properties. PLoS One 10, e0131476.
53. Kim Y, Holland AJ, Lan W, Cleveland DW. (2010) Aurora kinases and protein phosphatase 1 mediate chromosome congression through regulation of CENP-E. Cell. 142, 444–455.
54. Nijenhuis W, Vallardi G, Teixeira A, Kops GJPL, Saurin AT. (2014) Negative feedback at kinetochores underlies a responsive spindle checkpoint signal. Nature 16, 1257–1264.
55. Qian J, Beullens M, Huang J, De Munter S, Lesage B, Bollen M. (2015) Cdk1 orders mitotic

events through coordination of a chromosome-associated phosphatase switch. Nat. Commun. 6, 10215.
56. Sivakumar S, Janczyk P, Qu Q, Brautigam CA, Stukenberg PT, Yu H, et al. (2016) The human SKA complex drives the metaphase-anaphase cell cycle transition by recruiting protein phosphatase 1 to kinetochores. Elife. 5.
57. Roy J, Cyert MS. (2009) Cracking the phosphatase code: docking interactions determine substrate specificity. Sci. Signal. 2, re9.
58. Connor JH, Weiser DC, Li S, Hallenbeck JM, Shenolikar S. (2001) Growth arrest and DNA damage-inducible protein GADD34 assembles a novel signaling complex containing protein phosphatase 1 and inhibitor 1. Mol. Cell. Biol. 21, 6841–50.
59. Eto M. (2009) Regulation of cellular protein phosphatase-1 (PP1) by phosphorylation of the CPI-17 family, C-kinase-activated PP1 Inhibitors. J. Biol. Chem. 284, 35273–35277.
60. Mesman AW, Zijlstra-Willems EM, Kaptein TM, De Swart RL, Davis ME, Ludlow M, et al. (2014) Measles virus suppresses RIG-I-like receptor activation in dendritic cells via DC-SIGN-mediated inhibition of PP1 phosphatases. Cell Host Microbe. 16, 31–42.
61. Young LC, Hartig N, Muñoz-Alegre M, Oses-Prieto JA, Durdu S, Bender S, et al. (2013) An MRAS, SHOC2, and SCRIB complex coordinates erk pathway activation with polarity and tumorigenic growth. Mol. Cell. 52, 679–692.
62. Xing Z, Lin A, Li C, Liang K, Wang S, Liu Y, et al. (2014) LncRNA directs cooperative epigenetic regulation downstream of chemokine signals. Cell. 159, 1110–1125.
63. Santos CX, Hafstad AD, Beretta M, Zhang M, Molenaar C, Kopec J, et al. (2016) Targeted redox inhibition of protein phosphatase 1 by Nox4 regulates eIF2α-mediated stress signaling. EMBO J. 35, 319–34.
64. Hou H, Sun L, Siddoway BA, Petralia RS, Yang H, Gu H, et al. (2013) Synaptic NMDA receptor stimulation activates PP1 by inhibiting its phosphorylation by Cdk5. J. Cell Biol. 203, 521–535.
65. Vafiadaki E, Arvanitis DA, Sanoudou D, Kranias EG. (2013) Identification of a protein phosphatase-1/phospholamban complex that is regulated by cAMP-dependent phosphorylation. PLoS One. 8.
66. Minnebo N, Görnemann J, O'Connell N, Van Dessel N, Derua R, Vermunt MW, et al. (2013) NIPP1 maintains EZH2 phosphorylation and promoter occupancy at proliferation-related target genes. Nucleic Acids Res. 41, 842–854.
67. Zhang T, Wang S, Lin Y, Xu W, Ye D, Xiong Y, et al. (2012) Acetylation negatively regulates glycogen phosphorylase by recruiting protein phosphatase 1. Cell Metab. 15, 75–87.
68. Kelsall IR, Rosenzweig D, Cohen PTW. (2009) Disruption of the allosteric phosphorylase a regulation of the hepatic glycogen-targeted protein phosphatase 1 improves glucose tolerance in vivo. Cell. Signal. 21, 1123–1134.
69. Aow J, Dore K, Malinow R. (2015) Conformational signaling required for synaptic plasticity by the NMDA receptor complex. Proc. Natl. Acad. Sci. U. S. A. 112, 14711–6.
70. Brautigan DL. (2013) Protein Ser/ Thr phosphatases - The ugly ducklings of cell signalling. FEBS J. 280, 324–345.

# CHAPTER 3

# Aims and Strategies

The scaffold protein NIPP1 is ubiquitously expressed in eukaryotic cells and is one of the most ancient regulators of protein phosphatase PP1. Initial *in vitro* and cell-based studies revealed that the central domain of NIPP1 is an inhibitor of PP1 towards a subset of substrates. Besides PP1, several other NIPP1 interacting partners have been identified, suggesting that it is a multifunctional protein implicated in processes as diverse as transcription, pre-mRNA splicing and DNA replication. The role of NIPP1 in transcription is at least partially mediated by its ability to interact with the Polycomb group proteins EZH2 and EED. EZH2 binds to the N-terminal ForkHead-associated (FHA) domain of NIPP1 as a substrate for dephosphorylation by associated PP1. EED binds to the central and C-terminal domains of NIPP1. The latter domain also harbors RNA-binding and an additional PP1-inhibitory site.

At the start of my research project, it was already known that NIPP1 is essential during early embryonic development and cell proliferation. Indeed, NIPP1-null embryos die at the onset of gastrulation, resembling the phenotype observed in EZH2- or EED-null embryos. This precluded further exploration of the postnatal *in vivo* functions of NIPP1. Therefore, the main objective of my thesis was to **generate and phenotype an inducible NIPP1 knockout (iKO) mouse model**. Since of all the examined tissues the deletion of NIPP1 was only efficient in testis, I further focused the phenotyping on neonatal and adult testis where NIPP1 is abundantly expressed in all cell types except elongated spermatids and spermatozoa.

In Chapter 4, entitled 'Protein phosphatase PP1-NIPP1 maintains spermatogonia through stabilization of the Polycomb Repressive Complex 2' the postnatal function of NIPP1 in testis was explored by generating and phenotyping an inducible NIPP1 knockout mouse model. This model was based on the use of a tamoxifen-dependent Cre recombinase. Histological and histochemical analysis of the testis at several stages of development disclosed a likely function for NIPP1 in the survival of germ cells, including (un)differentiated spermatogonia.

To examine if the phenotype could be an extrinsic defect, we have investigated the contribution of Sertoli cells, which normally provide a sustentacular microenvironment (niche) for spermatogonia. These studies were complemented with proliferation assays performed in organotypic testis cultures. Next, we evaluated the effect of the deletion of NIPP1 on GFRA1$^{+}$-enriched cultures of undifferentiated spermatogonia, using

proliferation and viability assays. These studies revealed that the loss of germ cells was an intrinsic defect caused by the loss of NIPP1 from germ cells.

Additional experiments were performed to shed light on the molecular mechanism underlying the observed phenotype. First, we investigated by RNA sequencing and chromatin immunoprecipitation (ChIP) assays the effect of deletion of NIPP1 on EZH2-mediated gene silencing in testis. Second, immunohistological and biochemical studies were performed to examine whether the PP1-dependent phosphorylation status of EZH2 was compromised in the iKO spermatogonia. Finally, we evaluated whether the phenotype could be mimicked in organotypic testis cultures by the chemical inhibition of the EZH core components of the PRC2 complex. The data indicated that the observed phenotype is caused by the hyperphosphorylation of EZH2, resulting in its proteasomal degradation and the subsequent loss of associated regulatory subunits.

# CHAPTER 4

# Results

# Protein phosphatase PP1-NIPP1 maintains spermatogonia through stabilization of the Polycomb Repressive Complex 2

These results are part of:

**Mónica Ferreira**[1,2], Shannah Boens[1], Claudia Winkler[1], Kathelijne Szekér[1], Iris Verbinnen[1], Aleyde Van Eynde[1], Margarida Fardilha[2] and Mathieu Bollen[1]. The protein phosphatase 1 regulator NIPP1 is essential for mammalian spermatogenesis. *Scientific Reports*. 2017; 7:13364.

[1]Laboratory of Biosignaling & Therapeutics, KU Leuven Department of Cellular and Molecular Medicine, University of Leuven, Leuven, Belgium.
[2]Institute for Research in Biomedicine-iBiMED, Health Sciences Department, University of Aveiro, Aveiro, Portugal.

**Personal contribution:**

First author: all data/figures presented

## 4.1 Abstract

The Polycomb Repressive Complex 2 (PRC2) is required for spermatogonial stem-cell maintenance because it suppresses inappropriate gene expression via trimethylation of histone H3 at Lys27 (H3K27me3). Enhancer of zeste homolog 2 (EZH2), the canonical catalytic subunit of the PRC2 complex, is a substrate for phosphorylation by cyclin-dependent kinases 1/2 (CDK1/2) and dephosphorylation by protein phosphatase 1 (PP1). EZH2 also binds directly to NIPP1, a nuclear regulator of PP1, but the biological relevance of this interaction is not clear because NIPP1 has properties of both an inhibitor and facilitator of dephosphorylation by PP1. To study the *in vivo* function of NIPP1 we have generated an inducible knockout model. Here we show that the postnatal deletion of NIPP1 in mouse testis results in a decreased proliferation and survival capacity of (un)differentiated spermatogonia and meiotic spermatocytes, culminating within a couple of months in a Sertoli cells-only phenotype. The development of this phenotype is preceded by the proteasomal degradation of EZH2 and an associated loss of other PRC2 core components, resulting in a decreased trimethylation of H3K27 at target loci. Consistent with a contribution of PRC2 malfunction to the NIPP1 deletion phenotype, we find that it can be phenocopied by the chemical inhibition of H3K27 trimethylation. Mechanistically, the loss of NIPP1 destabilizes EZH2 due to a deficient dephosphorylation of CDK sites (Thr345 and Thr487) by PP1. Accordingly, non-phosphorylatable EZH2 mutants have a prolonged lifetime in spermatogonia. Our results show that NIPP1 is key regulator of PRC2 stability and the maintenance of male germ cells, at least in part because it controls the timely dephosphorylation of EZH2 at CDK sites by associated PP1.

**Keywords:** EZH2, NIPP1, Polycomb Group Proteins, Protein Phosphatase 1, Proliferation, Spermatogonia.

## 4.2 Introduction

Continuous sperm production in adult males depends on a tight balance between the proliferation and differentiation of undifferentiated spermatogonia [1,2]. Spermatogonial stem cells (SSCs) divide to generate more stem cells (self-renewal) or progeny committed to differentiate into primary spermatocytes. The latter cells undergo a first meiotic division to form secondary spermatocytes, which rapidly enter the second meiotic division to produce spermatids. Finally, spermatids develop into spermatozoa during a differentiation process that involves major morphological changes. The postnatal proliferation and differentiation of spermatogonia is epigenetically controlled, mainly through DNA methylation and covalent histone modifications [3–6]. This implies a tight regulation of the concentration, chromatin targeting and catalytic activity of DNA- and histone-modifying enzymes.

The key epigenetic regulators of self-renewal and differentiation in spermatogonia of postnatal testis are still poorly defined [6–9]. One notable exception is the Polycomb Repressive Complex 2 (PRC2), which is essential for the maintenance of male germ cells [10,11]. The PRC2 complex contributes to the transcriptional silencing of Polycomb group (PcG) target genes, which control pluripotency, cell proliferation and differentiation [12,13]. EZH (enhancer of zeste homolog) proteins, i.e. EZH1 and EZH2, function as mutually exclusive catalytic subunits of the PRC2 complex and trimethylate histone H3 at Lys27 (H3K27me3). EZH2 appears to be the major H3K27 methyltransferase but its loss in some cell types can be compensated for by EZH1 [11]. The non-catalytic PRC2 core components comprise SUZ12 (suppressor of zeste 12 homolog), EED (embryonic ectoderm development), and RBAP48 (retinoblastoma associated protein 48), which all promote methylation by EZH2. PRC2 represses the transcription of PcG targets mainly because the deposited H3K27me3 hampers the recruitment of ATP-dependent chromatin-remodeling complexes and RNA polymerase II [12–14].

In cultured cells PRC2-mediated gene silencing is antagonistically regulated by cyclin-dependent kinases 1/2 (CDK1/2) and protein phosphatase 1 (PP1), which (de)phosphorylate EZH2 at Thr345, Thr416 and Thr487 (mouse residues used throughout this manuscript) [15–18]. Phosphorylation at Thr345 increases the targeting of EZH2 to chromatin, resulting in enhanced H3K27 trimethylation of target loci [15,16]. EZH2 phosphorylation at Thr487 (and Thr345) is linked to its proteasomal degradation in late mitosis [19]. Thr487 phosphorylation has been reported to disrupt the interaction of EZH2

with other PRC2 components [20], but this is not a general finding [16]. Anyhow, free EZH2 is ubiquitinated by the SCF-type E3-ubiquitin ligase ß-TrCP (FBXW1), in particular when it is also phosphorylated by Jak2 at Tyr641, leading to its proteasomal degradation [21]. Finally, the CDK-mediated phosphorylation of EZH2 at Thr416 creates a docking site for NIPP1 (nuclear inhibitor of PP1), which transiently inhibits the dephosphorylation of CDK sites by PRC2-associated PP1 [17]. The essential role of NIPP1 in PRC2 signaling is also underscored by other studies. Thus, NIPP1 has independent interaction sites for both EZH2 and EED [17,22], and acts as a transcriptional repressor in a PRC2-dependent dependent manner [22,23]. In addition, NIPP1 binds to a subset of PcG target genes and promotes the association of EZH2 with proliferation-related target genes [17,24,25].

NIPP1, encoded by *Ppp1r8*, is one of nearly 200 known vertebrate regulators of PP1 [26]. It is a nuclear protein of 38 kDa and consists of an N-terminal ForkHead-associated (FHA) domain, a central PP1-anchoring domain and a C-terminal PP1-inhibitory domain. The FHA domain has a phosphate-binding loop that binds proteins, including EZH2, that are phosphorylated on specific phospho-Thr-Pro (pTP) dipeptide motifs by CDKs [17]. Purified NIPP1 is a potent inhibitor of PP1 towards all tested substrates, including FHA ligands. However, the deletion or allosteric removal of the C-terminal PP1-inhibitory domain allows the dephosphorylation of FHA ligands by NIPP1-associated PP1 [27–29]. The trigger and molecular details of this allosteric 'de-inhibition' mechanism are poorly understood but preliminary data suggest that it involves C-terminal phosphorylation and RNA binding [27]. Collectively, these data strongly suggest that NIPP1 inhibits associated PP1 but is also required to allow the timely dephosphorylation of FHA-ligands.

The genetic deletion of NIPP1 in mice is early embryonic lethal [30]. To study the postnatal functions of NIPP1 we have generated an inducible knockout model. Here, we show that the knockout of NIPP1 in mouse testis causes the hyperphosphorylation of EZH2 at CDK sites, confirming that NIPP1 is not only a PP1 inhibitor but is also required for the timely dephosphorylation of EZH2 by PP1. Hyperphosphorylated EZH2 is targeted for proteasomal degradation, which is associated with a diminished proliferation and survival potential of (un)differentiated spermatogonia, eventually leading to the total loss of germ cells. Our data identify PP1-NIPP1 as a key regulator of PRC2 signaling and spermatogenesis.

# 4.3 Results

## 4.3.1 Generation of an inducible NIPP1-knockout model

To study the postnatal functions of NIPP1 we developed an *in vivo* model for the inducible inactivation of *Ppp1r8*. Mice with floxed *Ppp1r8* alleles (*Ppp1r8*$^{fl/fl}$) were crossed with transgenic mice expressing tamoxifen-activated CRE-ERT2 recombinase under control of the Ubiquitin C (UBC) promotor (Figure S1A-C) [31]. Offspring with the *UBC-Cre-ERT2*$^{+/-}$; *Ppp1r8*$^{fl/+}$ genotype was crossed with heterozygous mice (*Ppp1r8*$^{+/-}$). The resulting *UBC-Cre-ERT2*$^{+/-}$; *Ppp1r8*$^{fl/-}$ mice were used as tamoxifen-inducible NIPP1 knockouts or iKOs (Figure 1A, Figure S1A-C). Since the deletion of one *Ppp1r8* allele does not affect the expression level of NIPP1 [30], the heterozygous *UBC-Cre-ERT2*$^{+/-}$; *Ppp1r8*$^{fl/+}$ mice were used as controls (CTRs). The adopted knockout strategy avoids phenotypic artefacts induced by CRE recombinase because one *Ppp1r8* allele is inactivated by recombination in both the CTRs and iKOs [32].

Following 4 consecutive tamoxifen injections at the age of 4 weeks, the CTR and iKO mice were sacrificed 2-16 weeks later (Figure 1B). The iKO mice appeared healthy and showed a normal growth (Figure S1D). In fact, the only macroscopic phenotype in the male iKOs was a gradually developing smaller testis size (Figure 1C and D). This correlated with a loss of NIPP1 from the testis, as shown by both immunohistochemistry (Figure 1C) and immunoblotting (Figure 1E and F). At the age of 12 weeks the expression level of NIPP1 in the iKO testes was reduced by ~80%, as compared to that in CTR mice. The remaining NIPP1 in the iKOs was mainly expressed in interstitial cells (Figure 1C). We confirmed that the expression level of NIPP1 in testis from wild-type and *Ppp1r8*$^{+/-}$ mice was about the same (Figure S1E and F), justifying the use of heterozygotes as controls. Remarkably, in the accessory sex glands (seminal vesicles and agglutination glands) and the epididymis, a depletion of NIPP1 was only detected in limited histological areas and this had no effect on the histological organization and size of these glands (Figure S2).

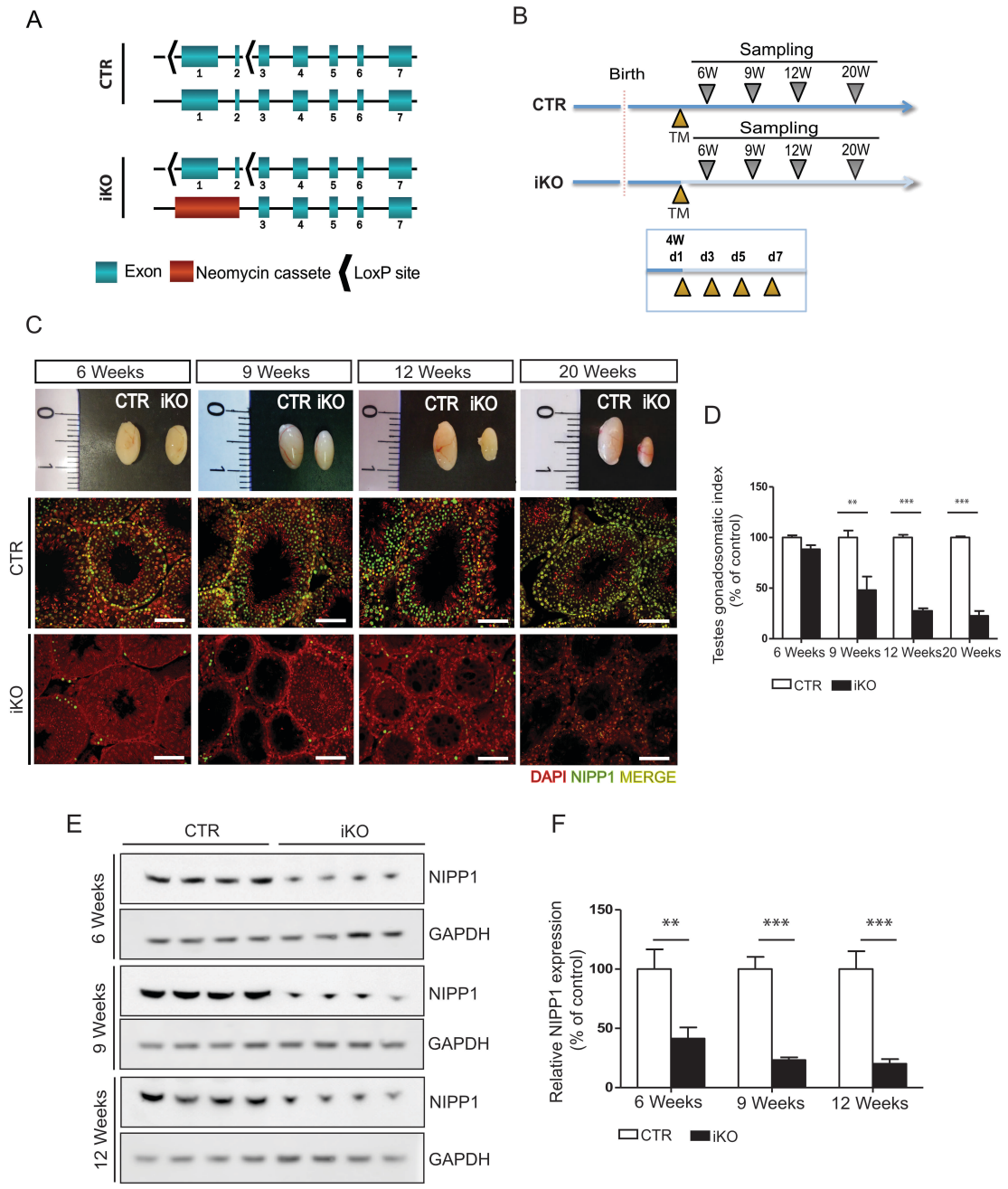


**Figure 1. The postnatal inactivation of *Ppp1r8* causes a reduced testis size.** (A) *Ppp1r8* alleles in control (CTR) and inducible NIPP1 knockout (iKO) mice. The exon numbers are indicated. (B) CTR and iKO mice express CRE-ERT2 recombinase under control of the UBC promoter (UBC-Cre-ERT2). Scheme of the 4-consecutive intraperitoneal tamoxifen (TM) injections at the age of 4 weeks (W) and the subsequent testes sampling. d, days. (C) Macroscopic view of tamoxifen-injected testes from control and iKO mice at the age of 6, 9, 12 and 20 weeks (upper panels). The lower panels show immunostainings of NIPP1 in testis from tamoxifen-treated CTRs and iKOs at the indicated ages. Scale bar, 50 µm. (D) Testes gonadosomatic index, as determined by the percentage of total testis weight (g) over the body weight (g) of 6, 9, 12 and 20 weeks-old adult CRT and iKO mice. (E-F) The level of NIPP1 in total testis extracts from tamoxifen-injected CTR

and TKO mice was visualized by immunoblotting (E) and quantified (F). GAPDH was used as a loading control. Data are represented as means ± SEM (n=4). **, $p<0.01$; ***, $p<0.001$.

### 4.3.2 The deletion of NIPP1 leads to a loss of male germ cells

In adult mouse testis NIPP1 is expressed in both germ cells and somatic cells, including Sertoli cells (Figure S3). Strikingly, the level of NIPP1 decreases upon spermatogenic differentiation and is nearly undetectable in terminally differentiated elongated spermatids, hinting at a key role of NIPP1 in the maintenance of male progenitor cells. This incited us to explore the fate of germ cells and the supporting Sertoli cells in the NIPP1 iKOs. The number of Sertoli cells (SOX9 staining) was not affected by the deletion of NIPP1 (Figure 2A and B). Moreover, the expression of factors secreted by Sertoli cells, including inhibins (*Inhba* and *Inha*) and the SSC self-renewal factor *Gdnf* (Figure 2C), was the same in the CTRs and iKOs, indicating that the function of Sertoli cells is probably not affected by the deletion of NIPP1. In contrast, H&E stainings revealed that the diameter of the seminiferous tubules gradually decreased due to a loss of germ cells (Figure 2A and D). In testis of 9 weeks, i.e. 5 weeks after the administration of tamoxifen, the seminiferous tubules already showed a clear decrease in the number of germ cells. The most severely affected tubules showed gross vacuolization and only contained occasional germ cells. By the age of 12 weeks most seminiferous tubules were agametic and only contained Sertoli cells. Quantitative RT-PCR for specific germ-cell markers confirmed the progressive loss of all types of germ cells in the iKOs (Figure 2E-G).

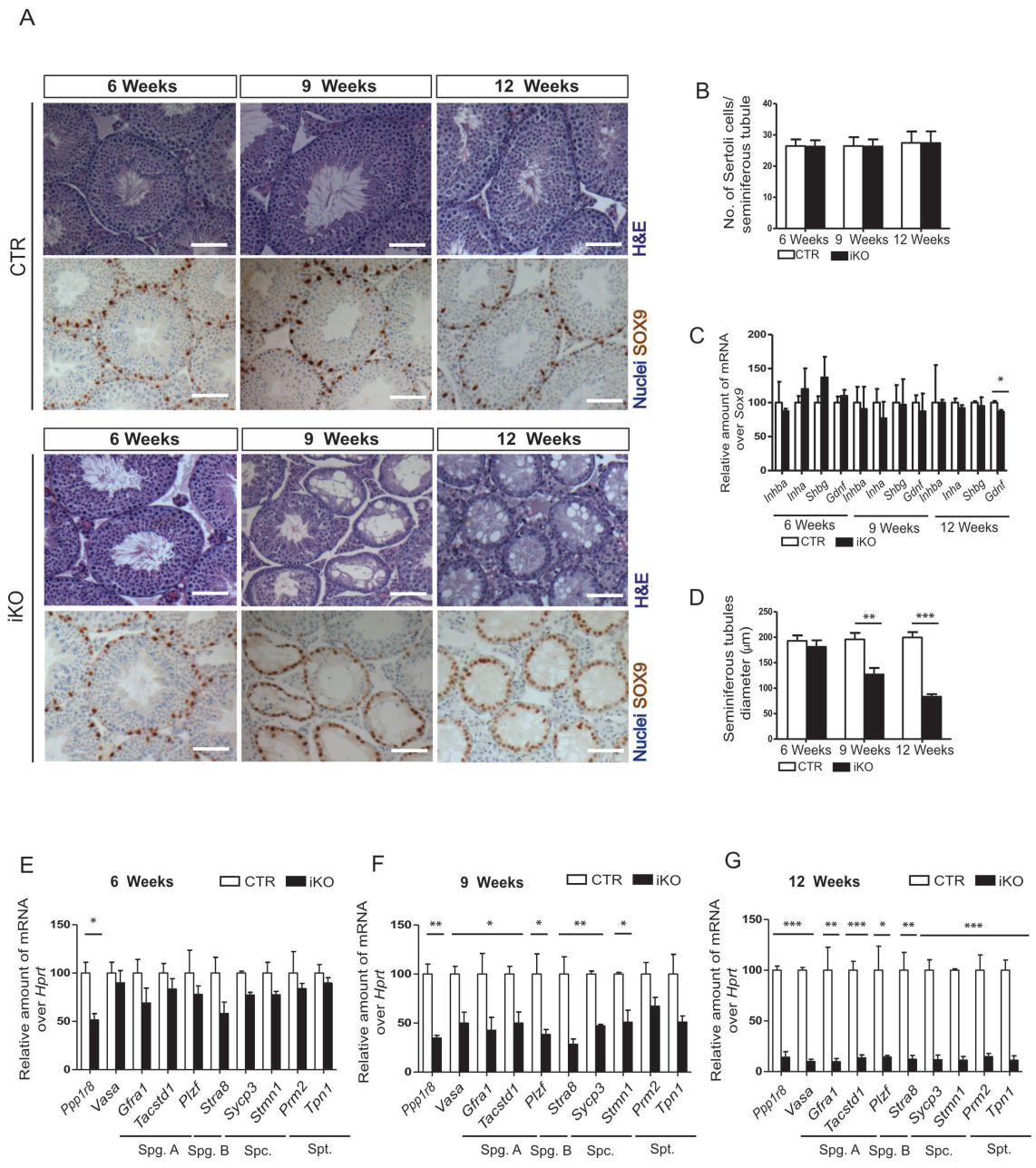


**Figure 2. The testicular deletion of NIPP1 leads to a loss of germ cells.** (A) Testis sections of tamoxifen-injected CTR and iKO mice at the indicated ages were stained with Hematoxylin-Eosin (H&E) and a Sertoli-cells (SOX9) marker. Scale bar, 50 µm. (B) The number of Sertoli cells per seminiferous tubule. (C, E-G) qRT- PCR analysis of the indicated genes, including markers for the different types of germ cells, at the indicated ages. *Sox9* or *Hprt* were used as housekeeping gene for normalization. Spg. A, spermatogonia A; Spg. B, spermatogonia B; Spc., spermatocytes; Spt., spermatids. (D) Quantification of cross-sectional diameter of the seminiferous tubules. The results are means ± SEM (n=4). *, p<0.05; ***, p0.01;* ****, p<0.001.*

### 4.3.3 NIPP1 is required for the proliferation and survival of spermatogonia and (pre)leptotene spermatocytes

We subsequently examined whether the testis phenotype in the iKOs can be explained by a reduced proliferation and/or increased apoptosis of germ cells. For these experiments, we used tamoxifen-treated mice of 6 weeks, when a testis phenotype is not yet histologically apparent. Stainings for the spermatogonia marker PLZF (promyelocytic leukemia zinc finger) did not yet show a significantly reduced number of PLZF-positive cells per tubule at this age (Figure 3A and B), in accordance with qRT-PCR data (Figure 2E). However, both BrdU (5'-bromo-2'-deoxyuridine) incorporation assays (Figure 3A and C) and PCNA (proliferating cell nuclear antigen) stainings (Figure 3A and D) disclosed a twofold lower proliferation rate of spermatogonia and (pre)leptotene spermatocytes in the iKOs. These conclusions were validated by stainings for cyclin D2 and histone H3 phosphorylation at Ser10 (H3S10P), which are markers for G1 and mitotic cells, respectively (Figure S4A-C). In contrast, TUNEL assays revealed a 3-fold increased level of apoptosis in germ cells from 7 weeks-old iKO mice (Figure 3A and E). Apoptosis was particularly increased in germ cells from the basal layers of the seminiferous epithelium, comprising spermatogonia and early meiotic spermatocytes. Stainings for the senescence marker $p16^{INK4a}$ (Figure S4A and D) and for fibrosis (Figure S4E) did not disclose differences between the CTRs and iKOs. Also, both groups contained similar proportions of tubules at different stages of development (Figure S4F). Collectively, our data indicate that the gradual loss of male germ cells after the deletion of NIPP1 is explained by their reduced proliferation and increased apoptosis rather than by the induction of senescence or fibrosis.

We have also investigated whether the loss of germ cells in the iKOs could be an indirect effect caused by the depletion of NIPP1 in peripheral tissues. For example, it could be argued that the deletion of NIPP1 from the brain interferes with the level of circulating testosterone, which is required for germ-cell survival [33]. However, the expression of NIPP1 in the iKOs was only marginally affected in the brain cortex and hypothalamus, and only reduced in a scattered fashion in the cerebellum (Figure S5A-D). Also, the levels of circulating testosterone were similar in the CTRs and iKOs and there was no correlation between testosterone levels and testis weight in 9 weeks-old mice (Figure S5E and F). To further differentiate between intrinsic and extrinsic defects, we aimed to generate a testis-specific NIPP1 mouse KO model by recombination with Cre under control of the gonocyte-specific *Vasa* promotor (Figure S5G and H). However, the CRE-recombinase

was expressed precociously, resulting in the global deletion of NIPP1. Such global recombination with *Vasa*-controlled CRE recombinase has also been noted for other genes (Diego Castrillon, personal communication). As an alternative approach to determine whether the testis phenotype was mediated by the loss of NIPP1 from peripheral tissues, we performed organ cultures using testis that were isolated from tamoxifen-treated mice of 6 weeks (Figure S6A), or testis isolated at the age of 4 weeks and treated *in vitro* with hydroxytamoxifen (Figure S6D). Under *in vitro* outgrowing conditions, BrdU incorporation (Figure S6A-C) and the level of PCNA (Figure S6D-F) were severely decreased in the iKOs, demonstrating that the observed phenotype is an intrinsic defect caused by the testicular depletion of NIPP1.

Although PLZF is predominantly expressed in undifferentiated spermatogonia, recent studies showed that PLZF can also be detected in differentiating spermatogonia [34]. Therefore, it was not clear whether the decreased number of PLZF-positive cells in the iKOs (Figure 2E-G) also reflected a loss of undifferentiated spermatogonia, which only represent a small fraction of the total pool of spermatogonia. Therefore, we also performed stainings for GFRA1, a specific marker for undifferentiated spermatogonia (Figure 3F and G). The number of GFRA1 positive cells ($GFRA1^+$) was not significantly affected in iKOs of 6 weeks, but was reduced by ≈50% and ≈90% at 9 and 12 weeks, respectively. To explore whether $GFRA1^+$ spermatogonia have a reduced proliferation capacity after the deletion of NIPP1, we isolated $GFRA1^+$-enriched testicular cells from CTR and iKO mice (Figure 3H and I). The 4-OHT-induced deletion of NIPP1 in $GFRA1^+$-enriched cultures reduced their proliferation by some 40%, as demonstrated by BrdU incorporation assays (Figure 3J and K), and increased the number of apoptopic cells, as shown by TUNEL assays (Figure 3L and M). We also examined testis of tamoxifen-treated neonates of 7 days. At this age, the seminiferous tubules only contain a heterogeneous pool of gonocyte-derived (un)differentiated spermatogonia and Sertoli-cells (Figure S7). In the neonatal iKOs NIPP1 was successfully deleted while the number of Sertoli cells (SOX9) was not significantly affected. Also, proliferation was reduced by some 50%, as determined by PCNA stainings. Strikingly, the number of $GFRA1^+$ cells was decreased by about 80%, showing that undifferentiated spermatogonia are also depleted in the first wave of spermatogenesis.

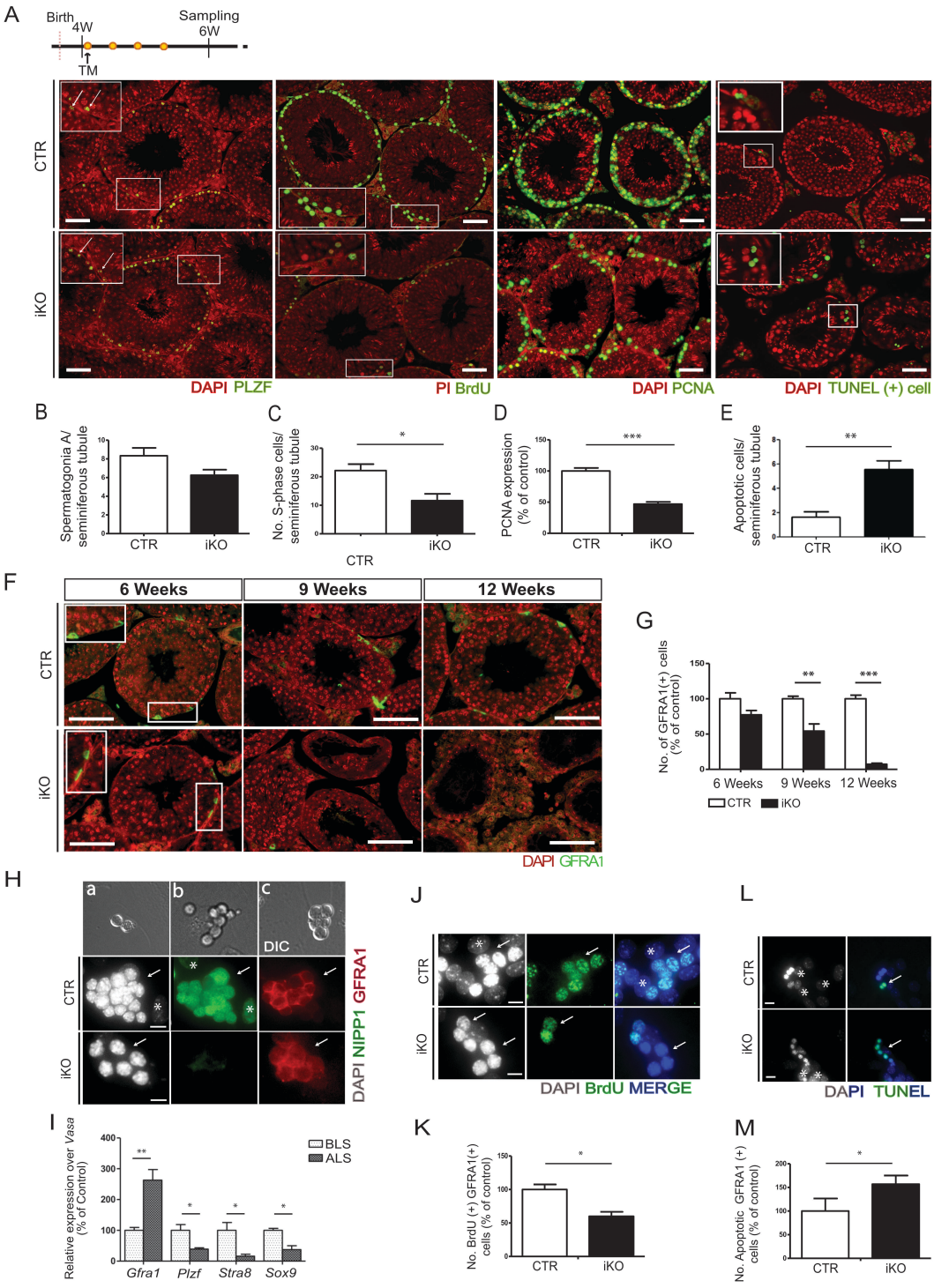


**Figure 3. *Ppp1r8*$^{-/-}$ testes show reduced proliferation and survival of germ cells.** (A) Testis sections of tamoxifen-treated mice of 6 weeks were stained for spermatogonia (PLZF), proliferation of spermatogonia and (pre)leptotene spermatocytes (BrdU incorporation, PCNA) and apoptosis (TUNEL) (7 weeks) in DAPI or propidium iodide (PI) stained nuclei. Scale bar, 50 µm. (B-E) Quantifications of the stainings as shown in panel (A) (n=4) (D) represents the total expression of PCNA per tubule. (F) Testis sections of tamoxifen-treated mice of the indicated age

were stained for the undifferentiated spermatogonia marker GFRA1. Scale bar, 50 μm. (G) Quantification of the relative number of undifferentiated spermatogonia (GFRA1$^+$ cells) per seminiferous tubule. **, p<0.01; ***, p<0.001. (H) Analysis of GFRA1$^+$-enriched cells isolated from CTR and iKO testis at 12 days after birth (P12), using the laminin selection method. GFRA1$^+$ cells immunostained for NIPP1 and GFRA1 show the efficient deletion of NIPP1 after treatment of GFRA1$^{+\ (Ppp1r8fl/+)}$ (CTR) and GFRA1$^{+\ (Ppp1r8fl/-)}$ (iKO) cells with 1 μM of 4-OHT during 72h. a, GFRA1$^+$-paired spermatogonia; b, GFRA1$^+$-aligned spermatogonia; c, GFRA1$^+$ spermatogonia colony. Arrows indicate GFRA1$^+$ colonies formed after 96h. *, mouse embryonic fibroblast (MEF) nucleus. Scale bar, 10 μm. (I) The relative enrichment of GFRA1$^+$ cells is represented by the expression of gene markers for the different populations of *Gfra1*$^+$, *Plzf*$^+$ or *Stra8*$^+$ spermatogonia and Sertoli cells (*Sox9*$^+$) after laminin selection, using *Vasa* as housekeeping gene. BLS, before laminin selection; ALS, after laminin selection. (J) BrdU incorporation assay for GFRA1$^+$-enriched cultures. Representative images are shown. Arrows indicate GFRA1$^+$ colonies. *, mouse embryonic fibroblast (MEF) nucleus. Scale bar, 10 μm. (K) Quantification (n=3) of the proportion of BrdU-incorporated nuclei. Scale bar, 10 μm. (L) Immunocytochemistry of apoptotic cells (green) using the TUNEL assay. Scarce apoptotic positive cells were nearly only observed in GFRA1$^{+\ (Ppp1r8fl/-)}$ (iKO) cells after 4-OTH treatment for 72 hours. *, mouse embryonic fibroblast (MEF) nucleus. Scale bar, 10 μm. (M) Quantification of the apoptotic cells as shown in (L). All data in this figure are represented as means ± SEM. *, $p$<0.05; **, $p$<0.01. DIC, differential interference contrast.

### 4.3.4 The deletion of NIPP1 results in the destabilization of EZH2

NIPP1 has an FHA-domain that recruits phosphoproteins for regulated dephosphorylation by associated PP1 (see Introduction). One of the established NIPP1 FHA-ligands is the histone methyltransferase EZH2. Double immunostainings showed a co-localization of NIPP1 and EZH2 in GFRA1$^+$-enriched cells (Figure S8A). Also, NIPP1 co-immunoprecipitated with EZH2 from total testis nuclear extracts and GFRA1$^+$-enriched cell lysates (Figure S8B), confirming that they are part of the same complex in germ cells, in particular in spermatogonia.

EZH2 is the catalytic subunit of the PRC2 complex. The non-catalytic core subunits of the PRC2 complex include EED, SUZ12 and RBAP48. Interestingly, the loss of any of these PRC2 subunits also destabilizes the other core components [35–38]. Since the deletion of PRC2 core components in mouse testis results in a loss of spermatogonia [10,11], we speculated that the testis phenotype of the NIPP1 iKOs might be caused by a phosphorylation-regulated degradation of EZH2, culminating in the destabilization of other PRC2 components. Consistent with this notion, we found that the levels of EZH2, RBAP48 and SUZ12, as determined by both immunohistochemistry and immunoblotting,

were reduced by 30-40% in iKOs of 6 weeks, when the seminiferous tubules still contain a normal number of germ cells (Figure 4A-G). Close inspection of the immunehistochemical pictures (see insets) revealed that the PRC2 components were mainly expressed in proliferating germ cells and were lost from a subset of these cells. RNA sequencing did not disclose changed transcript levels of the PRC2 core components in NIPP1 iKOs (Table S1), suggesting that their downregulation involves a (post)translational process. Intriguingly, we found that EZH2 from testis lysates migrated as two bands during SDS-PAGE and that the upper band was relatively more prominent (~40%) in the iKOs (Figure 4B and D). Since the slower migration of the upper band was abolished by a pre-treatment with lambda phosphatase (Figure S9A), we conclude that it represents hyperphosphorylated EZH2. Finally, we also examined the fate of other NIPP1 FHA-ligands (SAP155 and CDC5L) and PP1 (all isoforms), but their level was not affected in testis lysates of iKOs of 6 weeks (Figure S9B-G). In conclusion, our data suggest that the deletion of NIPP1 results in the hyperphosphorylation and destabilization of EZH2, which contributes to the (expected) destabilization of other PRC2 core components.

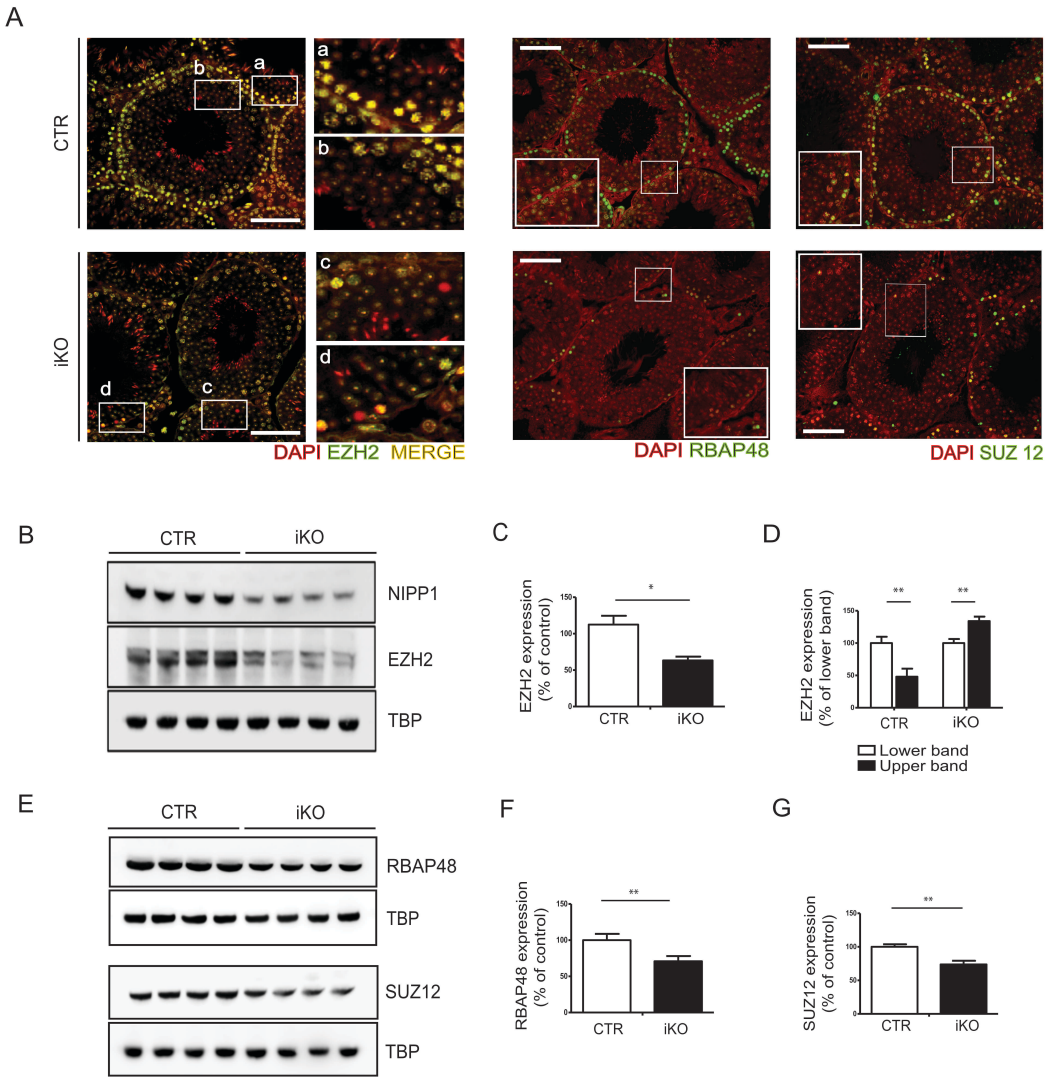


**Figure 4. The loss of NIPP1 is associated with the destabilization of PRC2 core components.** (A) Testis sections of tamoxifen-injected mice of 6 weeks were immunostained for EZH2, RBAP48 and SUZ12. Scale bar, 50 µm. (B) NIPP1 and EZH2 levels were detected by immunoblotting. TBP was used as a loading control. (C) Quantification of the EZH2 levels, as shown in panel (B). (D) Ratio of the higher and lower bands of EZH2, as shown in panel (B). (E) The same testis lysates (~100 µg) were immunoblotted for RBAP48 and SUZ12. (F-G) Quantifications of panel (E). All bar data are means ± SEM (n=4). *, $p<0.05$; **, $p<0.01$.

### 4.3.5 NIPP1 stabilizes EZH2 by promoting PP1-mediated dephosphorylation of CDK sites

Since EZH2 in HeLa cells is targeted for proteasomal degradation by its CDK1/2-mediated phosphorylation at Thr345 and Thr478 [19,20], we hypothesized that EZH2 in spermatogonia is also destabilized by phosphorylation of these residues. Therefore, we first compared the half-lives of EGFP-tagged EZH2-wildtype (WT), EZH2-T345A and EZH2-T487A in a spermatogonia-A cell line (C18-4) after the addition of the protein synthesis inhibitor cycloheximide (Figure 5A-C). EZH2-WT had a half-life of approximately 2 hours but this increased to about 6h for the non-phosphorylatable alanine mutants, similar to the half-life of EGFP. Thus, EZH2 in spermatogonia A is stabilized by preventing its phosphorylation at Thr345 or Thr487. We proceeded to examine whether these sites are hyperphosphorylated in the testes of the iKOs. Since Thr345 and Thr487 are followed by a proline, their phosphorylation status can be derived from immunoblotting with a pan pTP antibody, in particular since Thr345 and Thr487 represent the major TP-phosphorylation sites of EZH2 [15–18]. EZH2 that was immunoprecipitated from testis lysates (Figure 5D and E) or $GFRA1^{+}$-enriched cell lysates (Figure S9H and I) was hyperphosphorylated at pTP motifs in the iKOs. Moreover, EGFP-EZH2 that was ectopically expressed in spermatogonia-A showed a reduced phosphorylation at TP-dipeptide motifs after the co-expression of a Flag-PP1-NIPP1 fusion (Figure 5G-H), indicating that EZH2 is a potential substrate for dephosphorylation by PP1-NIPP1. This is in accordance with previous *in vitro* data showing that the TP-dipeptide motifs of EZH2 are dephosphorylated by purified PP1 [17]. We also found that the incubation of $GFRA1^{+}$-enriched cells with the CDK inhibitor roscovitin severely decreased the phosphorylation of EZH2 at TP-dipeptides (Figure S9H and J), in accordance with previous data that identified EZH2 as a CDK substrate [15,19,20]. Collectively, our data strongly indicate that the loss of EZH2 in the testis of the NIPP1 iKOs is due to a deficient dephosphorylation of CDK sites, resulting in its proteasomal degradation.

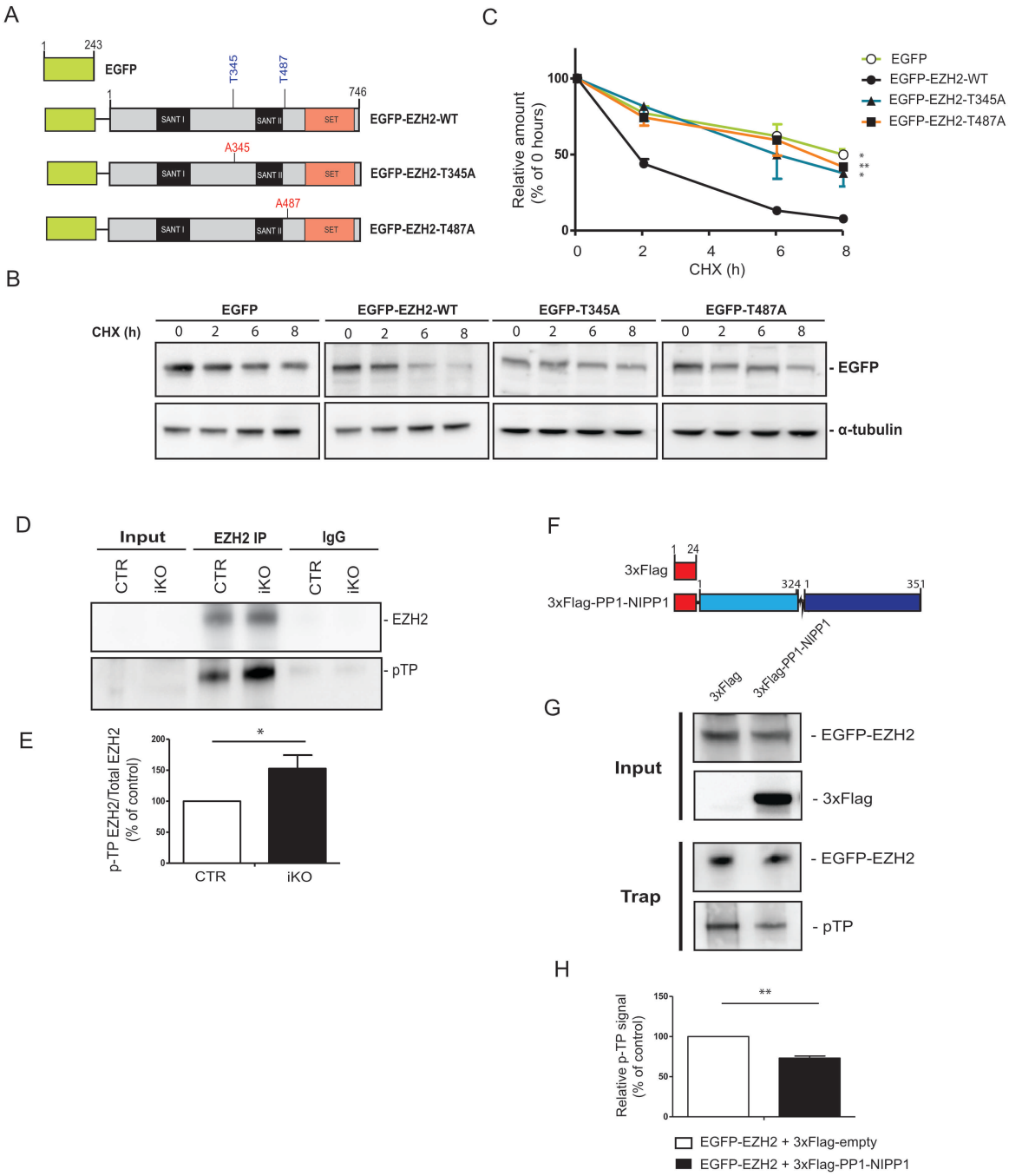


**Figure 5. NIPP1 regulates the dephosphorylation and stability of EZH2.** (A) Schematic representation of EGFP and the indicated EGFP-tagged EZH2 variants. (B) Non-synchronized C18-4 cells were transfected with EGFP or the EGFP-tagged EZH2 variants and treated with cycloheximide (CHX; 50 µg/ml) for the indicated time points. The fate of EGFP and the EGFP fusions was determined by immunoblotting with an anti-EGFP antibody. Data are represented as means ± SEM (n=3). *, $p<0.05$; **, $p<0.01$. (C) Representative example of the turnover of EGFP and EGFP-EZH2 fusions in the presence of cycloheximide. α-Tubulin was used as a loading control. (D) EZH2 was immunoprecipitated (IP) from testis extracts of tamoxifen-treated mice of 6

weeks. The IP loading was corrected for equal amounts of immunoprecipitated EZH2 in the CRT and iKO conditions. For the input, ~10 µg protein was loaded and IgGs were used as negative control. The blots were stained for total EZH2 and TP-dipeptide phosphorylated EZH2 (pTP). EZH2 immunoprecipitation (IP) and detection were performed with distinct antibodies from Cell signaling with catalog numbers 5246 and 3147, respectively, which were raised in different species. (E) Quantification of relative amounts of phosphorylated EZH2 (n=4). (F) Scheme of Flag and Flag-tagged PP1-NIPP1 fusion. (G) EGFP-EZH2 and either Flag or Flag-PP1-NIPP1 were transiently expressed in spermatogonia-A cells (C18-4) for 48h. The cells were synchronized in mitosis by a treatment with nocodazole for 16h. Cell lysates were analyzed for the presence of EGFP-EZH2 and Flag-PP1-NIPP1 (Flag). EGFP-traps were immunoblotted for EGFP-EZH2 and phosphorylated EZH2 (pTP). (H) Quantification of the relative amounts of phosphorylated EZH2 (n=3). *, $p<0.05$; **, $p<0.01$.

### 4.3.6 The loss of PRC2 affects the expression of proliferation and survival genes

We subsequently explored the consequence of the gradual loss of the PRC2 core components in the testes of the NIPP1 iKOs. The major substrate of EZH2 is histone H3, which is trimethylated at Lys27 (H3K27me3). Consistent with the decreased concentration of EZH2 in the iKOs, the testicular level of H3K27me3 in mice of 6 weeks was reduced, as shown by both immunostaining (Figure 6A) and immunoblotting (Figure 6B-C). Closer inspection of the stainings revealed that the loss of H3K27me3 in the iKOs was particularly strong in seminiferous tubules containing spermatogonia and (pre)leptotene spermatocytes (Figure 6A, panels 1-2), but was less obvious in tubules at later stages (Figure 6A, panel 3). A decreased H3K27me3 level was also observed in neonatal testis of tamoxifen-induced mice (Figure S10A-C) and tamoxifen-treated testis cultures from mice of 4 weeks (Figure S10D-F).

The histone methyltransferase EZH2 regulates cell proliferation and survival mainly by transcriptional repression of target genes via trimethylation of H3K27. To identify the transcriptome profile of CTR and iKO testis from mice of 6 weeks, we performed a comparative RNA sequencing. Data analysis identified 122 upregulated and 152 downregulated genes in the iKOs (Figure 6D, Table S2). Among the downregulated targets were genes that contribute to cell-cycle progression (*Cdkn2a*, *Kntc1*), MAP kinase signaling (*Dusp 9*), PcG signaling (*Dnmt3l*) and spermatogenesis (*Nanos 1*) (Figure 6E). The upregulated genes included pro-apoptotic genes (*Parp8*, *Bbc3, Ccnb3),* genes involved in cell-cycle progression (*Tnk, Ptprt, Kif2b*) and gonadal development genes (*Lhx9*). In

general, these altered expression profiles are consistent with the observed decreased proliferation and survival potential of testicular cells in the iKOs. The RNA sequencing data were largely confirmed by qRT-PCR (Figure 6F). Further analysis revealed that about 12% of the genes that were mapped in the RNA seq data are previously described PcG targets, based on PcG target lists [10,39–41]. Interestingly, 26% of the genes affected in the iKOs are established PcG targets (Figure S11A), reflecting a twofold enrichment. We have also verified by ChIP analysis that H3K27me3 was enriched at or around the promoter region of affected PRC2 target genes in testis (Figure 6G and Figure S11B) and that the deletion of NIPP1 was associated with decreased H3K27 trimethylation at these loci, except for *CDKn2a* (Figure 6H). Paradoxically, the decreased H3K27me3 level of *Pou3f3* correlated with a decreased transcript level, indicating that *Pou3f3* expression is also regulated by non-PcG related mechanisms or belongs to the subgroup of PcG targets that are activated by EZH2 [24,42].

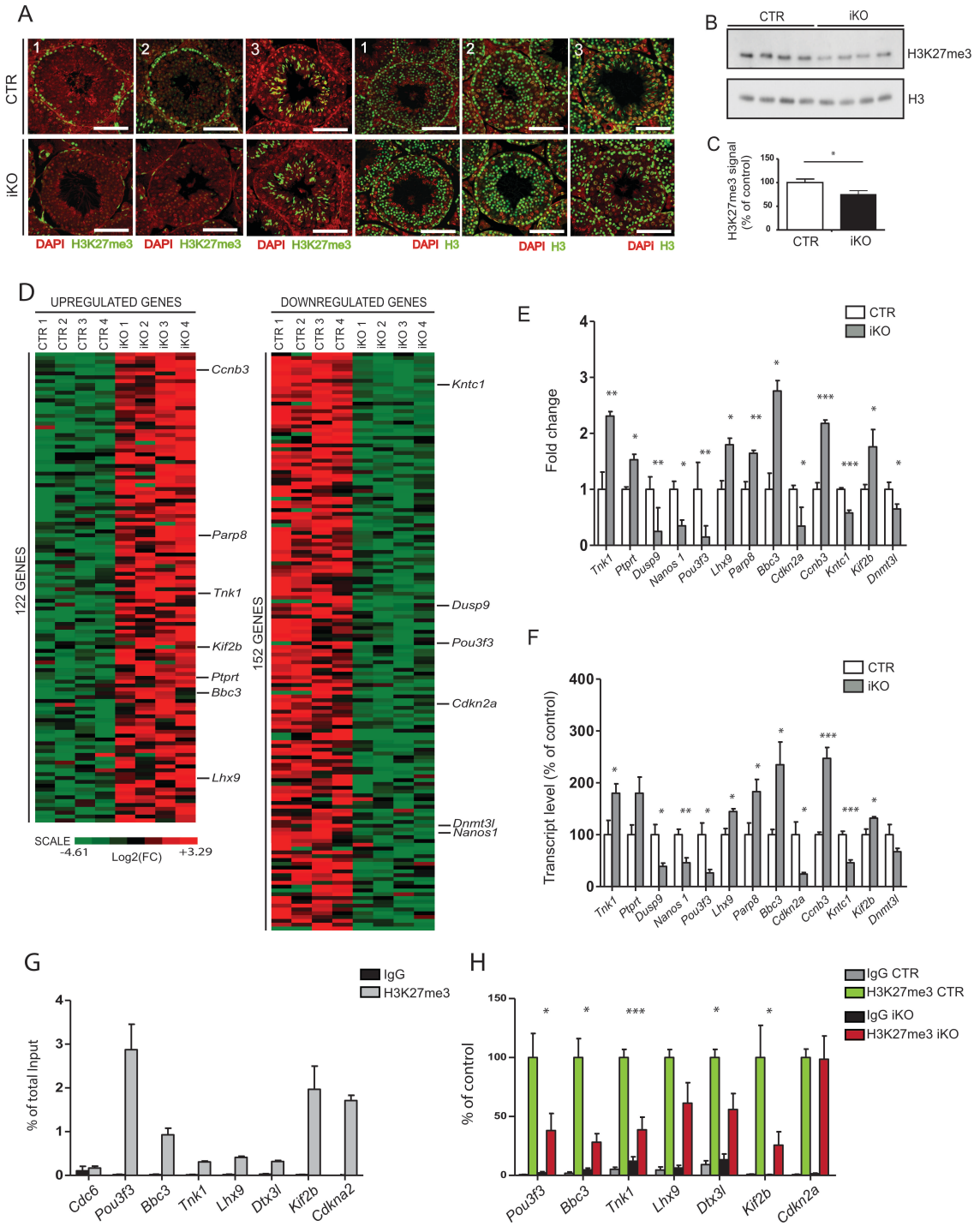


**Figure 6. PRC2 destabilization results in the deregulation of PcG target genes.** (A) Testis sections of tamoxifen-treated mice of 6 weeks were immunostained for histone H3 and H3K27me3. Shown are seminiferous tubules at different stages (1, Stage V-VIII; 2, Stage VIII-IX; 3, Stage X-XI). Scale bar, 50 µm. (B) Total H3 and H3K27me3 in histone extracts of testis were visualized by immunoblotting. (C) Quantification of H3K27me3, as shown in panel (B) (n=4). (D) Comparative RNA-sequencing profiling in testis of

tamoxifen-treated mice of 6 weeks. The figure shows the heat map of the significantly up- and downregulated genes. (E) Analysis of RNA-sequencing data showing changes in the level of the indicated transcripts in the iKOs. (F) qRT-PCR analysis of the same transcripts. The indicated genes encode proteins with the same name except for *Bbc3* and *Cdkn2a,* which encode PUMA and p16/INK4a, respectively. (G) ChIP assays for H3K27me3 of the indicated genes in testis of tamoxifen-treated CTR mice of 6 weeks. ChIPs with IgGs served as negative controls. *Cdc6* gene was used as non-PcG target control gene. ChIP enrichments were calculated as a percentage of the total input signal (n=6). (H) Comparison of the H3K27me3 ChIP data between CTR and iKO mice. H3K27me3 enrichment in the iKOs is presented as a percentage of the corresponding CTR value (n=6). Data are represented as means ± SEM. *, $p<0.05$; **, $p<0.01$; ***, $p<0.001$.

### 4.3.7 The *Ppp1r8*$^{-/-}$ testis phenotype can be phenocopied by the chemical inhibition of EZH proteins

EPZ011989 is an inhibitor of both EZH1 and EZH2, but is about 15 times more selective for EZH2 [43]. We have independently validated the importance of EZH1/2 for spermatogenesis by examining the effect of EPZ011989 on proliferation in cultured testis slices from mice that had not been pretreated with tamoxifen and, hence, contained 1 (iKO) or two (CTR) functional *Ppp1r8* alleles [43]. The addition of EPZ011989 reduced the level of both H3K27me3 and the proliferation marker PCNA by some 60% (Figure 7A-C), which is identical to the results obtained after the deletion of NIPP1 (Figure 3 and Figure S6). Thus, the testis hypoproliferation phenotype induced by the deletion of NIPP1 can be phenocopied by the chemical inhibition of EZH1/2.

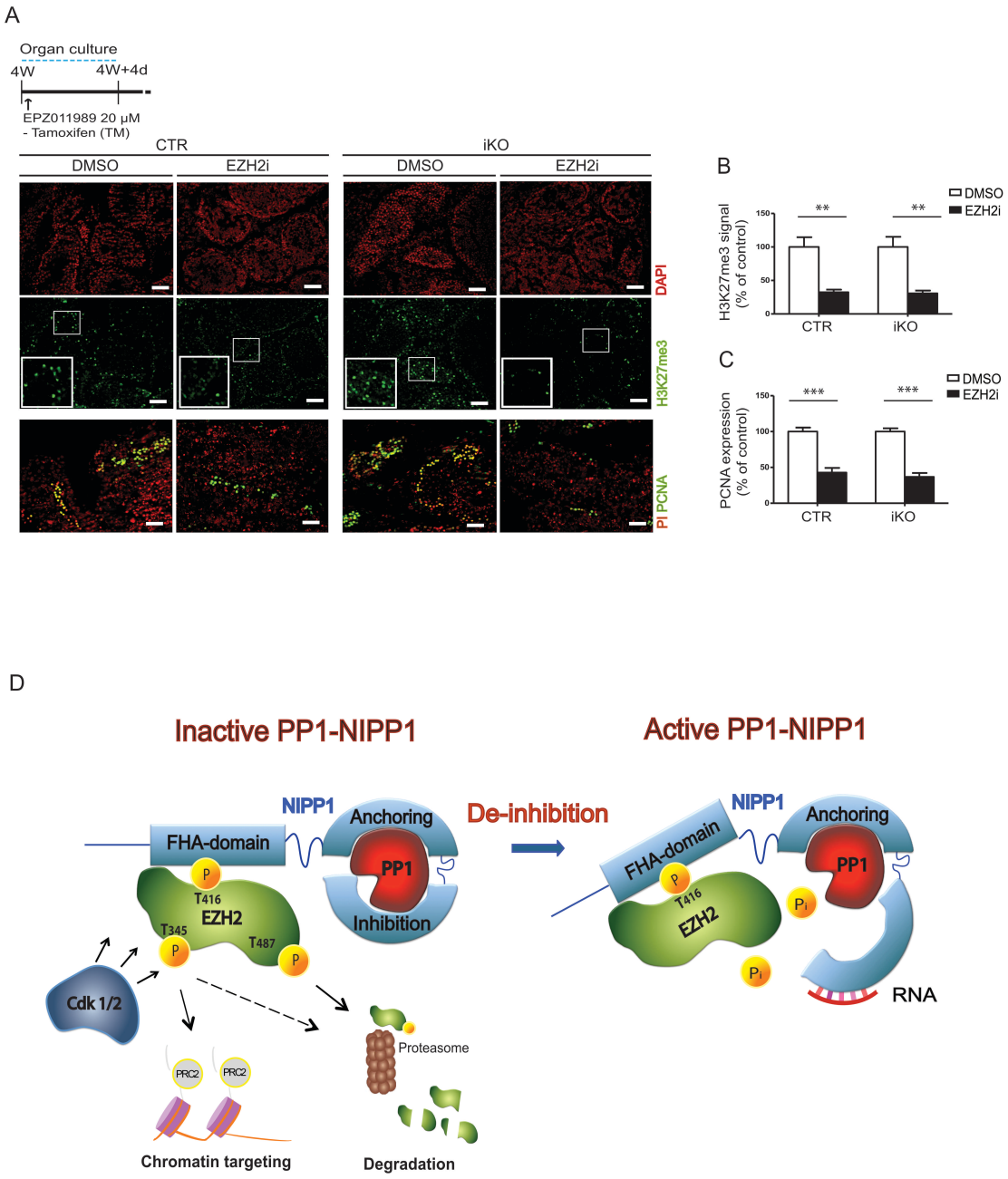


**Figure 7. The chemical inhibition of EZH1/2 in testis organ cultures mimics the *Ppp1r8*$^{-/-}$ phenotype.** (A) Testis slices from CTR and iKO mice of 4 weeks were cultured for 96 hours in the presence of vehicle (DMSO) or the EZH inhibitor EPZ011989 (EZHi), but in the absence of 4-OHT. Subsequently, testis sections were stained with DAPI and immunostained for H3K27me3 and PCNA. Scale bar, 50 µm. (B) Quantification of H3K27me3. Data are means ± SEM (n=4). (C) Quantification of PCNA. Data are means ± SEM (n=4). ***p<0.01, ***p<0.001.* (D) Model of the regulation of EZH2 by CDKs and PP1-NIPP1. CDKs phosphorylate EZH2 at Thr345, Thr416 and Thr487. Thr345 phosphorylation targets EZH2 to chromatin via non-coding RNAs, while Thr487 (and Thr345) phosphorylation results in the proteasomal degradation of EZH2. The

phosphorylation of EZH2 at Thr416 creates a docking site for the N-terminal FHA-domain of NIPP1. EZH2-recruited NIPP1 prevents the immediate dephosphorylation of EZH2 by PRC2-associated PP1. However, the inhibition of PP1 by NIPP1 can be alleviated (de-inhibition) by the allosteric disruption of the interaction between PP1 and the C-terminal PP1-inhibitory domain of NIPP1, resulting in the dephosphorylation of EZH2. *In vitro* such de-inhibition is seen after the binding of RNA to the C-terminus of PP1, even when de-inhibited NIPP1 remains tightly associated with PP1 via its PP1-anchoring domain.

## 4.4 Discussion

The inactivation of both *Ppp1r8* alleles in mice is early embryonic lethal [30]. This prompted us to develop an inducible knockout model to study postnatal functions of NIPP1. The only macroscopic consequence of the deletion of NIPP1 in adult mice was a reduced testis size (Figure1C and D). However, this does not preclude key functions for NIPP1 elsewhere as inactivation of the floxed *Ppp1r8* allele by UBC-CRE recombination was incomplete or patchy in all other examined tissues. Tamoxifen-induced UBC-CRE recombination is indeed known to be variable due to CRE expression in a tissue-dependent manner or mosaic fashion [32,44]. Nonetheless, UBC-CRE recombination was very efficient in the seminiferous tubules and the deletion of NIPP1 led to a reduced proliferation of spermatogonia and (pre)leptotene spermatocytes, culminating in the disappearance of all germ cells (Figure 2). The loss of the male germline was associated with the hypoproliferation of progenitor spermatogonia, comprising undifferentiated spermatogonia, as shown by tamoxifen-induced deletion of NIPP1 in $GFRA1^{+}$-enriched cell populations (Figure 3J-K). Although our data identify NIPP1 as a key regulator of the proliferation of spermatogonia and (pre)leptotene spermatocytes, they do not exclude additional functions for NIPP1 in other germ-cell processes, such as meiosis.

We have explored the events leading up to the testis phenotype in $Ppp1r8^{-/-}$ mice. For this purpose, we mainly analyzed testes of mice of 6 weeks, i.e. two weeks after the administration of tamoxifen, when the seminiferous tubules still appeared normal and the number of germ cells had not yet significantly decreased. Strikingly, at this age we already observed a reduced proliferation and increased apoptosis of spermatogonia and meiotic spermatocytes, and this correlated with a decreased level of EZH2 and other PRC2 core components (Figure 3 and 4). Importantly, none of the other examined NIPP1 interactors showed an altered expression in the iKOs. The lower concentration of EZH2 was clearly the consequence of a deregulated post-transcriptional control mechanism because the

EZH2 transcript level was not affected. PRC2 core components are well known to stabilize each other [35–38]. Accordingly, we found that the loss of EZH2 was associated with a similarly decreased level of other PRC2 components (Figure 4). Several independent lines of evidence indicate that the loss of PRC2 components can account for the testis phenotype in *Ppp1r8*$^{-/-}$ mice. First, the genetic deletion of EZH1/2, SUZ12 or EED in mice has also been shown to result in a loss of germ cells [10,11]. Second, the chemical inhibition of EZH1/2 causes a hypoproliferation phenotype similar to that observed after the deletion of NIPP1 (Figure 7A-C). Third, the loss of PRC2 components in *Ppp1r8*$^{-/-}$ mice was associated with a reduced H3K27 trimethylation and altered expression of PcG targets that are important for proliferation and cell survival (Figure 6). Importantly, it has recently been demonstrated that the loss of EZH2 in male germ cells can be compensated for by EZH1 [11]. Since the deletion of NIPP1 reduced the global trimethylation of H3K27 (Figure 6A-C), this suggest that EZH1 is probably also lost in *Ppp1r8*$^{-/-}$ testis. Consistent with this notion, the TP-dipeptide motif that mediates the binding of EZH2 to the FHA domain of NIPP1, termed TP5 in [17], is conserved in EZH1.

Our data suggest that the decreased level of EZH2 in spermatogonia of the iKOs is caused by its deficient PP1-NIPP1 mediated dephosphorylation at CDK sites (Figure 5). The activity modulation of the PP1-NIPP1 holoenzyme is complex. Indeed, NIPP1 has both a PP1-anchoring and PP1-inhibitory domain which, together, fully block the activity of PP1 (Figure 7D). This is particularly relevant for ligands of the FHA domain of NIPP1, including EZH2, that are recruited in a phosphorylation-dependent manner. CDKs phosphorylate EZH2 at Thr345, Thr416 and Thr487. Phosphorylation of Thr416 serves to recruit NIPP1, which inhibits PRC2-associated PP1 and thereby opposes the immediate dephosphorylation of EZH2 [17]. However, NIPP1 is not always inhibitory as it also enables the timely dephosphorylation of FHA ligands by associated PP1 [28]. The trigger and mechanism of this ‘de-inhibition’ are still unclear but we speculate that it involves the allosteric disruption of the interaction between PP1 and the C-terminal inhibitory domain of NIPP1. *In vitro*, such ‘de-inhibition’ is detected after the binding of the C-terminus of NIPP1 to RNA [27]. Intriguingly, the phosphorylation of EZH2 at Thr345 has been shown to promote its recruitment via non-coding RNAs (Figure 7D). Possibly, these non-coding RNAs or their degradation products also trigger the dephosphorylation of EZH2 by PP1-NIPP1, eventually resulting in the release of EZH2 from chromatin. Consistent with the notion that NIPP1 is an allosterically controlled facilitator of the dephosphorylation of EZH2 by associated PP1, we found that the deletion of NIPP1 causes the

hyperphosphorylation of EZH2 at CDK sites. The consequence of this hyperphosphorylation was difficult to predict since CDK-mediated phosphorylation of EZH2 has been linked to both its enhanced chromatin targeting (Thr345) and proteolytic degradation (Thr487 and Thr345) [15,16,19,20]. Possibly, the outcome depends on the cell-cycle regulated timing or duration of these phosphorylation events, or is determined by additional components that are (transiently) recruited to the PRC2 complex [45,46]. In any case, the permanent and complete deletion of NIPP1 causes the hyperphosphorylation and degradation of EZH2 in spermatogonia. At first glance, it may come as a surprise that the inactivation of *Ppp1cc,* encoding PP1γ1 and the testis-specific splice variant PP1γ2, does not cause a similarly strong phenotype as seen after deletion of the PP1 interactor NIPP1 [47–49]. However, spermatogonia also express other PP1 isoforms (PP1α and PP1β) and NIPP1 binds equally well to all of them [50]. Therefore, the deletion of PP1γ does not preclude the formation of the PP1-NIPP1 holoenzyme and is not expected to cause the same phenotype as seen after the deletion of NIPP1.

We have shown here that the postnatal deletion of NIPP1 in testis leads to the hypoproliferation and apoptosis of spermatogonia, and culminates within a few months in the loss of all germ cells. This phenotype stems from the loss of PRC2 core components, resulting in a reduced H3K27 trimethylation and altered expression of target genes that regulate cell survival and proliferation. The destabilization of PRC2 components is initiated by the proteasomal degradation of EZH2, and possibly also EZH1, caused by a deficient dephosphorylation of CDK sites by PP1-NIPP1.

## 4.5 Methods

**Handling of mice**

Mice were housed in a specific-pathogen free facility under standard 12h light/dark cycles with water and food *ad libitum*. All experiments were approved by the KU Leuven Ethical Committee and executed according to their guide of care of experimental animals. *Ubc-Cre-ERT2/Ppp1r8*$^{fl/+}$ (CTR) and *Ubc-Cre-ERT2/Ppp1r8*$^{fl/-}$ (iKO) mice were generated using the breeding scheme shown in Fig. S1A, involving previously described *Ppp*1r8$^{+/-}$ [30], *Ppp1r8*$^{fl/fl}$ [51] and *Ubc-Cre-ERT2* mice [31](gift from Dr. M. Baes, KU Leuven, Belgium). A testis-specific NIPP1 mouse KO model was generated as detailed in (Figure S5G), using transgenic *Vasa-Cre* mouse [52] (a gift from Dr. D.H. Castrillon, University of Texas Southwestern Medical Center. USA). For genotyping, tail-clip DNA was amplified

by PCR, using the primer sets described in Table S3. The PCR conditions are available on request.

Tamoxifen (Sigma-Aldrich) was dissolved in 10% (v/v) ethanol in oil at a concentration of 20 mg/ml. Deletion of the floxed *Ppp1r8* allele in adult males and neonates was induced by 4 intraperitoneal or 3 subcutaneous injections, respectively, of 0.2 mg tamoxifen/g body weight (Figure 1B and Figure S4G). BrdU (Sigma) was dissolved in phosphate-buffered saline (PBS) and injected intraperitoneally at 100 mg per kg mouse body weight. Testes were harvested 2h following BrdU injections. The testes from anaesthetized animals were either directly frozen in liquid nitrogen, fixed in Bouin's (Sigma-Aldrich) or 4% Paraformaldehyde (PFA) solutions.

**Organ and cell culture**

Testis organ culture was performed as described [53,54]. Briefly, a testis from adult male mice was sliced into four pieces and placed on agarose gels soaked in the organ culture medium containing 2x alpha-MEM (Sigma), 10% knockout serum replacement KSR (Sigma), 100 U/ml penicillin, 100 µg/ml streptomycin and 7% w/v sodium bicarbonate. Testis slices were maintained in culture for 4 days and 10 µM BrdU (Sigma) was added to the medium 6 hours before harvesting (Table S4). EZH1/2 was inhibited in cultured testis by treatment with 20 µM EPZ011989 (Tocris) [43]. *In vitro* deletion of the floxed *Ppp1r8* allele was done by addition of 2 µM (Z)-4-Hydroxytamoxifen (OHT) (Sigma-Aldrich) to the medium for 96h.

C18-4 cells were cultured in high-glucose Dulbecco's modified Eagle's medium/F12 (DMEM/F12), supplemented with 10% fetal bovine serum, 100 U/ml penicillin and 100 µg/ml streptomycin. Transfections were performed using Lipofectamine 2000 (Invitrogen) or JetPrime kit (Polyplus). Nocodazole (Sigma-aldrich) was used at a concentration of 0.3 µg/ml for 16h (M-phase). Cycloheximide (Sigma-aldrich) was used at a concentration of 50 µg/ml.

GFRA1$^{+}$-enriched cells (undifferentiated spermatogonia) were isolated from 12 days-old CTR and iKO mice, as described by Guan et al. (2009). Briefly, testicular cells were isolated by an enzymatic procedure using collagenase IV (Worthinghton biochem corp.) and dispase (Invitrogen), followed by enrichment of GFRA1$^{+}$-enriched spermatogonia through laminin (Sigma) selection. After enrichment, cells were co-cultured with freshly prepared MEF (mouse embryonic fibroblasts) as feeding cells. The MEFs had been pre-incubated with Mitomycin C (Sigma) and maintained in spermatogonia stem cells (SSCs)

growth medium, containing MEM alfa medium (Thermo fisher scientific) and supplemented with 10% FBS, 100 U/ml penicillin, non-essential amino acids (Thermo fisher scientific), β-Mercaptoethanol (Sigma), N2-1 supplement (Thermo fisher scientific), 4 ng/ml of recombinant GDNF (R&D systems) and $10^3$ U/ml of recombinant LIF (Sigma). NIPP1 deletion was induced by addition of 1 μM 4-OHT to the medium for 72h. For the proliferation assay, 15 μM BrdU was added to the medium 5 hours before harvesting cells.

**Immunohistochemistry**

Testes fixed in Bouin's (6h) or 4% PFA (24h) were embedded in paraffin and sectioned at a thickness of 6 μm. Testis sections were stained with Hematoxylin and Eosine (H&E) or the fibrosis marker Sirius red according to standard protocols. TUNEL assays were performed using the In-Situ-Cell-Death-Detection-Kit and Fluorescein (Roche) on paraffin-embedded testis tissue following the instructions of the manufacturer. Testis sections were stained using the antibodies listed in (Table S4) and using the TSA™ Fluorescein or TSA™ Biotin system (PerkinElmer). Detailed immunostaining protocols are available on request. The immunofluorescence images were acquired with a Leica TCS SPE laser scanning confocal system mounted on a Leica DMI 4000B microscope and equipped with a Leica ACS APO 20X objective. Quantifications shown in Figure 2B, 3B-C, E-G and Figure S4B-C were performed by counting the number of cells stained with the indicated cell markers per seminiferous tubule (30 randomly selected tubules per mouse, n=4). Leica MM AF 2.1 software was used for quantification (10 pictures of 10x objective magnification were randomly selected per mouse testis) of the relative expression of PCNA (Figure 3D, 7C, S6F, S7B), NIPP1 (Figure S1F, S6B and E), SOX 9 (Figure S7B), EZH2 (Figure S10B and E), H3K27m3 (Figure 7B, S10C and F) and p16 (Figure S4D) over DAPI (nucleus) signal.

**Plasmids**

Plasmids encoding eGFP-tagged mouse wild-type EZH2, EZH2-T345A and EZH2-T487A have been described [17]. The plasmid encoding Flag-tagged PP1γ-NIPP1 fusion was generated in three cloning steps. First, a flexible linker encompassing the sequence LSGGGGSGGGGSGGGGSGGGGSAAA [55] was C-terminally fused to PP1γ by an adapter-based cloning strategy. Second, cDNA encoding bovine NIPP1 was cloned in open reading frame with the cDNA encoding the PP1γ-linker at its 3' end. Finally, cDNA that

encodes PP1γ-linker-NIPP1 was cloned via *Xho*I and *Sac*II in the eGFP-C1 vector (Clontech), in which the eGFP-tag had been replaced by a 3x Flag-tag.

**Biochemical procedures**

Testes were homogenized using a dounce homogenizer (Sigma) and incubated in lysis buffer for 20 min at 4°C. The lysis buffer comprised modified RIPA buffer (50 mM Tris-HCl at pH 7.4, 1% Triton-X 100, 0.2% sodium deoxycholate, 0.2% sodium dodecyl sulfate (SDS), 1 mM EDTA, 0.3 M NaCl) or SDS-lysis buffer (50 mM Tris-HCl at pH 7.4, 2% SDS, 12% glycerol, 100 mM ß-mercaptoethanol). Lysis buffers were supplemented with 20 mM NaF, 5 µM leupeptin, 0.5 mM phenylmethanesulfonyl fluoride, 0.5 mM benzamidine and 1 mM orthovanadate. The lysates were centrifuged for 5 min at 1800 x *g* and the supernatant was used for immunoblotting or immunoprecipitation. The testis extracts for immunoblotting in Figure 1E, 4B and E, Figure 5B, D and G, Figure S9A, B, D and F were prepared with modified RIPA, while SDS-lysis buffer was used in Figure 6B and S7C. For in *vitro* dephosphorylation with lambda phosphatase, samples were incubated for 30 minutes at 30°C with 400 units of lambda phosphatase (Santa Cruz) in the presence of 5 mM DTT and 2 mM $MnCl_2$. For the immunoprecipitation assays in testis extracts, the supernatant was pre-cleared with 30 µl of protein-A-Sepharose beads (1:1 suspension in TBS) for 1 h at 4°C. After centrifugation (30 s at 425 x *g*) the supernatant was incubated overnight at 4°C with antibodies against EZH2 (Table S4) or anti-mouse IgG for control (Dako). Subsequently, 30 µl of protein-A-Sepharose (1:1 suspension in TBS) was added for 1 h at 4°C. After centrifugation for 30 s at 425 x *g* the pellet was washed five times with Tris-buffered saline (TBS), supplemented with 0.1% Triton X-100 and 0.25% NP-40, and subjected to SDS-PAGE.

C18-4 cells were harvested and lysed for 30 minutes at 4°C in 50 mM Tris-HCl at pH 7.4, 0.3 M NaCl, 0.5% Triton-X 100, 20 mM NaF, 5 µM leupeptin, 0.5 mM phenylmethanesulfonyl fluoride, 0.5 mM benzamidine and 1 mM orthovanadate. After centrifugation (10 min at 1800 x *g*), the supernatant was used for immunoblotting or EGFP-trapping [56].

To examine the interaction of NIPP1 and EZH2, isolated cells and testis nuclear extracts were prepared as described by Prieto et al. (2002). The nuclear extracts were used for immunoprecipitation studies as described above. $GFRA1^+$-enriched cells were pre-incubated with dimethylsulfoxide (DMSO) or 150 µM of the CDK-inhibitor roscovitine (LC Laboratories) for 2 h before immunoprecipitation.

Immunoblotting was performed following 10% SDS- PAGE with the indicated antibodies (Table S4). Immunoblots were visualized using ECL reagent (Perkin Elmer) in an ImageQuant LAS4000 imaging system (GE Healthcare) and were quantified using ImageQuant TL software (GE Healthcare).

**RNA sequencing and Quantitative Reverse Transcriptase PCR (qRT-PCR)**

Total RNA was isolated from 40 mg of snap-frozen mouse testis using the GenElute$^{TM}$ Mammalian Total RNA Miniprep kit (Sigma-aldrich). RNA integrity of the samples used for RNA sequencing was assessed using a Bioanalyser 2100 (Agilent). Library preparation, sequencing and statistical analysis of the RNA sequencing data were performed by VIB Nucleomics Core, as detailed in the Supplemental information.

Complementary DNA (cDNA) was synthetized from 2 µg of total RNA using oligo dT primers (Sigma-aldrich) RevertAid Premium Reverse Transcriptase and RiboLock RNase inhibitor enzymes (Fermentas). About 1.2% of the cDNA was amplified by PCR in duplicate using SYBR Green qPCR Mix (Invitrogen) and a Rotorgene detection system (Corbett Research). To compare the relative amount of target genes in different samples, values were normalized to the housekeeping gene *Hprt* (Hypoxanthine-guanine phosphoribosyltransferase). qRT-PCR primers are listed in Table S5.

**Chromatin immunoprecipitation (ChIP)**

ChIP assays were performed according to the protocol of Upstate with some modifications, as described in the section with Supplemental information. The immunoprecipitated DNA was quantified by real-time qPCR. Gene-specific primers for qChIP analysis are listed in (Table S6). Selection of the likely PcG target genes was performed by a comparative analysis of the top list ($Log_2$ (FC) > ±0.58; FDR < 0.05) genes derived from RNA-seq data and a list composed of PcG target genes that were previously described [10,39–41].

**Statistics**

All statistical analysis was performed using GraphPad Prism software. Two-way unpaired (Figure 1-2, 3B-E and G, Figure 4C-G, Figure 5E, Figure 6, Figure S1-S3, Figure S4-S5E, Figure S6-S7, Figure S9C-G, Figure S10) or paired (Figure 3J-M and Figure 5C and H) student's t-test, and Pearson's correlation test (Figure S5F) were used.

**Acknowledgments**

We acknowledge Dr. Karel De Gendt for expert advice and valuable discussions, and Prof. Dr. Marie-Claude Hofmann for kindly providing the C18-4 cell line. We thank Maud De Meyer, Annemie Hoogmartens and Fabienne Withof for technical assistance. Prof. M. Baes (KU Leuven, Belgium) is acknowledged for the donation of *UBC-Cre* mice, and Prof. DH. Castrillon (University of Texas Southwestern Medical Center, USA) for providing the *Vasa*-Cre mice. RNA sequencing library preparation, sequencing and statistical analysis was performed by the VIB Nucleomics Core (www.nucleomics.be).

**Data availability**

All gene expression data are available at GEO under the accession number GSE83145.

**Author contributions**

M.F., M.Fa., A.V.E. and M.B. designed the study. M.F. performed the experiments, isolated and cultured the GFRA1$^{+}$ cells and analyzed the data. M.F., S.B., K.S. and I.V. generated and histologically analyzed the NIPP1 knockout model. C.W. made the PP1-NIPP1 fusion and contributed for MEFs isolation. M.B. and A. V. E. supervised the execution of the experiments. M.F., A.V.E. and M.B. wrote the manuscript. M.B. coordinated the project. All authors read and approved the final version of the manuscript.

**Competing financial interests**

The authors declare no competing financial interests.

**Funding**

This work was financially supported by the Fund for Scientific Research - Flanders (grant GOA6213N). The FCT/Portuguese Ministry of Science and Technology provided a doctoral fellowship for M. F.

## 4.6 References

1. Yoshida S, Nabeshima YI, Nakagawa T. Stem cell heterogeneity: Actual and potential stem cell compartments in mouse spermatogenesis. Ann. N. Y. Acad. Sci. 2007. p. 47–58.
2. Oatley JM, Brinster RL. Regulation of spermatogonial stem cell self-renewal in mammals. Annu. Rev. Cell Dev. Biol. 2008;24:263–86.
3. Shirakawa T, Yaman-Deveci R, Tomizawa S, Kamizato Y, Nakajima K, Sone H, et al. An epigenetic switch is crucial for spermatogonia to exit the undifferentiated state toward a Kit-positive identity. Development. 2013;140:3565–76.
4. Sasaki H, Matsui Y. Epigenetic events in mammalian germ-cell development: reprogramming and beyond. Nat Rev Genet. 2008;9:129–40.
5. Kubo N, Toh H, Shirane K, Shirakawa T, Kobayashi H, Sato T, et al. DNA methylation and gene expression dynamics during spermatogonial stem cell differentiation in the early postnatal mouse testis. BMC Genomics. 2015;16:624.

6. Ly L, Chan D, Trasler JM. Developmental windows of susceptibility for epigenetic inheritance through the male germline. Semin. Cell Dev. Biol. 2015. p. 96–105.
7. Sasaki H, Matsui Y. Epigenetic events in mammalian germ-cell development: reprogramming and beyond. Nat Rev Genet. 2008;9:129–40.
8. Komai Y, Tanaka T, Tokuyama Y, Yanai H, Ohe S, Omachi T, et al. Bmi1 expression in long-term germ stem cells. Sci. Rep. 2014;4:6175.
9. Kubo N, Toh H, Shirane K, Shirakawa T, Kobayashi H, Sato T, et al. DNA methylation and gene expression dynamics during spermatogonial stem cell differentiation in the early postnatal mouse testis. BMC Genomics. 2015;16:624.
10. Mu W, Starmer J, Fedoriw AM, Yee D, Magnuson T. Repression of the soma-specific transcriptome by polycomb-repressive complex 2 promotes male germ cell development. Genes Dev. 2014;28:2056–69.
11. Mu W, Starmer J, ShibatYa Y, Yee D, Magnuson T. EZH1 in germ cells safeguards the function of PRC2 during spermatogenesis. Dev Biol. 2017;424:198–207.
12. Sparmann A, van Lohuizen M. Polycomb silencers control cell fate, development and cancer. Nat. Rev. Cancer. 2006;6:846–56.
13. Aranda S, Mas G, Di Croce L. Regulation of gene transcription by Polycomb proteins. Sci. Adv.. 2015;1:e1500737.
14. Comet I, Helin K. Revolution in the Polycomb hierarchy. Nat. Struct. Mol. Biol. 2014;21:573–5.
15. Chen S, Bohrer LR, Rai AN, Pan Y, Gan L, Zhou X, et al. Cyclin-dependent kinases regulate epigenetic gene silencing through phosphorylation of EZH2. Nat. Cell Biol. 2010;12:1108–14.
16. Kaneko S, Li G, Son J, Xu CF, Margueron R, Neubert TA, et al. Phosphorylation of the PRC2 component Ezh2 is cell cycle-regulated and up-regulates its binding to ncRNA. Genes Dev. 2010;24:2615–20.
17. Minnebo N, Goernemann J, O'Connell N, Van Dessel N, Derua R, Vermunt MW, et al. NIPP1 maintains EZH2 phosphorylation and promoter occupancy at proliferation-related target genes. Nucleic Acids Res. 2013;41:842–54.
18. Yang CC, LaBaff A, Wei Y, Nie L, Xia W, Huo L, Yamaguchi H, Hsu YH, Hsu JL, Liu D, Lang J, Du Y, Lien HC, Li LY, Deng R, Chan LC, Yao J, Kleer CG, Hortobagyi GN HM. Phosphorylation of EZH2 at T416 by CDK2 contributes to the malignancy of triple negative breast cancers. Am J Transl Res. 2015;15:1009–20.
19. Wu SC, Zhang Y. Cyclin-dependent kinase 1 (CDK1)-mediated phosphorylation of enhancer of zeste 2 (Ezh2) regulates its stability. J. Biol. Chem. 2011;286:28511–9.
20. Wei Y, Chen Y-H, Li L-Y, Lang J, Yeh S-P, Shi B, et al. CDK1-dependent phosphorylation of EZH2 suppresses methylation of H3K27 and promotes osteogenic differentiation of human mesenchymal stem cells. Nat. Cell Biol. 2011;13:87–94.
21. Sahasrabuddhe a a, Chen X, Chung F, Velusamy T, Lim MS, Elenitoba-Johnson KSJ. Oncogenic Y641 mutations in EZH2 prevent Jak2/β-TrCP-mediated degradation. Oncogene. 2014;34:1–10.
22. Jin Q, Van Eynde A, Beullens M, Roy N, Thiel G, Stalmans W, et al. The protein phosphatase-1 (PP1) regulator, nuclear inhibitor of PP1 (NIPP1), interacts with the polycomb group protein, embryonic ectoderm development (EED), and functions as a transcriptional repressor. J. Biol. Chem. 2003;278:30677–85.
23. Roy N, Van Eynde A, Beke L, Nuytten M, Bollen M. The transcriptional repression by NIPP1 is mediated by Polycomb group proteins. Biochim. Biophys. Acta - Gene Struct. Expr. 2007;1769:541–5.
24. Nuytten M, Beke L, Van Eynde a, Ceulemans H, Beullens M, Van Hummelen P, et al. The transcriptional repressor NIPP1 is an essential player in EZH2-mediated gene silencing. Oncogene. 2008;27:1449–60.
25. Van Dessel N, Beke L, Goernemann J, Minnebo N, Beullens M, Tanuma N, et al. The phosphatase interactor NIPP1 regulates the occupancy of the histone methyltransferase EZH2 at Polycomb targets. Nucleic Acids Res. 2010;38:7500–12.
26. Heroes E, Lesage B, Goernemann J, Beullens M, Van Meervelt L, Bollen M. The PP1 binding code: A molecular-lego strategy that governs specificity. FEBS J. 2013. p. 584–95.

27. Beullens M, Vulsteke V, Van Eynde A, Jagiello I, Stalmans W, Bollen M. The C-terminus of NIPP1 (nuclear inhibitor of protein phosphatase-1) contains a novel binding site for protein phosphatase-1 that is controlled by tyrosine phosphorylation and RNA binding. Biochem. J. 2000;352 Pt 3:651–8.
28. Tanuma N, Kim SE, Beullens M, Tsubaki Y, Mitsuhashi S, Nomura M, et al. Nuclear inhibitor of protein phosphatase-1 (NIPP1) directs protein phosphatase-1 (PP1) to dephosphorylate the U2 small nuclear ribonucleoprotein particle (snRNP) component, spliceosome-associated protein 155 (Sap155). J. Biol. Chem. 2008;283:35805–14.
29. Van Dessel N, Boens S, Lesage B, Winkler C, Gornemann J, Van Eynde A, et al. Protein phosphatase PP1-NIPP1 activates mesenchymal genes in HeLa cells. FEBS Lett. 2015;22:1314-21.
30. Van Eynde A, Nuytten M, Dewerchin M, Schoonjans L, Keppens S, Beullens M, et al. The Nuclear Scaffold Protein NIPP1 Is Essential for Early Embryonic Development and Cell Proliferation. Mol Cell Biol. 2004;24:5863–74.
31. Ruzankina Y, Pinzon-Guzman C, Asare A, Ong T, Pontano L, Cotsarelis G, et al. Deletion of the Developmentally Essential Gene ATR in Adult Mice Leads to Age-Related Phenotypes and Stem Cell Loss. Cell Stem Cell. 2007;1:113–26.
32. Kwan KM. Conditional alleles in mice: Practical considerations for tissue-specific knockouts. Genesis. 2002. p. 49–62.
33. Ruwanpura SM, McLachlan RI, Meachem SJ. Hormonal regulation of male germ cell development. J. Endocrinol. 2010;205:117–31.
34. Agrimson KS, Onken J, Mitchell D, Topping TB, Chiarini-Garcia H, Hogarth CA, et al. Characterizing the Spermatogonial Response to Retinoic Acid During the Onset of Spermatogenesis and Following Synchronization in the Neonatal Mouse Testis. Biol. Reprod. 2016;95:81.
35. Cao R, Zhang Y. SUZ12 is required for both the histone methyltransferase activity and the silencing function of the EED-EZH2 complex. Mol. Cell. 2004;15:57–67.
36. Cao R, Zhang Y. The functions of E(Z)/EZH2-mediated methylation of lysine 27 in histone H3. Curr. Opin. Genet. Dev. 2004. p. 155–64.
37. Pasini D, Bracken AP, Jensen MR, Lazzerini Denchi E, Helin K. Suz12 is essential for mouse development and for EZH2 histone methyltransferase activity. Embo J. 2004;23:4061–71.
38. Montgomery ND, Yee D, Chen A, Kalantry S, Chamberlain SJ, Otte AP, et al. The murine polycomb group protein Eed is required for global histone H3 lysine-27 methylation. Curr. Biol. 2005;15:942–7.
39. Bracken AP, Dietrich N, Pasini D, Hansen KH, Helin K. Genome-wide mapping of polycomb target genes unravels their roles in cell fate transitions. Genes Dev. 2006;20:1123–36.
40. Lee TI, Jenner RG, Boyer LA, Guenther MG, Levine SS, Kumar RM, et al. Control of Developmental Regulators by Polycomb in Human Embryonic Stem Cells. Cell. 2006;125:301–13.
41. Squazzo SL, O'Geen H, Komashko VM, Krig SR, Jin VX, Jang SW, et al. Suz12 binds to silenced regions of the genome in a cell-type-specific manner. Genome Res. 2006;16:890–900.
42. Xu K, Wu ZJ, Groner AC, He HH, Cai C, Lis RT, et al. EZH2 Oncogenic Activity in Castration-Resistant Prostate Cancer Cells Is Polycomb-Independent. Science (80). 2012;338:1465–9.
43. Campbell JE, Kuntz KW, Knutson SK, Warholic NM, Keilhack H, Wigle TJ, et al. EPZ011989, A potent, orally-available EZH2 inhibitor with robust in vivo activity. ACS Med. Chem. Lett. 2015;6:491–5.
44. Feil S, Valtcheva N, Feil R. Inducible cre mice. Methods Mol. Biol. 2009;530:343–63.
45. Caretti G, Palacios D, Sartorelli V, Puri PL. Phosphoryl-EZH-ion. Cell Stem Cell. 2011. p. 262–5.
46. Zeng X, Chen S, Huang H. Phosphorylation of EZH2 by CDK1 and CDK2: A possible regulatory mechanism of transmission of the H3K27me3 epigenetic mark through cell divisions. Cell Cycle. 2011. p. 579–83.
47. Chakrabarti R, Kline D, Lu J, Orth J, Pilder S, Vijayaraghavan S. Analysis of Ppp1cc-null mice suggests a role for PP1gamma2 in sperm morphogenesis. Biol. Reprod. 2007;76:992–1001.

48. Forgione N, Vogl AW, Varmuza S. Loss of protein phosphatase 1cc (PPP1CC) leads to impaired spermatogenesis associated with defects in chromatin condensation and acrosome development: An ultrastructural analysis. Reproduction. 2010;139:1021–9.
49. Sinha N, Puri P, Nairn AC, Vijayaraghavan S. Selective ablation of Ppp1cc gene in testicular germ cells causes oligo-teratozoospermia and infertility in mice. Biol. Reprod.. 2013;89:128.
50. Kim SE, Shima H, Nakamura K, Kikuchi K. Broad specificity in binding of NIPP-1, nuclear inhibitor of protein phosphatase-1, to PP1 isoforms in vivo. Tohoku J. Exp. Med. 2000;191:39–45.
51. Boens S, Verbinnen I, Verhulst S, Szekér K, Ferreira M, Gevaert T, et al. The deletion of the phosphatase regulator NIPP1 causes progenitor cell expansion in the adult liver. Stem Cells. 2016;34:2256-2262.
52. Gallardo T, Shirley L, John GB, Castrillon DH. Generation of a germ cell-specific mouse transgenic Cre line, Vasa-Cre. Genesis. 2007;45:413–7.
53. Sato T, Katagiri K, Kubota Y, Ogawa T. In vitro sperm production from mouse spermatogonial stem cell lines using an organ culture method. Nat. Protoc. 2013;8:2098–104.
54. Sato T, Katagiri K, Gohbara A, Inoue K, Ogonuki N, Ogura A, et al. In vitro production of functional sperm in cultured neonatal mouse testes. Nature. 2011;471:504–7.
55. Arai R, Ueda H, Kitayama a, Kamiya N, Nagamune T. Design of the linkers which effectively separate domains of a bifunctional fusion protein. Protein Eng. 2001;14:529–32.
56. Winkler C, Munter S De, Dessel N Van, Lesage B, Heroes E. The selective inhibition of protein phosphatase-1 results in mitotic catastrophe and impaired tumor growth. J. Cell Sci. 2015;128:4526–37.

# 4.7 Supplemental Information

## 4.7.1 Additional Experimental Procedures

**Testosterone assay**

Serum testosterone was determined at the Centre for Laboratory Medicine (Laboratoriumgeneeskunde UZ-KU Leuven, Belgium). Blood was extracted by cardiac puncture from male mice of 9 weeks that had been housed with an adult female for 2 weeks.

**Chromatin immunoprecipitation (ChIP)**

ChIP assays were performed as described [1]. Briefly, 100 mg of testis was cross-linked with 1% paraformaldehyde (PFA) in PBS during 10 min at room temperature before stopping the reaction with 250 mM glycine. After centrifugation (425 x *g*) for 5 minutes at 4°C, the pellet was dissolved in SDS lysis buffer (50 mM Tris/HCl at pH 8.0, 1% SDS, 10 mM EDTA), supplemented with 20 mM NaF, 5 µM leupeptin, 0.5 mM phenylmethanesulfonyl fluoride, 0.5 mM benzamidine and 1 mM orthovanadate, and sonicated in the Bioruptor sonicator with 30 sec on/30 sec off cycles during 35 minutes at 4°C. 500 µg of sheared chromatin ($OD_{260}$) was pre-cleared with 35 µl of pre-blocked Protein-A-Sepharose for 2 hours at 4°C. Protein-A-Sepharose was blocked with 1 mg/ml BSA, 1 mg/ml salmon sperm DNA and 1% Triton X-100. 150 µg of pre-cleared chromatin was incubated overnight at 4°C with 3 µl of anti-H3K27me3 antibody (1 mg/ml; Table S4) or with polyclonal rabbit anti-mouse immunoglobulins (IgG). Then 30 µl pre-blocked protein-A-Sepharose was added for 1h. The beads were washed once with low salt buffer (16.7 mM Tris-HCl at pH 8.1, 1% Triton X-100, 167 mM NaCl, 1.2 mM EDTA and 0.01% SDS), once with high salt buffer (20 mM Tris-HCl at pH 8.1, 1% Trition X-100, 500 mM NaCl, 0.1% SDS and 2 mM EDTA), once with LiCl buffer (10 mM Tris-HCl at pH 8.1, 0.25 M LiCl, 1% NP-40 and 1% Na-deoxycholate), and twice with TE buffer (10 mM Tris/HCl at pH 8.0, 1 mM EDTA). The histone/DNA complex was twice eluted at 65°C with fresh elution buffer (0.1 M NaHCO3 at pH 8.0, 1% SDS). After reversing the cross-links by incubation with 0.2 M NaCl and RNAase A for 4h at 65°C, the samples were treated with Proteinase K. Subsequently, the DNA was purified using the GenElute™ PCR Clean-up kit (Sigma).

**RNA sequencing**

The Nanodrop ND-1000 (Nanodrop Technologies) was used to determine the RNA concentration and purity and the Bioanalyser 2100 (Agilent) to assess the RNA integrity of all RNA samples. Library preparation, sequencing and analysis were performed by the VIB Nucleomics Core (www. nucleomics.be) according to their standard protocols. Briefly, 5 µg of total RNA per sample was used as input. rRNA was depleted using Illumina TruSeq® Stranded Total RNA Sample Prep Kit with Ribo-Gold (Illumina). cDNA was generated using random primers and double stranded cDNA was synthesized using DNA polymerase I and RNAase H. Next, multiple indexing adapters were ligated to introduce different barcodes for each sample, followed by an enrichment PCR. The sequence libraries of each sample were equimolarly pooled and sequenced (1/2 run of iIllumina NextSeq500 flow-cell at 2x 75 bp). Preprocessing was performed using FastX 0.013, Cutadapt 1.7.1 and Short read 1.16.3 to remove mainly low quality ends, adaptor sequences and unreliable reads [2–5]. For the mapping of the reads alignment with Tophat v2.0.13 to the reference genome of *Mus musculus* (GRCm38.73) was performed [6]. Reads with a mapping quality smaller than 20 were removed from the alignments using Samtools 1.1 [7]. Transcript coordinates were extracted from the GRC reference annotation (Gffread from the Cufflinks v2.1.1 suite), and merged to gene coordinates (mergeBed from the Bedtools v2.17.0 toolkit). Next, the number of aligned reads per gene was counted (HTSeq-count v0.6.1p1) [8,9]. Genes for which all samples had less than 1 cpm (count-per-million) were removed. Raw counts for the retained 17.344 genes were further corrected within samples for GC-content and between samples using full quantile-normalization, according to the EDASeq package from Bioconductor [10]. Differential gene expression was determined with the EdgeR 3.4.0 package by fitting a negative binomial generalized linear model (GLM) against the normalized counts [11]. Differential expression was tested for with a GLM likelihood ratio test and the resulting p-values were corrected for multiple testing with Benjamini-Hochberg to control the false discovery rate [12].

## 4.7.2 Additional Figures and Tables

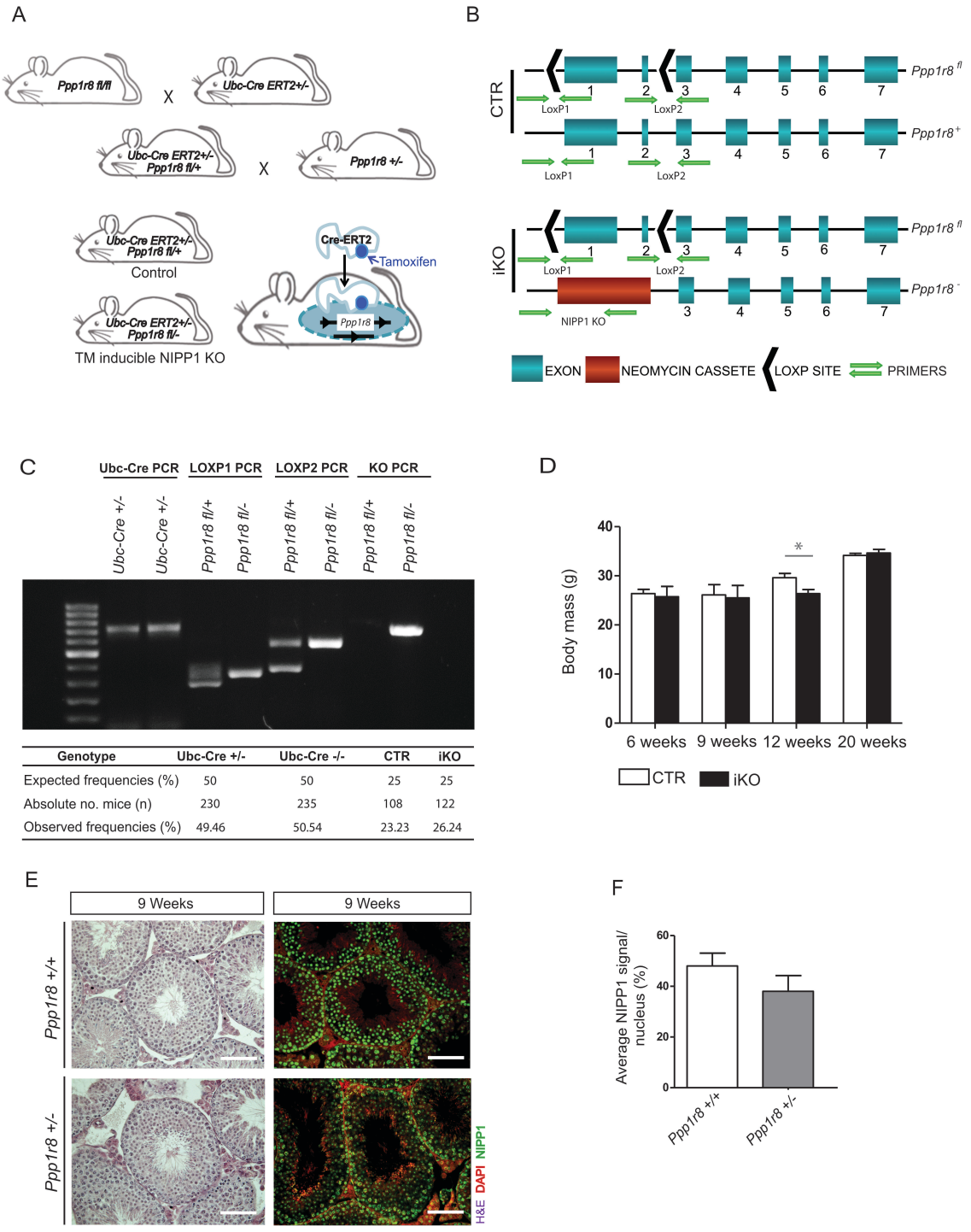


| Genotype | Ubc-Cre +/- | Ubc-Cre -/- | CTR | iKO |
|---|---|---|---|---|
| Expected frequencies (%) | 50 | 50 | 25 | 25 |
| Absolute no. mice (n) | 230 | 235 | 108 | 122 |
| Observed frequencies (%) | 49.46 | 50.54 | 23.23 | 26.24 |

**Figure S1. Breeding strategy and mice genotyping for inducible deletion of NIPP1.** (A) Scheme of crossing strategy for the generation of the inducible *Ppp1r8* knockout mice (iKO) and their controls (CTR). The administration of tamoxifen causes the nuclear translocation of CRE-ERT2 [13]. (B) Scheme of the localization of the primers used for PCR-based genotyping of the CTR and iKO. (C) Representative example of PCRs on genomic tail DNA used for genotyping

CTR and iKO. The primer sequences are shown in Table S3. Also indicated are frequencies of the offspring from the *Ubc-Cre-ERT2*$^{+/-}$, *Ppp1r8*$^{fl/+}$ and *Ppp1r8*$^{+/-}$ mice crosses. (D) Body mass of tamoxifen-injected CTR and iKO mice at 6, 9, 12 and 20 weeks. (E) Hematoxylin-Eosin staining (left panels) and immunostainings of NIPP1 (right panels) in testis from wild-type (WT) mice and *Ppp1r8*$^{+/-}$ mice at 9 weeks. Bar, 50 µm. (F) Quantification of NIPP1 immunostainings as described in panel (E). The data represent means ± SEM. (n=4).

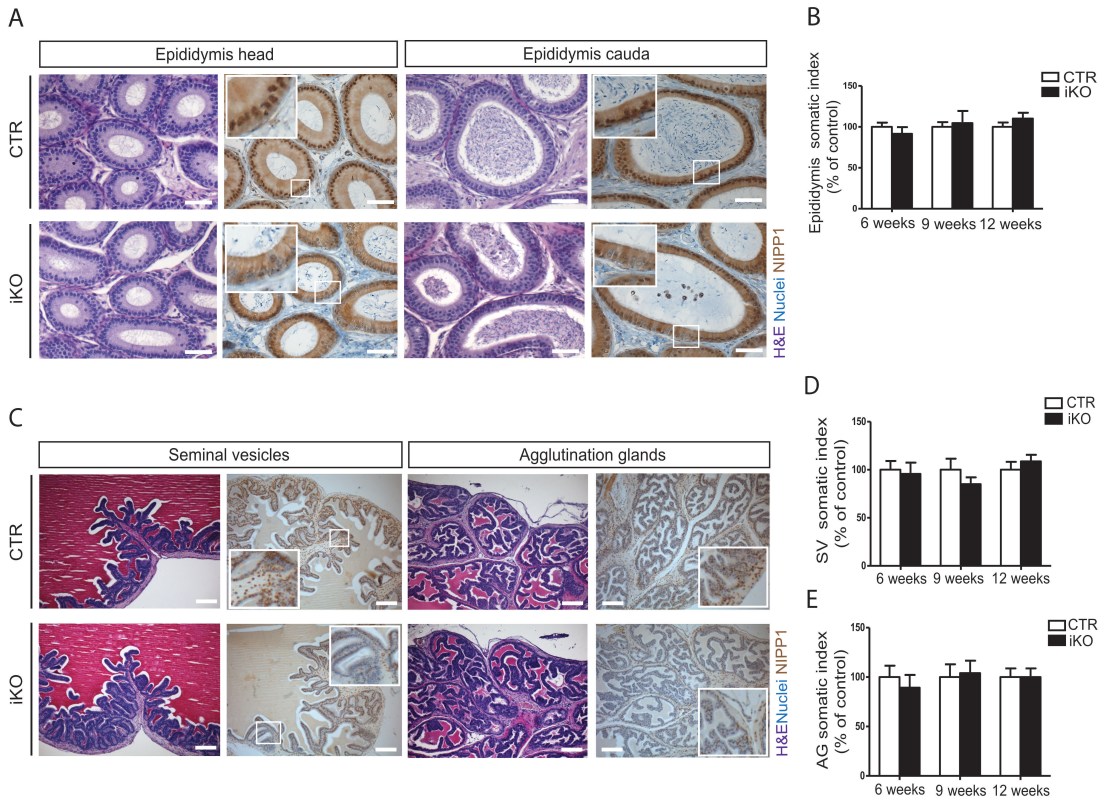


**Figure S2. The somatic index of the epididymis and the male accessory glands are not affected by the tamoxifen-induced deletion of NIPP1.** (A) Sections of the epididymis head and cauda from tamoxifen-injected mice at the age of 9 weeks were stained for Hematoxylin-Eosin (H&E) and NIPP1. Scale bars represent 50 µm in all panels of this figure. (B) The epididymis somatic index of tamoxifen-injected CTRs and iKOs at the indicated timepoints. The somatic index was determined by the percentage of total organ weight (g) over the body weight (g), and was expressed as a % of the value for the CTRs. All data are represented as means ± SEM. (n=4). (C) Sections of seminal vesicles (SV) and agglutination glands (AG) from tamoxifen-injected CTR and iKO mice at the age of 9 weeks were stained for H&E and NIPP1. (D) The SV somatic index of tamoxifen-injected CTRs and iKOs at the indicated time points. (E) The AG somatic index of tamoxifen-injected CTRs and iKOs at the indicated time points.

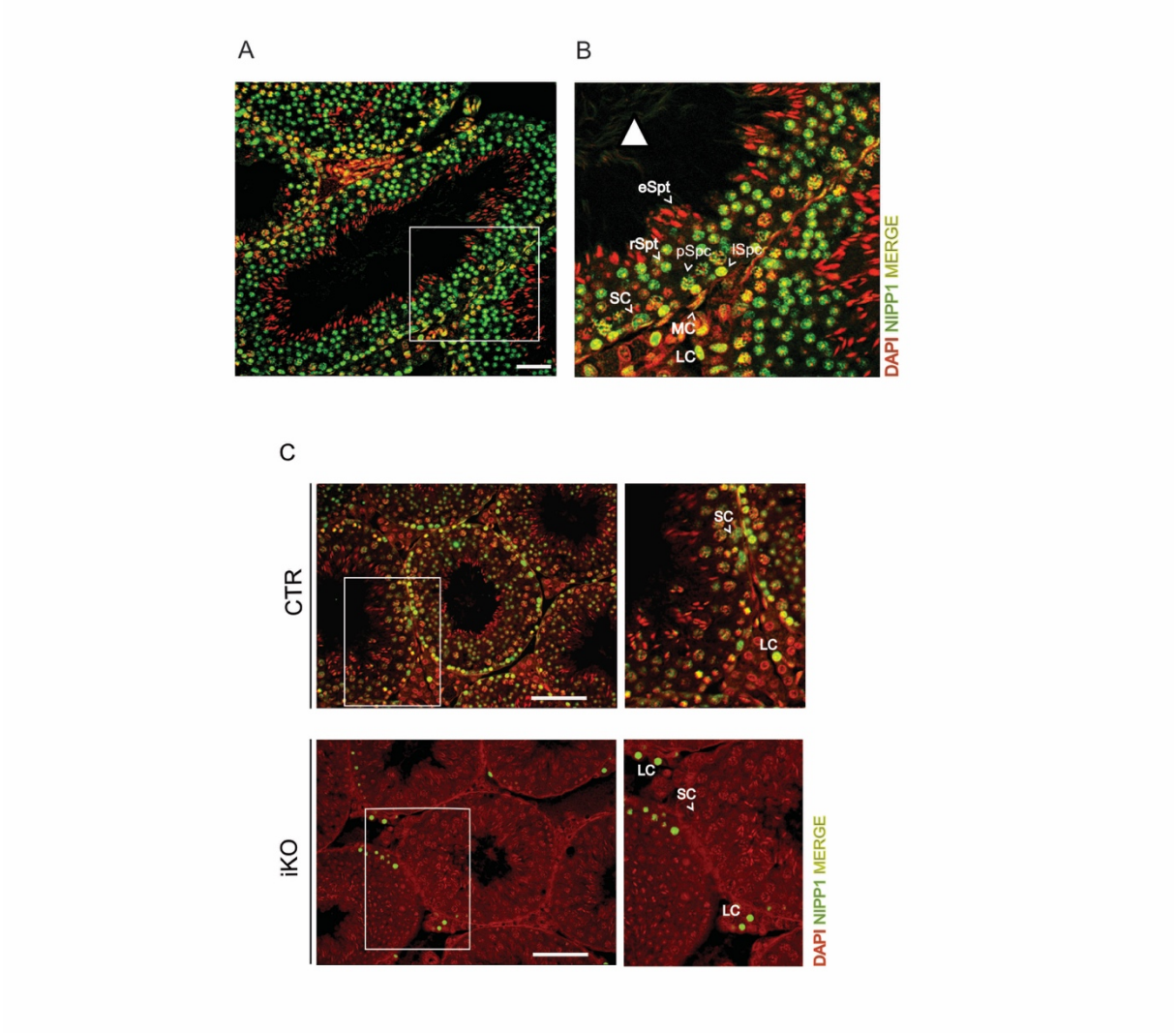


**Figure S3. Expression of NIPP1 in testis of adult mice.** (A) Immunostainings of NIPP1 in testis from wild-type mice at the age of 6 weeks. Scale bar, 25 µm. (B) Higher amplification of the square from panel (A). LC, Leydig cells; MC, Myoid cells; SC, Sertoli cells; Spc, spermatocytes; pSpg, pachytene spermatocytes; lSpc, leptotene spermatocytes; eSpt, elongated spermatids; rSpt, round spermatids. White triangle, lumen. (C) Magnifications of CTR and iKO testis sections immunostained for NIPP1, showing that NIPP1 is expressed in germ cells and somatic cells of the seminiferous tubules in the CTR mice and is efficiently deleted in the iKO mice. SC, Sertoli cells; LC, Leydig cells.

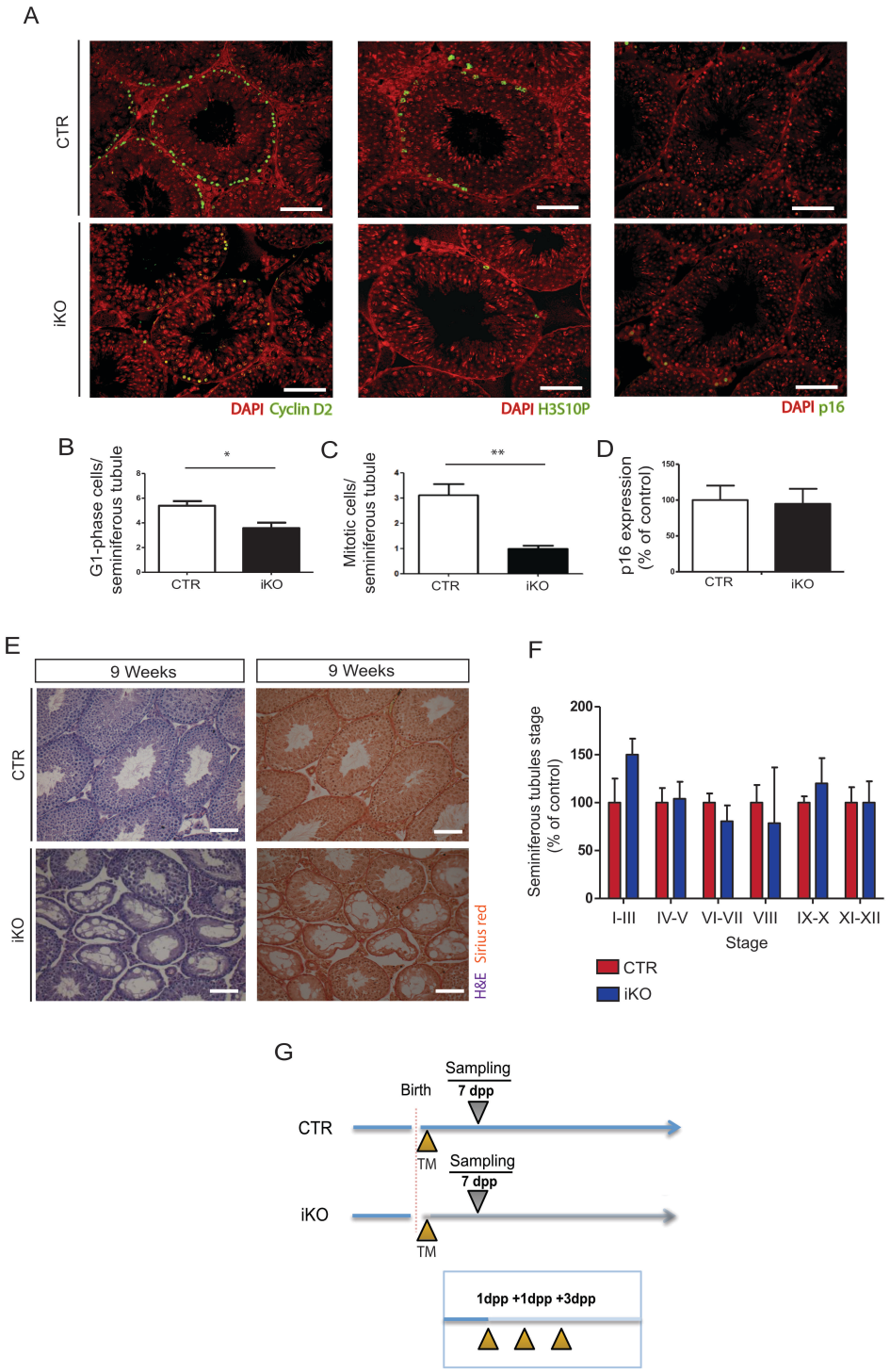


**Figure S4. The testicular loss of NIPP1 results in hypoproliferation but not senescence or fibrosis.** (A) Testis sections of tamoxifen-treated mice of 6 weeks were stained for Cyclin D2, phospho-Ser 10 of Histone H3 (H3S10P) and p16. Scale bar, 50 µm. (B) Quantification of G1-phase cells by counting the number of Cyclin D2 positive cells per seminiferous tubule of immunostainings as shown in panel (A). All data are represented as means ± SEM (n=4). *, $p<0.05$; **, $p<0.01$. (C) Quantification of mitotic cells by counting the number of H3S10P positive

cells in the immunostaining from panel (A). (D) Quantification of the immunostainings of the senescence marker p16 from panel (A). (E) Testis sections of tamoxifen-treated mice of 6 weeks were stained for fibrosis with Sirius red. Scale bar, 50 µm. (F) Quantification of the indicated seminiferous tubule stages (I-XII) stained testis sections of tamoxifen-treated mice at the age of 6 weeks [14]. (G) Scheme of tamoxifen induction and sampling of testis from neonates. UBC-CRE-ERT2 driven deletion of *Ppp1r8* was induced by the subcutaneous injection of 0.2 mg tamoxifen/g mouse in 1 dpp-old newborns. W, weeks; dpp, days post-partum; TM, tamoxifen.

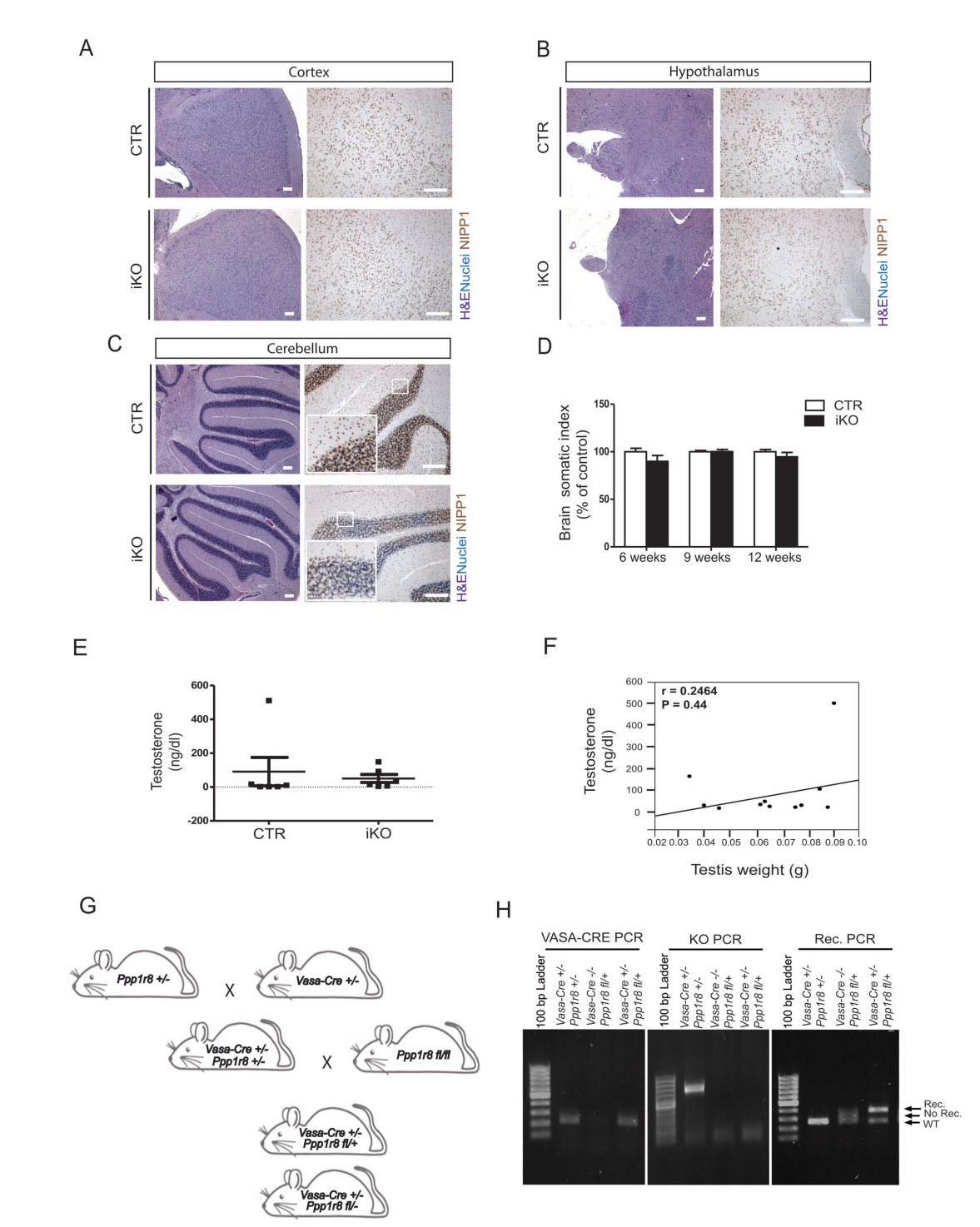


**Figure S5. The testis phenotype is an intrinsic testicular defect.** (A) Brain cortex sections of tamoxifen-treated mice of 6 weeks were stained for hematoxylin & eosin (H&E) and NIPP1. Scale bars represent 100 µm in all panels of this Figure. (B) Hypothalamus sections of tamoxifen-treated mice of 6 weeks were stained for H&E and NIPP1. (C) Cerebellum sections of tamoxifen-treated mice of 6 weeks were stained for H&E and NIPP1. (D) The brain somatic index of tamoxifen-treated CTR and iKO mice at the indicated timepoints. (E) Testosterone levels in blood serum of tamoxifen-treated mice of 9 weeks. Data are means ± SEM (n=6). (F) Scatter plot of the correlation

between testis weight (g) and blood testosterone basal levels (ng/dl). Pearson's correlation test: *r*, correlation coefficient; p, *p* value. (G) Scheme of breeding strategy for the generation of the testis specific *Ppp1r8* knockout mice using the transgenic *Vasa*-Cre mice. (H) Representative example of the PCR amplicons derived from PCR on tail DNA from mice with the indicated genotypes. The following primers were used: primers *VasaCre* forward and *VasaCre* reverse in lanes 2-4, primers NIPP1 KO forward and NIPP1 KO reverse in lanes 6-8 and primers LoxP1 forward, LoxP1 reverse and LoxP2 reverse in lanes 10-12. The efficiency and specificity of the *Vasa-Cre* recombinase is shown in lanes 10-12, where the resulting PCRs amplicons which correspond to NIPP1 wild-type (WT; 267 bp), no recombined $NIPP1^{fl}$ (No Rec; 329 bp) and recombined $NIPP1^{fl}$ (Rec; 389 bp) are represented. The sequence and location of the primers are indicated in Supplemental information. bp, base pairs; fl, loxP allele.

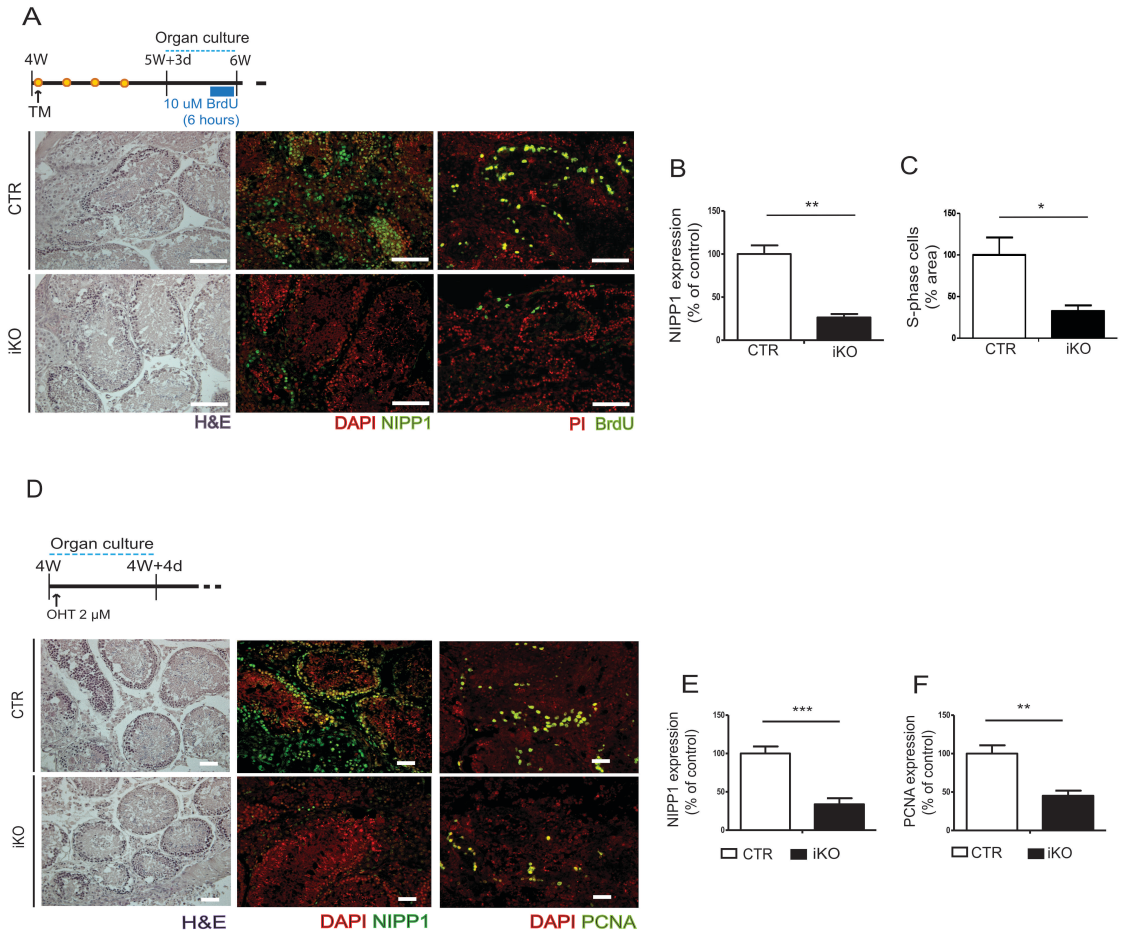


**Figure S6. The deletion of NIPP1 leads to a reduced proliferation of germ cells in cultured testis slices.** (A) Testis from tamoxifen-treated CTR and iKO mice were isolated at 5 weeks and 3 days, and cultured for 4 days. After incubation with BrdU for 6 hours, testis sections were prepared and stained for H&E, NIPP1 and incorporated BrdU. Scale bar, 50 µm. (B) Quantification of NIPP1 immunostainings as shown in panel (A). All data in this Figure are represented as means ± SEM (n=4). *, $p<0.05$; **, $p<0.01$. (C) Quantifications of BrdU immunostainings of panel (A). *, $p<0.05$. (D) Organ culture of testis slices that were isolated from non-treated CTRs and iKOs of 4 weeks. (Z)-4-Hydroxytamoxifen (4-OHT) was added to the slices for 96 hours to delete the floxed *Ppp1r8* allele. Subsequently, testis sections were stained for NIPP1 and PCNA. Scale bar, 50 µm. (E, F) Quantification of stainings as shown in (D) (n=4). **, $p<0.01$; ***, $p<0.001$.

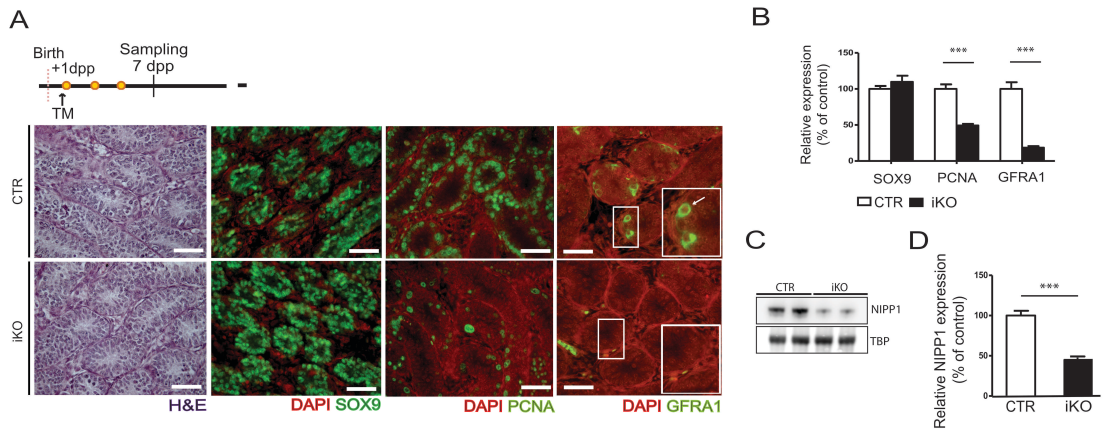


**Figure S7. The removal of NIPP1 from neonatal testis decreases the proliferation of gonocyte-derived cells.** (A) Testis sections from neonates of 7 days (dpp, days post-partum) that had been treated with tamoxifen were stained for H&E, SOX9, PCNA and GFRA1. Scale bar, 50 μm. (B) Quantifications of stainings as shown in panel (A) (n=4). (C) Testis lysates from the same mice were used for immunoblotting with the indicated antibodies. TBP was used as a loading control. (D) Quantifications of NIPP1 expression as shown in panel (C) (n=4).

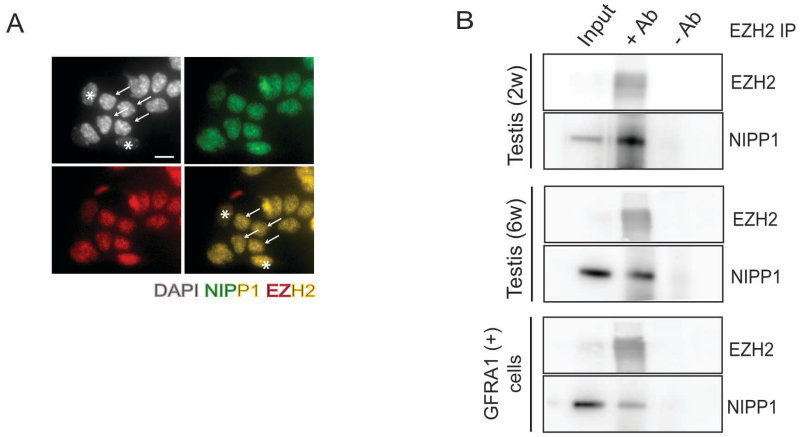


**Figure S8. NIPP1 forms a complex with EZH2 in testis and GFRA1$^+$ cells.** (A) Co-localization of NIPP1 (green) and EZH2 (red) in the nucleus of GFRA1$^+$-enriched cultured cells. Arrows indicate GFRA1$^+$ colonies formed after 96h. *, mouse embryonic fibroblast (MEF) nucleus. GFRA1$^+$, undifferentiated spermatogonia. (B) Endogenous EZH2 was immunoprecipitated from testis nuclear extracts and GFRA1$^+$-enriched cell lysates and, examined for associated NIPP1 by immunoblotting. IP, immunoprecipitation; W, weeks; + Ab, EZH2 antibody added; - Ab, no antibody added. Scale bar, 10 μm.

**Table S1.** Expression of the indicated genes in tamoxifen-treated CTR and iKO mice of 6 weeks, as derived from the RNA sequencing data. FC, Fold-change; FDR, False Discovery Rate.

| GENE ID | DESCRIPTION | FC | FDR |
|---|---|---|---|
| *Ezh2* | enhancer of zeste homolog 2 | 0.892 | 0.183 |
| *Eed* | embryonic ectoderm development | 0.988 | 0.954 |
| *Suz12* | suppressor of zester 12 homolog | 0.978 | 0.902 |
| *Rbbp4* | retinoblastoma binding protein 4 | 0.892 | 0.121 |
| *Cdc5l* | cell division cycle 5-like | 1.066 | 0.705 |
| *Sf3b1* | splicing factor 3b, subunit 1 | 0.960 | 0.811 |
| *Melk* | maternal embryonic leucine zipper kinase | 0.789 | 0.615 |
| *Ppp1ca* | protein phosphatase 1, catalytic subunit, alpha isoform | 0.919 | 0.200 |
| *Ppp1cb* | protein phosphatase 1, catalytic subunit, beta isoform | 0.854 | 0.385 |
| *Ppp1cc* | protein phosphatase 1, catalytic subunit, gamma isoform | 0.918 | 0.559 |

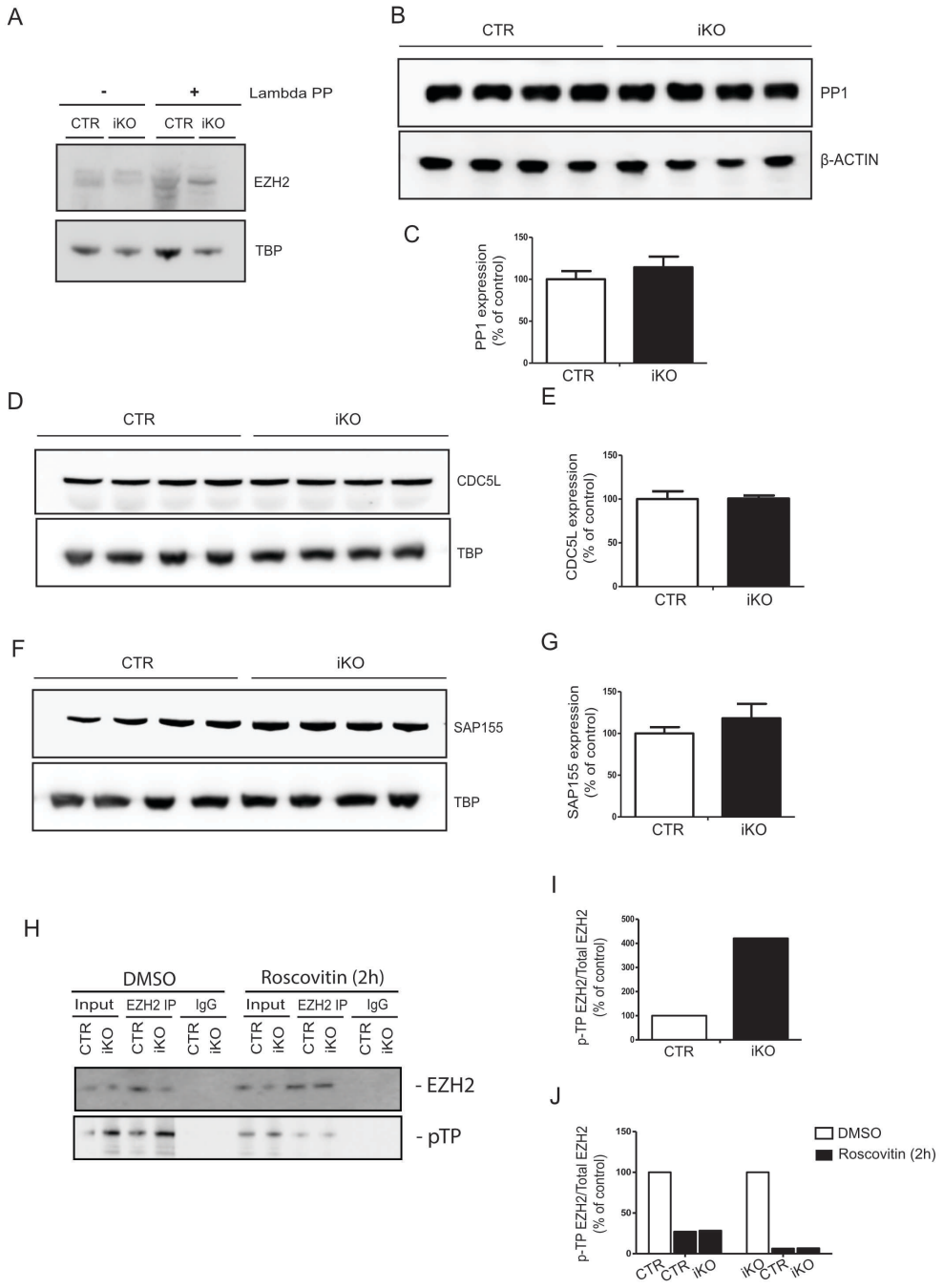


**Figure S9. The deletion of NIPP1 destabilizes EZH2 but has no effect on the level of other NIPP1 ligands.** (A) Lysates from tamoxifen-treated mice of 6 weeks were pre-incubated with phosphatase-inhibitors or with lambda phosphatase (PP) and the level of EZH2 was verified by immunoblotting. TATA-binding protein (TBP) was used as a loading control. (B) The level of PP1 in total testis extracts from tamoxifen-treated mice of 6 weeks was visualized by immunoblotting. β-actin was used as a loading control. (C) Quantifications of PP1 levels from panel (B). All bar data in this Figure are means ± SEM (n=4). (D) The level of CDC5L in total testis extracts from tamoxifen-treated mice of 6 weeks was detected by immunoblotting. TBP was used as a loading

control. (E) Quantifications of CDC5L levels from panel (D). (F) The level of SAP155 in total testis extracts from tamoxifen-treated mice of 6 weeks was visualized by immunoblotting. TBP was used as a loading control. (G) Quantifications of SAP155 levels from panel (F). (H) Endogenous EZH2 was immunoprecipitated from $GFRA1^{+}$-enriched cell lysates out of a pool of CTR and iKO 12 days-old mice (n=3). Cells were pre-incubated with 4-OTH for 72 hours and later with either dimethylsulfoxide (DMSO) or 150 μM of the Cdk-inhibitor roscovitine for 2 hours. Phosphorylation was further analyzed by immunoblotting with pan-pTP antibodies. (I) Quantification of pTP levels in CTR and iKO, as shown in panel (H). (J) Quantification of pTP/EZH2 ratio in CTR and iKO, before and after preincubation of the cells with roscovitine, as shown in panel (H).

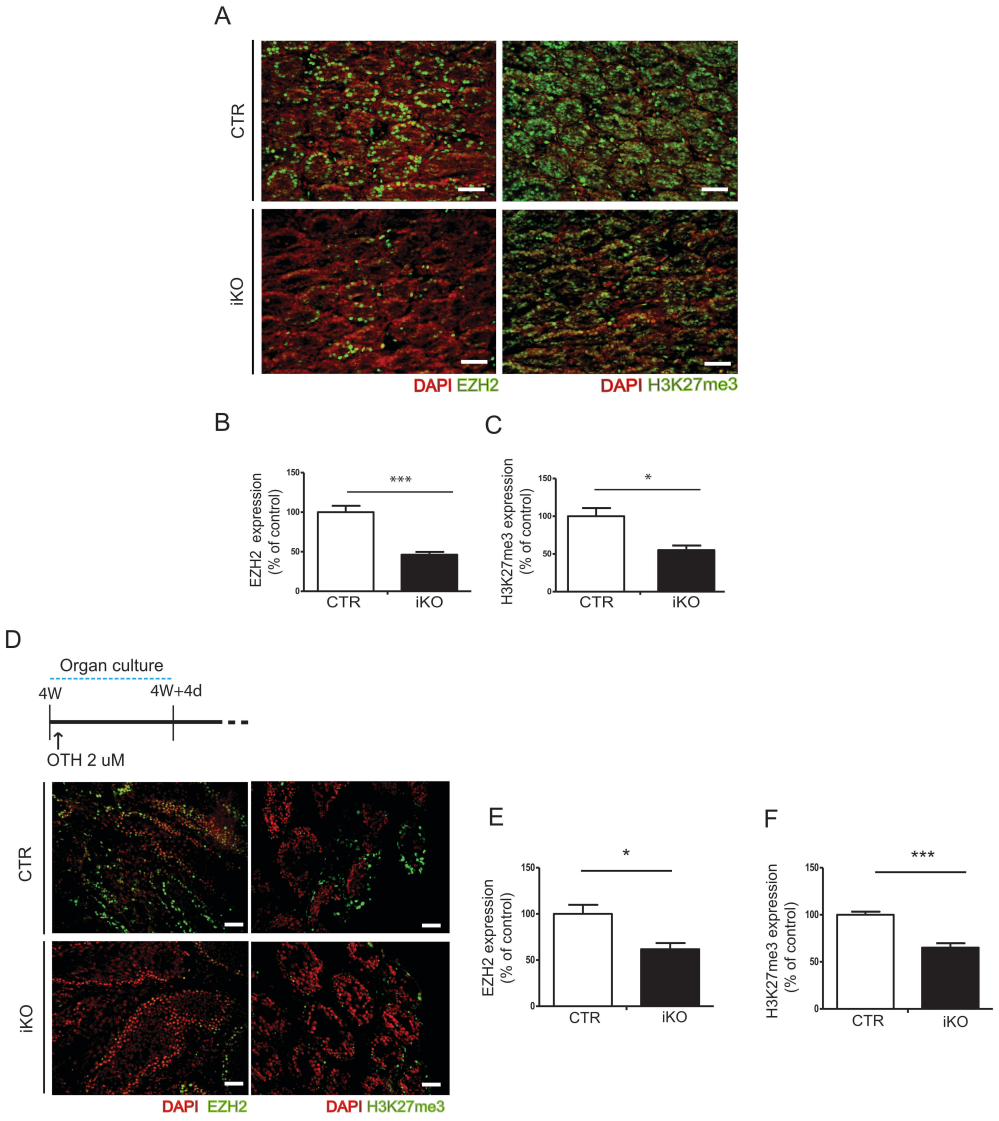


**Figure S10. The loss of NIPP1 is associated with decreased H3K27me3 levels.** (A) Testis slices from tamoxifen-treated CTR and iKO neonates of 7 days (dpp, days post-partum). Testis sections were immunostained for EZH2 and H3K27me3. Scale bar, 50 µM. (B) Quantifications of EZH2 immunostainings as shown in panel (A). All bar data in this Figure are represented as means ± SEM (n= 4). ***, $p<0.001$. (C) Quantifications of H3K27me3 immunostainings as shown in panel (A). *, $p<0.05$. (D) Organ culture of testis slices that were isolated from non-treated mice of 4 weeks. Hydroxytamoxifen (HTO) was added to the slices for 96 hours to delete the floxed *Ppp1r8* allele in CTRs and iKOs. Subsequently, testis sections were stained for EZH2 and H3K27me3. Scale bar, 50 µM. (E) Quantifications of EZH2 immunostainings as shown in panel (D). *, $p<0.05$. (F) Quantifications of H3K27me3 immunostainings as shown in panel (D). ***, $p<0.001$.

**Table S2.** Differentially expressed genes in iKO mice of 6 weeks, as derived from the RNA sequencing data. Genes are arranged by descendent order of FDR value.

| UPREGULATED GENES | | | | | | DOWNREGULATED GENES | | | | | |
|---|---|---|---|---|---|---|---|---|---|---|---|
| **GENE ID** | **FC** | **FDR** | **GENE ID** | **FC** | **FDR** | **GENE ID** | **FC** | **FDR** | **GENE ID** | **FC** | **FDR** |
| *Sgsh* | 3.814 | 4.344E-18 | Phkg1 | 3.296 | 1.177E-02 | Cuzd1 | 0.1858 | 6.6E-27 | Try5 | 0.4637 | 5.1E-03 |
| *Adh1* | 2.150 | 5.919E-14 | Wfs1 | 2.731 | 1.217E-02 | Slc9c1 | 0.5227 | 2.0E-25 | Cenpt | 0.5038 | 5.1E-03 |
| *C1qtnf4* | 1.611 | 2.010E-12 | *Adamtsl1* | 1.547 | 1.224E-02 | *Gmcl1* | 0.5875 | 2.0E-20 | *Gipc2* | 0.4858 | 5.2E-03 |
| *Rgs9* | 3.396 | 2.942E-10 | *Arhgap30* | 1.545 | 1.263E-02 | *Tdrd9* | 0.6161 | 4.3E-18 | *Nlrp4c* | 0.4366 | 5.3E-03 |
| *Ccnb3* | 2.184 | 1.857E-09 | *Nlrp10* | 4.526 | 1.424E-02 | *Lrpprc* | 0.5435 | 7.5E-18 | *Dnph1* | 0.2875 | 5.3E-03 |
| *Nmnat3* | 1.592 | 1.708E-07 | *Lrsam1* | 1.559 | 1.501E-02 | *Gm13941* | 0.6049 | 2.8E-17 | *Pigv* | 0.6283 | 5.4E-03 |
| *Ttn* | 1.559 | 2.245E-06 | *Otud6a* | 1.509 | 1.547E-02 | *Cpsf1* | 0.6317 | 1.7E-13 | *A1cf* | 0.5035 | 6.0E-03 |
| *Leng8* | 1.565 | 2.356E-06 | *Ptprt* | 1.533 | 1.586E-02 | *Hist1h1t* | 0.5530 | 7.4E-12 | *Hist1h2ak* | 0.4407 | 6.1E-03 |
| *Ppp1r1c* | 1.617 | 2.501E-06 | *Npr2* | 1.855 | 1.615E-02 | *Kntc1* | 0.5816 | 7.5E-12 | *Myh13* | 0.3547 | 6.7E-03 |
| *Zfp940* | 1.955 | 4.534E-06 | *Slc1a4* | 2.774 | 1.624E-02 | *Tuba3a* | 0.6482 | 3.4E-10 | *Pop5* | 0.5532 | 6.7E-03 |
| *Prss35* | 1.716 | 7.238E-06 | *Nfatc2* | 1.862 | 2.087E-02 | *Wdr63* | 0.6622 | 1.6E-09 | *Mal* | 0.5788 | 8.0E-03 |
| *Pmp2* | 2.266 | 9.900E-06 | *Bbc3* | 2.758 | 2.172E-02 | *Abca2* | 0.3703 | 2.7E-09 | *Large* | 0.6120 | 9.8E-03 |
| *Prdm8* | 2.630 | 1.032E-05 | *Abcg8* | 2.100 | 2.260E-02 | *Zbtb17* | 0.6102 | 4.0E-09 | *Adam7* | 0.0867 | 1.1E-02 |
| *Nsun5* | 1.931 | 1.131E-05 | *Mypn* | 1.588 | 2.465E-02 | *Ces5a* | 0.1387 | 6.4E-09 | *Jph1* | 0.3192 | 1.1E-02 |
| *Trpv1* | 2.573 | 1.962E-05 | *Icam2* | 3.094 | 2.479E-02 | *Wdr11* | 0.6369 | 6.6E-09 | *Rundc3b* | 0.5938 | 1.1E-02 |
| *Slc1a3* | 1.801 | 3.031E-05 | *Agmo* | 2.574 | 2.527E-02 | *Daw1* | 0.6004 | 7.4E-09 | *Cdkn2a* | 0.3445 | 1.1E-02 |
| *Pet2* | 1.788 | 3.566E-05 | *Xrcc3* | 1.729 | 2.527E-02 | *Ercc2* | 0.6209 | 1.7E-08 | *Hist1h2bj* | 0.3960 | 1.1E-02 |
| *Dact1* | 1.979 | 3.605E-05 | *Dtx3l* | 1.650 | 2.664E-02 | *Dnhd1* | 0.6257 | 2.3E-08 | *Prtg* | 0.2723 | 1.1E-02 |
| *Hist2h2be* | 1.566 | 3.615E-05 | *Hsd3b6* | 1.947 | 2.740E-02 | *Sord* | 0.4173 | 4.6E-08 | *Prpsap2* | 0.6400 | 1.2E-02 |
| *Ndufs5* | 8.252 | 5.923E-05 | *Atn1* | 2.221 | 2.794E-02 | *Suox* | 0.4370 | 1.2E-07 | *Kctd4* | 0.3809 | 1.3E-02 |
| *Farp1* | 2.226 | 8.815E-05 | *Mmp15* | 2.186 | 2.884E-02 | *Hspa12a* | 0.5700 | 1.4E-07 | *Dnd1* | 0.4309 | 1.3E-02 |
| *Bdkrb2* | 6.224 | 1.513E-04 | *Unc79* | 1.761 | 2.941E-02 | *Spink8* | 0.0417 | 1.4E-07 | *Trim71* | 0.5301 | 1.4E-02 |
| *Slc35c1* | 2.907 | 1.720E-04 | *Hcn1* | 3.993 | 2.983E-02 | *Cd52* | 0.1227 | 1.7E-07 | *Hist2h3b* | 0.2816 | 1.4E-02 |
| *Agr3* | 9.795 | 2.367E-04 | *Sema4g* | 1.877 | 2.983E-02 | *Crisp1* | 0.0396 | 2.7E-07 | *Wfdc13* | 0.0965 | 1.4E-02 |
| *Fam115a* | 1.552 | 2.397E-04 | *Csmd2* | 1.550 | 3.014E-02 | *Hist1h2ba* | 0.6530 | 5.1E-07 | *Wfdc15b* | 0.1410 | 1.4E-02 |
| *Ltbr* | 1.511 | 2.445E-04 | *Deaf1* | 1.565 | 3.075E-02 | *Glb1l2* | 0.3709 | 6.5E-07 | *Lin28b* | 0.6467 | 1.4E-02 |
| *Pmfbp1* | 1.600 | 2.700E-04 | *Krt10* | 1.681 | 3.089E-02 | *Haghl* | 0.6367 | 9.4E-07 | *Grik3* | 0.3156 | 1.5E-02 |
| *Ipo5* | 1.787 | 2.728E-04 | *Car3* | 3.403 | 3.179E-02 | *Pnkp* | 0.5810 | 1.9E-06 | *Hist1h2bk* | 0.4319 | 1.5E-02 |
| *Sult1e1* | 2.590 | 3.008E-04 | *Cml1* | 2.105 | 3.262E-02 | *Prss56* | 0.5915 | 2.3E-06 | *Cdc42bpg* | 0.6516 | 1.5E-02 |
| *Gfap* | 1.846 | 3.140E-04 | *Casp1* | 2.764 | 3.527E-02 | *Epsti1* | 0.6406 | 4.1E-06 | *Gpr82* | 0.3505 | 1.5E-02 |
| *Gldn* | 5.541 | 3.745E-04 | *Cuedc1* | 2.108 | 3.679E-02 | *Gclc* | 0.6557 | 5.7E-06 | *Kifc5b* | 0.5568 | 1.6E-02 |
| *Acp1* | 2.832 | 4.015E-04 | *Fbln2* | 1.811 | 3.829E-02 | *Gm4735* | 0.3668 | 6.7E-06 | *Apoa2* | 0.2225 | 1.6E-02 |
| *Chgb* | 1.635 | 4.518E-04 | *Fancb* | 3.216 | 3.892E-02 | *Rrm2* | 0.6324 | 1.8E-05 | *Sarm1* | 0.2913 | 1.6E-02 |
| *Jph2* | 1.763 | 4.561E-04 | *Lhx9* | 1.799 | 3.939E-02 | *Hba-a1* | 0.3332 | 2.1E-05 | *Ccdc36* | 0.6671 | 1.7E-02 |
| *Ptchd3* | 1.847 | 5.655E-04 | *Myh14* | 1.810 | 3.973E-02 | *Guca2b* | 0.1137 | 3.1E-05 | *Park2* | 0.6201 | 1.8E-02 |
| *Clec11a* | 1.910 | 6.322E-04 | *C8a* | 3.194 | 3.978E-02 | *Orc2* | 0.6620 | 6.7E-05 | *Defb23* | 0.0968 | 1.8E-02 |
| *Pdlim7* | 2.526 | 6.996E-04 | *Anks4b* | 1.846 | 3.978E-02 | *Smco2* | 0.6298 | 1.3E-04 | *Hbb-b1* | 0.5176 | 1.9E-02 |
| *Kitl* | 1.522 | 8.880E-04 | *Nfic* | 1.548 | 4.068E-02 | *Hist3h2ba* | 0.2640 | 1.3E-04 | *Cbx2* | 0.5446 | 2.0E-02 |
| *Klk1b21* | 2.018 | 9.406E-04 | *Arhgef15* | 1.602 | 4.129E-02 | *Serpina1f* | 0.1382 | 1.6E-04 | *Zfp524* | 0.6491 | 2.1E-02 |
| *Flot2* | 1.551 | 9.491E-04 | *Pyroxd2* | 1.881 | 4.143E-02 | *Spc25* | 0.6449 | 1.6E-04 | *Acad10* | 0.6039 | 2.2E-02 |
| *Asb2* | 1.780 | 9.541E-04 | *Camk1g* | 1.694 | 4.143E-02 | *Hist1h2bm* | 0.3920 | 2.0E-04 | *Grtp1* | 0.1032 | 2.2E-02 |
| *Adam23* | 1.845 | 9.798E-04 | *Glipr2* | 1.714 | 4.353E-02 | *Krt18* | 0.1505 | 2.5E-04 | *Spint5* | 0.3962 | 2.4E-02 |
| *Agt* | 1.736 | 1.058E-03 | *Gapt* | 3.653 | 4.458E-02 | *Plekhg4* | 0.5809 | 2.7E-04 | *Hist1h2ai* | 0.4636 | 2.4E-02 |
| *Col17a1* | 1.979 | 1.417E-03 | *Dsp* | 1.503 | 4.572E-02 | *Spint1* | 0.2862 | 4.3E-04 | *Plekha4* | 0.6682 | 2.4E-02 |
| *Cacng5* | 5.934 | 1.940E-03 | *Loxl2* | 1.691 | 4.834E-02 | *Gucy2g* | 0.4166 | 4.8E-04 | *Trpv6* | 0.3154 | 2.4E-02 |
| *Gjd3* | 2.242 | 1.988E-03 | | | | *Cpn1* | 0.1024 | 5.1E-04 | *Itpa-ps1* | 0.6288 | 2.4E-02 |
| *Artn* | 1.803 | 2.096E-03 | | | | *Spdyb* | 0.6366 | 5.1E-04 | *Grm6* | 0.4034 | 2.5E-02 |
| *Parp8* | 1.647 | 2.148E-03 | | | | *Myh6* | 0.3827 | 6.2E-04 | *Dnmt3l* | 0.6592 | 2.7E-02 |
| *Adprm* | 1.544 | 2.611E-03 | | | | *Hist1h4n* | 0.4344 | 7.5E-04 | *Nlrp4f* | 0.4994 | 2.8E-02 |
| *Gipc3* | 4.025 | 2.611E-03 | | | | *Thoc6* | 0.4894 | 7.5E-04 | *Nanos1* | 0.3539 | 2.9E-02 |
| *Mageb3* | 1.918 | 2.615E-03 | | | | *Ddx43* | 0.6380 | 1.0E-03 | *Pcyox1l* | 0.4139 | 2.9E-02 |
| *Pomc* | 1.627 | 2.615E-03 | | | | *Myoc* | 0.2787 | 1.1E-03 | *Dhps* | 0.6467 | 3.0E-02 |
| *Klk1b27* | 2.600 | 2.902E-03 | | | | *Cdo1* | 0.5676 | 1.1E-03 | *Cx3cr1* | 0.6635 | 3.1E-02 |
| *Vat1l* | 2.216 | 2.922E-03 | | | | *Pold1* | 0.4964 | 1.2E-03 | *Grb7* | 0.1383 | 3.1E-02 |
| *Rbp7* | 3.346 | 2.991E-03 | | | | *Hmga1* | 0.5587 | 1.4E-03 | *Gpm6a* | 0.5665 | 3.1E-02 |
| *Man1a* | 1.549 | 3.087E-03 | | | | *Pate2* | 0.5182 | 1.4E-03 | *Hist1h4j* | 0.5316 | 3.1E-02 |
| *Zbtb39* | 1.609 | 3.213E-03 | | | | *Ros1* | 0.5719 | 1.6E-03 | *Cd247* | 0.5862 | 3.2E-02 |
| *Wdr91* | 2.126 | 3.709E-03 | | | | *Uba1y* | 0.6377 | 1.6E-03 | *Hbb-b2* | 0.3539 | 3.4E-02 |
| *Cd93* | 1.663 | 4.431E-03 | | | | *Tyk2* | 0.6678 | 1.7E-03 | *Abcb5* | 0.1381 | 3.5E-02 |
| *Ryr1* | 1.595 | 4.544E-03 | | | | *Hist1h2aa* | 0.6413 | 1.7E-03 | *Sall4* | 0.3891 | 3.6E-02 |
| *Eps8l2* | 2.111 | 4.713E-03 | | | | *Wdhd1* | 0.6007 | 1.9E-03 | *Trhde* | 0.5816 | 3.7E-02 |
| *Dsc3* | 1.584 | 5.123E-03 | | | | *Mast3* | 0.5393 | 3.0E-03 | *Cdhr2* | 0.4974 | 3.8E-02 |
| *Tnk1* | 2.320 | 5.138E-03 | | | | *Cdca7* | 0.4558 | 3.0E-03 | *Tmem25* | 0.5274 | 4.1E-02 |
| *Il21* | 2.612 | 5.369E-03 | | | | *Hmga1-rs1* | 0.5868 | 3.1E-03 | *Gprc5c* | 0.5132 | 4.1E-02 |

| | | | | | | | | |
|---|---|---|---|---|---|---|---|---|
| *Tktl1* | 1.874 | 5.394E-03 | *Lat2* | 0.5559 | 3.3E-03 | *Prom2* | 0.1414 | 4.2E-02 |
| *Klk1b24* | 2.113 | 5.617E-03 | *Defb28* | 0.1006 | 3.5E-03 | *Nkx2-4* | 0.6329 | 4.2E-02 |
| *P4htm* | 1.781 | 6.112E-03 | *Dusp9* | 0.2509 | 3.5E-03 | *Bbox1* | 0.5955 | 4.3E-02 |
| *Wdsub1* | 1.540 | 6.112E-03 | *Ap4s1* | 0.6326 | 3.5E-03 | *Ankrd13d* | 0.4343 | 4.4E-02 |
| *Otog* | 6.190 | 6.112E-03 | *Fancl* | 0.6688 | 3.6E-03 | *Elovl7* | 0.3663 | 4.4E-02 |
| *Il20rb* | 2.986 | 6.658E-03 | *Car4* | 0.3578 | 3.7E-03 | *Kifc1* | 0.6595 | 4.4E-02 |
| *Myo7b* | 1.851 | 8.051E-03 | *Hist1h2bb* | 0.3460 | 3.9E-03 | *Hist1h2ah* | 0.3186 | 4.5E-02 |
| *Slc6a15* | 4.248 | 8.599E-03 | *Polr3gl* | 0.6650 | 4.2E-03 | *Mcm2* | 0.6028 | 4.5E-02 |
| *Ampd3* | 1.656 | 9.019E-03 | *Spocd1* | 0.5582 | 4.2E-03 | *Wfdc6b* | 0.3801 | 4.6E-02 |
| *Cdsn* | 2.581 | 9.706E-03 | *Hist1h4i* | 0.6000 | 4.3E-03 | *Gpr68* | 0.4121 | 4.9E-02 |
| *Slc38a6* | 1.632 | 9.706E-03 | *Rpia* | 0.6292 | 4.7E-03 | *Defb22* | 0.1461 | 5.0E-02 |
| *Kcnn3* | 2.462 | 1.102E-02 | *Hist1h1a* | 0.5801 | 4.7E-03 | | | |
| *Kif2b* | 1.762 | 1.109E-02 | *Pou3f3* | 0.15101 | 4.9E-03 | | | |

*FC, fold change; FDR, false discovery rate.

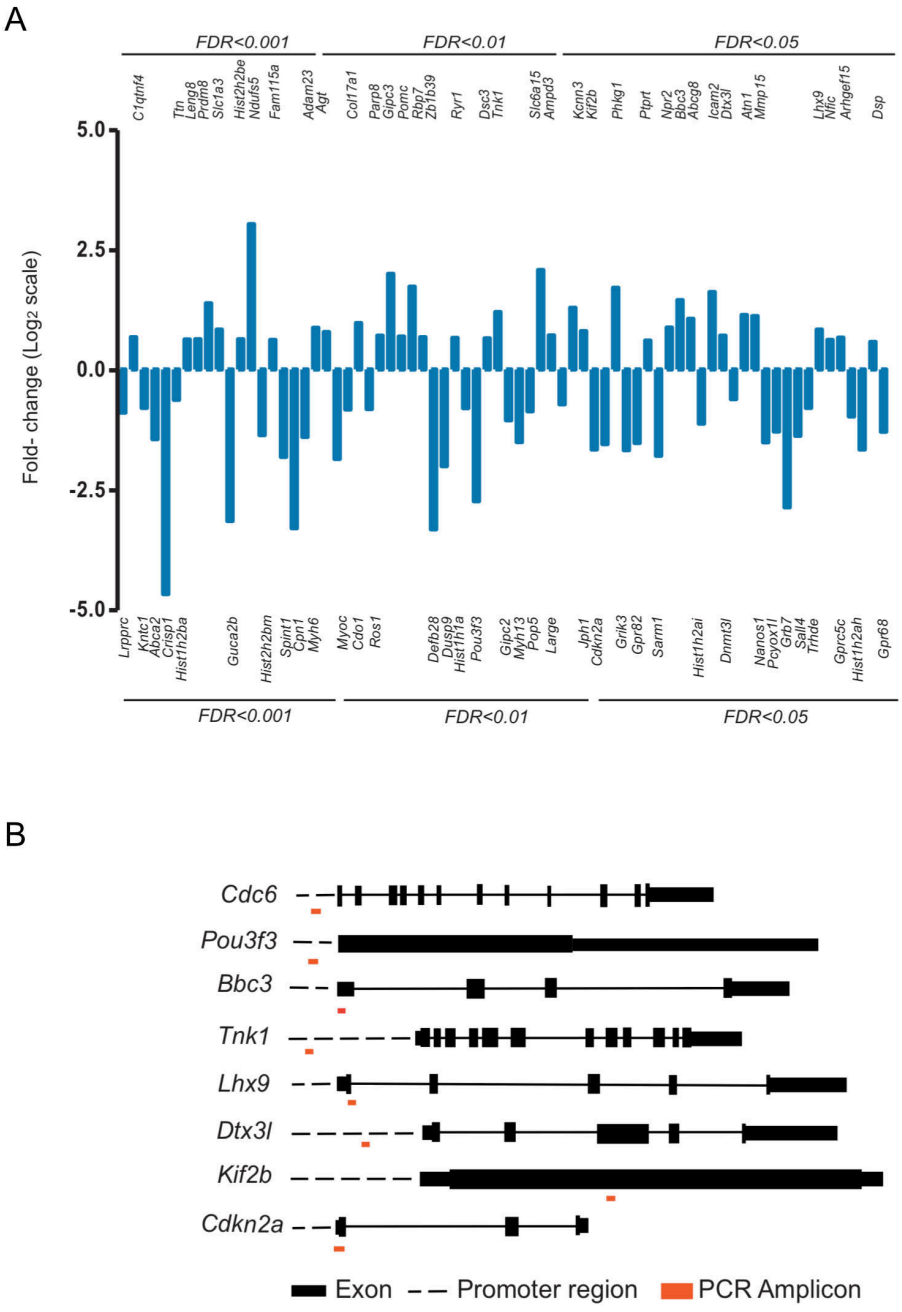


**Figure S11. The loss of NIPP1 from testis deregulates the expression of PcG targets.** (A) Bar chart of the RNA sequencing data showing the expression levels of the indicated PcG target genes represented as $Log_2$ fold-change. FC, fold change; FDR, False Discovery Rate. (B) The positions of the PCR-amplicons are indicated on each gene that is analyzed for H3K27me3 by chromatin immunoprecipitation (ChIP). The schemes of the genes are based on data generated by the Mouse Genome Browser (https://genome.ucsc.edu/; *Mus musculus* GRCmi37/mm10).

**Table S3.** Primers used for genotyping CTR and NIPP1 iKO mice.

| | |
|---|---|
| *Ubc*Cre forward | GCCTGCATTACCGGTCGATGCAACGA |
| *Ubc*Cre reverse | GTGGCAGATGGCGCGGCAACACCATT |
| *VasaCre* forward | CACGTGCAGCCGTTTAAGCCGCGT |
| *VasaCre* reverse | TTCCCATTCTAAACAACACCCTGAA |
| LoxP1 forward | CTTACAAGGAGTGGTATTCGAACC |
| LoxP1 reverse | ACTGTCTAGCAGGGCATAGTGTTG |
| LoxP2 forward | CCACCCTCTCCTTTACTTTGTCTTC |
| LoxP2 reverse | GGAGAGGAGTAATGAGAGGAGTTGTG |
| NIPP1 KO forward | CCTCAGCAGATAGCCCACGG |
| NIPP1 KO reverse | CGCATCGCCTTCTATCGCCTTCTTGAC |

**Table S4.** List of antibodies used in this study.

| Antibodies | Company (catalog no./ref) | Dilution used |
|---|---|---|
| NIPP1 | Sigma (HPA027452) | IF 1:250; WB 1:1000 |
| GAPDH | Cell Signalling (2118) | WB 1:5000 |
| SOX9 | Millipore (AB5535) | DAB 1:100 |
| $p16^{INK4A}$ | Cell Signalling (4824) | IF 1:50 |
| PLZF | Santa Cruz (SC-28319) | IF 1:50; WB 1:1000 |
| Cyclin D2 | Cell Signalling (3741) | IF 1:75 |
| BrdU | BD Biosciences (347580) | IF 1:100 |
| H3S10P | Upstate (06-570) | IF 1:500 |
| EZH2 | Cell Signalling (5246) | IF 1:50; WB 1:1000 |
| EZH2 | Home made [15,16] | IP 1:50 |
| EZH2 | Cell signalling (3147) | WB 1:1000 |
| SUZ12 | Abcam (ab12073) | IF 1:50; WB 1:1000 |
| RBAP48 | GenTex (GTX0232) | IF 1:50; WB 1:1000 |
| TBP | Abcam (ab51841) | WB 1:5000 |
| CDC5l | Home made [17] | WB 1:2500 |
| SAP155 | MBL (D221-3) | WB 1:2500 |
| FCM | Home made [7] | WB 1:2500 |
| β-Actin | Abcam (ab6276) | WB 1:10000 |
| Pan-pTP | Cell Signalling (9391) | WB 1:1000 |
| H3K27me3 | Upstate (07-449) | IF 1:50; WB 1:1000 |
| H3 | Santa Cruz (SC 10809) | IF 1:50; WB 1:5000 |
| α-Tubulin | Sigma (T6074) | WB 1:10000 |
| eGFP | Santa Cruz (SC-8334) | WB 1:1000 |
| Flag | Stratagene (200472) | WB 1:1000 |
| PCNA | Upstate (07-2162) | IF 1:100 |
| GFRA1 | R&D systems (AF560) | IF 1:50 |

**Table S5.** q-RT PCR primers used in this study

| Gene | mRNA Forward primer | mRNA Reverse primer |
|---|---|---|
| *Hprt* | CTGGTGAAAAGGACCTCTCG | TGAAGTACATTATAGTCAAGGGCA |
| *Ppp1r8 (Nipp1)* | AGCGCTGGTGTACCACAAACA | TTGTGAGGTTCCAGCCGAATGT |
| *Ddx4 (Vasa)* | TGGCAGAGCGATTTCTTTT | CGCTGTATTCAACGTGTGCT |
| *Plzf* | GAGCACACTCAAGAGCCACA | GTGGCAGAGTTTGCACTCAA |
| *Stra8* | GCTTTTGACGTGGCAAGTTT | AACACAGCCAAGGCTTTTGA |
| *Tacstd1* | CAGAATACTGTCATTTGCTCCA | GTTCTGGATCGCCCCTTC |
| *Sycp3* | GGACAGCGACAGCTCACC | TTCCCAGATTTCCCAGAATG |
| *Stmn1* | CTGCAGAAGAAAGACGCAAGT | TGCTGAAGTTGTTGTTCTCCTC |
| *Prm2* | CAGAAGGCGGAGGAGACAC | CTCCTCCTTCGGGATCTTCT |
| *Tpn1* | AGCCGCAAGCTAAAGACTCA | CGGTAATTGCGACTTGCAT |
| *Tnk1* | CTCAAGTGTCTGATTCCAGAGG | CCACTGGGTAGTGTCCATAAC |
| *Ptprt* | TTACCTGGGAGCAGATTAACAC | CCAGAGCTGTTCACCATCAT |
| *Dusp9* | CTTGAGCTGTGGCCTAGATT | TAGGTAGAGATTGGGCAGGA |
| *Nanos1* | CTACACCACACACATCCTCAA | CTTTGGAGAGCGGGCAATA |
| *Pou3f3* | AGCAGTTCGCTAAGCAGTT | CGAGAACACGTTGCCATAGA |
| *Lhx9* | CCGAGACTCTGTCTACCATCT | GCTGTCCTTCATCCCGAAAT |
| *Parp8* | GGATCACTTCCGAAACCACTT | TCTCTCTTGCCTTGAACACATC |
| *Bbc3* | GTCTAGCCCGCGACAGT | CGCAAAGGCTGCAGGATAC |
| *Cdkn2a* | GAACTCTTTCGGTCGTACCC | GTTCGAATCTGCACCGTAGT |
| *Ccnb3* | GCTGGTGGAGACTGAAGATTAC | CTCCTCAATGATGGTTGGATCTT |
| *Kntc1* | TCCGAAGATCCAAGCATTCAG | GACCACATCCACGTCAGTATC |
| *Kif2b* | GGATCTGTGTGTGTGTGAGAA | ACTACATTGTGCGAGGGAATAG |
| *Dnmt3l* | GAGACACCTTCTTCTTGCTCTAA | GGATTTCAGCCATTGCTCTTC |
| *Ggra1* | AAGAGAAGAATTGTCTGCGTATCT | CTGCTGTTAACCGGCTCAT |
| *Gdnf* | GCTGACCAGTGACTCCAATATG | CGCTGCCGCTTGTTTATCT |
| *Inhba* | AGAACGGGTATGTGGAGATAGA | GACTCGGCAAAGGTGATGAT |
| *Inha* | TCTGAACCAGAGGAGGAAGAT | GGGATGGCCGGAATACATAAG |
| *Shbg* | CACAGTAGGCTTTGGTCCTC | CTCAGGCATAGCATCTCCTTC |

| | | |
|---|---|---|
| *Sox9* | GAAGGAGAGCGAGGAAGATAAG | TGACGTGTGGCTTGTTCT |

**Table S6.** ChIP primers used in this study

| Gene | ChIP Forward primer | ChIP Reverse primer |
|---|---|---|
| *Bbc3* | gcagcaaggtgcctcaata | gcatgaacactccggagaaa |
| *Pou3f3* | ccacaggagttggttgtgtat | ggagaaggaggaggaagaaga |
| *Dtx3l* | gcagggcgacaggtttaata | gccatctctccagaacatgaa |
| *Tnk1* | gggtatctcagtttcccttctg | tgcctcctgtctcactctat |
| *Lhx9* | ctctgcatctgtagggagaatg | gtcggctccttccttagtaatc |
| *Kif2b* | cgtacactttgccaccataga | ctcaggatgtcttcctcctact |
| *Cdkn2a* | tccagtctctgatacccgttag | ggctttgagtcctggttctt |
| *Cdc6* | ggccttgtagccctcttaaa | gcctaacgtcctcattctactg |
| *Hoxa11* | aggagaaggggttccttcaa | ctccgcggtttgtcaataat |

## 4.7.3 Additional References


1. Van Dessel N, Beke L, Goernemann J, Minnebo N, Beullens M, Tanuma N, et al. The phosphatase interactor NIPP1 regulates the occupancy of the histone methyltransferase EZH2 at Polycomb targets. Nucleic Acids Res. 2010;38:7500–12.
2. Martin M. Cutadapt removes adapter sequences from high-throughput sequencing reads. EMBO journal. 2011;17:10.
3. Morgan M, Anders S, Lawrence M, Aboyoun P, Pagès H, Gentleman R. ShortRead: A bioconductor package for input, quality assessment and exploration of high-throughput sequence data. Bioinformatics. 2009;25:2607–8.
4. Langmead B, Salzberg SL. Fast gapped-read alignment with Bowtie 2. Nat Methods. 2012;9:357–9.
5. Trapnell C, Pachter L, Salzberg SL. TopHat: Discovering splice junctions with RNA-Seq. Bioinformatics. 2009;25:1105–11.
6. Li H, Handsaker B, Wysoker A, Fennell T, Ruan J, Homer N, et al. The Sequence Alignment / Map (SAM) Format and SAMtools 1000 Genome Project Data Processing Subgroup. Bioinformatics. 2009;25:1–2.
7. Trapnell C, Williams B a, Pertea G, Mortazavi A, Kwan G, van Baren MJ, et al. Transcript assembly and quantification by RNA-Seq reveals unannotated transcripts and isoform switching during cell differentiation. Nat. Biotechnol. 2010;28:511–5.
8. Quinlan AR, Hall IM. BEDTools: A flexible suite of utilities for comparing genomic features. Bioinformatics. 2010;26:841–2.
9. Anders S, Pyl PT, Huber W. HTSeq-A Python framework to work with high-throughput sequencing data. Bioinformatics. 2015;31:166–9.
10. Risso D, Schwartz K, Sherlock G, Dudoit S. GC-content normalization for RNA-Seq data. BMC Bioinformatics. 2011;12:480.
11. Robinson MD, Smyth GK. Moderated statistical tests for assessing differences in tag abundance. Bioinformatics. 2007;23:2881–7.
12. Benjamini Y, Hochberg Y. Controlling the false discovery rate: a practical and powerful approach to multiple testing. J. R. Stat. Soc. 1995. p. 289–300.
13. Feil S, Valtcheva N, Feil R. Inducible cre mice. Methods Mol. Biol. 2009;530:343–63.
14. Russell LD, Ettlin RA, SinhaHikim AP, C.E. (1990). Histological and histopathological evaluation of the testis. Clear-water, FL: Cache River Press.
15. Minnebo N, Goernemann J, O'Connell N, Van Dessel N, Derua R, Vermunt MW, et al. NIPP1 maintains EZH2 phosphorylation and promoter occupancy at proliferation-related target genes. Nucleic Acids Res. 2013;41:842–54.
16. Van Dessel N, Beke L, Goernemann J, Minnebo N, Beullens M, Tanuma N, et al. The phosphatase interactor NIPP1 regulates the occupancy of the histone methyltransferase EZH2 at Polycomb targets. Nucleic Acids Res. 2010;38:7500–12.
17. Boudrez A, Beullens M, Groenen P, Van Eynde A, Vulsteke V, Jagiello I, et al. NIPP1-mediated interaction of protein phosphatase-1 with CDC5L, a regulator of pre-mRNA splicing and mitotic entry. J. Biol. Chem. 2000;275:25411–7.

# CHAPTER 5

# General Discussion and Perspectives

NIPP1 forms a heterodimeric complex with a quantitatively important fraction of the nuclear pool of PP1 and affects key processes such as transcription, pre-mRNA splicing and chromatin remodeling, through regulated dephosphorylation of a subset of PP1 substrates [273,274,295,310]. NIPP1 is a conserved PIP with three functional domains: (1) a substrate recruiting N-terminal FHA domain, (2) a central PP1-anchoring domain, and (3) a C-terminal PP1-inhibitory and RNA binding domain [269–271]. The established FHA-ligands of NIPP1 include the chromatin modifier EZH2, the pre-mRNA splicing factors SAP155 and CDC5L, and protein kinase MELK [277,288–290].

In mammals, NIPP1 is already expressed during early embryonic development and in all adult tissues but its expression level is cell-type dependent. In this study, we focused on the *in vivo* function of NIPP1 in adult tissues by generating and phenotyping an inducible NIPP1 knockout (iKO) mouse model. Hereby, we identified NIPP1 as an essential factor for the maintenance of the spermatogenic lineage, including different pools of (un)differentiated spermatogonia.

## 5.1 NIPP1 regulates the expansion of specific pools of progenitor cells

I have found that the ablation of NIPP1 in mouse testis is associated with a progressive loss of germ cells from the seminiferous epithelium, resulting in a Sertoli cells-only phenotype. The observed phenotype resulted from the almost complete loss of both undifferentiated spermatogonia (GFRA1$^+$ spermatogonia [93]) and differentiating spermatogonia. To examine whether hypoproliferation of GFRA1$^+$ spermatogonia results from an intrinsic proliferative defect or from a deficient signaling by surrounding NIPP1 depleted sustentacular cells (e.g. Sertoli cells), we performed *in vitro* deletion of NIPP1 in GFRA1$^+$ spermatogonia isolated from CTR and iKO testis. Our results indicated that the deletion of NIPP1 in cultured GFRA1$^+$ cells also resulted in a reduced proliferation, indicating that it represents an intrinsic defect. Nevertheless, this effect could only be studied for a short period, which did not enable us to explore whether NIPP1 is also important for the self-renewal of spermatogonial stem cells (i.e. spermatogonia Asingle; see Introduction), which only represent a small population of GFRA1$^+$ cells. This can be further explored by transplantation assays, where GFRA1$^+$ cells isolated from CTR and iKO mice carrying a reporter gene (GFP or LacZ), are transplanted into a histocompatible recipient testis that has been pretreated with a chemical agent (Busulfan) that impairs spermatogenesis [85,311]. This assay would enable us to examine whether GFRA1$^+$ stem cells from iKOs

can repopulate the recipient testis *in vivo*. The function(s) of NIPP1 in the spermatogenic lineage could also be further addressed by generating an inducible gonocyte-specific NIPP1 *knockout* using available *Vasa*-CreERT2 inducible recombinases [312].

Gene-expression profiling by RNA sequencing showed that the deletion of NIPP1 from adult testis results in the deregulation of genes that are important for the proliferation and survival of germ cells. These included the upregulation of genes encoding pro-apoptotic factors such as PARP8 and BBC3/PUMA, in accordance with the increased level of apoptosis in the iKO testis. Importantly, p53-activated PUMA is involved in p53-dependent and p53-independent apoptotic pathways and is epigenetically regulated by Polycomb Group proteins (PcG) [313]. It will be important to explore whether this deregulation of apoptotic factors also applies to $GFRA1^+$ cells isolated from iKOs. For that purpose, $GFRA1^+$ cells can be isolated by FACs sorting prior to RNA sequencing [314].

The proliferation defects observed in undifferentiated spermatogonia did not come as a surprise since the global deletion of NIPP1 is embryonic lethal at E6.5-7.5 and also associated with a deficient proliferation [294]. In addition, *Ppp1r8*$^{-/-}$ embryonic stem cells (ES) could not be derived indicating that NIPP1-null ES cells are not viable. Other data from the host laboratory also support a role for NIPP1 in the proliferation of progenitor cells (Figure 15). Thus, the deletion of NIPP1 from liver-epithelial cells triggers the proliferation of perivenous (biliary) progenitor cells [315], but preliminary results suggest a partial loss of pericentral $Axin2^+$ progenitor cells. Likewise, the deletion of NIPP1 from keratinocytes results in an increased proliferation of transit amplifying cells but a loss of slow-cycling stem cells, most likely $Axin2^+$ cells, in the hair follicles and the interfollicular epidermis (Verbinnen *et al*., unpublished data). Interestingly, Axin2 is also expressed in undifferentiated spermatogonia, including stem cells, and contributes here to proliferation regulated by the Wtn/β-catenin pathway [316]. Wtn6 is specifically secreted by Sertoli cells and is essential to create a niche for undifferentiated spermatogonia [316]. Since genes of the Wtn/β-catenin pathway are epigenetically repressed by PcGs [180,181], it would be worthwhile to analyze whether the Wtn/β-catenin signaling pathway is disturbed in progenitor cells that lack NIPP1. Overall, our data suggest that NIPP1 is required for the maintenance of tissue-specific subpopulations of progenitor cells (Figure 15).

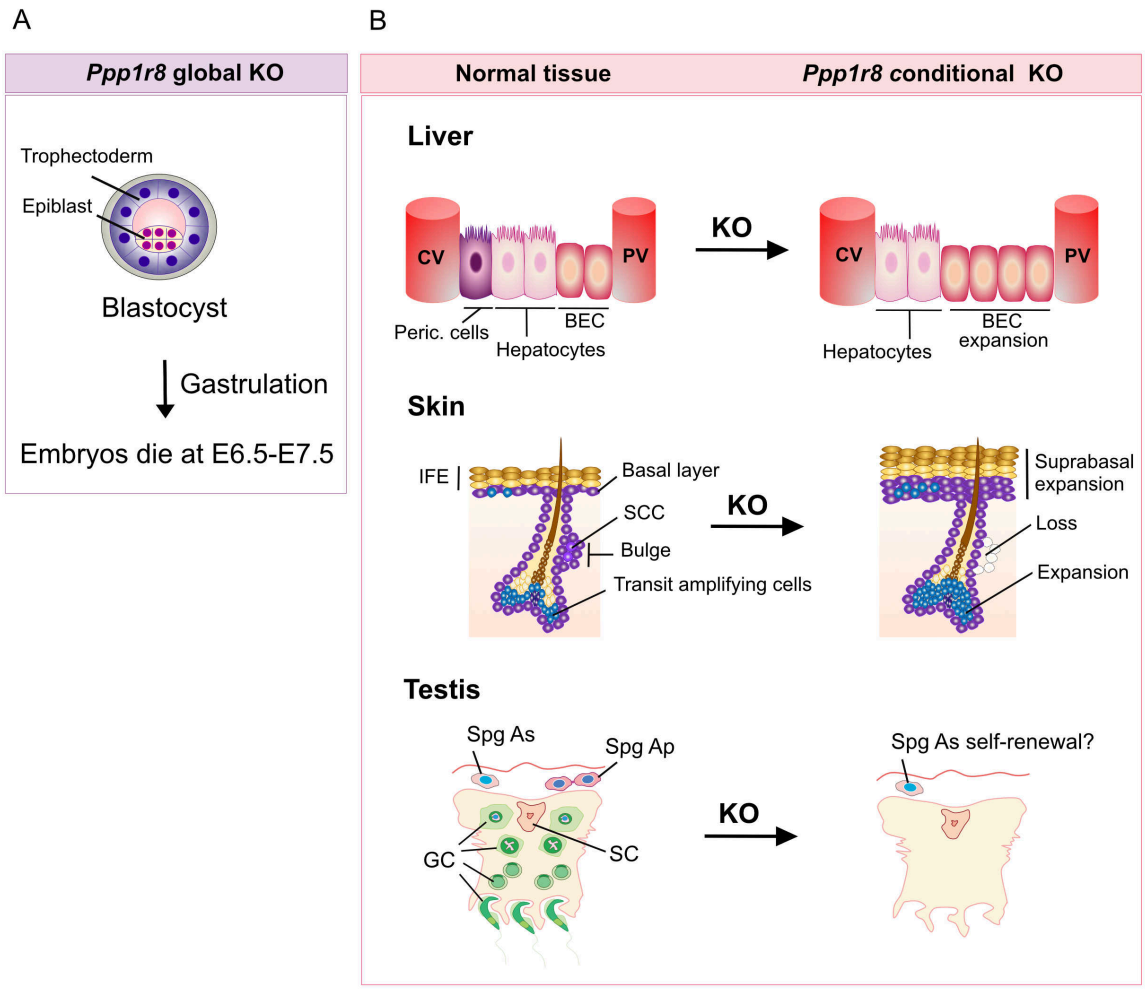


**Figure 15: Effects of the deletion of NIPP1 on the maintenance of progenitor cells during embryogenesis and in adult tissues.** (A) The global deletion of NIPP1 (*Ppp1r8*$^{-/-}$) is embryonic lethal at the onset of gastrulation. (B) *Ppp1r8*$^{-/-}$ livers show an expansion of perivenous progenitor cell compartment [315], but a loss of pericentral stem cells (preliminary unpublished data). Skin NIPP1 KO mice show a hyperproliferation of transit amplifying cells in the hair follicles and the interfollicular epidermis, but a loss of slowly cycling stem cells. *Ppp1r8*$^{-/-}$ testis exhibit a complete loss of germ cells associated with hypoproliferation of (un)differentiated spermatogonia. KO, *knockout*; Peric. cells, pericentral cells; BEC, Biliary epithelial cells; CV, central vein; PV, portal vein; IFE, Interfollicular epidermis; SCC, slowly cycling stem cells; Spg. As, Spermatogonia A single; Spg. Ap, Spermatogonia Apaired.

## 5.2 PP1-NIPP1 regulates the stability of EZH2

NIPP1 forms a complex with PP1 and the PRC2 core components EED and EZH2. Also, NIPP1 is associated with a subset of PRC2 target genes [274,290] and functions as a PRC2-dependent transcriptional repressor [274,275,290]. Phosphorylation of EZH2 by

cyclin dependent kinases (CDK1/2) at Thr416 creates a docking site for the recruitment of NIPP1 [290], which then enables the regulated dephosphorylation of EZH2 by associated PP1.

We found that the deletion of NIPP1 in mouse testis results in the downregulation of EZH2 and a global reduction of H3K27 trimethylation in seminiferous tubules at early stages of development. It remains to be established whether NIPP1 also stabilizes EZH1. Consistent with our observations, we noted an altered expression of PcG target genes and a decreased H3K27 trimethylation at these loci. These results are in accordance with previous observations demonstrating that *Ppp1r8*$^{-/-}$ blastocyst outgrows show a reduced trimethylation of H3K27 and a de-repression of PcG target genes [293,294]. In addition, mouse embryos lacking NIPP1 die at around the gastrulation stage, a phenotype that is similar to that observed after the loss of the PRC2 core components EZH2, EED or SUZ12 [317]. Collectively, these data suggest that NIPP1 affects the expression of proliferation-related genes, not only during embryogenesis but also postnatally in actively proliferating tissues like testis. Notably, recent studies have established the importance of the PRC2 complex in testis, as the gonocyte-specific deletion of either EZH1/2, EED or SUZ12 causes a postnatal testicular phenotype characterized by exhaustion of progenitor cells and a meiotic arrest [213,318]. Surprisingly, the single deletion of EZH1 or EZH2 has no effect on spermatogenesis, suggesting that EZH1 and EZH2 act redundantly. Further experiments are required to determine whether Sertoli cells-only phenotype after the deletion of NIPP1 can be rescued by the ectopic expression of EZH1/2 in GFRA1$^{+}$ cells. To this end, GFRA1$^{+}$ cells isolated from CTR and iKO mice can be treated in culture with hydroxytamoxifen to remove NIPP1 and transfected or transduced with EZH1/2 constructs. Another strategy involves the crossing of the CTR and iKO mice with mice that inducible overexpress EZH1/2 in testis.

We demonstrated that NIPP1 stabilizes EZH2 in spermatogonia by enabling the timely dephosphorylation of CDK1/2 sites by PP1. In addition to Thr416, EZH2 is also phosphorylated at Thr345 and Thr487 by CDK1/2 [290,319–322]. We found that the deletion of NIPP1 causes a hyperphosphorylation of EZH2 at these sites, whereas the overexpression of a PP1-NIPP1 fusion causes the hypophosphorylation of EZH2 at TP-dipeptide motifs. The hyperphosphorylation of EZH2 in the absence of NIPP1 was not expected as NIPP1 was previously reported to inhibit the dephosphorylation of EZH2 by PP1 in HeLa cells [290]. However, our results are in agreement with the global nuclear

hyperphosphorylation on threonine observed in the *Ppp1r8*$^{-/-}$ mouse embryos [323]. These paradoxal data can be rationalized by the view that NIPP1 is an inhibitor of PP1 under basal circumstances but can be 'de-inhibited' by poorly understood mechanisms (see below), resulting in the timely dephosphorylation of EZH2. We found that the persistent hyperphosphorylation of EZH2 at Thr345 and Thr487 results in its proteasomal degradation, consistent with previous reports [319].

## 5.3 NIPP1 is a modulator of associated PP1

NIPP1 is a very potent and highly specific inhibitor of PP1, preventing the dephosphorylation of all substrates except those are recruited by the FHA domain [277,292]. Consistent with this notion, EZH2 is hyperphosphorylated in the absence of NIPP1 in testis and the overexpression of a PP1-NIPP1 fusion in HeLa cells causes the hypophosphorylation of all known FHA ligands (Winkler et al, unpublished data). However, NIPP1 has also been found to inhibit the dephosphorylation of EZH2 by associated PP1 [290]. Collectively, these data suggest that NIPP1 is an inhibitor of associated PP1 but also allows the dephosphorylation of FHA ligands in a context-dependent manner. We propose that the dephosphorylation of FHA ligands requires the removal of the C-terminus of NIPP1 from the active site of PP1. *In vitro* data suggest that this 'de-inhibition' mechanism possibly involves an allosteric mechanism, induced by the RNA-dependent phosphorylation of NIPP1 at Tyr335 [269] (Figure 16). At present it is not clear which RNA is bound to NIPP1 *in vivo*. However, since EZH2 interacts with RNA to promote repression or PRC2-independent activation of genes [321,324,325] and since phosphorylation of EZH2 promotes its chromatin targeting via non-coding RNAs, it is tempting to speculate that these are also the RNAs that are recognized by NIPP1. In view of the latent endoribonuclease activity associated with NIPP1, we speculate that these RNAs may also be processed by NIPP1, possibly as a first step to re-(in)activate the PP1-NIPP1 complex.

Intriguingly, the testis-specific NIPP1ε/NIPP1T isoform lacks the C-terminal PP1-inhibitory and RNA-binding sites. Therefore, this isoform may represent a constructively 'de-inhibited' variant of NIPP1 that allows the persistent dephosphorylation of FHA ligands, including EZH2. A comparative analysis of EZH2 (de)phosphorylation after the knockdown of endogenous NIPP1 and the inducible expression of siRNA resistant NIPP1α or NIPP1ε/NIPP1T could be used to explore this hypothesis.

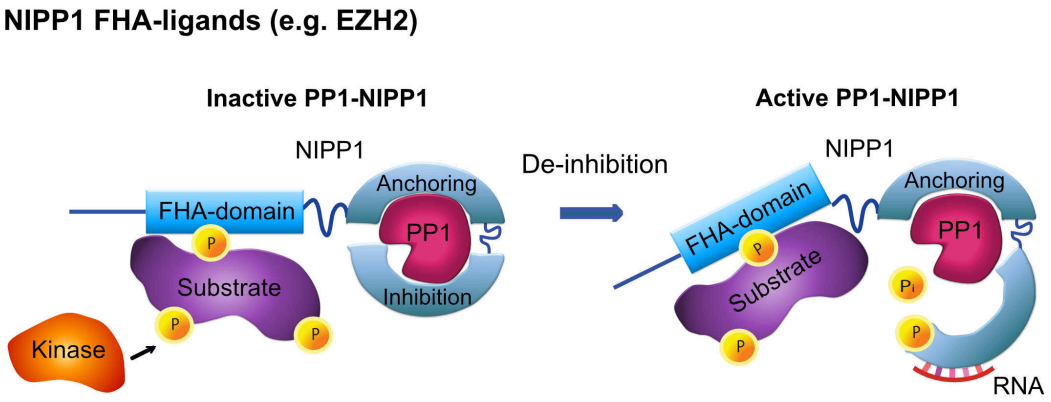


**Figure 16**: **Regulation of NIPP1 ligands by PP1-NIPP1.** NIPP1 restricts the PP1-dependent dephosphorylation to substrates with phosphorylated TP-dipeptides that are recruited by the FHA domain of NIPP1. Dephosphorylation of FHA ligands by the PP1-NIPP1 holoenzyme is suggested to be dependent on the allosteric removal (de-inhibition) of the C-terminal domain of NIPP1 from PP1, which is suggested to be induced by phosphorylation and/or RNA-binding. P, phosphate.

## 5.4 A role for NIPP1 in male infertility?

We have demonstrated that the targeted deletion of NIPP1 in murine adult testis culminates in a complete loss of germ cells. This phenotype resembles the Sertoli cells-only (SCO) syndrome in men. It cannot be excluded that some types of SCO are caused by mutations in the NIPP1 encoding gene (*PPP1R8*), which could be screened for by DNA sequence analysis of patients with the SCO syndrome. However, mutations in *PPP1R8* are likely to cause also dramatic effects in other tissues, unless they only affect the C-terminus of the testis-specific NIPP1ε/NIPP1T. The effects of such mutations are difficult to predict as the function of the C-terminus of NIPP1ε/NIPP1T remains to be explored. Also, it cannot be excluded that such mutations are compensated for by an increased expression of NIPP1α.

# CHAPTER 6

# References (Chapter 1 and 5)

1. Brinster RL. Male germline stem cells: from mice to men. Science. 2007;316:404–5.
2. Russell LD, Ettlin RA, SinhaHikim AP CE. Histological and histopathological evaluation of the testis. Clear-water, FL: Cache River Press; 1990.
3. Hinton BT, Urner TT. he seminiferous tubular microenvironment. In: Cell and Molecular Biology of the Testis. Desjardins C, Ewing LL, editors. New York: Oxford University Press; 1993.
4. Nistal M, Abaurrea MA, Paniagua R. Morphological and histometric study on the human Sertoli cell from birth to the onset of puberty. J. Anat. 1982;14:351–63.
5. Kretser D, Kerr J. The cytology of the testis. In: The physiology of reproduction. Knobil E, Neill J, Ewing L, Greenwald C, Markert C, Pfaff D, editors. New York: Raven press; 1988.
6. Weber J, Russell L, Wong V, Peterson R. Three dimensional reconstruction of a rat stage V Sertoli cell: II. Morphometry of Sertoli-Sertoli and Sertoli-germ cell relationships. Am. J. Anat. 1983;167:163–79.
7. Setchell BP. Blood-testis barrier, junctional and transport proteins and spermatogenesis. Adv. Exp. Med. Biol. 2008;636:212–23.
8. Sharpe R. M. Regulation of spermatogenesis. In The physiology of reproduction. Knobil E, Neill JD, editors. New York: NY: Raven Press; 1994.
9. Clermont Y. The cycle of the seminiferous epithelium in man. Am. J. Anat. 1963;112:35–51.
10. Clermont Y. Kinetics of spermatogenesis in mammals: seminiferous epithelium cycle and spermatogonial renewal. Physiol. Rev. 1972;52:198–236.
11. Stern H. The process of meiosis. In Cell and Molecular Biology of the Testis. Desjardins C, Ewing L, editors. New York: Oxford Univ. Press; 2013.
12. Cooke HJ, Saunders PTK. Mouse models of male infertility. Nat. Rev. Genet. 2002;3:790–801.
13. Richardson BE, Lehmann R. Mechanisms guiding primordial germ cell migration: strategies from different organisms. Nat. Rev. Mol. Cell Biol. 2010;11:37–49.
14. Saitou M, Barton SC, Surani MA. A molecular programme for the specification of germ cell fate in mice. Nature. 2002;418:293–300.
15. Ying Y, Liu XM, Marble A, Lawson KA, Zhao GQ. Requirement of Bmp8b for the Generation of Primordial Germ Cells in the Mouse. Mol. Endocrinol. 2000;14:1053–63.
16. Ying Y, Qi X, Zhao G. Induction of primordial germ cells from murine epiblasts by synergistic action of BMP4 and BMP8B signaling pathways. Proc Natl Acad Sci U S A. 2001;98:7858–62.
17. Besmer P. The kit ligand encoded at the murine Steel locus: a pleiotropic growth and differentiation factor. Curr. Opin. Cell Biol. 1991;3:939–46.
18. Tsuda M, Sasaoka Y, Kiso M, Abe K, Haraguchi S, Kobayashi S, et al. Conserved role of nanos proteins in germ cell development. Science. 2003;301:1239–41.
19. Kehler J, Tolkunova E, Koschorz B, Pesce M, Gentile L, Boiani M, et al. Oct4 is required for primordial germ cell survival. EMBO Rep. 2004;5:1078–83.
20. Zhao GQ, Garbers DL. Male germ cell specification and differentiation. Dev Cell. 2002;2:537–47.
21. Culty M. Gonocytes, the forgotten cells of the germ cell lineage. Birth Defects Res. Part C - Embryo Today Rev. 2009. p. 1–6.
22. Rouiller-Fabre V, Levacher C, Pairault C, Racine C, Moreau E, Olaso R, et al. Development of the foetal and neonatal testis. Andrologia. 2003. p. 79–83.
23. Maatouk DM, Loveland KL, McManus MT, Moore K, Harfe BD. Dicer1 is required for differentiation of the mouse male germline. Biol Reprod. 2008;79:696–703.
24. Maatouk DM, Dinapoli L, Alvers A, Parker KL, Taketo MM, Capel B. Stabilization of ß-catenin in XY gonads causes male-to-female sex-reversal. Hum. Mol. Genet. 2008;17:2949–55.
25. Durcova-Hills G, Tang F, Doody G, Tooze R, Surani MA. Reprogramming primordial germ cells into pluripotent stem cells. PLoS One. 2008;3.
26. Luo X, Ikeda Y, Parker KL. A cell-specific nuclear receptor is essential for adrenal and gonadal development and sexual differentiation. Cell. 1994;77:481–90.
27. Zhang L, Chen M, Wen Q, Li Y, Wang Y, Wang Y, et al. Reprogramming of Sertoli cells to fetal-like Leydig cells by Wt1 ablation. Proc. Natl. Acad. Sci. U. S. A. 2015;112:4003–8.

28. Birk OS, Casiano DE, Wassif C a, Cogliati T, Zhao L, Zhao Y, et al. The LIM homeobox gene Lhx9 is essential for mouse gonad formation. Nature. 2000;403:909–13.
29. Miyamoto N, Yoshida M, Kuratani S, Matsuo I, Aizawa S. Defects of urogenital development in mice lacking Emx2. Development. 1997;124:1653–64.
30. Nef S, Verma-Kurvari S, Merenmies J, Vassalli J-D, Efstratiadis A, Accili D, et al. Testis determination requires insulin receptor family function in mice. Nature. 2003;426:291–5.
31. Swain A, Lovell-Badge R. Mammalian sex determination: A molecular drama. Genes Dev. 1999. p. 755–67.
32. Gubbay J, Collignon J, Koopman P, Capel B, Economou A, Munsterberg A, et al. A gene mapping to the sex-determining region of the mouse Y chromosome is a member of a novel family of embryonically expressed genes. Nature. 1990;346:245–50.
33. Sinclair AH, Berta P, Palmer MS, Hawkins JR, Griffiths BL, Smith MJ, et al. A gene from the human sex-determining region encodes a protein with homology to a conserved DNA-binding motif. Nature. 1990;346:240–4.
34. Koopman P, Gubbay J, Vivian N, Goodfellow P, Lovell-Badge R. Male development of chromosomally female mice transgenic for Sry. Nature. 1991;351:117–21.
35. Bullejos M, Koopman P. Spatially dynamic expression of Sry in mouse genital ridges. Dev. Dyn. 2001;221:201–5.
36. Albrecht KH, Eicher EM. Evidence That Sry Is Expressed in Pre-Sertoli Cells and Sertoli and Granulosa Cells Have a Common Precursor. Dev. Biol. 2001;240:92–107.
37. Hacker A, Capel B, Goodfellow P, Lovellbadge R. Expression of sry, the mouse sex-determining gene. Development. 1995;121:1603–14.
38. Lovell-Badge R, Robertson E. XY female mice resulting from a heritable mutation in the primary testis-determining gene, Tdy. Development. 1990;109:635–46.
39. Tevosian SG, Albrecht KH, Crispino JD, Fujiwara Y, Eicher EM, Orkin SH. Gonadal differentiation, sex determination and normal Sry expression in mice require direct interaction between transcription partners GATA4 and FOG2. Development. 2002;129:4627–34.
40. Hammes A, Guo JK, Lutsch G, Leheste JR, Landrock D, Ziegler U, et al. Two splice variants of the wilms' tumor 1 gene have distinct functions during sex determination and nephron formation. Cell. 2001;106:319–29.
41. Hawkins JR, Taylor A, Berta P, Levilliers J, Van der Auwera B, Goodfellow PN. Mutational analysis of SRY: nonsense and missense mutations in XY sex reversal. Hum. Genet. 1992;88:471–4.
42. Vidal VP, Chaboissier MC, Rooij D de, Schedl A, de Rooij DG, Schedl A. Sox9 induces testis development in XX transgenic mice. Nat. Genet. 2001;28:216–7.
43. Sekido R, Lovell-Badge R. Sex determination involves synergistic action of SRY and SF1 on a specific Sox9 enhancer. Nature. 2008;453:930–4.
44. Kanai Y, Koopman P. Structural and functional characterization of the mouse Sox9 promoter: implications for campomelic dysplasia. Hum. Mol. Genet. 1999;8:691–6.
45. Colvin JS, Green RP, Schmahl J, Capel B, Ornitz DM. Male-to-female sex reversal in mice lacking fibroblast growth factor 9. Cell. 2001;104:875–89.
46. Meeks JJ, Weiss J, Jameson JL. Dax1 is required for testis determination. Nat. Genet. 2003;34:32–3.
47. Skinner MK, Fritz IB. Testicular peritubular cells secrete a protein under androgen control that modulates Sertoli cell functions. Proc. Natl. Acad. Sci. U. S. A. 1985;82:114–8.
48. Zhao L, Svingen T, Ng ET, Koopman P. Female-to-male sex reversal in mice caused by transgenic overexpression of Dmrt1. Development. 2015;1083–8.
49. Matson CK, Murphy MW, Sarver AL, Griswold MD, Bardwell VJ, Zarkower D. DMRT1 prevents female reprogramming in the postnatal mammalian testis. Nature. 2011;9:1–5.
50. Minkina A, Matson CK, Lindeman RE, Ghyselinck NB, Bardwell VJ, Zarkower D. DMRT1 protects male gonadal cells from retinoid-dependent sexual transdifferentiation. Dev. Cell. 2014;29:511–20.
51. Bohacek J, Mansuy IM. Molecular insights into transgenerational non-genetic inheritance of acquired behaviours. Nat. Rev. Genet. 2015;16:641–52.

52. Brennan J, Capel B. One tissue, two fates: molecular genetic events that underlie testis versus ovary development. Nat. Rev. Genet. 2004;5:509–21.
53. Saitou M, Kagiwada S, Kurimoto K. Epigenetic reprogramming in mouse pre-implantation development and primordial germ cells. Development. 2012;139:15–31.
54. Kluin PM, de Rooij DG. A comparison between the morphology and cell kinetics of gonocytes and adult type undifferentiated spermatogonia in the mouse. Int. J. Androl. 1981;4:475–93.
55. Vergouwen RP, Jacobs SG, Huiskamp R, Davids J a, de Rooij DG. Proliferative activity of gonocytes, Sertoli cells and interstitial cells during testicular development in mice. J. Reprod. Fertil. 1991;93:233–43.
56. Moreno SG, Attali M, Allemand I, Messiaen S, Fouchet P, Coffigny H, et al. TGFβ signaling in male germ cells regulates gonocyte quiescence and fertility in mice. Dev. Biol. 2010;342:74–84.
57. Bellve a R, Cavicchia JC, Millette CF, O'Brien DA, Bhatnagar YM, Dym M. Spermatogenic cells of the prepubertal mouse. Isolation and morphological characterization. J Cell Biol. 1977;74:68–85.
58. Huckins C. The spermatogonial stem cell population in adult rats. I. Their morphology, proliferation and maturation. Anat. Rec. 1971;169:533–57.
59. Hilscher W, Hilscher B. Kinetics of the Male Gametogenesis. Andrologia. 1976;8:105–16.
60. Mendis SH, Meachem SJ, Sarraj MA, Loveland KL. Activin A balances Sertoli and germ cell proliferation in the fetal mouse testis. Biol Reprod. 2011;84:379–91.
61. van den Ham R, van Dissel-Emiliani FMF, van Pelt a MM. Expression of the scaffolding subunit A of protein phosphatase 2A during rat testicular development. Biol. Reprod. 2003;68:1369–75.
62. Ohta H, Yomogida K, Dohmae K, Nishimune Y. Regulation of proliferation and differentiation in spermatogonial stem cells: the role of c-kit and its ligand SCF. Development. 2000;127:2125–31.
63. Nagano R, Tabata S, Nakanishi Y, Ohsako S, Kurohmaru M, Hayashi Y. Reproliferation and relocation of mouse male germ cells (gonocytes) during prespermatogenesis. Anat. Rec. 2000;258:210–20.
64. De Rooij DG, Russell LD. All you wanted to know about spermatogonia but were afraid to ask. J. Androl. 2000;6512:776–98.
65. Payne CJ, Gallagher SJ, Foreman O, Dannenberg JH, Depinho RA, Braun RE. Sin3a is required by Sertoli cells to establish a niche for undifferentiated spermatogonia, germ cell tumors, and spermatid elongation. Stem Cells. 2010;28:1424–34.
66. Pellegrino J, Castrillon DH, David G. Chromatin associated Sin3A is essential for male germ cell lineage in the mouse. Dev. Biol. 2012;369:349–55.
67. Gallagher SJ, Kofman AE, Huszar JM, Dannenberg JH, DePinho RA, Braun RE, et al. Distinct requirements for Sin3a in perinatal male gonocytes and differentiating spermatogonia. Dev. Biol. 2013;373:83–94.
68. Sokol RZ. Endocrinology of male infertility: Evaluation and treatment. Semin. Reprod. Med. 2009;27:149–58.
69. Walker WH. Testosterone signaling and the regulation of spermatogenesis. Spermatogenesis. 2011;1:116–20.
70. Smith LB, Walker WH. The regulation of spermatogenesis by androgens. Semin. Cell Dev. Biol. 2014. p. 2–13.
71. Moyle WR, Campbell RK, Myers R V, Bernard MP, Han Y, Wang X. Co-evolution of ligand-receptor pairs. Nature. 1994;368:251–5.
72. Moyle WR, Campbell RK, Rao SN V, Ayad NG, Bernard MP, Han Y, et al. Model of human chorionic gonadotropin and lutropin receptor interaction that explains signal transduction of the glycoprotein hormones. J. Biol. Chem. 1995;270:20020–31.
73. Carreau S, Hess RA. Oestrogens and spermatogenesis. Philos. Trans. R. Soc. Lond. B. Biol. Sci. 2010;365:1517–35.
74. McLachlan RI, Robertson DM, Pruysers E, Ugoni A, Matsumoto AM, Anawalt BD, et al. Relationship between Serum Gonadotropins and Spermatogenic Suppression in Men Undergoing Steroidal Contraceptive Treatment. J. Clin. Endocrinol. Metab. 2004;89:142–9.

75. Zhang FP, Poutanen M, Wilbertz J, Huhtaniemi I. Normal prenatal but arrested postnatal sexual development of luteinizing hormone receptor knockout (LuRKO) mice. Mol. Endocrinol. 2001;15:172–83.
76. Krishnamurthy H, Kumar KM, Joshi CV, Krishnamurthy HN, Moudgal RN, Sairam MR. Alterations in sperm characteristics of follicle-stimulating hormone (FSH)-immunized men are similar to those of FSH-deprived infertile male bonnet monkeys. J. Androl. 2000. p. 316–27.
77. Meehan T, Schlatt S, O'Bryan MK, de Kretser DM, Loveland KL. Regulation of germ cell and Sertoli cell development by activin, follistatin, and FSH. Dev Biol. 2000;220:225–37.
78. De Kretser DM, Buzzard JJ, Okuma Y, O'Connor AE, Hayashi T, Lin SY, et al. The role of activin, follistatin and inhibin in testicular physiology. Mol. Cell. Endocrinol. 2004. p. 57–64.
79. Wang C, Nieschlag E, Swerdloff R, Behre HM, Hellstrom WJ, Gooren LJ, et al. Investigation, Treatment, and Monitoring of Late-Onset Hypogonadism in Males: ISA, ISSAM, EAU, EAA, and ASA Recommendations. Eur. Urol. 2009;55:121–30.
80. De Gendt K, Swinnen J V, Saunders PTK, Schoonjans L, Dewerchin M, Devos A, et al. A Sertoli cell-selective knockout of the androgen receptor causes spermatogenic arrest in meiosis. Proc. Natl. Acad. Sci. U. S. A. 2004;101:1327–32.
81. Bhasin S, Basaria S. Diagnosis and treatment of hypogonadism in men. Best Pract. Res. Clin. Endocrinol. Metab. 2011. p. 251–70.
82. Tagelenbosch RAJ, de Rooij DG. A quantitative study of spermatogonial multiplication and stem cell renewal in the C3H/101 F1 hybrid mouse. Mutat. Res. - Fundam. Mol. Mech. Mutagen. 1993;290:193–200.
83. de Rooij DG. Proliferation and differentiation of spermatogonial stem cells. Reproduction. 2001;121:347–54.
84. Shinohara T, Orwig KE, Avarbock MR, Brinster RL. Spermatogonial stem cell enrichment by multiparameter selection of mouse testis cells. Proc. Natl. Acad. Sci. U. S. A. 2000;97:8346–51.
85. Brinster RL, Zimmermann JW. Spermatogenesis following male germ-cell transplantation. Proc. Natl. Acad. Sci. U. S. A. 1994;91:11298–302.
86. Nakagawa T, Sharma M, Nabeshima Y i., Braun RE, Yoshida S. Functional Hierarchy and Reversibility Within the Murine Spermatogenic Stem Cell Compartment. Science (80). 2010;328:62–7.
87. Nakagawa T, Sharma M, Nabeshima Y, Braun RE, Yoshida S. Functional hierarchy and reversibility within the murine spermatogenic stem cell compartment. Science. 2010;328:62–7.
88. Barroca V, Lassalle B, Coureuil M, Louis JP, Le Page F, Testart J, et al. Mouse differentiating spermatogonia can generate germinal stem cells in vivo. Nat Cell Biol. 2009;11:190–6.
89. Boitani C, Di Persio S, Esposito V, Vicini E. Spermatogonial cells: Mouse, monkey and man comparison. Semin. Cell Dev. Biol. 2016; 59:79-88.
90. Morrison SJ, Kimble J. Asymmetric and symmetric stem-cell divisions in development and cancer. Nature. 2006;441:1068–74.
91. Spradling A, Fuller MT, Braun RE, Yoshida S. Germline stem cells. Cold Spring Harb. Perspect. Biol. 2011;3.
92. Tseng YT, Liao HF, Yu CY, Mo CF, Lin SP. Epigenetic factors in the regulation of prospermatogonia and spermatogonial stem cells. Reproduction. 2015;150:R77–91.
93. Agrimson KS, Onken J, Mitchell D, Topping TB, Chiarini-Garcia H, Hogarth CA, et al. Characterizing the Spermatogonial Response to Retinoic Acid During the Onset of Spermatogenesis and Following Synchronization in the Neonatal Mouse Testis. Biol. Reprod. 2016;95:81.
94. Spradling A, Drummond-Barbosa D, Kai T. Stem cells find their niche. Nature. 2001;414:98–104.
95. Scadden DT. The stem-cell niche as an entity of action. Nature. 2006;441:1075–9.
96. Oatley JM, Oatley MJ, Avarbock MR, Tobias JW, Brinster RL. Colony stimulating factor 1 is an extrinsic stimulator of mouse spermatogonial stem cell self-renewal. Development. 2009;136:1191–9.

97. Hofmann M-C. Gdnf signaling pathways within the mammalian spermatogonial stem cell niche. Mol. Cell. Endocrinol. 2008;288:95–103.
98. Meng X, Lindahl M, Hyvönen ME, Parvinen M, de Rooij DG, Hess MW, et al. Regulation of Cell Fate Decision of Undifferentiated Spermatogonia by GDNF. Science. 2000;287:1489–93.
99. Tadokoro Y, Yomogida K, Ohta H, Tohda A, Nishimune Y. Homeostatic regulation of germinal stem cell proliferation by the GDNF/FSH pathway. Mech. Dev. 2002;113:29–39.
100. Kanatsu-Shinohara M, Ogonuki N, Inoue K, Miki H, Ogura A, Toyokuni S, et al. Long-term proliferation in culture and germline transmission of mouse male germline stem cells. Biol. Reprod. 2003;69:612–6.
101. Kubota H, Avarbock MR, Brinster RL. Growth factors essential for self-renewal and expansion of mouse spermatogonial stem cells. Proc. Natl. Acad. Sci. U. S. A. 2004;101:16489–94.
102. Oatley JM, Avarbock MR, Telaranta AI, Fearon DT, Brinster RL. Identifying genes important for spermatogonial stem cell self-renewal and survival. Proc. Natl. Acad. Sci. U. S. A. 2006;103:9524–9.
103. Airaksinen MS, Saarma M. the Gdnf Family: Signalling, Biological Functions and Therapeutic Value. Nat. Rev. Neurosci. 2002;3:383–94.
104. Naughton CK, Jain S, Strickland AM, Gupta A, Milbrandt J. Glial cell-line derived neurotrophic factor-mediated RET signaling regulates spermatogonial stem cell fate. Biol. Reprod. 2006;74:314–21.
105. Oatley JM, Avarbock MR, Brinster RL. Glial cell line-derived neurotrophic factor regulation of genes essential for self-renewal of mouse spermatogonial stem cells is dependent on Src family kinase signaling. J. Biol. Chem. 2007;282:25842–51.
106. Matsui Y, Zsebo K, Hogan BL. Derivation of pluripotential embryonic stem cells from murine primordial germ cells in culture. Cell. 1992;70:841–7.
107. Resnick JL, Bixler LS, Cheng L, Donovan PJ. Long-term proliferation of mouse primordial germ cells in culture. Nature. 1992;359:550–1.
108. Labosky PA, Barlow DP, Hogan BL. Embryonic germ cell lines and their derivation from mouse primordial germ cells. Ciba Found Symp. 1994;182:157–78.
109. Boyer L, Lee T, Cole M, Johnstone S, Levine S, Zucker J, et al. Core transcriptional regulatory circuitry in human embryonic stem cells. Cell. 2005;122:947–56.
110. Sada A, Suzuki A, Suzuki H, Saga Y. The RNA-binding protein NANOS2 is required to maintain murine spermatogonial stem cells. Science. 2009;325:1394–8.
111. Chambers I, Tomlinson SR. The transcriptional foundation of pluripotency. Development. 2009;136:2311–22.
112. Yoshida S, Takakura A, Ohbo K, Abe K, Wakabayashi J, Yamamoto M, et al. Neurogenin3 delineates the earliest stages of spermatogenesis in the mouse testis. Dev. Biol. 2004;269:447–58.
113. Yoshida S, Sukeno M, Nakagawa T, Ohbo K, Nagamatsu G, Suda T, et al. The first round of mouse spermatogenesis is a distinctive program that lacks the self-renewing spermatogonia stage. Development. 2006;133:1495–505.
114. Schrans-Stassen BH, Saunders PT, Cooke HJ, de Rooij DG. Nature of the spermatogenic arrest in Dazl -/- mice. Biol. Reprod. 2001;65:771–6.
115. Sada A, Hasegawa K, Pin PH, Saga Y. NANOS2 acts downstream of glial cell line-derived neurotrophic factor signaling to suppress differentiation of spermatogonial stem cells. Stem Cells. 2012;30:280–91.
116. Nichols J, Zevnik B, Anastassiadis K, Niwa H, Klewe-Nebenius D, Chambers I, et al. Formation of pluripotent stem cells in the mammalian embryo depends on the POU transcription factor Oct4. Cell. 1998;95:379–91.
117. Oatley JM, Brinster RL. Regulation of spermatogonial stem cell self-renewal in mammals. Annu. Rev. Cell Dev. Biol. 2008;24:263–86.
118. Dann CT, Alvarado AL, Molyneux LA, Denard BS, Garbers DL, Porteus MH. Spermatogonial Stem Cell Self Renewal Requires OCT4, A Factor Down-Regulated During Retinoic Acid Induced Differentiation. Stem Cells. 2008; 26:9828-37.

119. Pesce M, Gross MK, Schöler HR. In line with our ancestors: Oct-4 and the mammalian germ. Bioessays. 1998;20:722–32.
120. Rosner MH, Vigano MA, Ozato K, Timmons PM, Poirier F, Rigby PW, et al. A POU-domain transcription factor in early stem cells and germ cells of the mammalian embryo. Nature. 1990;345:686–92.
121. Costoya J a, Hobbs RM, Barna M, Cattoretti G, Manova K, Sukhwani M, et al. Essential role of Plzf in maintenance of spermatogonial stem cells. Nat. Genet. 2004;36:653–9.
122. Buaas FW, Kirsh AL, Sharma M, McLean DJ, Morris JL, Griswold MD, et al. Plzf is required in adult male germ cells for stem cell self-renewal. Nat. Genet. 2004;36:647–52.
123. Hobbs RM, Fagoonee S, Papa A, Webster K, Altruda F, Nishinakamura R, et al. Functional antagonism between Sall4 and Plzf defines germline progenitors. Cell Stem Cell. 2012;10:284–98.
124. Falender AE, Freiman RN, Geles KG, Lo KC, Hwang K, Lamb DJ, et al. Maintenance of spermatogenesis requires TAF4b, a gonad-specific subunit of TFIID. Genes Dev. 2005;19:794–803.
125. Manku G, Culty M. Mammalian gonocyte and spermatogonia differentiation: recent advances and remaining challenges. Reproduction. 2015. p. R139–57.
126. Bowles J, Knight D, Smith C, Wilhelm D, Richman J, Mamiya S, et al. Retinoid signaling determines germ cell fate in mice. Science (80-. ). 2006;312:596–600.
127. Koubova J, Menke DB, Zhou Q, Capel B, Griswold MD, Page DC. Retinoic acid regulates sex-specific timing of meiotic initiation in mice. Proc. Natl. Acad. Sci. U. S. A. 2006;103:2474–9.
128. Handel MA, Schimenti JC. Genetics of mammalian meiosis: regulation, dynamics and impact on fertility. Nat. Rev. Genet. 2010;11:124–36.
129. Suzuki H, Ahn HW, Chu T, Bowden W, Gassei K, Orwig K, et al. SOHLH1 and SOHLH2 coordinate spermatogonial differentiation. Dev. Biol. 2012;361:301–12.
130. Filipponi D, Hobbs RM, Ottolenghi S, Rossi P, Jannini EA, Pandolfi PP, et al. Repression of kit expression by Plzf in germ cells. Mol. Cell. Biol. 2007;27:6770–81.
131. Barrios F, Filipponi D, Pellegrini M, Paronetto MP, Di Siena S, Geremia R, et al. Opposing effects of retinoic acid and FGF9 on Nanos2 expression and meiotic entry of mouse germ cells. J. Cell Sci. 2010;123:871–80.
132. Zhang L, Tang J, Haines CJ, Feng H, Lai L, Teng X, et al. C-Kit Expression Profile and Regulatory Factors During Spermatogonial Stem Cell Differentiation. BMC Dev. Biol. 2013;13:38.
133. Carlomagno G, Bragt MPA Van, Korver CM, Repping S, Rooij DG De, Pelt AMM Van. BMP4-Induced Differentiation of a Rat Spermatogonial Stem Cell Line Causes Changes in Its Cell Adhesion Properties 1. Biol Reprod. 2010;749:742–9.
134. Nagano MC, Yeh JR. The Identity and Fate Decision Control of Spermatogonial Stem Cells. Where Is the Point of No Return? Curr. Top. Dev. Biol. 2013;102:61–95.
135. Oatley JM, Kaucher A V, Avarbock MR, Brinster RL. Regulation of mouse spermatogonial stem cell differentiation by STAT3 signaling. Biol. Reprod. 2010;83:427–33.
136. Kaucher A V, Oatley MJ, Oatley JM. NEUROG3 is a critical downstream effector for STAT3-regulated differentiation of mammalian stem and progenitor spermatogonia. Biol. Reprod. 2012;86:164, 1–11.
137. Zhang T, Murphy MW, Gearhart MD, Bardwell VJ, Zarkower D. The mammalian Doublesex homolog DMRT6 coordinates the transition between mitotic and meiotic developmental programs during spermatogenesis. Development. 2014;141:3662–71.
138. Ballow D, Meistrich ML, Matzuk M, Rajkovic A. Sohlh1 is essential for spermatogonial differentiation. Dev. Biol. 2006;294:161–7.
139. Hao J, Yamamoto M, Richardson TE, Chapman KM, Denard BS, Hammer RE, et al. Sohlh2 knockout mice are male-sterile because of degeneration of differentiating type A spermatogonia. Stem Cells. 2008;26:1587–97.
140. Chithalen J V, Luu L, Petkovich M, Jones G. HPLC-MS/MS analysis of the products generated from all-trans-retinoic acid using recombinant human CYP26A. J Lipid Res. 2002;43:1133–42.

141. MacQueen AJ, Hochwagen A. Checkpoint mechanisms: The puppet masters of meiotic prophase. Trends Cell Biol. 2011. p. 393–400.
142. Niederreither K, Dollé P. Retinoic acid in development: towards an integrated view. Nat. Rev. Genet. 2008;9:541–53.
143. Kanatsu-Shinohara M, Lee J, Inoue K, Ogonuki N, Miki H, Toyokuni S, et al. Pluripotency of a single spermatogonial stem cell in mice. Biol. Reprod. 2008;78:681–7.
144. de Rooij DG, Mizrak SC. Deriving multipotent stem cells from mouse spermatogonial stem cells: a new tool for developmental and clinical research. Development. 2008;135:2207–13.
145. Kanatsu-Shinohara M, Inoue K, Miki H, Ogonuki N, Takehashi M, Morimoto T, et al. Clonal origin of germ cell colonies after spermatogonial transplantation in mice. Biol. Reprod. 2006;75:68–74.
146. Kanatsu-Shinohara M, Ogonuki N, Matoba S, Morimoto H, Ogura A, Shinohara T. Improved serum- and feeder-free culture of mouse germline stem cells. Biol. Reprod. 2014;91:88.
147. Guan K, Nayernia K, Maier LS, Wagner S, Dressel R, Lee JH, et al. Pluripotency of spermatogonial stem cells from adult mouse testis. Nature. 2006;440:1199–203.
148. Seandel M, James D, Shmelkov S V, Falciatori I, Kim J, Chavala S, et al. Generation of functional multipotent adult stem cells from GPR125+ germline progenitors. Nature. 2007;449:346–50.
149. Glaser T, Opitz T, Kischlat T, Konang R, Sasse P, Fleischmann BK, et al. Adult germ line stem cells as a source of functional neurons and glia. Stem Cells. 2008;26:2434–43.
150. Streckfuss-Bomeke K, Vlasov A, Hulsmann S, Yin D, Nayernia K, Engel W, et al. Generation of functional neurons and glia from multipotent adult mouse germ-line stem cells. Stem Cell Res. 2009;2:139–54.
151. Guan K, Wagner S, Unsold B, Maier LS, Kaiser D, Hemmerlein B, et al. Generation of functional cardiomyocytes from adult mouse spermatogonial stem cells. Circ. Res. 2007;100:1615–25.
152. Cyranoski D. Human stem cells created by cloning. Nature. 2013;497:295–6.
153. Nayernia K, Li M, Jaroszynski L, Khusainov R, Wulf G, Schwandt I, et al. Stem cell based therapeutical approach of male infertility by teratocarcinoma derived germ cells. Hum. Mol. Genet. 2004;13:1451–60.
154. Ehmcke J, Wistuba J, Schlatt S. Spermatogonial stem cells: Questions, models and perspectives. Hum. Reprod. Update. 2006. p. 275–82.
155. Lewis EB. A gene complex controlling segmentation in Drosophila. Nature. 1978;276:565–70.
156. Müller J. Transcriptional silencing by the Polycomb protein in Drosophila embryos. EMBO J. 1995;14:1209–20.
157. Busturia a, Wightman CD, Sakonju S. A silencer is required for maintenance of transcriptional repression throughout Drosophila development. Development. 1997;124:4343–50.
158. Shao Z, Raible F, Mollaaghababa R, Guyon JR, Wu CT, Bender W, et al. Stabilization of chromatin structure by PRC1, a polycomb complex. Cell. 1999;98:37–46.
159. Levine SS, Weiss A, Erdjument-Bromage H, Shao Z, Tempst P, Kingston RE. The core of the polycomb repressive complex is compositionally and functionally conserved in flies and humans. Mol. Cell. Biol. 2002;22:6070–8.
160. Francis NJ, Kingston RE, Woodcock CL. Chromatin compaction by a polycomb group protein complex. Science. 2004;306:1574–7.
161. Qiu J. Epigenetics: unfinished symphony. Nature. 2006;441:143–5.
162. Levenson JM, Sweatt JD. Epigenetic mechanisms in memory formation. Nat. Rev. Neurosci. 2005;6:108–18.
163. Bhaumik SR, Smith E, Shilatifard A. Covalent modifications of histones during development and disease pathogenesis. Nat Struct Mol Biol. 2007;14:1008–16.
164. Kuzmichev A, Nishioka K, Erdjument-Bromage H, Tempst P, Reinberg D. Histone methyltransferase activity associated with a human multiprotein complex containing the Enhancer of Zeste protein. Genes Dev. 2002;16:2893–905.
165. Sawarkar R, Paro R. Interpretation of Developmental Signaling at Chromatin: The Polycomb

Perspective. Dev. Cell. 2010. p. 651–61.
166. Sparmann A, van Lohuizen M. Polycomb silencers control cell fate, development and cancer. Nat. Rev. Cancer. 2006;6:846–56.
167. Simon J a, Kingston RE. Mechanisms of polycomb gene silencing: knowns and unknowns. Nat. Rev. Mol. Cell Biol. 2009;10:697–708.
168. Di Croce L, Helin K. Transcriptional regulation by Polycomb group proteins. Nat. Struct. Mol. Biol. 2013;20:1147–55.
169. Cao R, Zhang Y. SUZ12 is required for both the histone methyltransferase activity and the silencing function of the EED-EZH2 complex. Mol. Cell. 2004;15:57–67.
170. Cao R, Zhang Y. The functions of E(Z)/EZH2-mediated methylation of lysine 27 in histone H3. Curr. Opin. Genet. Dev. 2004. p. 155–64.
171. Cao R, Wang L, Wang H, Xia L, Erdjument-Bromage H, Tempst P, et al. Role of histone H3 lysine 27 methylation in Polycomb-group silencing. Science. 2002;298:1039–43.
172. Smith ZD, Meissner A. DNA methylation: roles in mammalian development. Nat. Rev. Genet. 2013;14:204–20.
173. Margueron R, Reinberg D. The Polycomb complex PRC2 and its mark in life. Nature. 2011;469:343–9.
174. Margueron R, Li G, Sarma K, Blais A, Zavadil J, Woodcock CL, et al. Ezh1 and Ezh2 Maintain Repressive Chromatin through Different Mechanisms. Mol. Cell. 2008;32:503–18.
175. Margueron R, Justin N, Ohno K, Sharpe ML, Son J, Drury III WJ, et al. Role of the polycomb protein EED in the propagation of repressive histone marks. Nature. 2009;461:762–7.
176. Xu C, Bian C, Yang W, Galka M, Ouyang H, Chen C, et al. Binding of different histone marks differentially regulates the activity and specificity of polycomb repressive complex 2 (PRC2). Proc. Natl. Acad. Sci. U. S. A. 2010;107:19266–71.
177. Shen X, Liu Y, Hsu YJ, Fujiwara Y, Kim J, Mao X, et al. EZH1 Mediates Methylation on Histone H3 Lysine 27 and Complements EZH2 in Maintaining Stem Cell Identity and Executing Pluripotency. Mol. Cell. 2008;32:491–502.
178. Xu B, On DM, Ma A, Parton T, Konze KD, Pattenden SG, et al. Selective inhibition of EZH2 and EZH1 enzymatic activity by a small molecule suppresses MLL- rearranged leukemia. Blood. 2015;125:346–57.
179. Bracken AP, Pasini D, Capra M, Prosperini E, Colli E, Helin K. EZH2 is downstream of the pRB-E2F pathway, essential for proliferation and amplified in cancer. EMBO J. 2003;22:5323–35.
180. Boyer L a, Plath K, Zeitlinger J, Brambrink T, Medeiros L a, Lee TI, et al. Polycomb complexes repress developmental regulators in murine embryonic stem cells. Nature. 2006;441:349–53.
181. Lee TI, Jenner RG, Boyer LA, Guenther MG, Levine SS, Kumar RM, et al. Control of Developmental Regulators by Polycomb in Human Embryonic Stem Cells. Cell. 2006;125:301–13.
182. Pasini D, Bracken AP, Hansen JB, Capillo M, Helin K. The polycomb group protein Suz12 is required for embryonic stem cell differentiation. Mol. Cell. Biol. 2007;27:3769–79.
183. Pietersen AM, van Lohuizen M. Stem cell regulation by polycomb repressors: postponing commitment. Curr. Opin. Cell Biol. 2008. p. 201–7.
184. Surface LE, Thornton SR, Boyer LA. Polycomb group proteins set the stage for early lineage commitment. Cell Stem Cell. 2010. p. 288–98.
185. Sparmann A, van Lohuizen M. Polycomb silencers control cell fate, development and cancer. Nat. Rev. Cancer. 2006;6:846–56.
186. Bracken AP, Helin K. Polycomb group proteins: navigators of lineage pathways led astray in cancer. Nat. Rev. Cancer. 2009;9:773–84.
187. Sasaki H, Matsui Y. Epigenetic events in mammalian germ-cell development: reprogramming and beyond. Nat Rev Genet. 2008;9:129–40.
188. Lees-Murdock DJ, Walsh CP. DNA methylation reprogramming in the germ line. Adv. Exp. Med. Biol. 2008. p. 1–15.
189. Song HW, Wilkinson MF. Transcriptional control of spermatogonial maintenance and differentiation. Semin. Cell Dev. Biol. 2014. p. 14–26.

190. Seisenberger S, Andrews S, Krueger F, Arand J, Walter J, Santos F, et al. The Dynamics of Genome-wide DNA Methylation Reprogramming in Mouse Primordial Germ Cells. Mol. Cell. 2012;48:849–62.
191. Kobayashi H, Sakurai T, Miura F, Imai M, Mochiduki K, Yanagisawa E, et al. High-resolution DNA methylome analysis of primordial germ cells identifies gender-specific reprogramming in mice. Genome Res. 2013;23:616–27.
192. Li JY, Lees-Murdock DJ, Xu GL, Walsh CP. Timing of establishment of paternal methylation imprints in the mouse. Genomics. 2004;84:952–60.
193. Maatouk DM, Kellam LD, Mann MRW, Lei H, Li E, Bartolomei MS, et al. DNA methylation is a primary mechanism for silencing postmigratory primordial germ cell genes in both germ cell and somatic cell lineages. Development. 2006;133:3411–8.
194. La Salle S, Trasler JM. Dynamic expression of DNMT3a and DNMT3b isoforms during male germ cell development in the mouse. Dev. Biol. 2006;296:71–82.
195. Sakai Y, Suetake I, Shinozaki F, Yamashina S, Tajima S. Co-expression of de novo DNA methyltransferases Dnmt3a2 and Dnmt3L in gonocytes of mouse embryos. Gene Expr. Patterns. 2004;5:231–7.
196. Kato Y, Kaneda M, Hata K, Kumaki K, Hisano M, Kohara Y, et al. Role of the Dnmt3 family in de novo methylation of imprinted and repetitive sequences during male germ cell development in the mouse. Hum. Mol. Genet. 2007;16:2272–80.
197. Ng J-H, Kumar V, Muratani M, Kraus P, Yeo J-C, Yaw L-P, et al. In vivo epigenomic profiling of germ cells reveals germ cell molecular signatures. Dev. Cell. 2013;24:324–33.
198. Yokobayashi S, Liang CY, Kohler H, Nestorov P, Liu Z, Vidal M, et al. Re: PRC1 coordinates timing of sexual differentiation of female primordial germ cells. J. Urol. 2013. p. 1954–5.
199. Liu S, BrindAmour J, Karimi MM, Shirane K, Bogutz A, Lefebvre L, et al. Setdb1 is required for germline development and silencing of H3K9me3-marked endogenous retroviruses in primordial germ cells. Genes Dev. 2014;28:2041–55.
200. Hajkova P, Erhardt S, Lane N, Haaf T, El-Maarri O, Reik W, et al. Epigenetic reprogramming in mouse primordial germ cells. Mech. Dev. 2002;117:15–23.
201. Davis TL, Yang GJ, McCarrey JR, Bartolomei MS. The H19 methylation imprint is erased and re-established differentially on the parental alleles during male germ cell development. Hum. Mol. Genet. 2000;9:2885–94.
202. Kaneda M, Okano M, Hata K, Sado T, Tsujimoto N, Li E, et al. Essential role for de novo DNA methyltransferase Dnmt3a in paternal and maternal imprinting. Nature. 2004;429:900–3.
203. Bourc'his D, Bestor TH. Meiotic catastrophe and retrotransposon reactivation in male germ cells lacking Dnmt3L. Nature. 2004;431:96–9.
204. Webster KE, O'Bryan MK, Fletcher S, Crewther PE, Aapola U, Craig J, et al. Meiotic and epigenetic defects in Dnmt3L-knockout mouse spermatogenesis. Proc. Natl. Acad. Sci. U. S. A. 2005;102:4068–73.
205. Ueda T, Abe K, Miura A, Yuzuriha M, Zubair M, Noguchi M, et al. The paternal methylation imprint of the mouse H19 locus is acquired in the gonocyte stage during foetal testis development. Genes to Cells. 2000;5:649–59.
206. Sasaki H, Matsui Y. Epigenetic events in mammalian germ-cell development: reprogramming and beyond. Nat Rev Genet. 2008;9:129–40.
207. Shirakawa T, Yaman-Deveci R, Tomizawa S, Kamizato Y, Nakajima K, Sone H, et al. An epigenetic switch is crucial for spermatogonia to exit the undifferentiated state toward a Kit-positive identity. Development. 2013;140:3565–76.
208. Liao H-F, Chen WSC, Chen Y-H, Kao T-H, Tseng Y-T, Lee C-Y, et al. DNMT3L promotes quiescence in postnatal spermatogonial progenitor cells. Development. 2014;1–12.
209. Hermann BP, Mutoji KN, Velte EK, Ko D, Oatley JM, Geyer CB, et al. Transcriptional and translational heterogeneity among neonatal mouse spermatogonia. Biol. Reprod. 2015;92:54.
210. Hammoud SS, Low DHP, Yi C, Carrell DT, Guccione E, Cairns BR. Chromatin and transcription transitions of mammalian adult germline stem cells and spermatogenesis. Cell Stem Cell. 2014;15:239–53.

211. Kubo N, Toh H, Shirane K, Shirakawa T, Kobayashi H, Sato T, et al. DNA methylation and gene expression dynamics during spermatogonial stem cell differentiation in the early postnatal mouse testis. BMC Genomics. 2015;16:624.
212. Lesch BJ, Page DC. Poised chromatin in the mammalian germ line. Development. 2014;141:3619–26.
213. Mu W, Starmer J, Fedoriw AM, Yee D, Magnuson T. Repression of the soma-specific transcriptome by polycomb-repressive complex 2 promotes male germ cell development. Genes Dev. 2014;28:2056–69.
214. Kimmins S, Sassone-Corsi P. Chromatin remodelling and epigenetic features of germ cells. Nature. 2005;434:583–9.
215. Govin J, Escoffier E, Rousseaux S, Kuhn L, Ferro M, Thévenon J, et al. Pericentric heterochromatin reprogramming by new histone variants during mouse spermiogenesis. J. Cell Biol. 2007;176:283–94.
216. Li A, Eirín-López JM, Ausió J. H2AX: tailoring histone H2A for chromatin-dependent genomic integrity. Biochem. Cell Biol. 2005;83:505–15.
217. Boulard M, Gautier T, Mbele GO, Gerson V, Hamiche A, Angelov D, et al. The NH2 tail of the novel histone variant H2BFWT exhibits properties distinct from conventional H2B with respect to the assembly of mitotic chromosomes. Mol Cell Biol. 2006;26:1518–26.
218. Fernandez-Capetillo O, Mahadevaiah SK, Celeste A, Romanienko PJ, Camerini-Otero RD, Bonner WM, et al. H2AX is required for chromatin remodeling and inactivation of sex chromosomes in male mouse meiosis. Dev. Cell. 2003. p. 497–508.
219. Turner JMA, Aprelikova O, Xu X, Wang R, Kim S, Chandramouli GVR, et al. BRCA1, histone H2AX phosphorylation, and male meiotic sex chromosome inactivation. Curr. Biol. 2004;14:2135–42.
220. Namekawa SH, Park PJ, Zhang LF, Shima JE, McCarrey JR, Griswold MD, et al. Postmeiotic Sex Chromatin in the Male Germline of Mice. Curr. Biol. 2006;16:660–7.
221. Turner JMA, Mahadevaiah SK, Ellis PJI, Mitchell MJ, Burgoyne PS. Pachytene asynapsis drives meiotic sex chromosome inactivation and leads to substantial postmeiotic repression in spermatids. Dev. Cell. 2006;10:521–9.
222. Martianov I, Brancorsini S, Catena R, Gansmuller A, Kotaja N, Parvinen M, et al. Polar nuclear localization of H1T2, a histone H1 variant, required for spermatid elongation and DNA condensation during spermiogenesis. Proc. Natl. Acad. Sci. U. S. A. 2005;102:2808–13.
223. Heidaran MA, Kistler WS. Isolation of a cDNA clone for transition protein 1 (TP1), a major chromosomal protein of mammalian spermatids. Gene. 1987;54:281–4.
224. Kleene KC, Flynn JF. Characterization of a cDNA clone encoding a basic protein, TP2, involved in chromatin condensation during spermiogenesis in the mouse. J. Biol. Chem. 1987;262:17272–7.
225. Steger K, Failing K, Klonisch T, Behre HM, Manning M, Weidner W, et al. Round spermatids from infertile men exhibit decreased protamine-1 and -2 mRNA. Hum. Reprod. 2001;16:709–16.
226. Carrell DT, Emery BR, Hammoud S. Altered protamine expression and diminished spermatogenesis: What is the link? Hum. Reprod. Update. 2007;13:313–27.
227. Rousseaux S, Caron C, Govin J, Lestrat C, Faure AK, Khochbin S. Establishment of male-specific epigenetic information. Gene. 2005. p. 139–53.
228. Cohen P. The origins of protein phosphorylation. Nat. Cell Biol. 2002;4:E127–30.
229. Gupta GS. Proteomics of Spermatogenesis. NY: Springer US; 2006.
230. Visconti PE, Moore GD, Bailey JL, Leclerc P, Connors SA, Pan D, et al. Capacitation of mouse spermatozoa. II. Protein tyrosine phosphorylation and capacitation are regulated by a cAMP-dependent pathway. Development. 1995;121:1139–50.
231. A.p. Harrison R, Gadella BM. Bicarbonate-induced membrane processing in sperm capacitation. Theriogenology. 2005. p. 342–51.
232. Lefievre L, Jha KN, de Lamirande E, Visconti PE, Gagnon C. Activation of protein kinase A during human sperm capacitation and acrosome reaction. J Androl. 2002;23:709–16.
233. Baudat F, Imai Y, de Massy B. Meiotic recombination in mammals: localization and

regulation. Nat. Rev. Genet. 2013;14:794–806.
234. Xu Y, Ashley T, Brainerd EE, Bronson RT, Meyn MS, Baltimore D. Targeted disruption of ATM leads to growth retardation, chromosomal fragmentation during meiosis, immune defects, and thymic lymphoma. Genes Dev. 1996;10:2411–22.
235. Lam I, Keeney S. Mechanism and control of meiotic recombination initiation. Cold Spring Harb Perspet Biol. 2015;52:1–53.
236. Takubo K, Ohmura M, Azuma M, Nagamatsu G, Yamada W, Arai F, et al. Stem Cell Defects in ATM-Deficient Undifferentiated Spermatogonia through DNA Damage-Induced Cell-Cycle Arrest. Cell Stem Cell. 2008;2:170–82.
237. de Lamirande E, Gagnon C. The extracellular signal-regulated kinase (ERK) pathway is involved in human sperm function and modulated by the superoxide anion. Mol. Hum. Reprod. 2002;8:124–35.
238. Luconi M, Barni T, Vannelli GB, Krausz C, Marra F, Benedetti P a, et al. Extracellular signal-regulated kinases modulate capacitation of human spermatozoa. Biol. Reprod. 1998;58:1476–89.
239. du Plessis SS, Page C, Franken DR. Extracellular signal-regulated kinase activation involved in human sperm-zona pellucida binding. Andrologia. 2002;34:55–9.
240. Braydich-Stolle L, Kostereva N, Dym M, Hofmann M-C. Role of Src family kinases and N-Myc in spermatogonial stem cell proliferation. Dev. Biol. 2007;304:34–45.
241. Lee J, Kanatsu-Shinohara M, Inoue K, Ogonuki N, Miki H, Toyokuni S, et al. Akt mediates self-renewal division of mouse spermatogonial stem cells. Development. 2007;134:1853–9.
242. Sariola H, Saarma M. Novel functions and signalling pathways for GDNF. J. Cell Sci. 2003;116:3855–62.
243. Urner F, Sakkas D. Protein phosphorylation in mammalian spermatozoa. Reproduction. 2003. p. 17–26.
244. Leyton L, LeGuen P, Bunch D, Saling PM. Regulation of mouse gamete interaction by a sperm tyrosine kinase. Proc. Natl. Acad. Sci. U. S. A. 1992;89:11692–5.
245. Smith GD, Wolf DP, Trautman KC, da Cruz e Silva EF, Greengard P, Vijayaraghavan S. Primate sperm contain protein phosphatase 1, a biochemical mediator of motility. Biol. Reprod. 1996;54:719–27.
246. Naz RK. Involvement of protein serine and threonine phosphorylation in human sperm capacitation. Biol. Reprod. 1999;60:1402–9.
247. Chakrabarti R, Kline D, Lu J, Orth J, Pilder S, Vijayaraghavan S. Analysis of Ppp1cc-null mice suggests a role for PP1gamma2 in sperm morphogenesis. Biol. Reprod. 2007;76:992–1001.
248. Ashizawa K, Wishart GJ, Ranasinghe ARAH, Katayama S, Tsuzuki Y. Protein phosphatase-type 2B is involved in the regulation of the acrosome reaction but not in the temperature-dependent flagellar movement of fowl spermatozoa. Reproduction. 2004;128:783–7.
249. Beumer TL, Roepers-Gajadien HL, Gademan IS, Kal HB, de Rooij DG. Involvement of the D-type cyclins in germ cell proliferation and differentiation in the mouse. Biol. Reprod. 2000;63:1893–8.
250. Ryser S, Glauser D, Vigier M, Zhang YQ, Tachini P, Schlegel W, et al. Gene expression profiling of rat spermatogonia and Sertoli cells reveals signaling pathways from stem cells to niche and testicular cancer cells to surrounding stroma. BMC Genomics. 2011;12:29.
251. Puri P, Phillips BT, Suzuki H, Orwig KE, Rajkovic A, Lapinski PE, et al. The transition from stem cell to progenitor spermatogonia and male fertility requires the SHP2 protein tyrosine phosphatase. Stem Cells. 2014;32:741–53.
252. Sinha N, Puri P, Nairn AC, Vijayaraghavan S. Selective ablation of Ppp1cc gene in testicular germ cells causes oligo-teratozoospermia and infertility in mice. Biol. Reprod. 2013;89:128.
253. Sinha N, Pilder S, Vijayaraghavan S. Significant Expression Levels of Transgenic PPP1CC2 in Testis and Sperm Are Required to Overcome the Male Infertility Phenotype of Ppp1cc Null Mice. PLoS One. 2012;7.
254. Pan X, Chen X, Tong X, Tang C, Li J. Ppp2ca knockout in mice spermatogenesis. Reproduction. 2015;149:385–91.
255. Mizoguchi S, Kim KH. Expression of cdc25 phosphatases in the germ cells of the rat testis.

Biol. Reprod. 1997;56:1474–81.
256. Di Vizio D, Cito L, Boccia A, Chieffi P, Insabato L, Pettinato G, et al. Loss of the tumor suppressor gene PTEN marks the transition from intratubular germ cell neoplasias (ITGCN) to invasive germ cell tumors. Oncogene. 2005;24:1882–94.
257. Soler DC, Kadunganattil S, Ramdas S, Myers K, Roca J, Slaughter T, et al. Expression of transgenic PPP1CC2 in the testis of Ppp1cc-null mice rescues spermatid viability and spermiation but does not restore normal sperm tail ultrastructure, sperm motility, or fertility. Biol. Reprod. 2009;81:343–52.
258. Oppedisano-Wells L, Varmuza S. Protein phosphatase 1cgamma is required in germ cells in murine testis. Mol. Reprod. Dev. 2003;65:157–66.
259. Forgione N, Vogl AW, Varmuza S. Loss of protein phosphatase 1cc (PPP1CC) leads to impaired spermatogenesis associated with defects in chromatin condensation and acrosome development: An ultrastructural analysis. Reproduction. 2010;139:1021–9.
260. Fardilha M, Esteves SLC, Korrodi-Gregório L, Pelech S, da Cruz e Silva OAB, da Cruz e Silva E. Protein phosphatase 1 complexes modulate sperm motility and present novel targets for male infertility. Mol. Hum. Reprod. 2011. p. 466–77.
261. Fardilha M, Ferreira M, Pelech S, Vieira S, Rebelo S, Korrodi-Gregorio L, et al. "Omics" of human sperm: profiling protein phosphatases. OMICS. 2013;17:460–72.
262. Fardilha M, Esteves SLC, Korrodi-Gregório L, Vintém AP, Domingues SC, Rebelo S, et al. Identification of the human testis protein phosphatase 1 interactome. Biochem. Pharmacol. 2011. p. 1403–15.
263. Hrabchak C, Varmuza S. Identification of the spermatogenic zip protein Spz1 as a putative protein phosphatase-1 (PP1) regulatory protein that specifically binds the PP1cc2 splice variant in mouse testis. J. Biol. Chem. 2004;279:37079–86.
264. Beullens M, Van Eynde A, Vulsteke V, Connor J, Shenolikar S, Stalmans W, et al. Molecular determinants of nuclear protein phosphatase-1 regulation by NIPP-1. J. Biol. Chem. 1999;274:14053–61.
265. Ceulemans H, Stalmans W, Bollen M. Regulator-driven functional diversification of protein phosphatase-1 in eukaryotic evolution. BioEssays. 2002. p. 371–81.
266. Van Eynde A, Pérez-Callejón E, Schoenmakers E, Jacquemin M, Stalmans W, Bollen M. Organization and alternate splice products of the gene encoding nuclear inhibitor of protein phosphatase-1 (NIPP-1). Eur. J. Biochem. 1999;261:291–300.
267. Fardilha M, Wu W, Sá R, Fidalgo S, Sousa C, Mota C, et al. Alternatively spliced protein variants as potential therapeutic targets for male infertility and contraception. Ann. N. Y. Acad. Sci. 2004. p. 468–78.
268. Jagiello I, Van Eynde A, Vulsteke V, Beullens M, Boudrez a, Keppens S, et al. Nuclear and subnuclear targeting sequences of the protein phosphatase-1 regulator NIPP1. J. Cell Sci. 2000;113 Pt 21:3761–8.
269. Beullens M, Vulsteke V, Van Eynde A, Jagiello I, Stalmans W, Bollen M. The C-terminus of NIPP1 (nuclear inhibitor of protein phosphatase-1) contains a novel binding site for protein phosphatase-1 that is controlled by tyrosine phosphorylation and RNA binding. Biochem. J. 2000;352 Pt 3:651–8.
270. Trinkle-Mulcahy L, Ajuh P, Prescott A, Claverie-Martin F, Cohen S, Lamond AI, et al. Nuclear organisation of NIPP1, a regulatory subunit of protein phosphatase 1 that associates with pre-mRNA splicing factors. J Cell Sci. 1999;112 Pt 2:157–68.
271. Jagiello I, Beullens M, Vulsteke V, Wera S, Sohlberg B, Stalmans W, et al. NIPP-1, a Nuclear Inhibitory Subunit of Protein Phosphatase-1, Has RNA-binding Properties. J. Biol. Chem. 1997;272:22067–71.
272. Bollen M, Beullens M. Signaling by protein phosphatases in the nucleus. Trends Cell Biol. 2002. p. 138–45.
273. Tanuma N, Kim SE, Beullens M, Tsubaki Y, Mitsuhashi S, Nomura M, et al. Nuclear inhibitor of protein phosphatase-1 (NIPP1) directs protein phosphatase-1 (PP1) to dephosphorylate the U2 small nuclear ribonucleoprotein particle (snRNP) component, spliceosome-associated protein 155 (Sap155). J. Biol. Chem. 2008;283:35805–14.
274. Van Dessel N, Beke L, Gornemann J, Minnebo N, Beullens M, Tanuma N, et al. The

phosphatase interactor NIPP1 regulates the occupancy of the histone methyltransferase EZH2 at Polycomb targets. Nucleic Acids Res. 2010;38:7500–12.
275. Roy N, Van Eynde A, Beke L, Nuytten M, Bollen M. The transcriptional repression by NIPP1 is mediated by Polycomb group proteins. Biochim. Biophys. Acta - Gene Struct. Expr. 2007;1769:541–5.
276. Jin Q, Van Eynde A, Beullens M, Roy N, Thiel G, Stalmans W, et al. The protein phosphatase-1 (PP1) regulator, nuclear inhibitor of PP1 (NIPP1), interacts with the polycomb group protein, embryonic ectoderm development (EED), and functions as a transcriptional repressor. J. Biol. Chem. 2003;278:30677–85.
277. Vulsteke V, Beullens M, Boudrez A, Keppens S, Van Eynde A, Rider MH, et al. Inhibition of Spliceosome Assembly by the Cell Cycle-regulated Protein Kinase MELK and Involvement of Splicing Factor NIPP1. J. Biol. Chem. 2004;279:8642–7.
278. Boudrez A, Beullens M, Groenen P, Van Eynde A, Vulsteke V, Jagiello I, et al. NIPP1-mediated interaction of protein phosphatase-1 with CDC5L, a regulator of pre-mRNA splicing and mitotic entry. J. Biol. Chem. 2000;275:25411–7.
279. Jin Q, Beullens M, Jagiello I, Van Eynde A, Vulsteke V, Stalmans W, et al. Mapping of the RNA-binding and endoribonuclease domains of NIPP1, a nuclear targeting subunit of protein phosphatase 1. Biochem. J. 1999;342 Pt 1:13–9.
280. O'Connell N, Nichols SR, Heroes E, Beullens M, Bollen M, Peti W, et al. The molecular basis for substrate specificity of the nuclear NIPP1:PP1 holoenzyme. Structure. 2012;20:1746–56.
281. Chevalier D, Morris ER, Walker JC. 14-3-3 and FHA domains mediate phosphoprotein interactions. Annu. Rev. Plant Biol. 2009;60:67–91.
282. Mahajan A, Yuan C, Lee H, Chen ES-W, Wu P-Y, Tsai M-D. Structure and function of the phosphothreonine-specific FHA domain. Sci. Signal. 2008;1:re12.
283. Pennell S, Westcott S, Ortiz-Lombarda M, Patel D, Li J, Nott TJ, et al. Structural and functional analysis of phosphothreonine-dependent FHA domain interactions. Structure. 2010;18:1587–95.
284. Durocher D, Jackson SP. The FHA domain. FEBS Lett. 2002. p. 58–66.
285. Durocher D, Taylor IA, Sarbassova D, Haire LF, Westcott SL, Jackson SP, et al. The Molecular Basis of FHA Domain:Phosphopeptide Binding Specificity and Implications for Phospho-Dependent Signaling Mechanisms. Mol. Cell. 2000;6:1169–82.
286. Li J, Lee GI, Van Doren SR, Walker JC. The FHA domain mediates phosphoprotein interactions. J. Cell Sci. 2000;113 Pt 23:4143–9.
287. Bernstein NK, Williams RS, Rakovszky ML, Cui D, Green R, Karimi-Busheri F, et al. The molecular architecture of the mammalian DNA repair enzyme, polynucleotide kinase. Mol. Cell. 2005;17:657–70.
288. Kumeta H, Ogura K, Adachi S, Fujioka Y, Tanuma N, Kikuchi K, et al. The NMR structure of the NIPP1 FHA domain. J Biomol NMR. 2008;40:219–24.
289. Boudrez A, Beullens M, Waelkens E, Stalmans W, Bollen M. Phosphorylation-dependent interaction between the splicing factors SAP155 and NIPP1. J. Biol. Chem. 2002;277:31834–41.
290. Minnebo N, Gornemann J, O'Connell N, Van Dessel N, Derua R, Vermunt MW, et al. NIPP1 maintains EZH2 phosphorylation and promoter occupancy at proliferation-related target genes. Nucleic Acids Res. 2013;41:842–54.
291. Li H, Byeon I, Ju Y, Tsai M. Structure of human Ki67 FHA domain and its binding to a phosphoprotein fragment from hNIFK reveal unique recognition sites and new views to the structural basis of FHA domain functions. J Mol Biol. 2004;335:371–81.
292. Beullens M, Van Eynde A, Stalmans W, Bollen M. The isolation of novel inhibitory polypeptides of protein phosphatase 1 from bovine thymus nuclei. J. Biol. Chem. 1992;267:16538–44.
293. Nuytten M, Beke L, Van Eynde a, Ceulemans H, Beullens M, Van Hummelen P, et al. The transcriptional repressor NIPP1 is an essential player in EZH2-mediated gene silencing. Oncogene. 2008;27:1449–60.
294. Van Eynde A, Nuytten M, Dewerchin M, Schoonjans L, Keppens S, Beullens M, et al. The Nuclear Scaffold Protein NIPP1 Is Essential for Early Embryonic Development and Cell

Proliferation. Mol Cell Biol. 2004;24:5863–74.
295. Beullens M, Bollen M. The protein phosphatase-1 regulator NIPP1 is also a splicing factor involved in a late step of spliceosome assembly. J. Biol. Chem. 2002;277:19855–60.
296. Eynde A Van, Nuytten M, Dewerchin M, Keppens S, Beullens M, Carmeliet P, et al. The Nuclear Scaffold Protein NIPP1 Is Essential for Early Embryonic Development and Cell Proliferation. Mol. Cell. Biol. 2004;24:5863–74.
297. Wahl MC, Will CL, Lührmann R. The Spliceosome: Design Principles of a Dynamic RNP Machine. Cell. 2009. p. 701–18.
298. Johnson D, Cohen PT, Chen MX, Chen YH. Identification of the regions on the M110 subunit of protein phosphatase 1M that interact with the M21 subunit and with myosin. Eur J Biochem. 1997;244:931–9.
299. Claverie-Martin F, Wang M, Cohen SN. ARD-1 cDNA from human cells encodes a site-specific single-strand endoribonuclease that functionally resembles Escherichia coli RNase E. J. Biol. Chem. 1997;272:13823–8.
300. Chang ACY, Sohlberg B, Trinkle-Mulcahy L, Claverie-Martin F, Cohen P, Cohen SN. Alternative splicing regulates the production of ARD-1 endoribonuclease and NIPP-1, an inhibitor of protein phosphatase-1, as isoforms encoded by the same gene. Gene. 1999;240:45–55.
301. Wang M, Cohen SN. ard-1: a human gene that reverses the effects of temperature-sensitive and deletion mutations in the Escherichia coli rne gene and encodes an activity producing RNase E-like cleavages. Proc. Natl. Acad. Sci. U. S. A. 1994;91:10591–5.
302. Miczak A, Kaberdin VR, Wei CL, Lin-Chao S. Proteins associated with RNase E in a multicomponent ribonucleolytic complex. Proc. Natl. Acad. Sci. USA. 1996;93:3865–9.
303. Vanzo NF, Li YS, Py B, Blum E, Higgins CF, Raynal LC, et al. Ribonuclease E organizes the protein interactions in the Escherichia coli RNA degradosome. Genes Dev. 1998;12:2770–81.
304. Carpousis AJ. The RNA Degradosome of *Escherichia coli* : An mRNA-Degrading Machine Assembled on RNase E. Annu. Rev. Microbiol. 2007;61:71–87.
305. Ow MC, Kushner SR. Initiation of tRNA maturation by RNase E is essential for cell viability in E. coli. Genes Dev. 2002;16:1102–15.
306. Lin-Chao S, Wei CL, Lin YT. RNase E is required for the maturation of ssrA RNA and normal ssrA RNA peptide-tagging activity. Proc. Natl. Acad. Sci. U. S. A. 1999;96:12406–11.
307. Li Z, Deutscher MP. RNase E plays an essential role in the maturation of Escherichia coli tRNA precursors. RNA. 2002;8:97–109.
308. Kim KS, Lee Y. Regulation of 6S RNA biogenesis by switching utilization of both sigma factors and endoribonucleases. Nucleic Acids Res. 2004;32:6057–68.
309. Schein A, Sheffy-Levin S, Glaser F, Schuster G. The RNase E/G-type endoribonuclease of higher plants is located in the chloroplast and cleaves RNA similarly to the E. coli enzyme. RNA. 2008;14:1057–68.
310. Jagiello I, Beullens M, Stalmans W, Bollen M. Subunit structure and regulation of protein phosphatase-1 in rat liver nuclei. J. Biol. Chem. 1995;270:17257–63.
311. Medrano J V., Martínez-Arroyo AM, Sukhwani M, Noguera I, Quiñonero A, Martínez-Jabaloyas JM, et al. Germ cell transplantation into mouse testes procedure. Fertil. Steril. 2014;102:e11–2.
312. Gallardo T, Shirley L, John GB, Castrillon DH. Generation of a germ cell-specific mouse transgenic Cre line, Vasa-Cre. Genesis. 2007;45:413–7.
313. Nakano K, Vousden KH. PUMA, a novel proapoptotic gene, is induced by p53. Mol. Cell. 2001;7:683–94.
314. Orwig KE, Shinohara T, Avarbock MR, Brinster RL. Functional analysis of stem cells in the adult rat testis. Biol Reprod. 2002;66:944–9.
315. Boens S, Verbinnen I, Verhulst S, Szeker K, Ferreira M, Gevaert T, et al. Brief Report: The Deletion of the Phosphatase Regulator NIPP1 Causes Progenitor Cell Expansion in the Adult Liver. Stem Cells. 2016;34:2256–62.
316. Takase HM, Nusse R. Paracrine Wnt/β-catenin signaling mediates proliferation of

undifferentiated spermatogonia in the adult mouse testis. Proc. Natl. Acad. Sci. 2016;113:1489–97.
317. Kerppola TK. Polycomb group complexes-many combinations, many functions. Trends Cell Biol. 2009;19:692–704.
318. Mu W, Starmer J, ShibatYa Y, Yee D, Magnuson T. EZH1 in germ cells safeguards the function of PRC2 during spermatogenesis. Dev Biol. 2017;424:198–207.
319. Wu SC, Zhang Y. Cyclin-dependent kinase 1 (CDK1)-mediated phosphorylation of enhancer of zeste 2 (Ezh2) regulates its stability. J. Biol. Chem. 2011;286:28511–9.
320. Chen S, Bohrer LR, Rai AN, Pan Y, Gan L, Zhou X, et al. Cyclin-dependent kinases regulate epigenetic gene silencing through phosphorylation of EZH2. Nat. Cell Biol.2010;12:1108–14.
321. Kaneko S, Li G, Son J, Xu CF, Margueron R, Neubert TA, et al. Phosphorylation of the PRC2 component Ezh2 is cell cycle-regulated and up-regulates its binding to ncRNA. Genes Dev. 2010;24:2615–20.
322. Wei Y, Chen Y-H, Li L-Y, Lang J, Yeh S-P, Shi B, et al. CDK1-dependent phosphorylation of EZH2 suppresses methylation of H3K27 and promotes osteogenic differentiation of human mesenchymal stem cells. Nat. Cell Biol. 2011;13:87–94.
323. Lesage B, Beullens M, Nuytten M, Van Eynde A, Keppens S, Himpens B, et al. Interactor-mediated nuclear translocation and retention of protein phosphatase-1. J. Biol. Chem. 2004;279:55978–84.
324. Zovoilis A, Cifuentes-Rojas C, Chu HP, Hernandez AJ, Lee JT. Destabilization of B2 RNA by EZH2 Activates the Stress Response. Cell. 2016;167:1788–1802.e13.
325. Davidovich C, Zheng L, Goodrich KJ, Cech TR. Promiscuous RNA binding by Polycomb repressive complex 2. Nat. Struct. 38; Mol. Biol. 2013;20:1250–7.

# List of Publications

## Articles

**Mónica Ferreira**, Shannah Boens, Claudia Winkler, Kathelijne Szekér, Iris Verbinnen, Aleyde Van Eynde, Margarida Fardilha and Mathieu Bollen. The protein phosphatase 1 regulator NIPP1 is essential for mammalian spermatogenesis. Scientific Reports. 2017; 7:13364.

Iris Verbinnen**, Mónica Ferreira** and Mathieu Bollen. Biogenesis and activity regulation of protein phosphatase 1. Biochemical Society Transactions. 2017; 45: 89-99.

Shannah Boens, Iris Verbinnen, Stefaan Verhulst, Kathelijne Szekér, **Mónica Ferreira**, Thomas Gevaert, Myriam Baens, Tania Roskans, Leo Van Grunsven, Aleyde Van Eynde and Mathieu Bollen. The deletion of the phosphatase regulator NIPP1 causes progenitor cell expansion in the adult liver. Stem Cells. 2016; 34: 2256-2262.

Luis Korrodi-Gregório, **Mónica Ferreira**, Ana Paula Vintém, Wenjuan Wu, Thorsten Muller, Katrin Marcus, Srinivasan Vijayaraghavan, David Brautigan, Odete A. B. da Cruz e Silva, Edgar F. da Cruz e Silva. Identification and characterization of two distinct PPP1R2 isoforms in human sperm. BMC Cell Biology. 2013;14: 15.

Margarida Fardilha, **Mónica Ferreira**, Steven Pelech, Sandra Vieira, Sandra Rebelo, Luis Korrodi-Gregório, Mário Sousa, Alberto Barros, Vladimiro Silva, Odete A. B. da Cruz e Silva and Edgar F. da Cruz e Silva. "OMICS" of human sperm: profiling protein phosphatases. OMICS: a Journal of Integrative Biology. 2013; 17: 460-472.

**Mónica Ferreira**, Rita C. Matos, Helena Oliveira, Bruno Nunes and Maria de Lourdes Pereira. Impairment of spermatogenesis by sodium arsenite. Human and Experimental Toxicology. 2012; 31: 290-302.

## Book Chapters

Joana Rocha, **Mónica Ferreira** and Margarida Fardilha. Fosforilação de Proteínas na Transdução de Sinais. 1st ed. Departamento de Biologia, Universidade de Aveiro, Edições afrontamento, Porto; 2012. ISBN: 978-972-36.

## Abstracts

Iris Verbinnen, Liakath-Ali, Kathelijne Szekér, Shannah Boens, **Mónica Ferreira**, Maria Garmyn, Fiona Watt, Aleyde Van Eynde, Mathieu Bollen. Protein phosphatase PP1-NIPP1 regulates epidermal homeostasis and the repair capacity of carcinogen-induced DNA damage. Copenhagen Bioscience Conferences: Protein signaling-from pathways to networks. October 2016, Copenhagen, Denmark.

**Mónica Ferreira**, Shannah Boens, Claudia Winkler, Kathelijne Szekér, Iris Verbinnen, Aleyde Van Eynde, Margarida Fardilha and Mathieu Bollen. The protein phosphatase regulator NIPP1 is essential for the proliferation of male germ cells. 19th European Testis Workshop: Germ Cells Potential. June 2016, Saint-Malo, France.

Iris Verbinnen, Liakath-Ali, Kathelijne Szekér, Shannah Boens, **Mónica Ferreira**, Baes, M., Fiona Watt, Aleyde Van Eynde, Mathieu Bollen. Protein phosphatase PP1-NIPP1 controls epidermal

homeostasis and susceptibility to DMBA-induced skin carcinogenesis. Oncoforum. May 2016, Leuven, Belgium.

Iris Verbinnen, Kathelijne Szekér, Shannah Boens, **Mónica Ferreira**, Myriam Baes, Aleyde Van Eynde, Mathieu Bollen. Protein phosphatase PP1-NIPP1 regulates epidermal proliferation and hair-type determination. Montagna Symposium on the Biology of Skin. October 2015, Gleneden Beach, Oregon, USA.

**Mónica Ferreira**, Shannah Boens, Kathelijne Szekér, Aleyde Van Eynde, Margarida Fardilha and Mathieu Bollen. The phosphatase regulator NIPP1 is essential for the proliferation and differentiation of male germ cells. EMBO Cell Cycle meeting. September 2014, Budapest, Hungary.

**Mónica Ferreira**, Shannah Boens, Kathelijne Szekér, Karel De Gendt, Aleyde Van Eynde, Margarida Fardilha and Mathieu Bollen. NIPP1 depletion in postnatal male germ cells leads to infertility. IUAP meeting at the University of Leuven. December 2014, Leuven, Belgium.

**Mónica Ferreira**, Aleyde Van Eynde, Monique Beullens, Mathieu Bollen, Margarida Fardilha. In search of protein ligands for a testis-specific variant of NIPP1, a nuclear regulator of PP1. EMBO Workshop: Advances in Protein-Protein interaction analysis and modulation. June 2012, Roscoff, France.

**Mónica Ferreira**, Aleyde Van Eynde, Monique Beullens, Mathieu Bollen, Margarida Fardilha. Identification of the Interactome of a Testis-specific Splice-variant of NIPP1, a Nuclear Regulator of Protein Phosphatase 1. Research Day at the University of Aveiro. June 2013, Aveiro, Portugal.